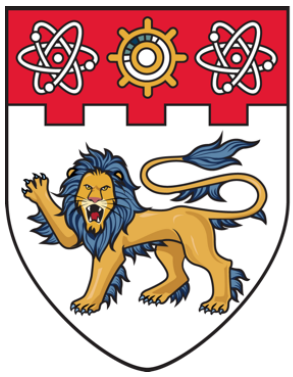

NANYANG TECHNOLOGICAL UNIVERSITY
SINGAPORE

TUNABLE AND STABLE SWOLLEN SURFACTANT LAMELLAR PHASES FOR HAIR-CARE APPLICATIONS

GONCALVES CARDOSO RUI ANDRE

SCHOOL OF MATERIALS SCIENCE AND ENGINEERING

2019

TUNABLE AND STABLE SWOLLEN SURFACTANT LAMELLAR PHASES FOR HAIR-CARE APPLICATIONS

GONCALVES CARDOSO RUI ANDRE

SCHOOL OF MATERIALS SCIENCE AND ENGINEERING

A thesis submitted to the Nanyang Technological University
in partial fulfilment of the requirement for the degree of
Doctor of Philosophy

2019

Statement of Originality

I hereby certify that the work embodied in this thesis is the result of original research, is free of plagiarised materials, and has not been submitted for a higher degree to any other University or Institution.

13 August 2019

Rui A. Gonçalves

Supervisor Declaration Statement

I have reviewed the content and presentation style of this thesis and declare it is free of plagiarism and of sufficient grammatical clarity to be examined. To the best of my knowledge, the research and writing are those of the candidate except as acknowledged in the Author Attribution Statement. I confirm that the investigations were conducted in accord with the ethics policies and integrity standards of Nanyang Technological University and that the research data are presented honestly and without prejudice.

13 August 2019

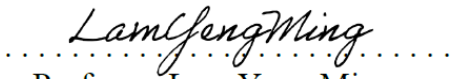

Professor Lam Yeng Ming

Authorship Attribution Statement

This thesis contains material from one paper published in the following peer-reviewed journal where I was the first and/or corresponding author.

Chapter 5 is published as Rui A. Gonçalves, B. Lindman, M. G. Miguel, T. Iwata and Yeng Ming Lam. Elucidating the effect of additives on the alkyl chain packing of a double tail cationic surfactant. *Journal of Colloid and Interface Science* 528 (2018) 400-409. DOI: 10.1016/j.jcis.2018.05.092.

Rui A. Gonçalves, B. Lindman, M. G. Miguel, T. Iwata and Yeng Ming Lam. Elucidating the additive effects on DODAC. *Journal of Colloid and Interface Science* (2020): *to be submitted*.

The contributions of the co-authors are as follows:

- Professor Lam provided the initial project direction and edited the manuscript drafts.
- I prepared the manuscript drafts. The manuscript was revised by Professor Lindman, Professor Miguel and Dr. Iwata.
- I co-designed the study with Professor Lam, Professor Lindman and Professor Miguel and performed all the laboratory work at the School of Materials Science and Engineering.
- All X-ray characterization, including sample preparation, was conducted by me in the Facility for Analysis, Characterisation, Testing and Simulation (FACTS).

Chapter 6 is under review as Rui A. Gonçalves, Polina Naidjonoka, Tommy Nylander, M. G. Miguel, B. Lindman and Yeng Ming Lam. Facile control of surfactant lamellar phase transition and adsorption behavior. *RSC Advances* (2020).

The contributions of the co-authors are as follows:

- Professor Lam provided the initial project direction and edited the manuscript drafts.
- I wrote the drafts of the manuscript. The manuscript was revised together with Professor Nylander, Professor Miguel and Professor Lindman.
- I co-designed the study with Professor Lam, Professor Nylander, Professor Lindman and Professor Miguel.

- I performed all the laboratory work at the School of Materials Science and Engineering.
- All ellipsometry data were collected by Ms. Polina Naidjonoka and me in the Division of Physical Chemistry, Department of Chemistry, Centre for Chemistry and Chemical Engineering, Lund University, Lund, Sweden.
- All the X-ray scattering, including synchrotron source, data collection and data treatment were conducted by me in the Facility for Analysis, Characterisation, Testing and Simulation and in the Australian Synchrotron (ANSTO), Clayton, Australia.

13 August 2019

Rui Gonçalves

.....

Rui A. Gonçalves

Abstract

Double-tailed surfactants have been commonly used in the formulation of personal-care products so as to provide some unique properties in the final product. These include the ability to deposit particles on surfaces and storage stability at ambient conditions. The challenge is to develop a single and stable lamellar gel (L_β) phase to achieve maximum swelling without coexisting water phase. Hair-conditioner compositions are generally formulated with various active compounds, such as cationic surfactants and molecules with specific functionalities. The concentration of various compounds will give rise to formulation with a variety of microstructures which will in turn provide different desirable material properties. Therefore, it is important to have good understanding of the phase behavior of such formulations to improve the formulation of products for hair-care applications. The investigation on the effect of additives is performed on dioctadecyldimethylammonium chloride mainly.

In this study, the thermal behavior, swelling behavior (in the presence of water), packing structure and deposition profile of double-tailed surfactant systems have been investigated. Initially, a phase study of dioctadecyldimethylammonium bromide (DODAB) and chloride (DODAC) in aqueous solution was conducted to determine the effect of the counterion on lamellar stability. Next, the effects of fifteen commonly used compounds, such as "ureas", hydrotrope molecules and short and intermediate-chain fatty acids and alcohols on the lamellar stability and packing structure upon thermal changes were examined. The physical appearance of these surfactant systems was examined optically and with the use of cross-polarizers to enable a facile way to detect the formation of birefringent structures, manifested by the observation of Maltese cross or oily streak textures. Differential scanning calorimetry (DSC) was used to establish the main phase transition (often called gel-to-liquid crystalline, L_α-L_β) temperature (T_m) and small/wide-angle X-ray scattering (SAXS and WAXS) was employed to determine the surfactant packing structure, polar and non-polar domain thickness and area per surfactant molecule below and above the T_m. Synchrotron SAXS and WAXS was used to determine the surfactant packing of diluted samples used for surfactant deposition investigation. In-situ null ellipsometry was used to

monitor and characterize time-dependent surfactant film deposition on a surface with respect to the layer thickness and adsorbed amount of surfactant. The deposition was performed upon rinsing and presented and discussed as a function of sample composition and concentration.

This Ph.D. work shows that stable L_α phases are yielded by incorporating small polar additives to the DODAC bilayer, thus lowering the L_α-L_β phase transition temperature. These stable L_α phases can spontaneously be changed into the L_β phase and subsequently deposited on a substrate. Ellipsometry studies demonstrate that dilution of the surfactant-additive-water phases leads to the deposition of well-defined robust layers onto silica. The adsorbed surfactant layers having approximately the same thickness of the surfactant chain length, are stable and are not affected by extensive dilution.

Lay Summary

Surfactants are molecules that can solubilize both polar and non-polar compounds. In other words, they solubilize two immiscible compounds in one single phase. These special molecules display a hierarchical organization structure which defines their field of application. Surfactants that self-assemble into lamellar structures are of great importance in biology can mimic bio-membranes and can be used as drug carriers because they can deliver compounds that are incompatible with the surrounding medium. Remarkably, they can be used in consumer-care applications. Positively charged lamellar phases can also deliver conditioning properties to surfaces and have been the foundation of fiber conditioner formulations, such as fabric softeners and hair conditioners. Above a specific temperature, lamellar structures show a "fluid-like" behavior (liquid crystalline phase), whereas below that temperature they display a "solid-like" behavior, named gel phase. This phase provides long shelf-life to the products, but they are not as stable as liquid crystalline phases. The function of a surfactant lamellar phase in conditioner formulation is analogous to coacervates in shampoo: it is crucial to deliver the smooth and anti-static feel of hair fibers [1, 2]. The layered structure of this surfactant phase can furthermore facilitate to stabilize dispersions of non-polar additives, for instance, oils and fragrances, while depositing the active conditioning compounds. This work is focused on the elucidation of the underlying surfactant-additive interactions. Additives of different chemical nature were added into the lamellar structure to tune the gel-to-liquid crystalline phase transition temperature. The packing structure of the resulting systems was examined. Small water-soluble molecules show an ability to fluidize the bilayer and decrease the phase transition temperature. On extensive dilution with water, these polar molecules were removed from the "fluid-like" bilayers. Consequently, a spontaneous transition from the "fluid-like" phase to the gel phase occurred whilst the additive was washed away on rinsing. Eventually well-defined layers of gel phase were deposited on a surface. These layers were shown to be stable on continuous rinsing due to high insolubility of the surfactant in water. All these works have demonstrated the possibility of designing a stable formulation that will deliver stable gel phases on a substrate for maximized conditioning efficacy.

References

[1] R.Y. Lochhead, *Practical Modern Hair Science, Chapter 3: Shampoo and Conditioner Science*, Allured Pub Corp2012.

[2] J. Yang, Chapter 36 - Hair Care Cosmetics, in: K. Sakamoto, R.Y. Lochhead, H.I. Maibach, Y. Yamashita (Eds.), *Cosmetic Science and Technology, Elsevier*, Amsterdam, 2017, pp. 601-615.

Acknowledgements

This doctoral dissertation would not have been possible without funding from the Agency for Science, Technology and Research (A*STAR, Singapore) under the Singapore International Graduate Award granted to me to pursue my Ph.D. studies at Nanyang Technological University, Singapore. Thanks to the A*STAR and Procter & Gamble research grants, I had the chance to travel to the Australian Synchrotron and to Lund University to conduct research work.

I would also like to thank the School of Materials Science and Engineering for the financial support of various conferences I have attended during the past four years and for providing well-equipped facilities to conduct research.

I would like to express my gratitude to my supervisor, Professor Yeng Ming Lam, who was abundantly helpful and offered invaluable guidance. Her mentorship and leadership inspired me to think critically and always explore our research ideas.

I want to thank Professor Björn Lindman and Professor Maria da Graça Miguel, my co-supervisors, mentors and source of inspiration for their passion and dedication to teaching. Their advice and guidance made me step out from my comfort zone and embrace this new chapter of my life in Asia, far away from my sunny Portugal.

I am most grateful to Dr. Toshi Iwata (P&G Innovation Centre, Singapore), Professor Tommy Nylander, Dr. Pio Buenconsejo, Dr. Samuel Morris, Final Year Project students and all our group members for the valuable comments, remarks and engagement on my research.

I would like to thank all the friends I made at NTU (faculty, staff and students), NTU SAO, NTU GSA and MSE GSC for the companionship, support and inspiration. A special word of gratitude to my friends and family members back in Portugal for their love, patience and support.

“Have a mission, plan ahead, question everything, assume nothing, roll up your sleeves, study the past, take risks, dream higher, welcome change, have an amazing haircut, laugh, be curious, pay attention to details, make mistakes, think sideways, do things with passion, don't forget to play, take it to the edge, breath.

Creativity takes courage.”
(Joana Astolfi).

Table of Contents

Table Captions

Figure Captions

Figure 1.1 Schematic illustration of the lamellar surfactant tunability in the presence of additives. A L_α single-phase (1Φ) is attained at a lower temperature and converted to a two-phase (2Φ) region to deposit a lamellar gel phase on a surface.

Figure 2.1 Schematic representation of the surfactant molecules. (a) Mono-tail nonionic surfactant, (b) mono-tail anionic surfactant, (c) mono-tail cationic surfactant, and (d) mono-tail zwitterionic surfactant.

Figure 2.2 Representation of the surfactant self-assembly evolution at different values of CPP and the geometrical constraints. The box highlights the various liquid crystalline phases.

Figure 2.3 Schematic representation of a lamellar structure with the polar domain in blue color (water, water-soluble molecules, surfactant head-groups, and counterions) and the non-polar domain in orange color (hydrocarbon chains and non-polar molecules).

Figure 2.4 Chemical structure of a quaternary ammonium double-tailed cationic amphiphile (swelling-type). X^- : anion as counterion, bromide (Br) or chloride (Cl).

Figure 2.5 (a) Phase diagram of the DODAB-water binary system. a: water melting points, b: crystals to lamellar mesophase transition, c: border between mesophase and mesophase + solid biphase region, d: mesophase to isotropic liquid transition. L-1 and L-2: proposed two different lamellar mesophases, H-2: reversed hexagonal phase, WS: waxy solid, I: isotropic liquid, A: crystal paste, B: crystals immersed in continuous isotropic liquid (*Reprinted with permission from P. C. Schulz, J. L. Rodríguez, F. A. Soltero-Martínez et al (1998) Phase behaviour of the dioctadecyldimethylammonium bromide-*

water system. Journal of Thermal Analysis and Calorimetry, 51, 49–62. Copyright 1998). (b) Phase diagram of the DODAC-water binary system. X_α and X_β: two dry crystals, XW: monohydrate crystal, X2W: dihydrate crystal, L: water, D: lamellar. (*Reprinted with permission from Laughlin, R.G., Munyon, R.L., Fu, Y.C. and Fehl, A.J. (1990) Physical science of the dioctadecyldimethylammonium chloride—water system. 1. Equilibrium phase behavior. Journal of Physical Chemistry, 94, 2546–2552. Copyright 1990, American Chemical Society*).

Figure 2.6 Schematic representation of the gel (L_β) and coagel (L_c) phases from different perspectives. The surfactant molecules adopt a hexagonal packing in the L_β phase which allows alkyl chain rotations; and an orthorhombic packing in the L_c phase which does not allow alkyl chain rotation.

Figure 2.7 Various structures of bilayers in the gel phase. (a) Gel phase, L_β; (b) Rippled gel phase, P_β; (c) Interdigitated gel phase, $L_{\beta int}$; (d) Tilted gel phase, $L_{\beta'}$.

Figure 2.8 Variations in the lamellar repeat distance with the composition of the urea-water solutions in systems with limited access to the solvent: L_β phase, 20 °C (■) and L_α phase, 25 °C (○). (A) The effect of water replacement by urea: The composition of the water-urea solution was varied, and the lipid composition in all samples was kept at 80 wt % (i.e., 20 wt % water-urea solution). (B) The effect of urea addition to a lipid-water system: The composition of the water-urea solution was varied, and the lipid-water ratio remained the same in all samples. In the sample with no urea, the composition was 80 wt % lipid and 20 wt % water. Urea was then added in different proportions to this mixture. (*Reprinted with permission from Fátima O. Costa-Balogh, Håkan Wennerström, Lars Wadsö, et al (2006) How Small Polar Molecules Protect Membrane Systems against Osmotic Stress: The Urea−Water−Phospholipid System. The Journal of Physical Chemistry B, 110, 23845-23852 Copyright 2006, American Chemical Society*).

Figure 2.9 Schematic phase diagram of the ternary DMPC-urea-water system at different temperatures. The phase diagrams contain three-phase triangles (dark grey), two-phase regions (light grey) and one-phase regions (white). (a) T<22 ^{o}C; (b) 22 ^{o}C<T<24 ^{o}C; (c) T>24 ^{o}C. *(Reprinted with permission from Emma Sparr and Håkan Wennerström (2011) Interlamellar forces and the thermodynamic characterization of lamellar phospholipid systems. Current Opinion in Colloid & Interface Science, 16, 561–567. Copyright 2011).*

Figure 2.10 Schematic representation of C18 fatty acid monolayers at the air/water interface. Note the effect of the degree of unsaturation on the area per molecule and the intermolecular distance, D, in the spread monolayers. (*Reprinted with permission from James R. Kanicky, Dinesh O. Shah (2002) Effect of Degree, Type, and Position of Unsaturation on the pKa of Long-Chain Fatty Acids. Journal of Colloid and Interface Science, 256, 201–207. Copyright 2002*).

Figure 2.11 Partial phase diagram of the poly(acrylamide)-b-complex salts-water-n-alcohols. The phase diagram shows the various liquid crystalline structures found at different mixture compositions. (*Reprinted with permission from Guilherme A. Ferreira, Lennard Piculell and Watson Loh (2016) Addition of n-Alcohols Induces a Variety of Liquid-Crystalline Structures in Surfactant-Rich Cores of Dispersed Block Copolymer/Surfactant Nanoparticles. ACS Omega, 1, 1104-1113 Copyright 2016, American Chemical Society*).

Figure 2.12 Schematic representation of the effect of the addition of butanol to the bilayer. (A) Illustration of the location of butanol in the membrane. (B) Summary of the parameters measured in this investigation. (*Reproduced from J. Guo, J. C. S. Ho, H. Chin, A. E. Mark, C. Zhou, S. Kjelleberg, B. Liedberg, A. N. Parikh, N. Cho, J. Hinks, Y. Mu and T. Seviour, Phys. Chem. Chem. Phys., 2019, 21, 11903 with permission from the PCCP Owner Societies*).

Figure 2.13 Schematic representation of the aggregates deposited on the silicon substrate. (a) Deposited layered structures of dodecyltrimethylammonium bromide (DTAB) (I) and DNA-DTAB complexes. (b) Deposited aggregates of DTAB (I) and coil-like aggregates deposited by carboxymethyl cellulose-DTAB complexes. (*Reprinted with permission from Sarathi Kundu (2010) Polyelectrolyte–surfactant complexes on solid surface. Journal of Colloid and Interface Science, 344, 547–555. Copyright 2010*).

Figure 2.14 Schematic ternary phase diagram showing an associative phase separation. The one-phase region and the two-phase region are labelled with 1Φ and 2Φ, respectively. On the right hand of the image, the polyelectrolyte–surfactant association is schematically depicted. (*Reprinted with permission from Tommy Nylander, Yulia Samoshina and Björn Lindman (2006) Formation of polyelectrolyte–surfactant complexes on surfaces. Advances in Colloid and Interface Science, 123-126, 105–123. Copyright 2006*).

Figure 2.15 Adsorbed amount from surfactant at hydrophilic and hydrophobic surfaces. (*Reprinted with permission from Maryline Clauzel, Eric S. Johnson, Tommy Nylander, Rajan K. Panandiker, Mark R. Sivik, Lennart Piculell (2011) Surface Deposition and Phase Behavior of Oppositely Charged Polyion-Surfactant Ion Complexes. Delivery of Silicone Oil Emulsions to Hydrophobic and Hydrophilic Surfaces. ACS Applied Materials and Interfaces, 3, 2451–2462 Copyright 2011, American Chemical Society*).

Figure 3.1 Molecular structure of: (a) dioctadecyldimethylammonium bromide – DODAB, (b) dioctadecyldimethylammonium chloride – DODAC, (c) urea – U, (d) methyl urea – MU, (e) dimethyl urea – DMU, (f) acetic acid – AA, (g) propionic acid – PA, (h) butyric acid – BA, (i) sodium butyrate – SB, (j) hexanoic acid – HA, (k) benzyl alcohol – BenOH, (l) phenoxyethanol – PhEtOH, (m) butanol – ButOH, (n) hexanol – HexOH, (o) octanol – OctOH, (p) decanol – DecOH, and (q) dodecanol – DodecOH.

Figure 3.2 Schematic polarized optical microscope setup. (*Reprinted with permission from Ingo Dierking (2004) Polarizing Microscopy, Textures of Liquid Crystals, John Wiley and Sons. Copyright 2004*).

Figure 3.3 Distinctive optical textures of a lamellar phase, showing (a) Maltese crosses and (b) oily streaks by aligned molecules observed between cross-polarizers revealing sample birefringence.

Figure 3.4 A schematic representation of a DSC cell cross-section. The reference and sample pan are heated simultaneously, and the difference in the amount of heat is recorded.

Figure 3.5 The variation of excess specific heat during a two-state transition process. T_m indicated the temperature at which the thermal transition occurs, and ΔH is the enthalpy associated with the thermal transition (area under the peak).

Figure 3.6 A schematic diagram of the entire range of the electromagnetic spectrum with the corresponding wavelength and frequency from the lowest energy (left) to the highest (right).

Figure 3. 7 A schematic representation of the Bragg diffraction. Periodic particles or structures scatter the incoming beam, and a beam with the same wavelength (λ) and in phase is scattered providing the distance (d) between aligned particles or structures, as stated by Bragg's law.

Figure 3.8 Schematic representation of the surfactant lamellar L_β phase packing structure. d_{sp} – interlamellar spacing, d_{bi} – bilayer thickness, d_w – polar domain thickness.

Figure 3.9 A schematic diagram of the SAXS and WAXS experimental setup. X-rays are generated, pass through a set of pinholes to define the resolution, a collimated beam of

X-rays irradiates the sample, and detectors collect the coherent scattered beams at different sample-to-detector distances.

Figure 3.10 A schematic representation of the coherent scattering from a lamellar surfactant structure following the Bragg's law for diffraction, thus allowing to determine the interlamellar spacing (d_{sp}) of an aggregate system.

Figure 3.11 A schematic representation of the coherent scattering from (a) a cubic (*Pn3m*) structure and (b) a hexagonal structure following the Bragg's law for diffraction, thus allowing the determination of different distances between neighboring aligned structures.

Figure 3.12 A schematic representation of the automated ellipsometer used in this study. The polarized light from the laser is depolarized with a circular polarizer. After the polarizer, the emerging linearly polarized light is transformed into elliptically polarized light when passing through the compensator, which is a quarter wave plate. The ellipticity can be varied by rotating the polarizer. As the reflection against the surface of the sample also changes the ellipticity of the light, the polarizer can be rotated in such a way that the light after reflection again is linearly polarized. The relative rotation of this light is measured by using another polarizer, the analyzer, which is rotated until a minima in light intensity as measured by the detector. (*Adapted with permission from Maryline Clauzel, Eric S. Johnson, Tommy Nylander, Rajan K. Panandiker, Mark R. Sivik, Lennart Piculell (2011) Surface Deposition and Phase Behavior of Oppositely Charged Polyion-Surfactant Ion Complexes. Delivery of Silicone Oil Emulsions to Hydrophobic and Hydrophilic Surfaces. ACS Applied Materials and Interfaces, 3, 2451–2462 Copyright 2011, American Chemical Society*).

Figure 4.1 POM micrographs of the textures of DODAB in water at increasing surfactant concentration: (a) to (m) correspond to 5 wt. %, 7.5 wt. %, 10 wt. %, 12.5 wt. %, 15 wt. %, 17.5 wt. %, 20 wt. %, 22.5 wt. %, 25 wt. %, 30 wt. %, 32.5 wt. %, 35 wt. % and

37.5 wt. %, respectively. The scale was set at 50 μm and applied to all micrographs. Temperature was kept constant at 25 ^{o}C.

Figure 4.2 POM micrographs of the textures of DODAC in water at increasing surfactant concentration: (a) to (m) correspond to 5 wt. %, 7.5 wt. %, 10 wt. %, 12.5 wt. %, 15 wt. %, 17.5 wt. %, 20 wt. %, 22.5 wt. %, 25 wt. %, 30 wt. %, 32.5 wt. %, 35 wt. % and 37.5 wt. %, respectively. The scale was set at 50 μm and applied to all micrographs. Temperature was kept constant at 25 ^{o}C.

Figure 4.3 Thermograms under (a) heating and (b) cooling of 35 wt. % DODAC in water at four different scan rates (1, 2, 5, and 10 ^{o}C /min). The endothermic event corresponds to the downwards deflection.

Figure 4.4 $DODA^{+}$ Br^{-} thermograms from 5 (bottom) to 37.5 wt. % of surfactant (top). On the left (a) is represented the heating scan, and on the right (b) is represented the cooling scan. The measurements were conducted from 10 to 60 ^{o}C, and back to 10 ^{o}C at 2 ^{o}C/min. The endothermic event corresponds to the downwards deflection.

Figure 4.5 Two-cycle thermograms under heating and cooling of 25 wt. % DODAB in water. The full line corresponds to the first cycle and dotted line to the second cycle. The measurements were conducted from 10 to 60 ^{o}C, and back to 10 ^{o}C at 2 ^{o}C/min. The endothermic event corresponds to the downwards deflection.

Figure 4.6 $DODA^{+}$ Cl^{-} thermograms from 5 (bottom) to 37.5 wt. % of surfactant (top). On the left (a) is represented the heating scan, and on the right (b) is represented the cooling scan. The measurements were conducted from 10 to 60 ^{o}C, and back to 10 ^{o}C at 2 ^{o}C/min. The endothermic event corresponds to the downwards deflection.

Figure 4.7 Two-cycle thermograms under heating and cooling of 35 wt. % of DODAC in water. The full line corresponds to the first cycle and dotted line to the second cycle. The measurements were conducted from 10 to 60 ^{o}C, and back to 10 ^{o}C at 2 ^{o}C/min. The endothermic event corresponds to the downwards deflection.

Figure 4.8 SAXS and WAXS profiles of 25 wt. % of DODAB in water under the heating cycle at 40 ^{o}C (grey; bottom profile) and 47 ^{o}C (red; top profile).

Figure 4.9 SAXS and WAXS profiles of 25 wt. % of DODAB in water under heating ((a) and (b)) and cooling ((c) and (d)) from top to bottom.

Figure 4.10 SAXS profile of 25 wt. % of DODAB in water at 47 ^{o}C under cooling showing the coexistence of two lamellar phases. The arrows represented lamellar reflections: in red the liquid crystalline phase and blue the gel phase.

Figure 4.11 SAXS and WAXS profiles of 35 wt. % of DODAC in water under heating ((a) and (b)) and cooling ((c) and (d)) from top to bottom.

Figure 4.12 Plot of double logarithmic of interlamellar spacing (d_{sp}, Å) versus inverse bilayer volume fraction (Φ_{bi}) for DODAC in water at: (a) 25 ^{o}C and (b) 50 ^{o}C.

Figure 4.13 Double logarithmic plot of interlamellar spacing (d_{sp}, Å) versus inverse bilayer volume fraction (Φ_{bi}) for DODAC in water. Star symbol corresponds to the theoretical maximum interlamellar spacing (d_{max}, Å). Circle symbol corresponds to the experimental results calculated from SAXS and WAXS analysis of the L_{β} gel phase (25 ^{o}C, blue color) and L_{α} liquid crystalline phase (50 ^{o}C, red color).

Figure 5.5 Effect of added additives on the main phase transition temperature of DODAC-*hydrotropes*-water ternary systems. BenOH- benzyl alcohol, PhEtOH- phenoxyethanol.

Figure 5.6 Effect of added additives on the main phase transition temperature of DODAC-*fatty alcohols*-water ternary systems. ButOH- butanol, HexOH- hexanol, OctOH- octanol, DecOH- decanol, DodecOH- dodecanol.

Figure 5.7 Effects of the presence of *ureas* in the interlamellar spacing (d_{sp}), bilayer thickness (d_{bi}), and area per surfactant molecule (a) of the DODAC lamellar structure. The variation of interlamellar spacing, bilayer thickness and area per surfactant molecule as a function of additive concentration is a useful view of the trends, but data are referred to different T_m temperatures. The top panels (a, b and c) correspond to the gel phase, and the bottom panels (d, e and f) correspond to the liquid crystalline phase. U- urea (black square), MU- methyl urea (red circle), DMU- dimethyl urea (blue triangle).

Figure 5.8 Effects of the presence of *SCFAs* in the interlamellar spacing (d_{sp}), bilayer thickness (d_{bi}), and area per surfactant molecule (a) of the DODAC lamellar structure. The variation of interlamellar spacing, bilayer thickness and area per surfactant molecule as a function of additive concentration is a useful view of the trends, but data are referred to different T_m temperatures. The top panels (a, b and c) correspond to the gel phase, and the bottom panels (d, e and f) correspond to the liquid crystalline phase. AA- acetic acid (green triangle), PA- propionic acid (purple rhombus), BA- butyric acid (yellow triangle), SB- sodium butyrate (cyan triangle), HA- hexanoic acid (brown hexagon).

Figure 5.9 Schematic representation of the packing structure for the fully interdigitated DODAC-sodium butyrate-water system.

Figure 5.10 SAXS and WAXS profiles for DODAC with (a) 1.3 and (b) 20 wt. % of sodium butyrate at 50 ^{o}C showing the L_{α}-L_{3} phase transition with excess amounts of additive.

Figure 5.11 SAXS profiles for DODAC in the presence of hexanoic acid. Top panels: 5.0 wt. % of the additive, T_m = 26.4 ^{o}C: (a) below the T_m, and (b) above the T_m. Bottom panels: 12.5 wt. % of the additive, T_m = 13.4 ^{o}C: (c) below the T_m, and (d) above the T_m. In the top two panels, a co-existence of a lamellar and cubic (*Pn3m*) phase was found, and the bottom two panels show the evolution to a reversed cubic (*Pn3m*) phase. The green color arrows represented cubic phase reflections, the black arrows represented lamellar phases.

Figure 5.12 Effects of the presence of *hydrotropes* in the interlamellar spacing (d_{sp}), bilayer thickness (d_{bi}), and area per surfactant molecule (a) of the DODAC lamellar structure. The variation of interlamellar spacing, bilayer thickness and area per surfactant molecule as a function of additive concentration is a useful view of the trends, but data are referred to different T_m temperatures. The top panels (a, b and c) correspond to the gel phase, and the bottom panels (d, e and f) correspond to the liquid crystalline phase. BenOH- benzyl alcohol (yellow star), PhEtOH- phenoxyethanol (orange pentagon).

Figure 5.13 Effects of the presence of *fatty alcohols* in the interlamellar spacing (d_{sp}), bilayer thickness (d_{bi}), and area per surfactant molecule (a) of the DODAC lamellar structure. The variation of interlamellar spacing, bilayer thickness and area per surfactant molecule as a function of additive concentration is a useful view of the trends, but data are referred to different T_m temperatures. The top panels (a, b and c) correspond to the gel phase, and the bottom panels (d, e and f) correspond to the liquid crystalline phase. ButOH- butanol (blue dot), HexOH- hexanol (green plus), OctOH- octanol (black cross), DecOH- decanol (red plus-crossed), DodecOH- dodecanol (blue minus).

Figure 5.14 SAXS profiles for DODAC in the presence of butanol. Top panels: 10.0 wt. % of the additive: (a) below the T_m, and (b) above the T_m. Bottom panels: 15.0 wt. % of the additive: (c) below the T_m (12 ^oC), and (d) above the T_m. In the top two panels, a L_β-L_α phase transition was found, and the bottom two panels show the evolution to a reversed sponge (L_3) phase was determined.

Figure 5.15 SAXS profiles for DODAC in the presence of hexanol. Top panels: 5.0 wt. % of the additive: (a) below the T_m (12 ^oC), and (b) above the T_m. Bottom panels: 10.0 wt. % of the additive: (c) below the T_m (12 ^oC), and (d) above the T_m. In the top two panels, a L_β-L_α phase transition was found, and the bottom two panels show the evolution to a reversed cubic phase was determined.

Figure 5.16 Schematic representation of (a) a reversed cubic (cub_b) phase and (b) a reversed hexagonal (rev hex) phase.

Figure 5.17 SAXS profiles for DODAC in the presence of octanol. Top panels: 5.0 wt. % of the additive: (a) below the T_m (15 ^oC), (b) during the phase transition (25 ^oC), and (c) above the T_m (50 ^oC). Bottom panels: 12.5 wt. % of the additive: (d) below the T_m (15 ^oC), (e) during the phase transition (25 ^oC), and (f) above the T_m (50 ^oC). In the top panels, a coexistence of lamellar gel and cubic phase evolution to a single lamellar liquid crystalline phase was found, and the bottom panels a coexistence of lamellar gel and hexagonal phase evolution to cubic and hexagonal phase transition was determined. The black color arrows represented lamellar phase reflections, the green arrows represented cubic phase, and the orange stars represented hexagonal phase.

Figure A.5.1 Glass vials with the ternary DODAC-water-urea mixtures. Increasing additive concentration from left to right (5.0, 7.5, 10.0, 12.5, 15.0 and 20.0 wt. %).

Figure A.5.2 Glass vials with the ternary DODAC-water-methyl urea mixtures. Increasing additive concentration from left to right (5.0, 7.5, 10.0, 12.5, 15.0 and 20.0 wt. %).

Figure A.5.3 Glass vials with the ternary DODAC-water-dimethyl urea mixtures. Increasing additive concentration from left to right (5.0, 7.5, 10.0, 12.5, 15.0 and 20.0 wt. %).

Figure A.5.4 Glass vials with the ternary DODAC-water-acetic acid mixtures. Increasing additive concentration from left to right (5.0, 7.5, 10.0, 12.5, 15.0 and 20.0 wt. %).

Figure A.5.5 Glass vials with the ternary DODAC-water-propionic acid mixtures. Increasing additive concentration from left to right (5.0, 7.5, 10.0, 12.5, 15.0 and 20.0 wt. %).

Figure A.5.6 Glass vials with the ternary DODAC-water-butyric acid mixtures. Increasing additive concentration from left to right (1.3, 2.1, 4.5, 5.0, 7.5, 10.0, 12.5, 15.0 and 20.0 wt. %).

Figure A.5.7 Glass vials with the ternary DODAC-water-sodium butyrate mixtures. Increasing additive concentration from left to right (1.3, 2.6, 5.0, 6.6, 7.5, 10.0, 12.5, 15.0 and 20.0 wt. %).

Figure A.5.8 Glass vials with the ternary DODAC-water-hexanoic acid mixtures. Increasing additive concentration from left to right (5.0, 7.5, 10.0, 12.5, 15.0 and 20.0 wt. %).

Figure A.5.9 Glass vials with the ternary DODAC-water-benzyl alcohol mixtures. Increasing additive concentration from left to right (5.0, 7.5, 10.0, 12.5, 15.0 and 20.0 wt. %).

Figure A.5.10 Glass vials with the ternary DODAC-water-phenoxyethanol mixtures. Increasing additive concentration from left to right (5.0, 7.5, 10.0, 12.5, 15.0 and 20.0 wt. %).

Figure A.5.11 Glass vials with the ternary DODAC-water-butanol mixtures. Increasing additive concentration from left to right (5.0, 7.5, 10.0, 12.5, 15.0 and 20.0 wt. %).

Figure A.5.12 Glass vials with the ternary DODAC-water-hexanol mixtures. Increasing additive concentration from left to right (5.0, 7.5, 10.0, 12.5, 15.0 and 20.0 wt. %).

Figure A.5.13 Glass vials with the ternary DODAC-water-octanol mixtures. Increasing additive concentration from left to right (5.0, 7.5, 10.0, 12.5, 15.0 and 20.0 wt. %).

Figure A.5.14 Glass vials with the ternary DODAC-water-decanol mixtures. Increasing additive concentration from left to right (5.0, 7.5, 10.0, 12.5, 15.0 and 20.0 wt. %).

Figure A.5.15 Glass vials with the ternary DODAC-water-dodecanol mixtures. Increasing additive concentration from left to right (5.0, 7.5, 10.0, 12.5, 15.0 and 20.0 wt. %).

Figure A.5.16 DODAC-water-urea thermograms from 5 (top) to 20 wt. % urea (bottom) at fixed 35 wt. % surfactant. On the left (a) is represented the heating scan, and on the right (b) is represented the cooling scan. The measurements were conducted from 10 to 60 ^{o}C,

and back to 10 ^{o}C at 2 ^{o}C/min. The endothermic event corresponds to the downwards deflection.

Figure A.5.17 DODAC-water-methyl urea thermograms from 5 (top) to 20 wt. % methyl urea (bottom) at fixed 35 wt. % surfactant. On the left (a) is represented the heating scan, and on the right (b) is represented the cooling scan. The measurements were conducted from 10 to 60 ^{o}C, and back to 10 ^{o}C at 2 ^{o}C/min. The endothermic event corresponds to the downwards deflection.

Figure A.5.18 DODAC-water-dimethyl urea thermograms from 5 (top) to 20 wt. % dimethyl urea (bottom) at fixed 35 wt. % surfactant. On the left (a) is represented the heating scan, and on the right (b) is represented the cooling scan. The measurements were conducted from 10 to 60 ^{o}C, and back to 10 ^{o}C at 2 ^{o}C/min. The endothermic event corresponds to the downwards deflection.

Figure A.5.19 DODAC-water-acetic acid thermograms from 5 (top) to 20 wt. % acetic acid (bottom) at fixed 35 wt. % surfactant. On the left (a) is represented the heating scan, and on the right (b) is represented the cooling scan. The measurements were conducted from 10 to 60 ^{o}C, and back to 10 ^{o}C at 2 ^{o}C/min. The endothermic event corresponds to the downwards deflection.

Figure A.5.20 DODAC-water-propionic acid thermograms from 5 (top) to 20 wt. % propionic acid (bottom) at fixed 35 wt. % surfactant. On the left (a) is represented the heating scan, and on the right (b) is represented the cooling scan. The measurements were conducted from 10 to 60 ^{o}C, and back to 10 ^{o}C at 2 ^{o}C/min. The endothermic event corresponds to the downwards deflection.

Figure A.5.21 DODAC-water-butyric acid thermograms from 1.3 (top) to 20 wt. % butyric acid (bottom) at fixed 35 wt. % surfactant. On the left (a) is represented the heating scan, and on the right (b) is represented the cooling scan. The measurements were conducted from 10 to 60 ^{o}C, and back to 10 ^{o}C at 2 ^{o}C/min. The endothermic event corresponds to the downwards deflection.

Figure A.5.22 DODAC-water-sodium butyrate thermograms from 1.3 (top) to 20 wt. % sodium butyrate (bottom) at fixed 35 wt. % surfactant. On the left (a) is represented the heating scan, and on the right (b) is represented the cooling scan. The measurements were conducted from 10 to 60 ^{o}C, and back to 10 ^{o}C at 2 ^{o}C/min. The endothermic event corresponds to the downwards deflection.

Figure A.5.23 DODAC-water-hexanoic acid thermograms from 5 (top) to 20 wt. % hexanoic acid (bottom) at fixed 35 wt. % surfactant. On the left (a) is represented the heating scan, and on the right (b) is represented the cooling scan. The measurements were conducted from 10 to 60 ^{o}C, and back to 10 ^{o}C at 2 ^{o}C/min. The endothermic event corresponds to the downwards deflection.

Figure A.5.24 DODAC-water-benzyl alcohol thermograms from 5 (top) to 20 wt. % benzyl alcohol (bottom) at fixed 35 wt. % surfactant. On the left (a) is represented the heating scan, and on the right (b) is represented the cooling scan. The measurements were conducted from 10 to 60 ^{o}C, and back to 10 ^{o}C at 2 ^{o}C/min. The endothermic event corresponds to the downwards deflection

Figure A.5.25 DODAC-water-phenoxyethanol thermograms from 5 (top) to 20 wt. % phenoxyethanol (bottom) at fixed 35 wt. % surfactant. On the left (a) is represented the heating scan, and on the right (b) is represented the cooling scan. The measurements were

conducted from 10 to 60 ^{o}C, and back to 10 ^{o}C at 2 ^{o}C/min. The endothermic event corresponds to the downwards deflection.

Figure A.5.26 DODAC-water-butanol thermograms from 5 (top) to 20 wt. % butanol (bottom) at fixed 35 wt. % surfactant. On the left (a) is represented the heating scan, and on the right (b) is represented the cooling scan. The measurements were conducted from 10 to 60 ^{o}C, and back to 10 ^{o}C at 2 ^{o}C/min. The endothermic event corresponds to the downwards deflection.

Figure A.5.27 DODAC-water-hexanol thermograms from 5 (top) to 15 wt. % hexanol (bottom) at fixed 35 wt. % surfactant. On the left (a) is represented the heating scan, and on the right (b) is represented the cooling scan. The measurements were conducted from 10 to 60 ^{o}C, and back to 10 ^{o}C at 2 ^{o}C/min. The endothermic event corresponds to the downwards deflection.

Figure A.5.28 DODAC-water-octanol thermograms from 5 (top) to 20 wt. % octanol (bottom) at fixed 35 wt. % surfactant. On the left (a) is represented the heating scan, and on the right (b) is represented the cooling scan. The measurements were conducted from 10 to 60 ^{o}C, and back to 10 ^{o}C at 2 ^{o}C/min. The endothermic event corresponds to the downwards deflection.

Figure A.5.29 DODAC-water-decanol thermograms from 5 (top) to 20 wt. % decanol (bottom) at fixed 35 wt. % surfactant. On the left (a) is represented the heating scan, and on the right (b) is represented the cooling scan. The measurements were conducted from 10 to 60 ^{o}C, and back to 10 ^{o}C at 2 ^{o}C/min. The endothermic event corresponds to the downwards deflection.

Figure A.5.30 DODAC-water-dodecanol thermograms from 5 (top) to 20 wt. % dodecanol (bottom) at fixed 35 wt. % surfactant. On the left (a) is represented the heating scan, and on the right (b) is represented the cooling scan. The measurements were conducted from 10 to 60 ºC, and back to 10 ºC at 2 ºC/min. The endothermic event corresponds to the downwards deflection.

Figure A.5.31 SAXS and WAXS profiles of DODAC in water with increasing urea concentration from top to bottom (5-20 wt. %). (a) and (b) correspond to measurements at 25 ºC, and (c) and (d) to 50 ºC.

Figure A.5.32 SAXS and WAXS profiles of DODAC in water with increasing methyl urea concentration from top to bottom (5-20 wt. %). (a) and (b) correspond to measurements at 25 ºC, and (c) and (d) to 50 ºC.

Figure A.5.33 SAXS and WAXS profiles of DODAC in water with increasing dimethyl urea concentration from top to bottom (5-20 wt. %). (a) and (b) correspond to measurements at 25 ºC, and (c) and (d) to 50 ºC.

Figure A.5.34 SAXS and WAXS profiles of DODAC in water with increasing acetic acid concentration from top to bottom (5-20 wt. %). (a) and (b) correspond to measurements at 25 ºC, and (c) and (d) to 50 ºC.

Figure A.5.35 SAXS and WAXS profiles of DODAC in water with increasing propionic acid concentration from top to bottom (5-20 wt. %). (a) and (b) correspond to measurements at 25 ºC, and (c) and (d) to 50 ºC.

Figure A.5.36 SAXS and WAXS profiles of DODAC in water with increasing butyric acid concentration from top to bottom (5-20 wt. %). (a) and (b) correspond to measurements at 25 ^{o}C, and (c) and (d) to 50 ^{o}C.

Figure A.5.37 SAXS and WAXS profiles of DODAC in water with increasing sodium butyrate concentration from top to bottom (1.3-20 wt. %). (a) and (b) correspond to measurements at 25 ^{o}C, and (c) and (d) to 50 ^{o}C.

Figure A.5.38 SAXS and WAXS profiles of DODAC in water with increasing hexanoic acid concentration from top to bottom (5-20 wt. %). (a) and (b) correspond to measurements at 12 ^{o}C, and (c) and (d) to 50 ^{o}C.

Figure A.5.39 SAXS and WAXS profiles of DODAC in water with increasing benzyl alcohol concentration from top to bottom (5-20 wt. %). (a) and (b) correspond to measurements at 25 ^{o}C, and (c) and (d) to 50 ^{o}C.

Figure A.5.40 SAXS and WAXS profiles of DODAC in water with increasing phenoxyethanol concentration from top to bottom (5-20 wt. %). (a) and (b) correspond to measurements at 25 ^{o}C, and (c) and (d) to 50 ^{o}C.

Figure A.5.41 SAXS and WAXS profiles of DODAC in water with increasing butanol concentration from top to bottom (5-20 wt. %). (a) and (b) correspond to measurements at 12 ^{o}C, and (c) and (d) to 50 ^{o}C.

Figure A.5.42 SAXS and WAXS profiles of DODAC in water with increasing hexanol concentration from top to bottom (5-20 wt. %). (a) and (b) correspond to measurements at 12 ^{o}C, and (c) and (d) to 50 ^{o}C.

Figure A.5.43 SAXS and WAXS profiles of DODAC in water with increasing octanol concentration from top to bottom (5-20 wt. %). (a) and (b) correspond to measurements at 25 ^{o}C, and (c) and (d) to 50 ^{o}C.

Figure A.5.44 SAXS and WAXS profiles of DODAC in water with increasing decanol concentration from top to bottom (5-20 wt. %). (a) and (b) correspond to measurements at 25 ^{o}C, and (c) and (d) to 50 ^{o}C.

Figure A.5.45 SAXS and WAXS profiles of DODAC in water with increasing dodecanol concentration from top to bottom (5-20 wt. %). (a) and (b) correspond to measurements at 25 ^{o}C, and (c) and (d) to 50 ^{o}C.

Figure 6.1 (a) DSC heating thermograms of 35 wt. % DODAC in water. Ternary surfactant mixtures with 5 wt. % (blue color) and 12.5 wt. % (orange color) of additive. Full line represents the original sample and dotted line corresponds to the sample diluted ten times. (b-c) Acetic acid (AA) samples. (d-e) Propionic acid (PA) samples. (f-g) Butyric acid (BA) samples. (h-i) Benzyl alcohol (BenOH) samples. (j-k) Phenoxyethanol (PhEtOH) samples. Endothermic down.

Figure 6.2 Thermodynamic parameters of the gel-to-liquid crystalline phase transition temperature (T_m) and the enthalpy of phase transition (ΔH_m) of the DODAC-water-additive mixtures at the original composition ((a) and (b)) and after dilution ten times ((c) and (d)). DODAC was fixed at 35 wt. % for all the samples. *a: Main phase transition peak; *b: Peak split that appears to indicate two thermal transitions, hence ΔH_m could not be determined.

Figure 6.3 Synchrotron scattering profiles of diluted mixtures of 5 wt. % acetic acid in DODAC-water at 20 ^{o}C (below T_m) and 55 ^{o}C (above T_m). (a) SAXS and (b) WAXS.

Figure 6.4 Schematic representation of the experimental procedure used to study the deposition from DODAC-water-additive mixtures at the silica/water interface at 25 ^{o}C by in-situ null ellipsometry. At t = 0 s the silica wafer was immersed in water. The diluted surfactant sample was injected into the cuvette at t = 300 s, followed by start/stop rinsing and repeat of rinsing.

Figure 6.5 Time evolution of the adsorbed amount (Γ) and average layer thickness (*d*) of DODAC-water mixture at the silica/water interface (T = 25 ^{o}C).

Figure 6.6 Time evolution of the adsorbed amount (cf. equation 3.9), Γ, and average layer thickness, *d*, of DODAC-water-additive mixtures at the silica/water interface (T = 25 ^{o}C). (a) to (d) DODAC-water-5 wt. % additive. (e) to (h) DODAC-water-12.5 wt. % additive.

Figure 6.7 (a) Time evolution of the adsorbed amount, Γ, and (b) average layer thickness, d, of DODAC-water-butyric acid mixtures at the silica/water interface (T = 25 ^{o}C). Mixtures with increasing concentration in the ellipsometry cuvette, 3.6 mM (C1), 6.0 mM (C2), 7.2 mM (C3) and 12.0 mM (C4).

Figure 6.8 (a) Adsorbed amount (Γ) and area per surfactant molecule, and (b) average layer thickness (*d*) of mixtures of 12.5 wt. % of butyric acid in DODAC-water. Mixtures with increasing concentration in the ellipsometry cuvette, 3.6 mM (C1), 6.0 mM (C2), 7.2 mM (C3) and 12.0 mM (C4).

Figure A.6.1 Stacked SAXS/WAXS profiles for the original mixtures of 35 wt. % DODAC-water-acetic acid (AA). (i) SAXS/WAXS of 5 wt. % AA in the L_β (gel) phase; (ii) SAXS/WAXS of 5 wt. % AA in the L_α (liquid crystalline) phase; (iii) SAXS/WAXS of 12.5 wt. % AA in the L_β phase; (iv) SAXS/WAXS of 12.5 wt. % AA in the L_α phase. The Bragg reflections on SAXS reveal the lamellar peak ratio of 1: 2: 3… On the WAXS regime the L_β phase peak at q = 1.50 $Å^{-1}$, and the L_α phase peak broadening at ca. 1.42 $Å^{-1}$ are determined.

Figure A.6.2 Stacked SAXS/WAXS profiles for the original mixtures of 35 wt. % DODAC-water-propionic acid (PA). (i) SAXS/WAXS of 5 wt. % PA in the L_β (gel) phase; (ii) SAXS/WAXS of 5 wt. % PA in the L_α (liquid crystalline) phase; (iii) SAXS/WAXS of 12.5 wt. % PA in the L_β phase; (iv) SAXS/WAXS of 12.5 wt. % PA in the L_α phase. The Bragg reflections on SAXS reveal the lamellar peak ratio of 1: 2: 3… On the WAXS regime the L_β phase peak at q = 1.49 $Å^{-1}$, and the L_α phase peak broadening at ca. 1.38 $Å^{-1}$ are determined.

Figure A.6.3 Stacked SAXS/WAXS profiles for the original mixtures of 35 wt. % DODAC-water-benzyl alcohol (BenOH). (i) SAXS/WAXS of 5 wt. % BenOH in the L_β (gel) phase; (ii) SAXS/WAXS of 5 wt. % BenOH in the L_α (liquid crystalline) phase; (iii) SAXS/WAXS of 12.5 wt. % BenOH in the L_β phase; (iv) SAXS/WAXS of 12.5 wt. % BenOH (unidentified phase). The Bragg reflections on SAXS reveal the lamellar peak ratio of 1: 2: 3… On the WAXS regime the L_β phase peak at q = 1.49 $Å^{-1}$, and the L_α phase peak broadening at ca. 1.40 $Å^{-1}$ are determined.

Figure A.6.4 Stacked SAXS/WAXS profiles for the original mixtures of 35 wt. % DODAC-water-phenoxyethanol (PhEtOH). (i) SAXS/WAXS of 5 wt. % PhEtOH in the L_β (gel) phase; (ii) SAXS/WAXS of 5 wt. % PhEtOH in the L_α (liquid crystalline) phase; (iii) SAXS/WAXS of 12.5 wt. % PhEtOH in the L_β phase; (iv) SAXS/WAXS of 12.5 wt. % PhEtOH in the L_α (liquid crystalline) phase. The Bragg reflections on SAXS reveal the

lamellar peak ratio of 1: 2: 3… On the WAXS regime the L_β phase peak at q = 1.52 $Å^{-1}$, and the L_α phase peak broadening at ca. 1.38 $Å^{-1}$ are determined.

Figure A.6.5 Scattering profiles of diluted mixtures at 20 ^oC (below T_m) and 55 ^oC (above T_m). (a) SAXS of 5 wt. % acetic acid in DODAC-water, (b) SAXS of 12.5 wt. % acetic acid in DODAC-water, (c) WAXS of 5 wt. % acetic acid in DODAC-water, and (d) WAXS of 12.5 wt. % acetic acid in DODAC-water.

Figure A.6.6 Scattering profiles of diluted mixtures at 20 ^oC (below T_m) and 55 ^oC (above T_m). (a) SAXS of 5 wt. % propionic acid in DODAC-water, (b) SAXS of 12.5 wt. % propionic acid in DODAC-water, (c) WAXS of 5 wt. % propionic acid in DODAC-water, and (d) WAXS of 12.5 wt. % propionic acid in DODAC-water.

Figure A.6.7 Scattering profiles of diluted mixtures at 20 ^oC (below T_m) and 55 ^oC (above T_m). (a) SAXS of 5 wt. % butyric acid in DODAC-water, (b) SAXS of 12.5 wt. % butyric acid in DODAC-water, (c) WAXS of 5 wt. % butyric acid in DODAC-water, and (d) WAXS of 12.5 wt. % butyric acid in DODAC-water.

Figure A.6.8 Scattering profiles of diluted mixtures at 20 ^oC (below T_m) and 55 ^oC (above T_m). (a) SAXS of 5 wt. % benzyl alcohol in DODAC-water, (b) SAXS of 12.5 wt. % benzyl alcohol in DODAC-water, (c) WAXS of 5 wt. % benzyl alcohol in DODAC-water, and (d) WAXS of 12.5 wt. % benzyl alcohol in DODAC-water.

Figure A.6.9 Scattering profiles of diluted mixtures at 20 ^oC (below T_m) and 55 ^oC (above T_m). (a) SAXS of 5 wt. % phenoxyethanol in DODAC-water, (b) SAXS of 12.5 wt. % phenoxyethanol in DODAC-water, (c) WAXS of 5 wt. % phenoxyethanol in DODAC-water, and (d) WAXS of 12.5 wt. % phenoxyethanol in DODAC-water.

Figure 7.1 The model used to derive the Gouy-Chapman theory from the Poisson-Boltzmann equation. A positively charged wall that it infinite in *x* or *y* direction has associated with it a charge density and a potential. Valency and concentration of electrolyte and the dielectric permittivity of the solvent determine the variation in potential in *z* direction. The ions are treated as point charges.

Figure 7.2 A schematic illustration of the lamellar system. Addition of oil to the system swells the $C_{12}E_5$ bilayers. Since the volume fraction of surfactant is kept constant, the interlamellar distance, *d*, is constant, while the bilayer thickness, $d_m = 2d_s + d_o = 2d_s (1 + R)$, increases with increasing R, where d_s and d_o are the surfactant molecular length and the oil layer thickness. R = 0 corresponds to the case of pure bilayers. R is the ratio between the volume fraction of oil ϕ_o and that of surfactant ϕ_s, $R = \phi_o/\phi_s$. (*Reproduced from M. Nagao, S. Chawang and T. Hawa, Soft Matter, 2011, 7, 6598-6605 with permission from The Royal Society of Chemistry*).

Figure 7.3 (a) The *q* dependence of relaxation state (Γ) for hydrogenated and tail-contrast-matched samples at T = 65°C. The enhancement in the decay rates of the tail-contrast-matched sample corresponds to membrane thickness fluctuations. Error bars represent ± 1 SD in the entire article and are smaller than the symbol size in this figure. (*Reprinted with permission from Rana Ashkar, Michihiro Nagao, Paul D. Butler, Andrea C. Woodka, Mani K. Sen and Tadanori Koga (2015) Tuning Membrane Thickness Fluctuations in Model Lipid Bilayers. Biophysical Journal, 109(1), 106–112. Copyright 2015*). (b) A schematic illustration of the lamellar system. Addition of oil to the system swells the $C_{12}E_5$ bilayers. Since the volume fraction of surfactant is kept constant, the interlamellar distance, *d*, is constant, while the bilayer thickness, $d_m = 2d_s + d_o = 2d_s (1 + R)$, increases with increasing R, where d_s and d_o are the surfactant molecular length and the oil layer thickness. R = 0 corresponds to the case of pure bilayers. (*Reprinted with permission from Michihiro Nagao, Elizabeth G. Kelley, Rana Ashkar, et al. (2017) Probing Elastic and Viscous Properties of Phospholipid Bilayers Using Neutron Spin Echo*

Spectroscopy. J. Phys. Chem. Lett., 8, 4679-4684 Copyright (2017) American Chemical Society).

Figure 7.4 (a) A schematic of a model liquid/silica interface with a lipid bilayer and an adsorbed biopolymer. The lower panel shows profiles of the scattering length density ρ as a function of the distance z from the planar surface in the cases where the alkyl chain regions of the lipids are normal hydrogenous groups (continuous blue line) and deuterated groups (dashed red line). In both cases, the solvent is matched in scattering length density to that of the substrate. The different regions shown are (A) silicon, (B) silicon dioxide, (C) lipid head groups, (D) lipid alkyl chains, (E) adsorbed biopolymer, and (F) solvent. (*Reprinted with permission from T. Nylander, R. A. Campbell, P. Vandoolaeghe, et al. (2008) Neutron reflectometry to investigate the delivery of lipids and DNA to interfaces (Review) Biointerphases, Vol. 3, No. 2, FB64-82 Copyright (2008) AIP Publishing*). (b) (A) Functionalized single-stranded DNA (HS-ss-DNA) that adsorbs to the gold substrate through the thiol end group as well as through backbone-substrate contacts. A multitude of adsorption states exists. (B) The formation of a mercaptohexanol (MCH) monolayer that prevents contacts between the DNA backbone and the substrate, the HS-ss-DNA is left attached by the thiol end. (C) The end-tethered HS-ss-DNA is shown after hybridization to complementary oligonucleotides. (*Reprinted with permission from R. Levicky, T. M. Herne, M. J. Tarlov and S. K. Satija (1998) Using Self-Assembly To Control the Structure of DNA Monolayers on Gold: A Neutron Reflectivity Study J. Am. Chem. Soc., 120, 38, 9787-9792 Copyright (1998) American Chemical Society*).

Abbreviations

AA	Acetic Acid
ANSTO	Australian Nuclear Science and Technology Organization
BA	Butyric Acid
BenOH	Benzyl alcohol
ButOH	1-Butanol
CPP	Critical Packing Parameter
DecOH	1-Decanol
DODAB	Dioctadecyldimethylammonium Bromide
DODAC	Dioctadecyldimethylammonium Chloride
DodecOH	1-Dodecanol
DMU	Dimethyl Urea
DSC	Differential Scanning Calorimetry
FACTS	Facility for Analysis Characterisation Testing & Simulation
HA	Hexanoic Acid
HexOH	1-Hexanol
MU	Methyl Urea
OctOH	1-Octanol
PA	Propionic Acid
PhEtOH	Phenoxyethanol
POM	Polarized Optical Microscopy
SAXS	Small-Angle X-ray Scattering
SB	Sodium Butyrate
U	Urea
WAXS	Wide-Angle X-ray Scattering

Chapter 1

Introduction

This chapter outlines the applications of lamellar surfactant systems followed by the analysis of the significant limitations of contemporary surfactant systems and the opportunities for the use of additive molecules to expand applications and new avenues in this field of research. An illustrative summary of the proposed hypothesis, the objectives, and scope of this dissertation are presented based on those limitations. The outline of the thesis is briefly described, followed by the key findings, outcomes and innovative ideas of this doctoral dissertation.

1.1 Hypothesis/Problem Statement

In the present investigation, it is hypothesized that the alkyl chain fluidity and stability of a cationic double-tailed lamellar phase forming surfactant can be tuned in the presence of additives to deposit robust layers of surfactant onto surfaces. By careful phase mapping characterization of the ternary surfactant systems, a single liquid crystalline (L_α) phase can be shifted towards a two-phase region of the phase diagram by water addition and the deposition of a gel (L_β) phase can be attained (Figure 1.1).

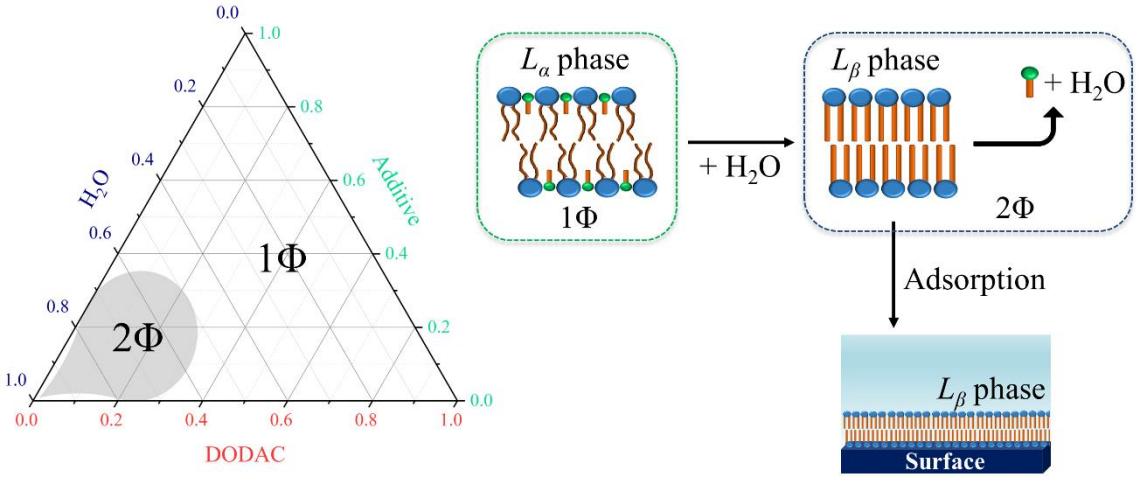

Figure 1.1 Schematic illustration of the lamellar surfactant tunability in the presence of additives. A L_α single-phase (1Φ) is attained at a lower temperature and converted to a two-phase (2Φ) region to deposit a lamellar gel phase on a surface.

One of the goals of this work is to achieve single and stable surfactant lamellar phases for hair-care applications. In order to formulate such systems, double-tailed surfactants are commonly used. However, the melting temperature (T_m) of these surfactants is generally too high for personal-care applications, which precludes their usage in such applications. This is related to the fact that a hair conditioner should display "flowability" (usually L_α phase) when used, but gel phases are preferred to deliver enhanced conditioning properties.

This work is a proof-of-concept, and hence the focus here is given to additives that can tune the T_m of the surfactant. The desired temperature value will, therefore, depend on particular applications of these surfactant systems, geographical location, etc.

With such requirements, the introduction of additives of different chemical nature would allow us to understand how the nature of these additives affects the phase behavior of the double-tailed surfactant. The location of these additives in the lamellar system can result in different packing structures, thus demonstrating their potential to tune the surfactant phase behavior [1-7].

Double-tailed surfactant systems are known to show very extensive swelling of their L_α phase and this swelling is generally controlled by electrostatic interactions. Gel phases also showed expected limitations in the surfactant miscibility. Thus while there is generally an extensive miscible regime for surfactants in liquid-like phases, the miscibility in solid-like phases such as L_β can be expected to be low [8-10]. These desirable gel phases can be used for conditioner deposition onto hair fibers without any compromise on the sensorial factor [11-14].

1.2 Objectives and Scope

This Ph.D. dissertation aims to develop ternary surfactant systems that tune the gel-to-liquid crystalline phase transition temperature which will give a single and stable gel (L_β) lamellar phase and propose a novel approach for surfactant deposition and surface modification for future hair conditioner application. This will be achieved by:

i. Understanding phase behavior and characterization of self-assembled double tailed cationic surfactant systems with bromide and chloride counterions in water;
ii. Understanding phase behavior and characterization of ternary surfactant-additive-water systems;
iii. Understanding how the aggregate structure is affected by the presence of different additives to tune and stabilize the self-assembled structure;
iv. Demonstrate the tunability of lamellar phases with water dilution;
v. Deposition and characterization of the adsorbed layer of the gel phase on surfaces.

A wide variety of experimental techniques, namely polarized optical microscopy, differential scanning calorimetry, small and wide-angle X-ray scattering and null-ellipsometry will be employed to elucidate the effects of additives on the bilayer structure and characterize the gel deposited on a surface.

1.3 Dissertation Overview

Chapter 1 provides a brief outline of the work contained within this dissertation. The goals and scope of this study are presented and essential aspects of surfactant self-assembly explained.

Chapter 2 reviews the literature concerning decisive aspects of surfactant self-assembly in water, driving forces governing the packing into different structures and phase transitions within lamellar surfactant structures. Lastly, the underlying principles for the selection of additives are presented, and the lamellar packing usefulness to hair-care applications is discussed.

Chapter 3 presents the method of formulation of surfactant systems, discusses the experimental techniques employed and the principles and methods of data analysis used in this investigation. The characterization methods with relevance to surfactant phase determination, the instrumental setup and data treatment are discussed.

Chapter 4 discusses a study of packing of lamellar phases of double-chained cationic surfactants with bromide and chloride counterions. These binary surfactant-water systems were formulated, the main phase transition temperature, and the self-assembled structure are determined. In addition, the swelling of surfactant bilayers with water is presented, and a one-dimensional swelling with chloride counterion in the gel and liquid crystalline phases is observed. The presence of interdigitated alkyl chains in the gel phase is identified.

Chapter 5 presents a series of ternary surfactant-additive-water systems and the effect of the additives on the lamellar packing structure. This chapter investigates the inclusion of "ureas", short-chain fatty acids, hydrotrope molecules, and short and intermediate-chain fatty alcohols on the main phase transition temperature, self-assembled structure, and stability in the gel and liquid crystalline phases. The results of these systems characterization and the effects on composition are discussed. The tunability of the gel-to-liquid crystalline phase transition temperature in the presence of additives is demonstrated.

Chapter 6 discusses the liquid crystalline to gel phase transition on dilution with water. This chapter presents the results of an in-situ study of surfactant gel deposition on surfaces. The effects of dilution and surfactant packing are discussed. Also, a focus on the surface deposition and modification by surfactant gel deposition are presented.

Chapter 7 presents the main conclusions and the significance of this work to the scientific community and its potential applicability. The unanswered questions from this investigation are presented, and the trends for future work in this field of research are suggested.

1.4 Innovation, Findings and Outcomes

In this Ph.D. study, effective ternary surfactant-additive-water systems were formulated, and their thermal behavior and packing structure were characterized; the gel-to-liquid crystalline phase transition with additive addition was established; their potential to hair-care applications has been demonstrated. The innovation of this work is summarized as follows:

1. Characterization of single and stable lamellar phases of cationic double-chained surfactants;
2. Investigation of the effects of additives of different polarities on the lamellar packing and the gel-to-liquid crystalline phase transition temperature decrease;
3. Demonstration of the phase tunability on dilution with water by additive removal

from the bilayers;

4. Demonstration of the potential of these surfactant systems to hair-care applications by proposing a novel approach of surfactant deposition and surface modification to deliver conditioning properties.

The key outcomes of this work are summarized as follows:

1. Single and stable lamellar surfactant phases of double-chained cationic surfactants can be prepared following an appropriate protocol;
2. The introduction of additives in the bilayer structure can tune the gel-to-liquid crystalline (L_β-L_α) phase transition temperature of the surfactant system;
3. Lamellar phase reversibility (L_α-L_β) can be attained by additive removal from the bilayer on dilution with water, and a gel phase is formed;
4. Deposition of well-defined robust layers of a gel phase on a substrate with a thickness of the order of the double surfactant molecule length has been demonstrated.

References

[1] P. Alexandridis, R. Ivanova, B. Lindman, Effect of glycols on the self-assembly of amphiphilic block copolymers in water. 2. Glycol location in the microstructure, *Langmuir* 16(8) **2000** 3676-3689.

[2] G. Montalvo, A. Khan, Self-Assembly of Mixed Ionic and Zwitterionic Amphiphiles: Associative and Dissociative Interactions between Lamellar Phases, *Langmuir* 18(22) **2002** 8330-8339.

[3] F.O. Costa-Balogh, H. Wennerstrom, L. Wadso, E. Sparr, How small polar molecules protect membrane systems against osmotic stress: The urea-water-phospholipid system, *Journal of Physical Chemistry B* 110(47) **2006** 23845-23852.

[4] A. Blanazs, S.P. Armes, A.J. Ryan, Self-Assembled Block Copolymer Aggregates: From Micelles to Vesicles and their Biological Applications, *Macromol. Rapid Commun.* 30(4-5) **2009** 267-277.

[5] E. Sparr, H. Wennerstrom, Interlamellar forces and the thermodynamic characterization of lamellar phospholipid systems, *Current Opinion in Colloid & Interface Science* 16(6) **2011** 561-567.

[6] G.A. Ferreira, W. Loh, Structural Parameters of Lamellar Phases Formed by the Self-Assembly of Dialkyldimethylammonium Bromides in Aqueous Solution, *J. Braz. Chem. Soc.* 27(2) **2016** 392-+.

[7] G.A. Ferreira, L. Piculell, W. Loh, Addition of n-Alcohols Induces a Variety of Liquid-Crystalline Structures in Surfactant-Rich Cores of Dispersed Block Copolymer/Surfactant Nanoparticles, *ACS Omega* 1(6) **2016** 1104-1113.

[8] T. Adachi, H. Takahashi, K. Ohki, I. Hatta, Interdigitated structure of phospholipid-alcohol systems studied by x-ray diffraction, *Biophysical Journal* 68(5) **1995** 1850-1855.

[9] D.J. Fairhurst, M.E. Baker, N. Shaw, S.U. Egelhaaf, Swelling and shrinking kinetics of a lamellar gel phase, *Appl. Phys. Lett.* 92(17) **2008** 3.

[10] A.K. Iwata T, Effect of the behenyl trimethyl ammonium counterion on the lamellar gel property, IFSCC Mag, **2013**, pp. 249-54.

[11] H. Kunieda, K. Shinoda, Solution behavior of dialkyldimethylammonium chloride in water. Basic properties of antistatic fabric softeners, *The Journal of Physical Chemistry* 82(15) **1978** 1710-1714.

[12] A.V. Svensson, E.S. Johnson, T. Nylander, L. Piculell, Surface Deposition and Phase Behavior of Oppositely Charged Polyion−Surfactant Ion Complexes. 2. A Means to Deliver Silicone Oil to Hydrophilic Surfaces, *ACS Appl. Mater. Interfaces* 2(1) **2010** 143-156.

[13] M. Clauzel, E.S. Johnson, T. Nylander, R.K. Panandiker, M.R. Sivik, L. Piculell, Surface Deposition and Phase Behavior of Oppositely Charged Polyion-Surfactant Ion Complexes. Delivery of Silicone Oil Emulsions to Hydrophobic and Hydrophilic Surfaces, *ACS Appl. Mater. Interfaces* 3(7) **2011** 2451-2462.

[14] D.P. Chang, M. Jankunec, J. Barauskas, F. Tiberg, T. Nylander, Adsorption of Lipid Liquid Crystalline Nanoparticles on Cationic, Hydrophilic, and Hydrophobic Surfaces, *ACS Appl. Mater. Interfaces* 4(5) **2012** 2643-2651.

Chapter 2

Literature Review

This chapter summarizes the literature available to date on the phase behavior of surfactant systems in solution. A review on the lamellar phase stability, with an emphasis on the bilayer-additive interactions is presented. This is followed by a discussion on the governing forces driving the lamellar formation and the phase transitions observed in lamellar systems. The phase behavior and stability of various complex surfactant systems are reviewed. The latest contributions in exploring their phase-rich behavior and the importance of gel phase stability are presented, with the main discussion on additive location, packing structure and adsorption on surfaces for hair-care applications.

2.1 Overview of surfactant systems

2.1.1 Amphiphilic structure of the surfactant molecule and classification

Surfactant is a term used to describe a surface active agent. These are generally amphiphilic molecules that possess both polar (nonionic, ionic, or zwitterionic) and non-polar (single/double alkyl chain) domains in their structure and as their name implied, they are well known to lower the surface tension at interfaces. Figure 2.1 shows a schematic representation of different categories of surfactants.

An exciting class of surfactants is the double-tailed surfactants due to their ability to spontaneously self-assemble into lamellar structures in aqueous solutions [1]. The charge of the polar functional group will, therefore, drive their application in different fields from biology [2], food [3], nano-science [4], consumer-care industry [5] and so many more.

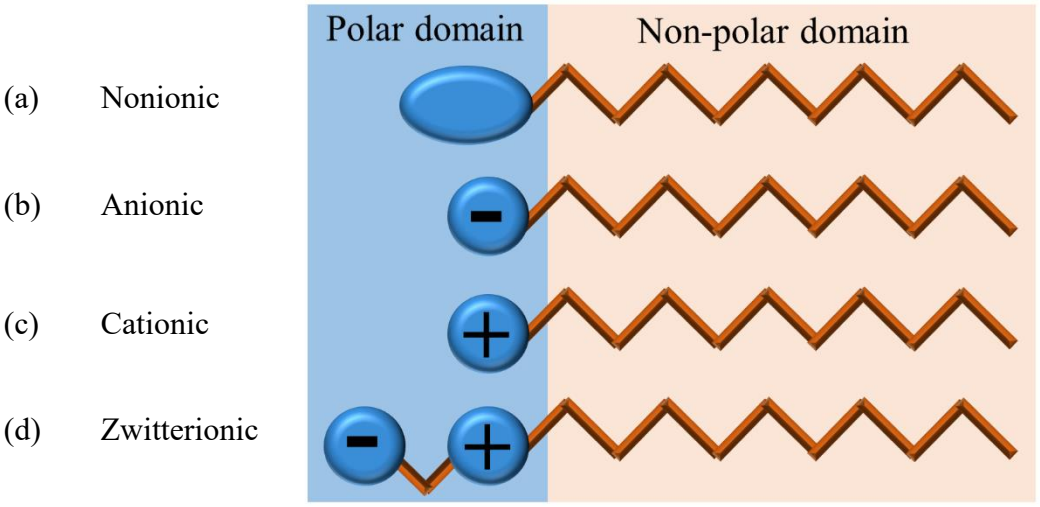

Figure 2.1 Schematic representation of the surfactant molecules. (a) Mono-tail nonionic surfactant, (b) mono-tail anionic surfactant, (c) mono-tail cationic surfactant, and (d) mono-tail zwitterionic surfactant.

2.1.2 Critical packing parameter

When in solution, a fundamental property of these species is their ability to self-aggregate. Thus, Tanford formulated one of the first theories regarding the effect of the molecular structure of the amphiphiles [6, 7] and Israelachvili investigated how that can affect the shape and size of the aggregates [8]. According to their studies, they put forward a concept of critical packing parameter (CPP) where the combination of general thermodynamic principles and geometrical packing considerations can predict the shape of the aggregate in equilibrium [6-8]. Hence, it is possible to predict a sequence of different surfactant aggregates related to its geometrical parameters. For instance, different aggregates such spherical micelles, planar bilayers, and reversed structures can be found corresponding to the various critical parameters as shown in Figure 2.2. Table 2.1 summarizes the different symbols used to describe self-assembled surfactant systems.

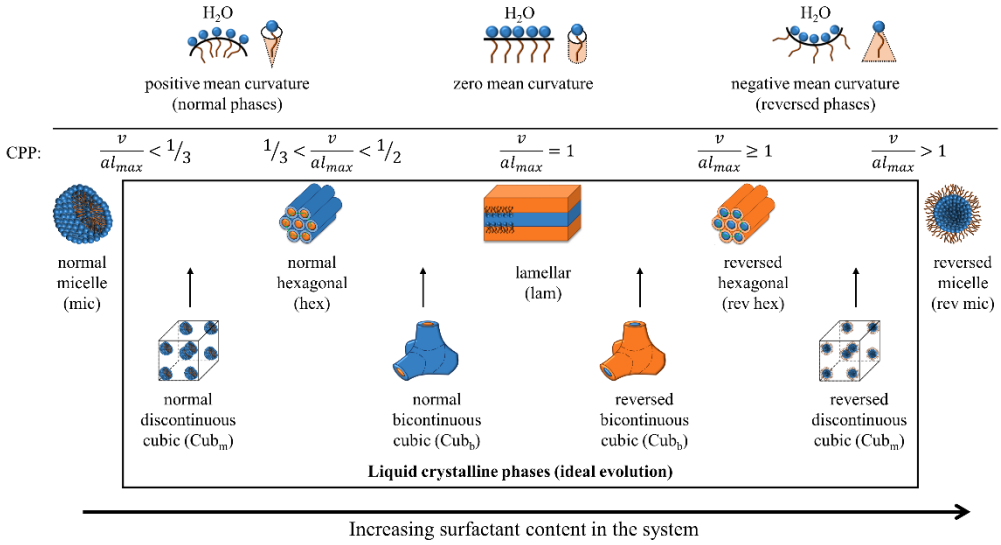

Figure 2.2 Representation of the surfactant self-assembly evolution at different values of CPP and the geometrical constraints. The box highlights the various liquid crystalline phases.

Table 2.1 Various notations for the self-assembled surfactant aggregates commonly found in the literature.

Self-assembled structure	**Notations**
Micellar	mic, L_1, S
Reversed micellar	rev mic, L_2, S
Hexagonal	hex, H_1, E, M_1, middle
Reversed hexagonal	rev hex, H_2, F, M_2
Lamellar (gel)	gel, lam L_β, L_β
Lamellar (liquid crystalline)	lam L_α, L_α
Vesicular	ves
Discrete cubic (normal micellar)	cub_m, I_1, S_{1c}
Discrete cubic (reversed micellar)	cub_m, I_2
Cubic (normal bicontinuous)	cub_b, V_1
Cubic (reversed bicontinuous)	cub_b, V_2
Sponge (reversed)	spo, L_3
Microemulsion	μem, L, S, μE

The critical packing parameter (CPP) is defined by the expression:

$$CPP = \frac{v}{a\, l_{max}} \tag{1}$$

where CPP is a dimensionless quantity, v is the volume of the alkyl chain, a is the optimal head-group area and l_{max} is the critical hydrocarbon length.

It is possible to estimate the volume of the alkyl chains of a saturated hydrocarbon chain from the expression, in cubic angstroms, [9]:

$$v = 27.4 + 26.9 n_c \tag{2}$$

where n_c corresponds to the total number of carbon atoms per saturated hydrocarbon chain. The maximum length, in angstroms, of a fully extended hydrocarbon chain can be estimated from, in angstroms, [9]:

$$l_{max} = 1.50 + 1.27 n_c \tag{3}$$

Lamellar phases with zero mean curvature

The difference between a lamellar liquid crystalline phase (L_α) and a gel phase (L_β) lies in the state of the hydrocarbon chains. In L_α phase, the hydrocarbon chains are in a melted state and in L_β phase, the chains are in a more rigid configuration. These phases consist of a stack of bilayers separated by an aqueous film (henceforth called interlamellar water), Figure 2.3. With a CPP value smaller than 0.5, amphiphiles with single hydrocarbon chains in dilute solution will form micellar aggregates at low surfactant concentration. Upon adding a second hydrocarbon chain in the molecule, the volume of the tail, v, doubles while the head-group area and the hydrocarbon length, a and l_{max}, respectively, remain relatively unchanged. Consequently, double-chained amphiphiles tend to spontaneously form bilayer structures such as vesicles and lamellar liquid crystals, whose curvatures are inherently lower than those formed by their single-chain counterparts.

The structural characteristics of these lamellar systems (often called “swelling-type”), as well as their thermodynamic characteristics, are attracting widespread interest and opened a challenging field in the study of lamellae-type systems. The presence of additives in these systems can tune the main phase transition temperature between the gel and the liquid crystalline phases.

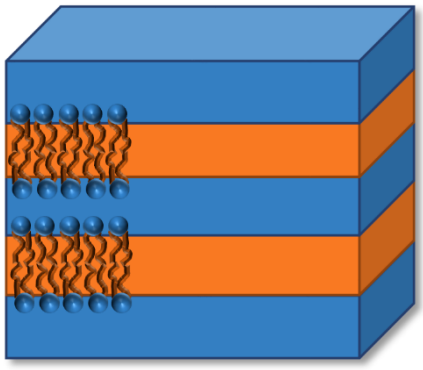

Figure 2.3 Schematic representation of a lamellar structure with the polar domain in blue color (water, water-soluble molecules, surfactant head-groups, and counterions) and the non-polar domain in orange color (hydrocarbon chains and non-polar molecules).

As mentioned before, the phase behavior of the "swelling-type" surfactants has been investigated by many researchers due to its ability to spontaneously form molecular organized aggregates, more specifically, lamellar structures. Ferreira and Loh conducted investigations on the phase behavior of these lamellar systems to look into the bilayer formation [10]. Their research was on the study of structural parameters at more concentrated regimes focusing on both L_β and L_α phases as an extension from vesicle structures studied before. No significant difference on the main phase transition temperature (T_m) of dioctadecyldimethylammonium bromide (DODAB) in water at different concentrations was found.

Dioctadecyldimethylammonium bromide and chloride

As mentioned earlier, double-tailed quaternary ammonium surfactants are potential candidates for applications that required swelling behavior as they are able to form single and stable lamellar phases across a broad range of surfactant concentrations and temperatures. This class of surfactants, in particular, cationic surfactants (often known as *quats*), has been widely used in fabric- and hair-care formulation attributed to their conditioning properties [11].

Dioctadecyldimethylammonium bromide (DODAB) and chloride (DODAC) are cationic surfactants with two 18-carbon chains covalently bonded to its head-group, Figure 2.4. The chemical structure of these surfactants makes them highly insoluble in water, and according to pure geometrical constraints (cf. above), they spontaneously self-assemble into lamellar structures [12]. The phase diagrams of these two double-tailed cationic surfactants are somewhat similar, as shown in Figure 2.5. However, a significant difference was observed. At a surfactant concentration below ≈ 33 wt. % of surfactant, DODAC showed a broad two-phase region (L+D) above the Krafft temperature. With increasing surfactant concentration a stable L_α (D) phase was found. Below this temperature, the gel phase coexisted with water. DODAB did not form a single and stable lamellar phase, only a L_α phase above the Krafft temperature, but with other metastable structures coexisting.

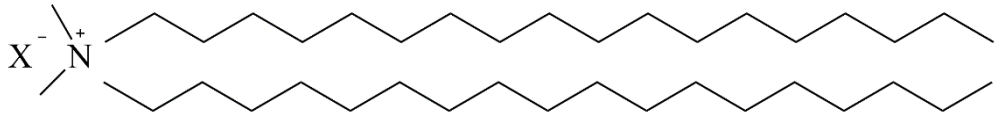

Figure 2.4 Chemical structure of a quaternary ammonium double-tailed cationic amphiphile (swelling-type). X^- : anion as counterion, bromide (Br) or chloride (Cl).

(a) (b)

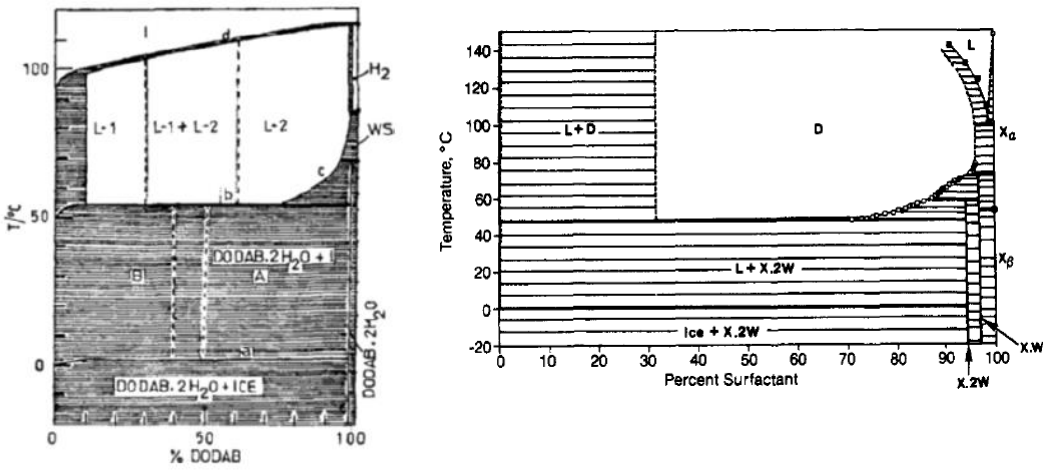

Figure 2.5 (a) Phase diagram of the DODAB-water binary system. a: water melting points, b: crystals to lamellar mesophase transition, c: border between mesophase and mesophase + solid biphase region, d: mesophase to isotropic liquid transition. L-1 and L-2: proposed two different lamellar mesophases, H-2: reversed hexagonal phase, WS: waxy solid, I: isotropic liquid, A: crystal paste, B: crystals immersed in continuous isotropic liquid (*Reprinted with permission from P. C. Schulz, J. L. Rodríguez, F. A. Soltero-Martínez et al (1998) Phase behaviour of the dioctadecyldimethylammonium bromide-water system. Journal of Thermal Analysis and Calorimetry, 51, 49–62. Copyright 1998*) [13]. (b) Phase diagram of the DODAC-water binary system. X_α and X_β: two dry crystals, XW: monohydrate crystal, X2W: dihydrate crystal, L: water, D: lamellar. (*Reprinted with permission from Laughlin, R.G., Munyon, R.L., Fu, Y.C. and Fehl, A.J. (1990) Physical science of the dioctadecyldimethylammonium chloride—water system. 1. Equilibrium phase behavior. Journal of Physical Chemistry, 94, 2546–2552. Copyright 1990, American Chemical Society*) [14].

In 1978, Kunieda and Shinoda reported the first phase study of the DODAC in water and showed the formation of a lamellar phase. A careful analysis of the results showed that it is possible to determine the amount of hydrated water and its optimum hydrophile-lipophile balance. The combination of those two factors and driven by insolubility, these

amphiphiles can adsorb on surfaces, such as fabric and hair fibers, efficiently, resulting in the softening and conditioning effect [11]. In the 1990s, Laughlin et al. developed a more extensive study based on phase behavior [14], kinetics [15] and colloidal stability [16] of this particular binary surfactant-water system. In this investigation of the DODAC in solution, an extensive lamellar phase region from around 31.5 wt. % to 95 wt. % above the Krafft temperature was observed, as illustrated in the phase diagram in Figure 2.5 (b). Furthermore, an unusually fast hydration of the dry crystals driven by heating the monohydrate crystal was observed. Last but not the least, a gel-like state by heating solutions of the monohydrate crystal was detected propelling more studies of micro-emulsion formation and phase behavior of shorter homologs [17].

Goto et al. have addressed the bilayer phase behavior of DODAB and DODAC in water under hydrostatic pressure. Different sample preparation methods showed the presence of different metastable phases in the vesicular systems. Besides, the study of the gel-to-liquid (L_β-L_α) phase transition temperature (T_m) found that those transitions occurred around 45 ^oC and 40 ^oC for DODAB and DODAC, respectively, for concentrations from 1 to 10 mM [18, 19].

Although double-tailed surfactant systems were actively studied [18-30] and their phase behavior suggested a broad single and stable region, which in theory, would be optimal to take up large amounts of water. So far, no research has been done regarding the counterion and co-surfactant/additive effects in their structural properties. As a result, it is crucial to carry out a thermodynamic study, complemented by phase characterization to revise and compare the studies carried out before. From literature, it was clear there is a lack in understanding characterization of the DODAC lamellar systems, whereas the DODAB-water system was densely characterized and understood.

2.2 Lamellar packing

2.2.1 Swelling, hydration and inter- and intra-lamellar forces

This study focuses on planar lamellar structures, so therefore, other self-assembled lamellar structures with positive or negative mean curvature will not be considered in this discussion.

The lamellar surfactant packing consists of periodically distributed bilayers of alkyl chains (non-polar domain) with layers of water (polar domain), as previously shown in Figure 2.3. Planar lamellar surfactant phases, both ionic and nonionic, are expected to display extensive swelling behavior. This phenomenon occurs naturally, and it can also be enhanced by the addition of polar or non-polar compounds to the system, which leads to swelling of the different domains of the lamellar structure. In the case of ionic surfactants, the swelling is driven by the osmotic pressure of counterion, as described by the Derjaguin, Landau, Verwey and Overbeek (DLVO) theory [31]. Generally, beyond this maximum swelling, the remaining water present in the system exists as an excess water phase. Nonetheless, the repulsive forces from electric double layer repulsion are the driving force for the swelling of lamellar phases formed by ionic surfactants. It has been shown that a careful selection of additives added to the bilayer structure can tune the electrostatics of the head-groups and therefore control the lamellar swelling [32-34]. It is noteworthy that the swelling potential of the L_β phase is different and usually lower than the L_α phase. On the one hand, the "solid-like" state of the alkyl chains of a gel phase do not facilitate the swelling of the gel. On the other hand, at higher temperatures (with the surfactant in the L_α phase), there is higher mobility of the counterions which increases the osmotic pressure of the excess water phase thus enhance the swelling of the liquid crystalline phase [35].

The head-groups of a surfactant gel phase typically pack in a hexagonal array [36]. This arrangement allows the hydrocarbon chains to acquire rotational movement, which prevents the chain crystallization. When the alkyl chains experience a closer packing, the surfactant head-groups arrange in an orthorhombic packing, as presented in Figure 2.6. Stronger hydrophobic chain-to-chain interactions stabilize this geometry, but it inhibits the

free rotation of the alkyl chains, thus leading to crystallization of the gel phase. This thermodynamically more stable gel phase is called the coagel (L_c) phase and should be prevented in order to achieve a stable gel phase.

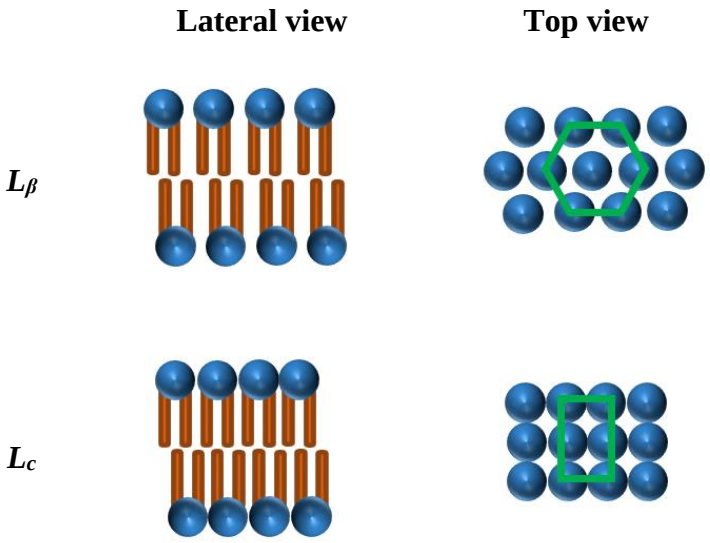

Figure 2.6 Schematic representation of the gel (L_β) and coagel (L_c) phases from different perspectives. The surfactant molecules adopt a hexagonal packing in the L_β phase which allows alkyl chain rotations; and an orthorhombic packing in the L_c phase which does not allow alkyl chain rotation.

2.2.2 Advantages and importance of a lamellar gel phase

Gel phases are the structural packing unit of many formulations in consumer-care products attributed to its packing structure which is capable of incorporating polar and non-polar compounds, and their rheological properties arising from the rigidity of the bilayers. This kinetically stable gel phase has allowed to increase the storage time (shelf-life) of formulations, even though they are not thermodynamically stable.

Many parameters are taken into consideration when developing a formulation with a specific purpose. For instance, one can consider the texture, the stability at different temperatures and the performance. Therefore the underlying interactions of these multi-component systems must be adequately understood. Briefly, among several advantages of gel formulations, Iwata has highlighted five key vectors to its usage in current consumer-care products: i) rich and creamy texture at low amphiphile concentration ($\leq$ 5 wt. %); ii) enhanced tactile properties irrespective the low concentration of oily components; iii) displays a slippery behavior attributed to its shear-thinning rheological property; iv) cost-effective due to the low concentration of the formulation components; and v) kinetically stable and capable of solubilizing molecules with different chemical properties, such as polar, non-polar or insoluble [36].

2.2.3 Stability of a lamellar gel phase

Single-component planar lamellar surfactant systems are, in general, morphologically more stable when compared to curved bilayer structures. This is also dependent on the energy cost of bending the surfactant surface [1]. During the L_α–L_β phase transition, the formation of a coagel (cf. above) or other stable and metastable gel phases can occur. However, amphiphiles in various gel phases essentially behave like a hydrated 2-D solid. Figure 2.7 shows different gel structures that can be formed to accommodate possible mismatches between the area per surfactant head-group and the cross-section area of the alkyl chains,

which ultimately resulted in tilted or interdigitated alkyl chains, or rippled surfaces [9, 37-39].

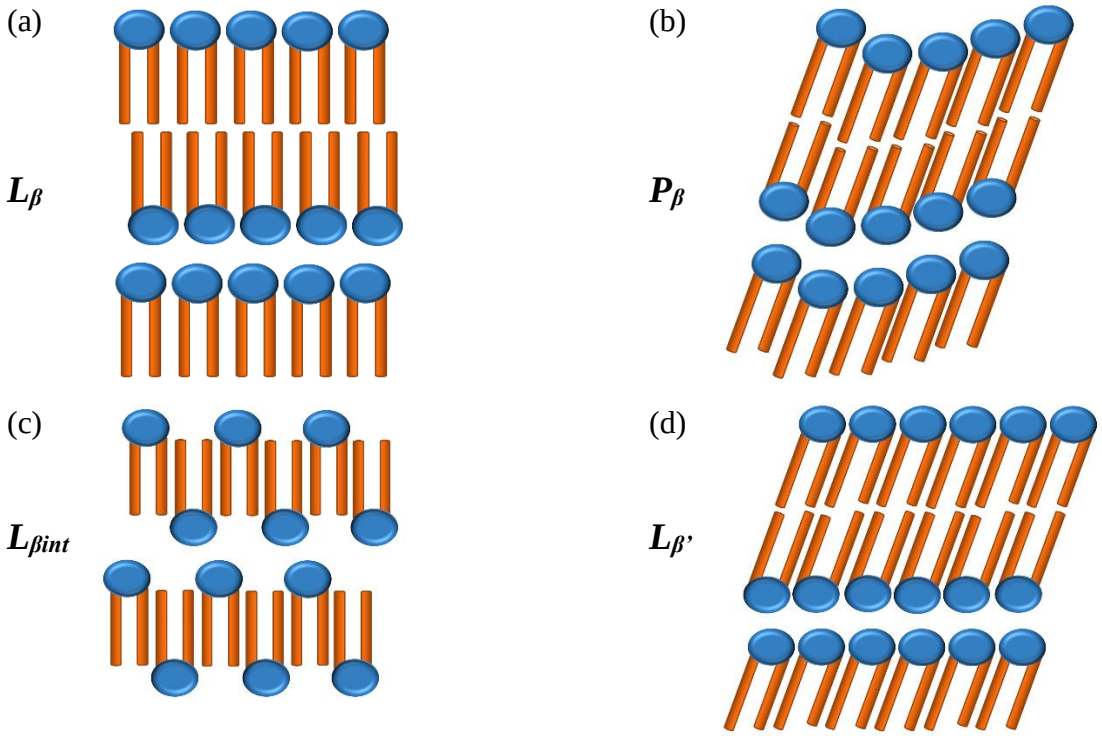

Figure 2.7 Various structures of bilayers in the gel phase. (a) Gel phase, L_β; (b) Rippled gel phase, P_β; (c) Interdigitated gel phase, $L_{\beta int}$; (d) Tilted gel phase, $L_{\beta'}$.

As discussed above, a gel phase can show several "irregularities", and it is important to discuss what are the factors contributing to the instability of a L_β phase.

The hexagonally packed lamellar structure, L_β phase, is not thermodynamically stable; instead, it is kinetically stable. Surfactant molecules have a tendency to adopt an orthorhombic packing, with alkyl chains closely packed, with no rotation, thus forming a coagel phase. However, the prevention of closely packed alkyl chains or the maintenance of a stable gel phase in a hexagonal packing will stop the formation of a coagel phase by allowing the hydrocarbon chains to rotate freely. An investigation of lamellar gels composed of long aliphatic alcohols showed that they adopted an orthorhombic packing with a density slightly higher than water. As a consequence, the coagel phase sank and displaced the interlamellar water out from the lamellar structure [40]. To prevent the coagel

phase formation, one may add other amphiphilic molecules to inhibit the alkyl chains of the surfactant to pack closer. Another mechanism could be to increase the stability of the gel phase by decreasing the kinetics of the L_c-L_β phase transition, or even suppress it. In other words, create a kinetically stable L_β phase.

The control of the flux of water that goes in and out of the water domain of the lamellar structure is a way to control and improve the gel stability. It has been reported that the gel phase stability is tightly related to the formulation protocol, more specifically, the thermal treatment/history. When the surfactant undergoes the L_α-L_β phase transition, it moves from a "fluid-like" phase to a phase with less "flowability" and deformation capacity. Ideally, all the water added to the formulation should remain as interlamellar water. However, an excess water phase coexisting with the gel phase is commonly found. An advantage of using ionic amphiphiles to formulate planar lamellar structures lies on the existence of counterions in the system. These counterions are the key to an ionic gradient that drives the water from the excess water phase to the interlamellar water. Such movement of water ultimately results in thicker interlamellar water layers and corresponds to the increase in viscosity [41]. Therefore, the optimization of the L_α-L_β phase transition is pivotal for the formation of a stable gel phase. Eccleston proposed a protocol which consisted of intense mixing of the melted amphiphiles followed by a slow cool down process to maximize the incorporation of excess water to the interlamellar water domain [42].

To formulate a stable L_β phase, one should carefully design the laboratory protocol, and could also add molecules that, ideally, suppress the formation of a coagel phase. Another parameter to take into consideration is the equilibration of the lamellar surfactant system after the inclusion of an additive. The polarity of the additive will dictate the best protocol to follow. It has been suggested that to mix a non-polar molecule to a lamellar system, the system should be melted first (above the surfactant melting temperature) and mix the additive while keeping the system in the melted state. This step potentiates the formation of a single-phase mixture. Only then, the hot water should be added to the mixture, followed by a slow cooling down of the temperature to allow equilibrium of the molecules partitioning [36].

2.3 Additives in the lamellar structure

2.3.1 Structure and functionality

2.3.1.1 Small polar additives

Lamellar self-assembled structures have been intensively investigated for many years. These lamellar structures are easily obtained by surfactant, polymer and block copolymer systems as demonstrated in many investigations [43-51]. However, in this dissertation, the discussion will focus on the lamellar systems composed by the surfactants in water. In some cases, the addition of a third compound to the lamellar surfactant structure in water may increase the stability of the gel phase.

The chemical structure of the additive allows us to estimate its location when added to the bilayer and the possible impacts on the lamellar stability. Researchers have been working on synthetic surfactants in the vesicular and lamellar phases because these surfactant systems are expected to be not only reliable models of the biological membrane but also used as drug carriers [51-53] attributed to their resemblance to bio-membranes, especially 1,2-dimyristoyl-s*n*-glycero-3-phosphatidylcholine (DMPC), the main constituent of the lipid membrane.

For a long time, the presence of small water-soluble additives in lamellae-type systems has been investigated, focusing on lipid-protein systems that self-assembled into lamellar structures [54-57] due to its importance creating a synthetic model for the study of the biological membrane. These studies suggested that small polar substances with low vapor pressure, such as urea, glycerol, betaine, and sugars could affect the molecular mobility of those lipid bilayers. Due to the polarity of these additives, they are mainly distributed in the aqueous regions, triggering an increase in the lipid alkyl chain mobility. Costa-Balong et al. demonstrated that replacing water by urea with a fixed surfactant concentration had a negligible effect on the interlamellar spacing (d-spacing), but an increased lamellar swelling with varying surfactant/water ratio was observed (Figure 2.8). The authors

suggested that the addition of these small molecules could reduce osmotic stress and thus reducing system dehydration. Interestingly, a preferred location of the urea molecule at the polar/non-polar interface was determined, that can be explained by the zwitterionic nature of the surfactant used in their study.

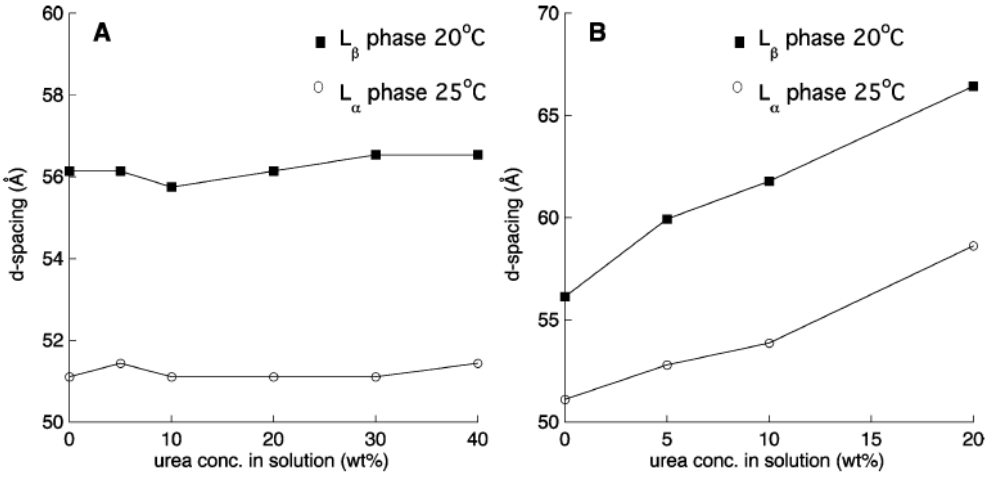

Figure 2.8 Variations in the lamellar repeat distance with the composition of the urea-water solutions in systems with limited access to the solvent: L_β phase, 20 °C (■) and L_α phase, 25 °C (○). (A) The effect of water replacement by urea: The composition of the water-urea solution was varied, and the lipid composition in all samples was kept at 80 wt % (i.e., 20 wt % water-urea solution). (B) The effect of urea addition to a lipid-water system: The composition of the water-urea solution was varied, and the lipid-water ratio remained the same in all samples. In the sample with no urea, the composition was 80 wt % lipid and 20 wt % water. Urea was then added in different proportions to this mixture. (*Reprinted with permission from Fátima O. Costa-Balogh, Håkan Wennerström, Lars Wadsö, et al (2006) How Small Polar Molecules Protect Membrane Systems against Osmotic Stress: The Urea−Water−Phospholipid System. The Journal of Physical Chemistry B, 110, 23845-23852 Copyright 2006, American Chemical Society*) [54].

A different study has also demonstrated the increasing polarity of the solvent solution when urea was added to the system. These increased polarities rely on stronger electrostatic interactions along with stronger hydrophobic interactions. As a result, an increase in the dielectric permittivity of the urea with water molecules was observed [58].

Hence, Sparr and Wennerström reported a thorough discussion on the thermodynamic characterization of the isothermal swelling of the lamellar-lipid system allowed to conclude that this mechanism was entropy-driven. The central equation in this regard is the definition of Gibbs free energy, ΔG:

$$\Delta G = \Delta H - T\Delta S \quad (4)$$

where ΔH stands for the variation in enthalpy, T is the absolute temperature, and ΔS is the variation in entropy. In this study, it was observed that free energy had an opposite sign with respect to enthalpy, thus determining an entropically driven swelling process. Another exciting highlight in these studies was the formation of lamellar structures in other polar solvents than water [59-61].

From the interpretation of the phase diagram in Figure 2.9, it is possible to realize that the availability of solvent drives both swelling and phase transition of the surfactant system. Analyzing, mainly, Figure 2.9 (a) is possible to conclude that the addition of urea induced a single L_α phase at higher water amounts. Souza et al. have shown the water-urea mixture results in a more polar medium leading to stronger electrostatic and hydrophobic interactions. Moreover, it was also denoted that the phase swelling is more long-ranged in the L_α phase rather than in the L_β phase [55].

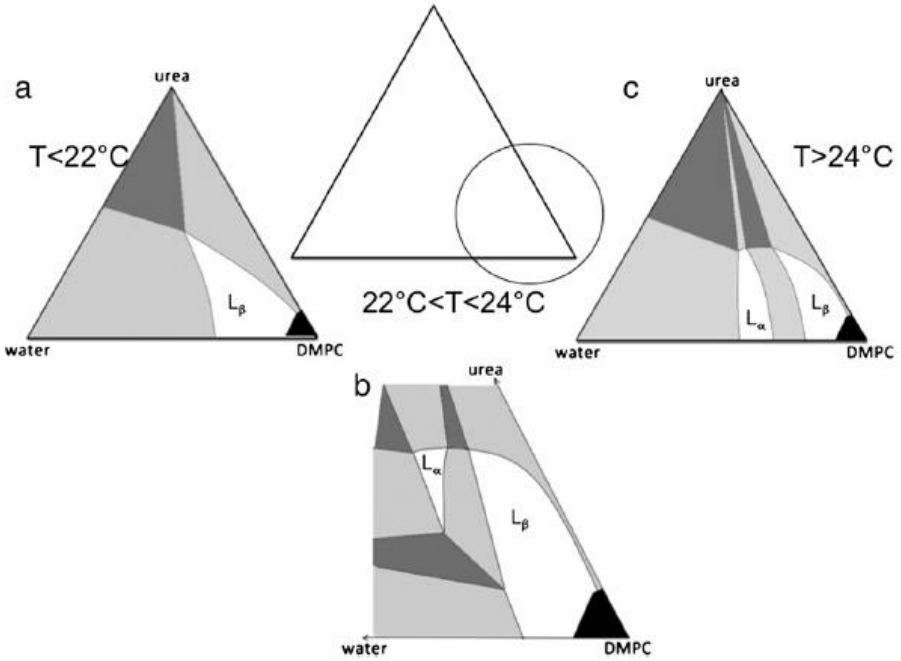

Figure 2.9 Schematic phase diagram of the ternary DMPC-urea-water system at different temperatures. The phase diagrams contain three-phase triangles (dark grey), two-phase regions (light grey) and one-phase regions (white). (a) T<22 ºC; (b) 22 ºC<T<24 ºC; (c) T>24 ºC. *(Reprinted with permission from Emma Sparr and Håkan Wennerström (2011) Interlamellar forces and the thermodynamic characterization of lamellar phospholipid systems. Current Opinion in Colloid & Interface Science, 16, 561–567. Copyright 2011)* [55].

Furthermore, it was also demonstrated that the amount of solvent, urea, or glycerol solution available was responsible for determining the extent of the lamellar swelling. Consequently, the presence of these polar compounds promoted a larger swelling of the L_α phase compared to the L_β phase [54].

Another molecule that had an effect on the lamellar stability is cholesterol, and its presence resulted in the formation of distinct lamellar structures. Maulik and Shipley have investigated the interaction of M-palmitoyl sphingomyelin with cholesterol and dipalmitoylphosphatidylcholine (DPPC) and the effects on the lamellar hydration [62]. The authors demonstrated that increasing amounts of cholesterol tuned the bilayer fluidity showing a progressive decrease in enthalpy associated with the phase transition. In addition, a decrease of the bilayer thickness of the L_β phase and a slight increase of bilayer thickness in the L_α phase was observed with cholesterol. More importantly, it was suggested that

cholesterol affected the inter-bilayer forces leading to a small reduction of the hydration layer thickness. More recently, Tanasescu and Zumbuehl et al. designed intricate bilayer structures in the presence of cholesterol, which prevented the formation of chain interdigitation and induced a L_α phase formation [63].

2.3.1.2 Fatty acids and fatty alcohols

In the discussion presented on the stability of lamellar structures, the addition of long-tailed molecules to prevent the formation of a coagel phase was suggested. There is vast amount of literature on those studies and researchers have investigated the formation of lamellar surfactant systems in the presence of fatty alcohols and its acids counterparts.

Kanicky and Shah have investigated how long-chained fatty acids behave by varying the length and saturation of the hydrocarbon chain and the effect on the pK_a [64]. This is an essential parameter because one may expect different self-assembled structures based on the electrostatics between surfactant head-groups. Full saturated alkyl chains were found to pack closely, and the introduction of several steric constraints by *cis* double bonds prevented a closer packing of the alkyl chains, Figure 2.10 [64]. This work provided further evidence that one can prevent the formation of a coagel phase, thus stabilizing the gel phase, by adding a long-chained fatty acid with a certain degree of chain unsaturation. The surfactant/fatty-acid ratio is another parameter to take into consideration to yield a stable lamellar phase. It has been demonstrated that lamellar phases are initially formed, but the system can evolve to isotropic phases (reversed L_3 phase, often called sponge phase) increasing the concentration of fatty-acid or the temperature [65, 66].

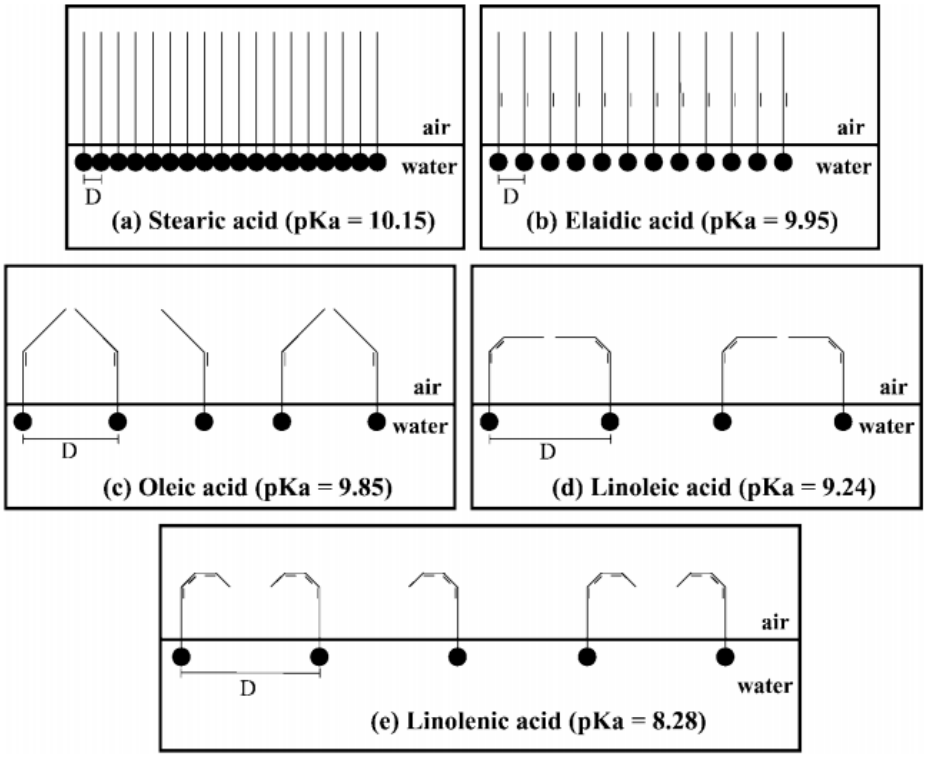

Figure 2.10 Schematic representation of C18 fatty acid monolayers at the air/water interface. Note the effect of the degree of unsaturation on the area per molecule and the intermolecular distance, D, in the spread monolayers. (*Reprinted with permission from James R. Kanicky, Dinesh O. Shah (2002) Effect of Degree, Type, and Position of Unsaturation on the pKa of Long-Chain Fatty Acids. Journal of Colloid and Interface Science, 256, 201–207. Copyright 2002*) [64].

Maldonado et al. investigated a mixed nonionic/ionic surfactant system in the presence of a short-chain fatty alcohol, hexanol [67]. Here, the authors observed the formation of an isotropic phase, a sponge phase. Also, the increase of ionic surfactant concentration in the system led to thickening of the bilayers, which the authors assumed that both lamellar and sponge phases were composed of the same bilayers, however, oriented with different curvature [67, 68].

Rowe worked on the effects of alcohols on phosphatidylethanolamines (PEs) and phosphatidylcholines (PCs) [69]. In this study, methanol, ethanol, and propanol were evaluated focusing on the gel-to-liquid crystalline phase transition temperature. In the presence of high alcohol concentrations (irrespective of the alcohol), the PCs phase

transitions were not thermodynamically reversible; instead, a two-phase region developed, and it was attributed to the formation of an interdigitated gel phase.

Lei and Safinya et al. investigated an intricate quaternary surfactant system composed of sodium dodecyl sulfate (SDS), water, pentanol, and dodecane [70]. This work evaluated the effects of addition of an alcohol molecule, but also a pure 12-carbon chain oil, dodecane, to the packing structure of the quaternary system. This mixture formed a sponge phase which is in the vicinity of a liquid crystalline phase. A L_3 phase displays a negative curvature towards the oil phase, thus forcing the surfactant to pack in a way that infinite bilayers of SDS separated by dodecane oil channels were determined. Here, the short-chain alcohol was used to stabilize the SDS into a liquid crystalline structure, and the addition of oil led to the development of a L_3 phase.

Usma, Renamayor, and Pacios have demonstrated the behavior of an ionic liquid lamellar phase in the presence of decanol [71]. A large liquid crystalline phase at different compositions and temperatures was found. However, at high temperatures, the lamellar phase was reported to be not stable, possibly due to the increased hydrophobicity of decanol, which resulted in a decanol-rich phase. The phase transition observed with increasing temperatures shows the versatility of decanol when added to a lamellar system to tune the phase behavior.

Ferreira, Piculell, and Loh investigated the phase behavior of a block copolymer/surfactant system with the addition of alcohols of different polarities [72]. In particular, the effects of octanol and decanol on the packing structure were studied. At varying the concentration of the different compounds, a broad series of kinetically stable liquid crystalline phases was formed as shown in Figure 2.11. The alcohols used in this investigation acted as co-surfactants, which tuned the CPP value and therefore allowed the formation of structures with different curvature. Also, excess amounts of octanol, acting as a co-solvent, stabilized the reversed structures.

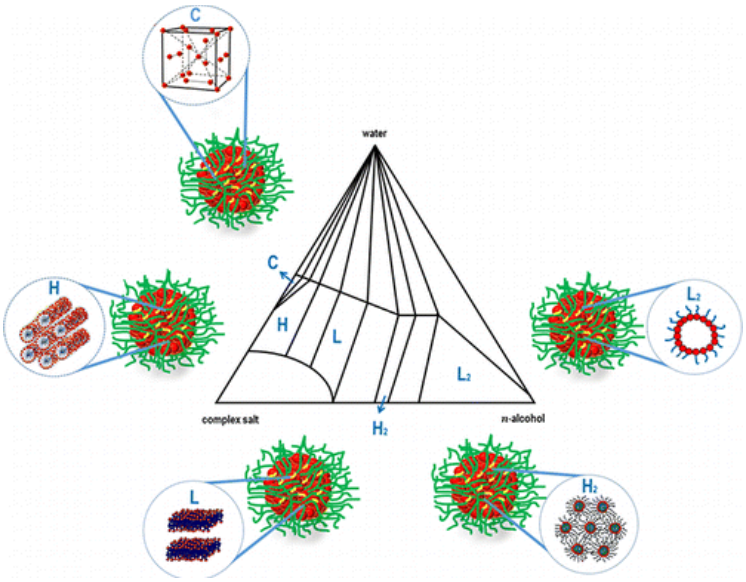

Figure 2.11 Partial phase diagram of the poly(acrylamide)-b-complex salts-water-n-alcohols. The phase diagram shows the various liquid crystalline structures found at different mixture compositions. (*Reprinted with permission from Guilherme A. Ferreira, Lennard Piculell and Watson Loh (2016) Addition of n-Alcohols Induces a Variety of Liquid-Crystalline Structures in Surfactant-Rich Cores of Dispersed Block Copolymer/Surfactant Nanoparticles. ACS Omega, 1, 1104-1113 Copyright 2016, American Chemical Society*) [72].

Early this year, Guo et al. have reported the effects of the presence of short-chain fatty alcohol in microbial membranes and discussed it in terms of bilayer interdigitation and bilayer disorder, Figure 2.12 [73]. The authors noted that a butanol/amphiphile ratio of 2:1 did not compromise the lamellar integrity and swelled the bilayer from full interdigitation to a 20 % thicker bilayer. Although this study focused on physiological temperatures, butanol only caused partial interdigitation of the bilayers attributed to its accumulation at the amphiphile head-group region. Furthermore, the response of the bilayer to butanol was attributed to multiple vectors, inter alia, partial interdigitation, and bilayer disorder. The inclusion of this short-chain fatty alcohol led to bilayer fluidization and, consequently, bilayer disorder.

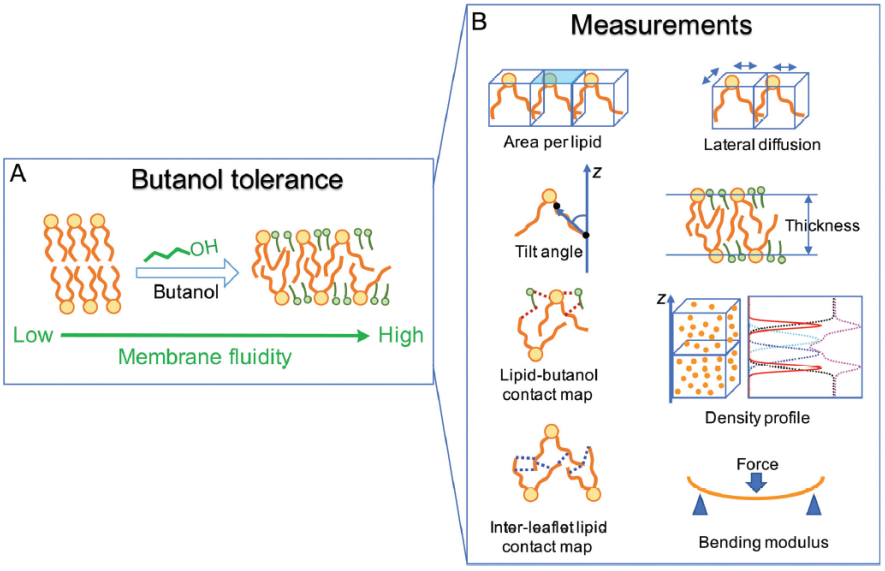

Figure 2.12 Schematic representation of the effect of the addition of butanol to the bilayer. (A) Illustration of the location of butanol in the membrane. (B) Summary of the parameters measured in this investigation. (*Reproduced from J. Guo, J. C. S. Ho, H. Chin, A. E. Mark, C. Zhou, S. Kjelleberg, B. Liedberg, A. N. Parikh, N. Cho, J. Hinks, Y. Mu and T. Seviour, Phys. Chem. Chem. Phys., 2019, 21, 11903 with permission from the PCCP Owner Societies*) [73].

The effects of additives in the lamellar packing of surfactant systems have been studied using different methods. However, the majority of those investigations were performed on zwitterionic surfactant systems and, most commonly, in a very dilute regime. Therefore, a deep understanding of the response of planar lamellar structures made up from an ionic double-tailed surfactant to additives seems to be currently lacking in the literature. This dissertation aims to focus on cationic surfactant systems which display conditioning properties in different areas of research, such as personal care and laundry. Moreover, those investigations discussed above opened the "door" not only for the study of the thermodynamic behavior and structural characterization of cationic surfactant systems in the presence of additives but also to the swelling potential with water and the gel-to-liquid crystalline phase transition tunability.

2.4 Surfactant adsorption at solid-liquid interfaces

Surfactant systems have been deposited onto different substrates to provide desirable properties. Depending on the application, a suitable surfactant should be selected. Many applications rely on the deposition of surfactant layers onto surfaces for a particular property such as the conditioning of fibers [9, 11, 31, 36, 74]. Ideally, the deposition of the surfactant is expected to occur in the gel phase since this structure would result in robust layers deposited on the fibers and should remain stable at the interface. The studies to be discussed demonstrated that the deposition of surfactant/polymer and surfactant systems on surfaces is possible and different deposition conditions may result in different structures. Therefore, researchers have dedicated their effort to this topic.

Kundu et al. studied the Langmuir monolayers deposition of a saturated fatty acid with an 18-carbon tail on silica in the presence of a divalent counterion to understand the growth of the films. Initially, an asymmetric monolayer with the surfactant head-groups at the water interface and the hydrophobic tails facing the air was deposited. The formation of islands of symmetrically aligned amphiphiles on top of a monolayer of asymmetrical amphiphiles was detected suggesting that the geometry of the surfactant deposited was pressure-dependent [75]. On a different investigation, Kundo deposited a polyelectrolyte-surfactant complex and studied the structure and morphology of the deposited aggregated at different amphiphile concentrations. The results showed that the morphology is dependent on the polyelectrolyte used. For instance, DNA-surfactant complexes deposited in a multilayered lamellar structure, whereas carboxymethyl cellulose-surfactant aggregates formed coil-like structures, Figure 2.13. These investigations highlighted that the structure of the deposited aggregate depended not only on the surfactant/polyelectrolyte-surface interactions but also the inter-aggregate interactions [76].

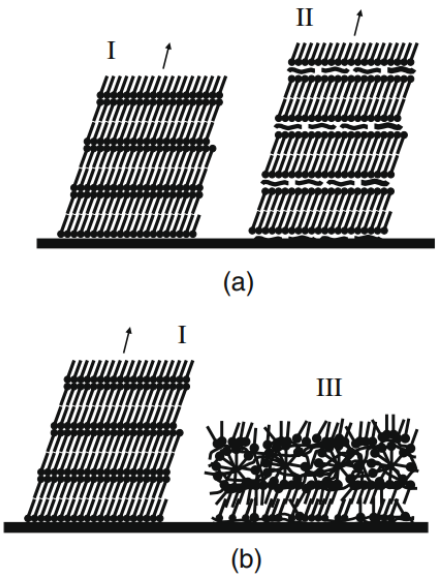

Figure 2.13 Schematic representation of the aggregates deposited on the silicon substrate. (a) Deposited layered structures of dodecyltrimethylammonium bromide (DTAB) (I) and DNA-DTAB complexes. (b) Deposited aggregates of DTAB (I) and coil-like aggregates deposited by carboxymethyl cellulose-DTAB complexes. (*Reprinted with permission from Sarathi Kundu (2010) Polyelectrolyte–surfactant complexes on solid surface. Journal of Colloid and Interface Science, 344, 547–555. Copyright 2010*) [76].

Nylander and Lindman et al. conducted a series of studies on the formation of polyelectrolyte-surfactant complexes on surfaces [77]. The focus of their investigations were on the kinetic aspects of deposition and the reversibility phenomenon of the adsorption. Research has shown that the structure of the deposited aggregate was dependent on several factors such as the chemical composition of the solution (polymers, surfactants, electrolytes, and pH) and the bulk solution phase behavior. For instance, the adsorption of polyelectrolyte systems, which are widely used in consumer-care applications, showed to be partially reversible and this is attributed to its strong affinity to the interface that in turn slowed down the adsorption process. Mixed surfactant-polymer systems demonstrated to be strongly dependent on the phase diagram. An example is a system composed of a negatively charged surfactant and a positively charged polymer, and associative phase separation occurs which is not desirable in formulations, Figure 2.14. To overcome this problem, the addition of electrolytes is used and this can result in three possibilities : i) at low salt amounts, the association of the polyelectrolyte and surfactant occurred; ii) at intermediate salt amounts, the miscibility of the two phases is observed due to self-

screening effect (usually in presence of excess of the surfactant); iii) at high salt amounts, a segregative phase separation happens with micelles to one phase and the polymers to the other (typical of nonionic surfactant systems) [77].

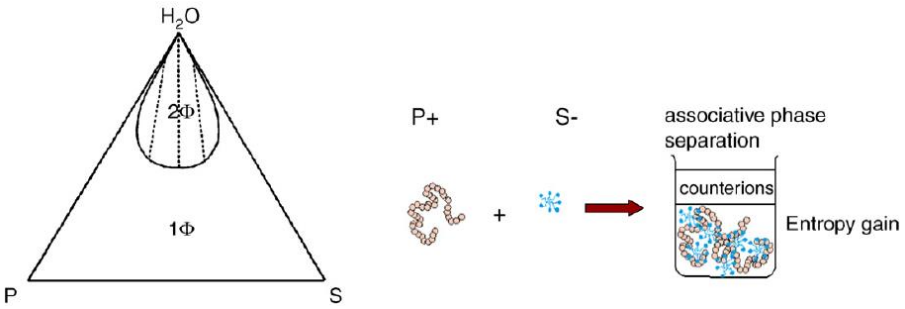

Figure 2.14 Schematic ternary phase diagram showing an associative phase separation. The one-phase region and the two-phase region are labelled with 1Φ and 2Φ, respectively. On the right hand of the image, the polyelectrolyte–surfactant association is schematically depicted. (*Reprinted with permission from Tommy Nylander, Yulia Samoshina and Björn Lindman (2006) Formation of polyelectrolyte–surfactant complexes on surfaces. Advances in Colloid and Interface Science, 123-126, 105–123. Copyright 2006*) [77].

Tonigold and Nylander et al. used ellipsometry to characterize inhomogeneities on deposited mixed polymer-surfactant complexes onto surfaces [78]. This work showed that the sample preparation method and surface cleaning could influence the ellipsometry results. Different aggregated particles in bulk solution resulted in inhomogeneous patches at the interface, which in turn culminated in fluctuating ellipsometry signal. The authors suggested that first spontaneous adsorption to the surface occurs, and given some time, the smaller aggregates fused into larger ones. This process was found to be affected by pH since it changes the charge density. Most importantly, the evidence of the presence of structures in the bulk solution should be considered to evaluate the structures deposited on the surface.

Svensson et al. investigated the deposition from the oil phase to hydrophilic surfaces [79], and Clauzel et al. performed a similar investigation but also on hydrophobic surfaces [80]. In the first study, the authors highlighted the effects of using a hydrophobically modified polymer which determined the solubility of the complex, found to be the driving force for adsorption [79]. The latter work, two protocols were evaluated: i) a titration experiment, where increasing amounts of surfactant were added to bulk poly-ion solution; ii) the adsorption from a bulk solution followed by a rinsing cycle with water. The results did not show significant differences of deposition on the hydrophilic and hydrophobic silica surface and agreed with previously reported results that pointed to low adsorption with increasing hydrophobicity of the poly-ion. This was attributed to the disappearance of the two-phase region, in the phase diagram, needed for deposition of the complex on dilution. Interestingly, selective adsorption from surfactant at hydrophobized silica was detected, and not observed at hydrophilic silica. Figure 2.15 shows the co-adsorption of the cationic polymer at the hydrophilic silica, a result of the non-selective adsorption [80].

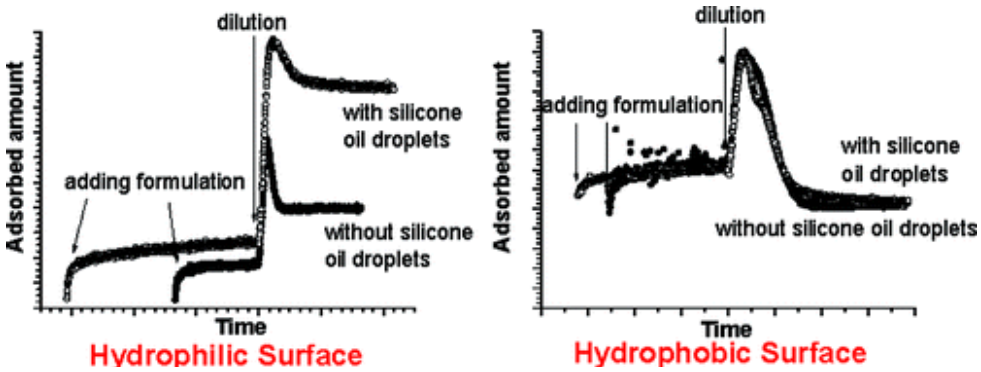

Figure 2.15 Adsorbed amount from surfactant at hydrophilic and hydrophobic surfaces. (*Reprinted with permission from Maryline Clauzel, Eric S. Johnson, Tommy Nylander, Rajan K. Panandiker, Mark R. Sivik, Lennart Piculell (2011) Surface Deposition and Phase Behavior of Oppositely Charged Polyion-Surfactant Ion Complexes. Delivery of Silicone Oil Emulsions to Hydrophobic and Hydrophilic Surfaces. ACS Applied Materials and Interfaces, 3, 2451–2462 Copyright 2011, American Chemical Society*) [80].

2.5 Ph.D. in the Context of Literature

The continuous progress of new consumer-care products and the enhancement of existing formulations enabled the use of surfactant-based systems to a wide range of applications. Complex polymer-surfactant systems were synthesized to deliver conditioning properties, but the hair-care industry had to also address other aspects relating to the stability of the formulations. Investigations on simpler systems, such as double-tailed ionic surfactants are lacking in literature. This is partially because of their limited applicability due to their high gel-to-liquid phase transition temperature (T_m). In Chapter 4, the phase behavior of two "swelling-type" cationic surfactants in water was studied using polarized optical microscopy (POM), small and wide-angle X-ray scattering (SAXS/WAXS) and differential scanning calorimetry (DSC), and the stability of the lamellar aggregates and their swelling is presented.

Though there are studies conducted on the effect of additives to tune the self-assembled structures of surfactants as discussed in the previous sections, systematic investigation on the effects of additives on the packing of lamellar structures is still required. Efforts should be directed to planar lamellar structures and how additives with different chemical nature tune the T_m of the surfactant without compromising the lamellar integrity. In particular, a transition from a stable gel (L_β) phase to a stable liquid crystalline (L_α) phase. Ternary surfactant-water-additive systems were studied, and the stability of the lamellar phases is investigated in Chapter 5. Additives were added to the lamellar systems to disturb the gel packing and induce the lowering of the T_m, resulting in ternary systems that display a tunable T_m. The location of the additives and the packing structure of these ternary surfactant systems were also studied using POM, SAXS/WAXS, and DSC to elucidate the mechanism of action.

The tunability of lamellar phases in the presence of additives has been demonstrated, and stable L_β and L_α phases determined. It is pivotal to demonstrate that lamellar cationic surfactant systems can be adsorbed onto surfaces. In Chapter 6, L_α phases are converted to L_β phases and deposited on a substrate. By means of time-resolved ellipsometry and

synchrotron SAXS/WAXS, the adsorption process was followed. Irreversible adsorption of robust layers of pure surfactant in the gel phase has been achieved by careful selection of the additives that are dissociated from the bilayers with water. These results have demonstrated a new principle of surfactant deposition and surface modification by tuning the gel-to-liquid crystalline phase transition temperature of lamellar surfactant systems with water-soluble additives.

References

[1] E.F. Marques, B.F.B. Silva, Surfactant Self-Assembly, in: T. Tadros (Ed.), *Encyclopedia of Colloid and Interface Science*, *Springer Berlin Heidelberg*, Berlin, Heidelberg, 2013, pp. 1202-1241.

[2] M. Kepczynski, T. Rog, Functionalized lipids and surfactants for specific applications, *Biochim. Biophys. Acta-Biomembr.* 1858(10) **2016** 2362-2379.

[3] M.A. Bos, T. van Vliet, Interfacial rheological properties of adsorbed protein layers and surfactants: a review, *Adv. Colloid Interface Sci.* 91(3) **2001** 437-471.

[4] M.E. Ali, M. Ullah, A. Maamor, S.B. Abd Hamid, Surfactant Assisted Ball Milling: A Simple Top down Approach for the Synthesis of Controlled Structure Nanoparticle, in: M.H. Mamat, Z. Khusaimi, S.A. Bakar, A.M. Nor, T. Soga, M.R. Mahmood (Eds.), *Nanoscience, Nanotechnology and Nanoengineering*2014, pp. 356-361.

[5] T. Tadros, R. Izquierdo, J. Esquena, C. Solans, Formation and stability of nano-emulsions, *Adv. Colloid Interface Sci.* 108 **2004** 303-318.

[6] C. Tanford, The hydrophobic effect : formation of micelles and biological membranes, New York : Wiley, [1973]1973.

[7] C. Tanford, Micelle shape and size, *Journal of Physical Chemistry* 76(21) **1972** 3020-&.

[8] J.N. Israelachvili, D.J. Mitchell, B.W. Ninham, Theory of self-assembly of hydrocarbon amphiphiles into micelles and bilayers, *Journal of the Chemical Society-Faraday Transactions Ii* 72 **1976** 1525-1568.

[9] D.F. Evans, H. Wennerström, The colloidal domain : where physics, chemistry, biology, and technology meet, 2nd ed. ed., New York : Wiley-VCH, 1999.1999.

[10] G.A. Ferreira, W. Loh, Structural Parameters of Lamellar Phases Formed by the Self-Assembly of Dialkyldimethylammonium Bromides in Aqueous Solution, *J. Braz. Chem. Soc.* 27(2) **2016** 392-+.

[11] H. Kunieda, K. Shinoda, Solution behavior of dialkyldimethylammonium chloride in water. Basic properties of antistatic fabric softeners, *The Journal of Physical Chemistry* 82(15) **1978** 1710-1714.

[12] A.K. Eduardo F. Marques, Björn Lindman, A calorimetric study of the gel-to-liquid crystal transition in catanionic surfactant vesicles, *Thermochimica Acta* **2002** 31–37.

[13] P.C. Schulz, J.L. Rodriguez, F.A. Soltero-Martinez, J.E. Puig, Z.E. Proverbio, Phase behaviour of the dioctadecyldimethylammonium bromide water system, *J. Therm. Anal. Calorim.* 51(1) **1998** 49-62.

[14] R.G. Laughlin, R.L. Munyon, Y.C. Fu, A.J. Fehl, Physical Science of the Dioctadecyldimethylammonium Chloride Water-System. 1. Equilibrium Phase-Behavior, *Journal of Physical Chemistry* 94(6) **1990** 2546-2552.

[15] R.G. Laughlin, R.L. Munyon, Y.C. Fu, T.J. Emge, Physical science of the dioctadecyldimethylammonium chloride-water system. 2. Kinetic and mechanistic aspects, *Journal of Physical Chemistry* 95(9) **1991** 3852-3856.

[16] R.G. Laughlin, R.L. Munyon, J.L. Burns, T.W. Coffindaffer, Y. Talmon, Physical science of the dioctadecyldimethylammonium chloride-water system. 3. Colloidal aspects, *The Journal of Physical Chemistry* 96(1) **1992** 374-383.

[17] J. Yang, G. Rong, S.E. Friberg, Temporary phase-behavior of a system containing di(hydrogenated tallowalkyl) dimethyl ammonium chloride-water-hexane, *J. Dispersion Sci. Technol.* 16(6) **1995** 469-493.

[18] M. Goto, S. Ishida, Y. Ito, N. Tamai, H. Matsuki, S. Kaneshina, Thermotropic and Barotropic Phase Transitions of Dialkyldimethylammonium Bromide Bilayer Membranes: Effect of Chain Length, *Langmuir* 27(10) **2011** 5824-5831.

[19] M. Goto, Y. Ito, S. Ishida, N. Tamai, H. Matsuki, S. Kaneshina, Hydrostatic Pressure Reveals Bilayer Phase Behavior of Dioctadecyldimethylammonium Bromide and Chloride, *Langmuir* 27(5) **2011** 1592-1598.

[20] M. Dubois, T. Zemb, Phase-behavior and scattering of double-chain surfactants in diluted aqueous-solutions, *Langmuir* 7(7) **1991** 1352-1360.

[21] A.M. Carmona-Ribeiro, B.R. Midmore, Surface potential in charged synthetic amphiphile vesicles, *The Journal of Physical Chemistry* 96(8) **1992** 3542-3547.

[22] L.R. Tsuruta, A.M. Carmona-Ribeiro, Counterion Effects on Colloid Stability of Cationic Vesicles and Bilayer-Covered Polystyrene Microspheres, *The Journal of Physical Chemistry* 100(17) **1996** 7130-7134.

[23] E. Feitosa, W. Brown, Fragment and Vesicle Structures in Sonicated Dispersions of Dioctadecyldimethylammonium Bromide, *Langmuir* 13(18) **1997** 4810-4816.

[24] E. Feitosa, P.C.A. Barreleiro, G. Olofsson, Phase transition in dioctadecyldimethylammonium bromide and chloride vesicles prepared by different methods, *Chem. Phys. Lipids* 105(2) **2000** 201-213.

[25] E.F. Marques, O. Regev, A. Khan, B. Lindman, Self-organization of double-chained and pseudodouble-chained surfactants: counterion and geometry effects, *Adv. Colloid Interface Sci.* 100 **2003** 83-104.

[26] E. Feitosa, P.C.A. Barreleiro, The effect of ionic strength on the structural organization of dioctadecyldimethylammonium bromide in aqueous solution, *Surface and Colloid Science*, *Springer Berlin Heidelberg*, Berlin, Heidelberg, 2004, pp. 163-168.

[27] E. Feitosa, G. Karlsson, K. Edwards, Unilamellar vesicles obtained by simply mixing dioctadecyldimethylammonium chloride and bromide with water, *Chem. Phys. Lipids* 140(1–2) **2006** 66-74.

[28] E. Feitosa, F.R. Alves, The role of counterion on the thermotropic phase behavior of DODAB and DODAC vesicles, *Chem. Phys. Lipids* 156(1–2) **2008** 13-16.

[29] A. Lopes, K. Edwards, E. Feitosa, Extruded vesicles of dioctadecyldimethylammonium bromide and chloride investigated by light scattering and cryogenic transmission electron microscopy, *Journal of Colloid and Interface Science* 322(2) **2008** 582-588.

[30] F.R. Alves, W. Loh, Vesicles prepared with the complex salts dioctadecyldimethylammonium polyacrylates, *Journal of Colloid and Interface Science* 368(1) **2012** 292-300.

[31] B. Kronberg, K. Holmberg, B. Lindman, Surface chemistry of surfactants and polymers, Chichester, West Sussex, United Kingdom : Wiley, 2014.2014.

[32] T. Adachi, H. Takahashi, K. Ohki, I. Hatta, Interdigitated structure of phospholipid-alcohol systems studied by x-ray diffraction, *Biophysical Journal* 68(5) **1995** 1850-1855.

[33] D.J. Fairhurst, M.E. Baker, N. Shaw, S.U. Egelhaaf, Swelling and shrinking kinetics of a lamellar gel phase, *Appl. Phys. Lett.* 92(17) **2008** 3.

[34] A.K. Iwata T, Effect of the behenyl trimethyl ammonium counterion on the lamellar gel property, IFSCC Mag, **2013**, pp. 249-54.

[35] G.M. Eccleston, Functions of mixed emulsifiers and emulsifying waxes in dermatological lotions and creams, *Colloids and Surfaces A: Physicochemical and Engineering Aspects* 123-124 **1997** 169-182.

[36] T. Iwata, Chapter 25 - Lamellar Gel Network, *Cosmetic Science and Technology*, *Elsevier*, Amsterdam, 2017, pp. 415-447.

[37] E. Evans, D. Needham, Physical properties of surfactant bilayer membranes: thermal transitions, elasticity, rigidity, cohesion and colloidal interactions, *The Journal of Physical Chemistry* 91(16) **1987** 4219-4228.

[38] K. Akabori, J.F. Nagle, Structure of the DMPC lipid bilayer ripple phase, *Soft Matter* 11(5) **2015** 918-926.

[39] M. Kranenburg, B. Smit, Phase Behavior of Model Lipid Bilayers, *The Journal of Physical Chemistry B* 109(14) **2005** 6553-6563.

[40] S. Fukushima, M. Yamaguchi, The effect of cetostearyl alcohol in cosmetic emulsions, *Cosmetics & Toiletries* 98(5) **1983** 89-&.

[41] G.M. Eccleston, M.K. Behan-Martin, G.R. Jones, E. Towns-Andrews, Synchrotron X-ray investigations into the lamellar gel phase formed in pharmaceutical creams prepared with cetrimide and fatty alcohols, *Int. J. Pharm.* 203(1-2) **2000** 127-139.

[42] E.G. M, The microstructure and properties of fluid and semisolid lotions and creams, IFSCC Mag, **2010**, pp. 167-74.

[43] L. Piculell, Understanding and Exploiting the Phase Behavior of Mixtures of Oppositely Charged Polymers and Surfactants in Water, *Langmuir* 29(33) **2013** 10313-10329.

[44] P. Alexandridis, T.A. Hatton, Poly(ethylene oxide)-poly(propylene oxide)-poly(ethylene oxide) block-copolymer surfactants in aqueous-solutions and at interfaces - Thermodynamics, structure, dynamics, and modeling, *Colloid Surf. A-Physicochem. Eng. Asp.* 96(1-2) **1995** 1-46.

[45] P. Alexandridis, U. Olsson, B. Lindman, Self-Assembly of Amphiphilic Block-Copolymers - The (EO)(13)(PO)(30)(EO)(13)-Water-P-Xylene System, *Macromolecules* 28(23) **1995** 7700-7710.

[46] P. Alexandridis, Poly(ethylene oxide) poly(propylene oxide) block copolymer surfactants, *Current Opinion in Colloid & Interface Science* 2(5) **1997** 478-489.

[47] P. Alexandridis, U. Olsson, B. Lindman, Structural polymorphism of amphiphilic copolymers: Six lyotropic liquid crystalline and two solution phases in a poly(oxybutylene)-b-poly(oxyethylene)-water-xylene system, *Langmuir* 13(1) **1997** 23-34.

[48] P. Holmqvist, P. Alexandridis, B. Lindman, Modification of the microstructure in poloxamer block copolymer-water-"oil" systems by varying the "oil" type, *Macromolecules* 30(22) **1997** 6788-6797.

[49] P. Alexandridis, R. Ivanova, B. Lindman, Effect of glycols on the self-assembly of amphiphilic block copolymers in water. 2. Glycol location in the microstructure, *Langmuir* 16(8) **2000** 3676-3689.

[50] A. Blanazs, S.P. Armes, A.J. Ryan, Self-Assembled Block Copolymer Aggregates: From Micelles to Vesicles and their Biological Applications, *Macromol. Rapid Commun.* 30(4-5) **2009** 267-277.

[51] M.A.C. Stuart, W.T.S. Huck, J. Genzer, M. Muller, C. Ober, M. Stamm, G.B. Sukhorukov, I. Szleifer, V.V. Tsukruk, M. Urban, F. Winnik, S. Zauscher, I. Luzinov, S. Minko, Emerging applications of stimuli-responsive polymer materials, *Nat. Mater.* 9(2) **2010** 101-113.

[52] A. Blanazs, S.P. Armes, A.J. Ryan, Self-Assembled Block Copolymer Aggregates: From Micelles to Vesicles and their Biological Applications, *Macromol. Rapid Commun.* 30(4-5) **2009** 267-277.

[53] S.P. Hong, P.R. Leroueil, E.K. Janus, J.L. Peters, M.M. Kober, M.T. Islam, B.G. Orr, J.R. Baker, M.M.B. Holl, Interaction of polycationic polymers with supported lipid

bilayers and cells: Nanoscale hole formation and enhanced membrane permeability, *Bioconjugate Chem.* 17(3) **2006** 728-734.

[54] F.O. Costa-Balogh, H. Wennerstrom, L. Wadso, E. Sparr, How small polar molecules protect membrane systems against osmotic stress: The urea-water-phospholipid system, *Journal of Physical Chemistry B* 110(47) **2006** 23845-23852.

[55] E. Sparr, H. Wennerstrom, Interlamellar forces and the thermodynamic characterization of lamellar phospholipid systems, *Current Opinion in Colloid & Interface Science* 16(6) **2011** 561-567.

[56] A. Nowacka, S. Douezan, L. Wadso, D. Topgaard, E. Sparr, Small polar molecules like glycerol and urea can preserve the fluidity of lipid bilayers under dry conditions, *Soft Matter* 8(5) **2012** 1482-1491.

[57] S. Bjorklund, J.M. Andersson, Q.D. Pham, A. Nowacka, D. Topgaard, E. Sparr, Stratum corneum molecular mobility in the presence of natural moisturizers, *Soft Matter* 10(25) **2014** 4535-4546.

[58] S.M.B. Souza, E.B. Alvarez, M.J. Politi, Effect of Urea on Surfactant Aggregates: A Comprehensive Review, *Recent Trends in Surface and Colloid Science* 12 **2012** 155-169.

[59] R.V. McDaniel, T.J. McIntosh, S.A. Simon, Nonelectrolyte substitution for water in phosphatidylcholine bilayers, *Biochimica et Biophysica Acta (BBA) - Biomembranes* 731(1) **1983** 97-108.

[60] P.K. Persson, B.A. Bergenståhl, Repulsive forces in lecithin glycol lamellar phases, *Biophysical Journal* 47(5) **1985** 743-746.

[61] W. Patrick Williams, P.J. Quinn, L.I. Tsonev, R.D. Koynova, The effects of glycerol on the phase behaviour of hydrated distearoylphosphatidylethanolamine and its possible relation to the mode of action of cryoprotectants, *Biochimica et Biophysica Acta (BBA) - Biomembranes* 1062(2) **1991** 123-132.

[62] P.R. Maulik, G.G. Shipley, N-Palmitoyl Sphingomyelin Bilayers: Structure and Interactions with Cholesterol and Dipalmitoylphosphatidylcholine, *Biochemistry* 35(24) **1996** 8025-8034.

[63] R. Tanasescu, M.A. Lanz, D. Mueller, S. Tassler, T. Ishikawa, R. Reiter, G. Brezesinski, A. Zumbuehl, Vesicle Origami and the Influence of Cholesterol on Lipid Packing, *Langmuir* 32(19) **2016** 4896-4903.

[64] J.R. Kanicky, D.O. Shah, Effect of Degree, Type, and Position of Unsaturation on the pKa of Long-Chain Fatty Acids, *Journal of Colloid and Interface Science* 256(1) **2002** 201-207.

[65] S.S. Funari, G. Rapp, F. Richter, Double-bilayer: a new phase formed by lysophospholipids and the corresponding fatty acid, *Quim. Nova* 32(4) **2009** 908-912.

[66] R.A. Gonçalves, B. Lindman, M.G. Miguel, T. Iwata, Y.M. Lam, Elucidating the effect of additives on the alkyl chain packing of a double tail cationic surfactant, *Journal of Colloid and Interface Science* 528 **2018** 400-409.

[67] A. Maldonado, R. Ober, T. Gulik-Krzywicki, W. Urbach, D. Langevin, The sponge phase of a mixed surfactant system, *Journal of Colloid and Interface Science* 308(2) **2007** 485-490.

[68] H.F. Mahjoub, K.M. McGrath, M. Kleman, Phase transition induced by shearing of a sponge phase, *Langmuir* 12(13) **1996** 3131-3138.

[69] E.S. Rowe, Thermodynamic reversibility of phase transitions. Specific effects of alcohols on phosphatidylcholines, *Biochim. Biophys. Acta* 813(2) **1985** 321-330.

[70] N. Lei, C.R. Safinya, D. Roux, K.S. Liang, Synchrotron x-ray-scattering studies on the sodium dodecyl sulfate-water-pentanol-dodecane L-3 sponge phase, *Phys. Rev. E* 56(1) **1997** 608-613.

[71] C.L. Usma, C.S. Renamayor, I.E. Pacios, Structural behavior of the lamellar mesophase formed by ternary mixtures of a two-tailed ionic liquid, 1-decanol and water, *Colloids and Surfaces A: Physicochemical and Engineering Aspects* 509 **2016** 174-181.

[72] G.A. Ferreira, L. Piculell, W. Loh, Addition of n-Alcohols Induces a Variety of Liquid-Crystalline Structures in Surfactant-Rich Cores of Dispersed Block Copolymer/Surfactant Nanoparticles, *ACS Omega* 1(6) **2016** 1104-1113.

[73] J. Guo, J.C.S. Ho, H. Chin, A.E. Mark, C. Zhou, S. Kjelleberg, B. Liedberg, A.N. Parikh, N.-J. Cho, J. Hinks, Y. Mu, T. Seviour, Response of microbial membranes to butanol: interdigitation vs. disorder, *Physical Chemistry Chemical Physics* 21(22) **2019** 11903-11915.

[74] J.N. Israelachvili, Chapter 14 - Electrostatic Forces between Surfaces in Liquids, in: J.N. Israelachvili (Ed.), *Intermolecular and Surface Forces (Third Edition)*, *Academic Press*, San Diego, 2011, pp. 291-340.

[75] S. Kundu, A. Datta, S. Hazra, Growth of a collapsing Langmuir monolayer, *Phys. Rev. E* 73(5) **2006** 7.

[76] S. Kundu, Polyelectrolyte-surfactant complexes on solid surface, *Journal of Colloid and Interface Science* 344(2) **2010** 547-555.

[77] T. Nylander, Y. Samoshina, B. Lindman, Formation of polyelectrolyte-surfactant complexes on surfaces, *Adv. Colloid Interface Sci.* 123 **2006** 105-123.

[78] K. Tonigold, I. Varga, T. Nylander, R.A. Campbell, Effects of Aggregates on Mixed Adsorption Layers of Poly(ethylene imine) and Sodium Dodecyl Sulfate at the Air/Liquid Interface, *Langmuir* 25(7) **2009** 4036-4046.

[79] A.V. Svensson, E.S. Johnson, T. Nylander, L. Piculell, Surface Deposition and Phase Behavior of Oppositely Charged Polyion−Surfactant Ion Complexes. 2. A Means to Deliver Silicone Oil to Hydrophilic Surfaces, *ACS Appl. Mater. Interfaces* 2(1) **2010** 143-156.

[80] M. Clauzel, E.S. Johnson, T. Nylander, R.K. Panandiker, M.R. Sivik, L. Piculell, Surface Deposition and Phase Behavior of Oppositely Charged Polyion-Surfactant Ion Complexes. Delivery of Silicone Oil Emulsions to Hydrophobic and Hydrophilic Surfaces, *ACS Appl. Mater. Interfaces* 3(7) **2011** 2451-2462.

Chapter 3

Experimental Methodology

This chapter describes the rationale for this Ph.D. project and provides an overview of the experimental procedures, including the selection of materials, method of sample preparation, characterization techniques and data processing. The careful selection of the surfactants and the additives used in the formulations is explained, followed by details of the sample formulation. The surfactant system characterization was performed using various techniques, such as optical microscopy for birefringence studies, differential scanning calorimetry for thermally induced phase-transition investigations, laboratory-based and synchrotron small and wide-angle X-ray scattering for structural analysis and ellipsometry for surface analysis. The fundamentals, instrumental configuration and data treatment and processing of each technique are expounded.

3.1 Rationale for selection

In this Ph.D. project, it is proposed that the alkyl chain fluidity and stability of a cationic double-tailed lamellar surfactant can be tuned in the presence of additives to deposit robust layers of surfactant onto surfaces. Systems of positively charged polymers (two-in-one shampoo) have been successfully used owing to the electrostatic interactions that helps them interact favorably with negatively charged surfaces. However, similar studies on double-tailed cationic surfactants seem to be lacking in the literature. From the investigation of the stability of the lamellar phases, it has been found that the weak stability of the gel phase arises from its inherent low solubility in water and the rigidity of the bilayers, which ultimately results in a kinetically stable phase. Despite being the key to increase the "shelf-time" of formulations, this phase is not thermodynamically stable.

Double-chained surfactants are known to show a significant swelling of their liquid crystalline phase, which is generally governed by electrostatic interactions. Also, gel phases are enticing in industrial formulations because they are robust and can be used as conditioning agents once adsorbed onto fibers of different nature.

In the first section of this project, the phase behavior of cationic double-tailed surfactants with bromide and chloride in water was investigated. These surfactant systems allow to infer the swelling with water and the lamellar stability at different surfactant concentrations. The selection of these two surfactants is based on two considerations: the surfactant geometry and head-group charge. Double-tailed surfactants spontaneously self-assemble into lamellar structures [1], which allow us to formulate lamellar phases at low surfactant concentration, and the charged head-groups provide the system with electrostatics, thus driving the swelling phenomenon.

The second section focuses on the study of the effects of additives on the lamellar packing and stability based on their location and interactions with the surfactant bilayer. Small polar molecules, hydrotrope molecules and aliphatic alcohols/acids were added

to the bilayer to tune the main phase transition temperature. By studying the additives with varying chemical characteristics, the underlying interactions with the bilayer can be elucidated and their effect on bilayer stability clarified.

In the third section of this work, a rinsing experiment was employed for the liquid crystalline phases to study the liquid crystalline-to-gel phase shift and subsequent gel phase adsorption on a surface upon dilution. The ternary surfactant systems were formulated with water-soluble additives that could be removed with water. Therefore, the resulting gel phases can be effectively deposited, and the layer thickness and adsorbed amount of surfactant on a surface can be determined.

3.2 Materials

Dioctadecyldimethylammonium chloride (DODAC, 96.7 % purity) was supplied by Evonik Corporation, USA. Dioctadecyldimethylammonium bromide (DODAB, 98.0 % purity), urea, 1-methyl urea, 1,3-dimethyl urea and sodium butyrate were purchased from Tokyo Chemical Industry Co., Ltd., Japan. Acetic acid, propionic acid, butyric acid, hexanoic acid, 1-butanol, 1-hexanol, 1-octanol, 1-decanol and 1-dodecanol were purchased from Sigma-Aldrich, Singapore. Benzyl alcohol was supplied by Ineos Chlorotoluenes, Belgium, and phenoxyethanol supplied by Clariant Produkte GmbH, Germany. The physico-chemical properties of these compounds (Figure 3.1) are summarized in Table 3.1, and they were used as received. Ultrapure water of 18 S/m conductivity was used to prepare the samples.

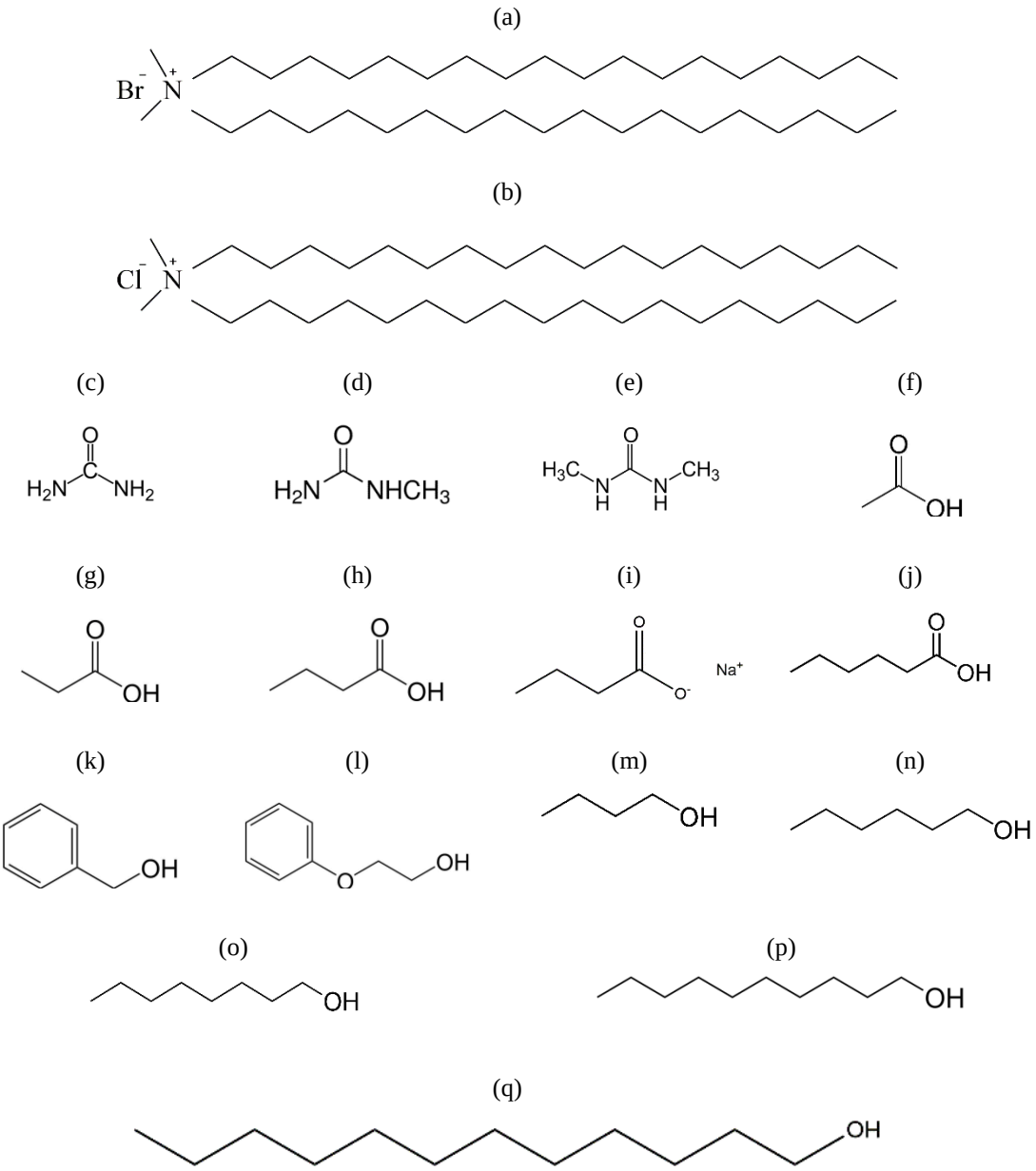

Figure 3.1 Molecular structure of: (a) dioctadecyldimethylammonium bromide – DODAB, (b) dioctadecyldimethylammonium chloride – DODAC, (c) urea – U, (d) methyl urea – MU, (e) dimethyl urea – DMU, (f) acetic acid – AA, (g) propionic acid – PA, (h) butyric acid – BA, (i) sodium butyrate – SB, (j) hexanoic acid – HA, (k) benzyl alcohol – BenOH, (l) phenoxyethanol – PhEtOH, (m) butanol – ButOH, (n) hexanol – HexOH, (o) octanol – OctOH, (p) decanol – DecOH, and (q) dodecanol – DodecOH.

Table 3.1 Physico-chemical characteristic properties of the compounds. Molar mass, melting point, boiling point, density and logarithm of the octanol/water partition coefficient. The data are taken from [2].

Compound	MM ($g\ mol^{-1}$)	Density ($g\ cm^{-3}$)	Melting point (^oC)	Boiling point (^oC)	Log *P*
Water	18.02	0.998	0.0	100.0	-
DODAB	630.97	0.840	157.2	-	3.80
DODAC	586.64	0.840	70.0	-	3.80
Urea	60.06	1.323	132.4	-	-2.11
Methyl urea	74.08	1.204	101.3	-	-1.40
Dimethyl urea	88.11	1.142	106.0	269.0	-0.49
Acetic acid	60.06	1.045	17.0	117.9	-0.17
Propionic acid	74.08	0.988	-20.5	141.5	0.33
Butyric acid	88.11	0.953	-5.1	163.7	0.79
Sodium butyrate	110.09	0.960	253.0	-	0.79
Hexanoic acid	116.16	0.927	-3.0	204.0	1.92
Benzyl alcohol	108.14	1.045	-16.0	203.0	1.05
Phenoxyethanol	138.16	1.110	11.8	245.5	1.13
Butanol	74.12	0.810	-90.0	116.0	0.84
Hexanol	102.17	0.814	-52.0	156.0	2.03
Octanol	130.23	0.827	-15.0	196.0	3.07
Decanol	158.28	0.829	5.0	231.0	4.57
Dodecanol	186.34	0.833	22.0	260.0	5.13

3.3 Sample preparation

Binary DODAB and DODAC mixtures were prepared by adding water to the surfactant. The method consisted of melting the surfactant at a temperature above T_m and then adding hot water (≈ 80°C), as described in [3]. The mixing was performed inside 20 mL transparent screw-cap glass vials. Due to the possible formation of different self-assembled structures or even the occurrence of phase separation, the sample preparation procedure takes an essential step for the success of the experiments. Therefore, vortex mixing was used to homogenize the mixture considering the possible formation of vesicles by sonication technique [4-6]. A slow cooling down protocol was employed to maximize the incorporation of water from the bulk water into the interlamellar water domain, as suggested in [7, 8]. The vials were kept inside a thermostated water bath (Julabo F25-ME) at a slow cooling down rate of 1 °C min^{-1} until it reached 25 °C. All the samples were equilibrated at room temperature for at least seven days before characterization.

Ternary DODAC-water-additive mixtures were prepared with a fixed surfactant concentration of 35 wt. % corresponding to a pure lamellar phase with no water coexistence, according to the DODAC-water phase diagram [9, 10]. The samples were prepared with concentrations of additive ranging from 1.3 to 20.0 % in weight. Sample homogeneity was attained using the protocol described above.

3.4 Surface preparation

Hydrophilic silica was used as the surface in this study, which was prepared from a silicon wafer, p-type, boron-doped, resistivity 1-20 Ω cm, purchased from SWI (Semiconductor Wafer, Inc., Taiwan). This substrate was thermally oxidized at ca. 900 °C to yield a 300 Å-thick layer of silicon oxide in order to increase the resolution of the ellipsometry measurements. The silicon wafer was cut into 12 x 20 mm slices. The silicon substrates were cleaned in a boiling mixture (1:1:5 by volume) of 25% NH_4OH (pro analysis, Merck), 30% H_2O_2 (pro analysis, Merck) and H_2O at 80 °C for 5 min, followed by cleaning in a

boiling mixture (1:1:5 by volume) of 32% HCl (pro analysis, Merck), 30% H_2O_2 (pro analysis, Merck) and H_2O at 80 ^oC for 5 min, as described in [11]. Then the slides were thoroughly rinsed with deionized water and ethanol and stored in absolute ethanol until use. Before use in the ellipsometry measurement, the substrate was dried with nitrogen and treated in a plasma cleaner (Harrick Scientific Corp., model PDC-3XG) for 5 min in air plasma at 0.02 mbar.

3.5 Characterization

3.5.1 Polarized optical microscopy

The phase's mosaic texture observation was attained under polarized light, resulting in a fast and straightforward method to determine the phase structure. Polarized optical microscopy (POM) is one of the few inexpensive methods often used to determine whether birefringence is present in the prepared samples. The instrument setup is depicted in Figure 3.2.

The sample is isotropic if the phase appears dark when observed under cross-polarizers, while those that appear bright correspond to an anisotropic phase. It is noteworthy that cubic phases do not show birefringence while hexagonal phases do. Accordingly, the observation of oily streaks or Maltese-cross optical birefringence patterns, as can be seen in Figure 3.3, is an indication of the presence of anisotropic lamellar structures [12-14]. Although POM mainly detects the anisotropic lamellar phases by illuminating the samples under cross-polarizers, it is still a useful technique to verify the presence of lamellar phases. In some cases, although birefringence could be detected, those domains were not observed using small-angle X-ray scattering (SAXS) due to the small extent of the lamellar domains. SAXS will be later discussed in section 3.5.3.

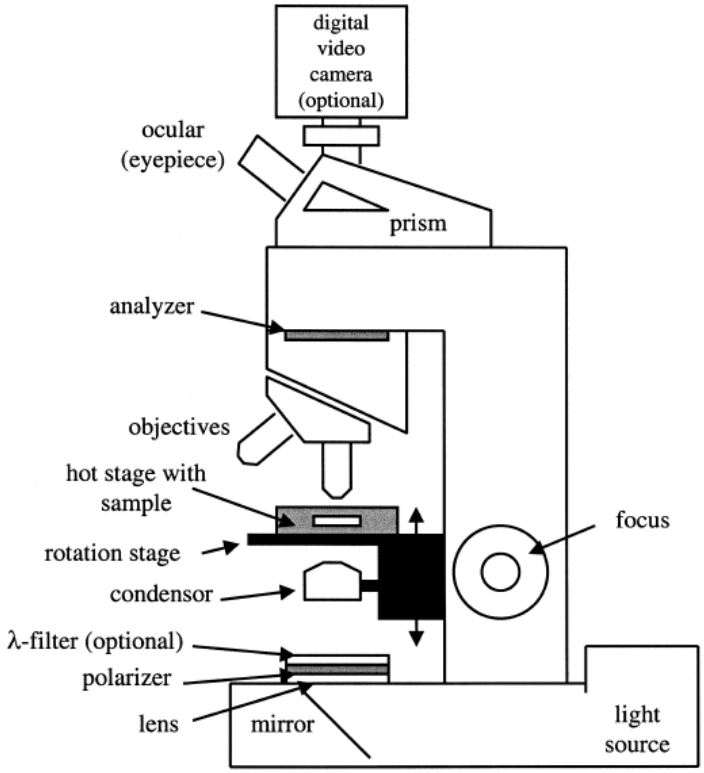

Figure 3.2 Schematic polarized optical microscope setup. (*Reprinted with permission from Ingo Dierking (2004) Polarizing Microscopy, Textures of Liquid Crystals, John Wiley and Sons. Copyright 2004*) [15].

(a) (b)

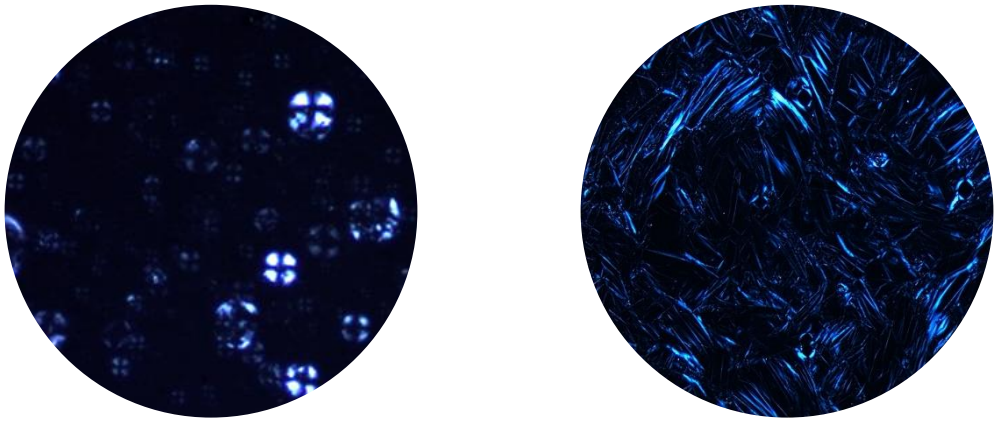

Figure 3.3 Distinctive optical textures of a lamellar phase, showing (a) Maltese crosses and (b) oily streaks by aligned molecules observed between cross-polarizers revealing sample birefringence.

To perform POM, a drop of the mixture was deposited on a glass slide and covered with a cover glass. All micrographs were obtained using an Olympus BX53 (Olympus Corporation, Japan) optical microscope with a polarizer filter, coupled with an *Infinity 1* camera (Lumenera). The micrographs were analyzed using Infinity Analyze software (Lumenera).

3.5.2 Differential scanning calorimetry

Differential scanning calorimetry (DSC) was used to study the thermal behavior of the surfactant systems. Different phase transitions/transformations, such as the first-order gel-to-liquid crystalline (L_β-L_α) phase transition can be determined by measuring the thermodynamic properties of thermally induced transitions, allowing us to infer conformational changes in the alkyl chain of the surfactant. A DSC measurement consists of two pans (hermetically sealed), the reference and the sample, both of which are electrically heated at a constant rate (Figure 3.4). Both pans will heat differently and the instrument will, therefore, record the difference in the amount of heat required to vary the temperature of both pans as a function of temperature. The L_β-L_α phase transition (often called T_m) was determined by using a Discovery DSC differential scanning calorimeter (TA Instruments, USA) at a rate of 2 $^oC\ min^{-1}$ from 10 ^oC to 60 ^oC and back to 10 ^oC. The chamber was kept under a nitrogen environment.

The enthalpy (ΔH) associated with a thermal transformation was determined by integrating the endothermic or exothermic peak areas under the thermogram peak (Figure 3.5) by use of the software Trios (TA Instruments, USA). It is noteworthy that the shape of the peak can provide information about the purity of the system and the cooperativity of the thermal transition. For instance, impurities usually result in peak broadening and peak asymmetry, and sharp peaks indicate cooperative thermal transitions [16-18].

By dividing the enthalpy change (*J/mol*) by the temperature (*K*) of the transformation, it is possible to obtain the corresponding entropy change:

$$\Delta S = \frac{\Delta H}{T_m} \tag{3.1}$$

where ΔS is normally expressed in $J\ K^{-1}\ mol^{-1}$ [19].

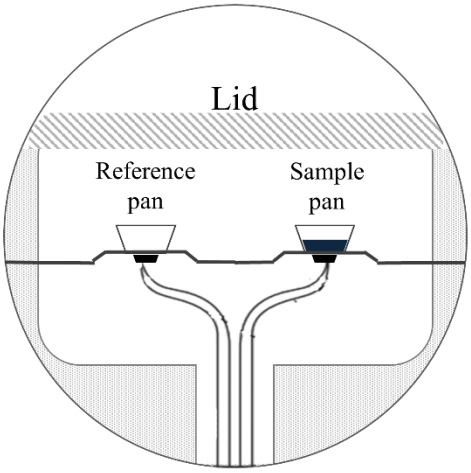

Figure 3.4 A schematic representation of a DSC cell cross-section. The reference and sample pan are heated simultaneously, and the difference in the amount of heat is recorded.

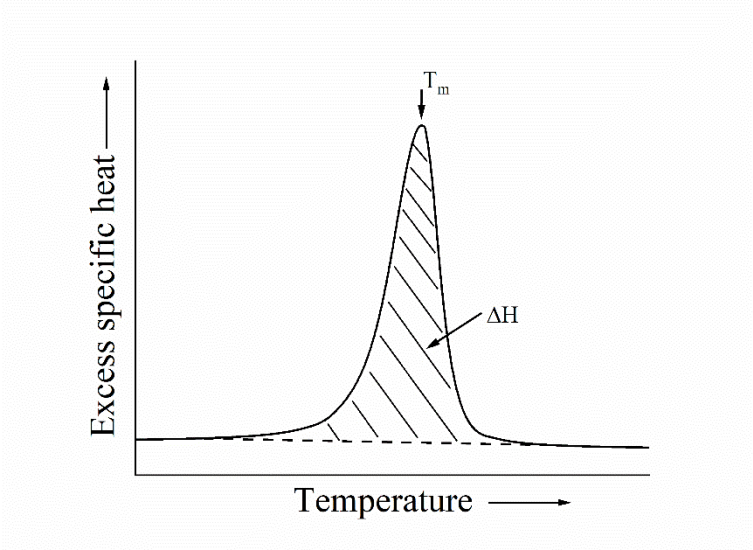

Figure 3.5 The variation of excess specific heat during a two-state transition process. T_m indicated the temperature at which the thermal transition occurs, and ΔH is the enthalpy associated with the thermal transition (area under the peak).

3.5.3 Small and wide-angle X-ray scattering

Small and wide-angle X-ray scattering (SAXS and WAXS) is a non-destructive analytical method that takes advantage of X-rays to ascertain the organization structure of molecular systems concerning averaged particle sizes and shapes. This method allows us to "see" ordered matter in materials in reciprocal space by scattering. When X-rays penetrate the sample (i.e., transmission mode), two phenomena are observed:

1) scattering into all directions from the atoms composing the sample occurs and generates background radiation;
2) ordered elements in the sample (in the scale-range of X-ray wavelength) with different materials or densities (providing contrast) will, therefore, produce additional scattering.

X-rays are electromagnetic waves with a much stronger wavelength (<3 Å) than visible light (≈5000 Å), Figure 3.6. This type of radiation interacts with matter mainly by absorption and scattering. When X-rays penetrate a sample, a portion passes through it, a portion is absorbed and transformed into other forms of energy, such as heat and fluorescence radiation, and a portion is scattered. Due to the nature of this work, the focus is on the scattered radiation.

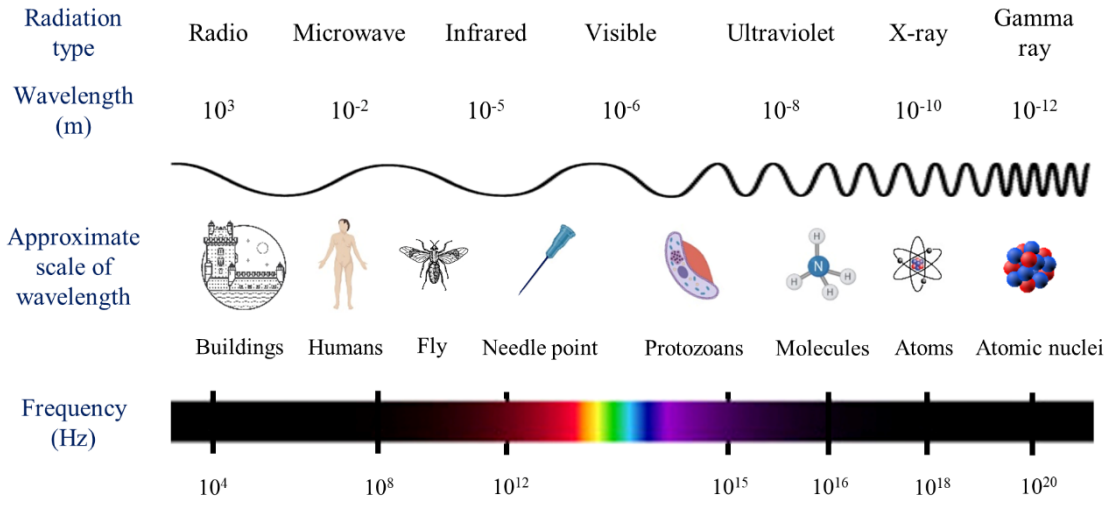

Figure 3.6 A schematic diagram of the entire range of the electromagnetic spectrum with the corresponding wavelength and frequency from the lowest energy (left) to the highest (right).

The scattering of radiation can occur with and without loss of energy. If the scattered radiation wavelength has a different wavelength than the incoming radiation, it is identified as Compton (or inelastic/incoherent) scattering [20]. When the incoming and scattering radiation have the same wavelength, it is identified as Rayleigh or Thomson (or elastic/coherent) scattering [21]. Compton scattering is produced when a photon hits an electron, and it is bounced away and becomes part of the featureless background radiation. On the other hand, Rayleigh scattering arises from photon collision with strongly bound electrons without energy transfer producing coherent scattering, thus carrying information about the particle structure.

SAXS is described by the reciprocal law, which postulates that the scattering vector (q) is determined as a result of the scattered intensity and vector [22]. This implies that every distance is measured relative to the wavelength of the income radiation (λ). Therefore, scattering profiles are usually presented as a function of q:

$$q = \frac{4\pi}{\lambda} \sin\theta \tag{3.2}$$

where θ is the angle of incidence. The dimension of q is one over the length and for that reason the scattering profile is commonly termed “the structure in reciprocal space”, whereas the particles are said to have a “structure in real space”.

When particle systems are densely packed (e.g., lamellar surfactant systems), the scattering profile will show pronounced peaks due to such highly ordered and periodic packing. From the Bragg peak (the first and most intense) and the position of its maximum (q^*), it is possible to determine the distance (d) between aligned particles and structures:

$$d = \frac{2\pi}{q^*} \tag{3.3}$$

Bragg's Law and setup

First and foremost, and I quote Cullity and Stock, "*A diffracted beam may be defined as a beam composed of a large number of scattered rays mutually reinforcing one another. Diffraction is, therefore, essentially a scattering phenomenon and not one involving any 'new' kind of interaction between X-rays and atoms*" [23]. Bragg's law of diffraction postulates that scattering vectors will be completely in phase if:

$$n\lambda = 2d \sin\theta \tag{3.4}$$

where *n* is an integer, and it states the necessary conditions which must be met if diffraction is to occur, as illustrated in Figure 3.7. These conditions are:

1) the incoming and scattered beam are always coplanar;
2) the angle between the scattered and transmitted beam is always 2θ.

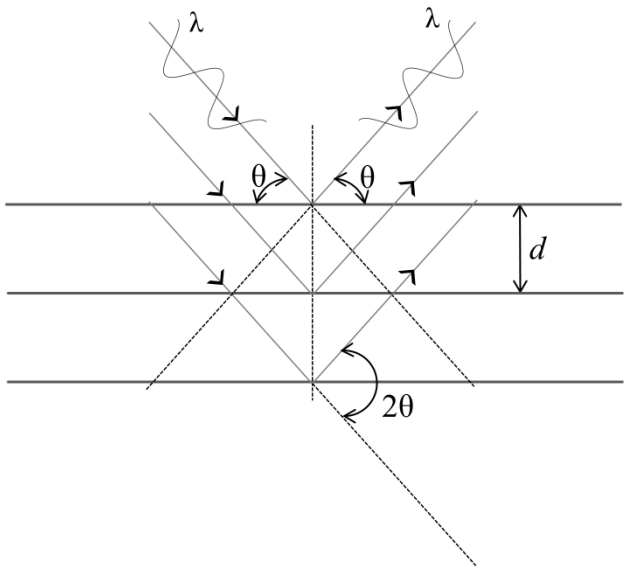

Figure 3. 7 A schematic representation of the Bragg diffraction. Periodic particles or structures scatter the incoming beam, and a beam with the same wavelength (λ) and in phase is scattered providing the distance (d) between aligned particles or structures, as stated by Bragg's law [23].

Quantification of the lamellar components

To determine parameters such as, the surfactant bilayer thickness (d_{bi}), the water layer thickness (d_w), and the area per surfactant molecule (a), an analysis of the scattering profiles was carried out. As shown in Figure 3.8, the surfactant system was assumed to comprise of two regions, the bilayer – containing the surfactant hydrocarbon chains; and the water layer – containing the water, the surfactant head-groups, and the counterions.

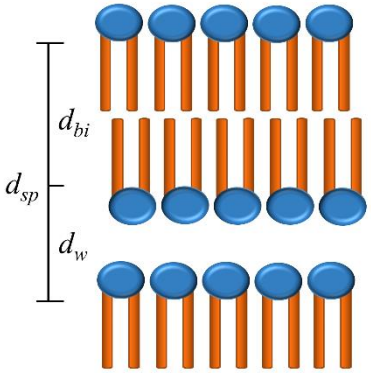

Figure 3.8 Schematic representation of the surfactant lamellar L_β phase packing structure. d_{sp} – interlamellar spacing, d_{bi} – bilayer thickness, d_w – polar domain thickness.

Structural parameters of the lamellar phase, such as the bilayer volume fraction (Φ_{bi}), the area per surfactant molecule (a), and the bilayer thickness (d_{bi}), were calculated from the SAXS and WAXS results, using Equations 3.5 and 3.6 [24]:

$$d_{sp} = \frac{2\pi}{q} \tag{3.5}$$

$$q = \frac{2\pi}{d_{sp}} = 2\pi\frac{\Phi_{bi}}{d_{bi}} = \pi\frac{\Phi_{bi}a}{v_{bi}} \tag{3.6}$$

where q is the first-order Bragg peak; Φ_{bi} is the volume fraction of the total hydrophobic constituents, and v_{bi} is the molar volume of the total amphiphiles present in the bilayer.

The non-polar domain only contains the hydrophobic segments of the surfactant, therefore, the Φ_{bi} can be calculated using Equation 3.7 [24]:

$$\Phi_{bi} = \frac{v_{hc,S} \times \frac{w_S}{M_S}}{v_S \times \frac{w_S}{M_S} + v_W \times \frac{w_W}{M_W}} \tag{3.7}$$

where w is the weight fraction, and *M* is the molar mass of the various components denoted as surfactant (*S*) and water (*W*); *v* is the molecular volume given by the sum of the partial molar volume of the hydrocarbon chain (*hc*) and the polar head-group of the molecule.

To analyze the SAXS and WAXS results, the values used for the various parameters were: $v_{hc,S}$ = 1026 Å^3 [1], v_S = 1126 Å^3 [25], and v_W = 30 Å^3 [24]. Since the hydrated radius of bromide and chloride was the same, 3.3 Å [26], the volume of DODAB and DODAC was considered to be similar.

Instrumentation setup

In the present work, the interlamellar spacing (d_{sp}) determination was carried out using two laboratory-based X-rays sources, and a synchrotron radiation source. SAXS and WAXS analytical method operates as described in Figure 3.9, and it shows a schematic representation of a simultaneous SAXS and WAXS setup. When only one detector is used, the sample-to-detector distance is varied to collect small or wide-angle profiles. The technical specifications of the different instruments are summarized in Table 3.2.

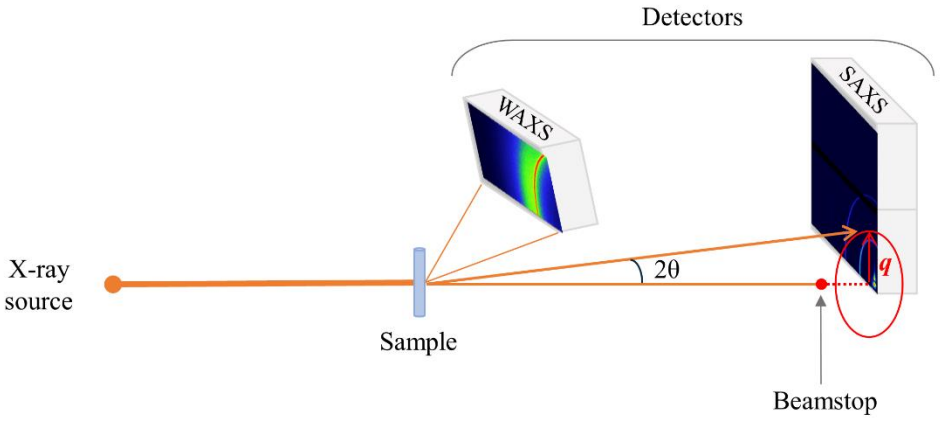

Figure 3.9 A schematic diagram of the SAXS and WAXS experimental setup. X-rays are generated, pass through a set of pinholes to define the resolution, a collimated beam of X-rays irradiates the sample, and detectors collect the coherent scattered beams at different sample-to-detector distances.

Table 3.2 Technical specifications of the three SAXS and WAXS instruments used: a SAXSess (Anton Paar, Austria), a Nano-inXider (Xenocs, France), and a synchrotron SAXS/WAXS beamline (ANSTO, Australia).

Instrument	**SAXSees (Anton Paar) @ FACTS**	**Nano-inXider SW-L (Xenocs) @ FACTS**	**SAXS/WAXS beamline (Australian synchrotron) @ ANSTO**
Source	Sealed tube (40 kV and 50 mA). Cu Kα λ = 1.542 Å	Microfocus sealed tube (50 kV and 0.6 mA). Cu Kα λ = 1.542 Å	In-vacuum undulator, 22 mm period, 3 m length. SAXS: λ = 1.512 Å (8.2 keV beam). WAXS: λ = 0.827 Å (15 keV beam).
Optics	Focusing multilayer mirror	Single-reflection multilayer optics optimized to reflect Cu Kα line	Horizontal and vertical focusing mirrors for a monochromatic beam with variable focus for different camera lengths.
Collimation	Line collimation	Point collimation. Medium (MR), high (HR), and very-high (VHR) resolution	Point collimation.
Beam path	Vacuum (≈1 mbar)	Vacuum (≈0.1 mbar)	Vacuum (≈0.005 mbar)
Detector	Image-plate. Cyclone Plus imaging-plate reader (Perkin Elmer)	Dectris Pilatus 3 (2 SAXS and 1 WAXS)	Dectris Pilatus 2M
Sample-to-detector distance	265 mm	SAXS: 938 mm WAXS: 79 mm (33º detector tilt)	SAXS: 7000 mm WAXS: 320 mm
Exposure time	1800 s	600 s	1 s
Temperature control	TCU 50 and TCS 300	Linkam HFSC350 stage	Water bath controlled by a Peltier system
Data-processing software	SAXSquant 3	Foxtrot	ScatterBrain

For effective and reliable data collection, the background scattering was minimized by keeping the system under vacuum during all measurements. For all the samples, the measurements were done at temperatures both under and above the main phase transition temperature.

In the presence of intermediate thermodynamic phases, such as lyotropic liquid crystalline phases, these show flow properties and degrees of molecular ordering between the crystalline solid and simple liquid states. In these densely packed particle systems, the positions and orientations of its particles can align themselves with each other. Therefore, the formation of a long-range ordered system occurs. The structure factor, in these liquid crystalline phases, is normally called lattice factor. It is translated to a set of narrow and intense peaks at well-defined angles. Consequently, the ratios of the peak positions on the *q*-scale have typical values and should obey the relationship as follows [1]:

- Lamellar symmetry √1, √4, √9, √16, √25, …
- Cubic (*Pn3m*) symmetry √1, √2, √3, √4, √6, √8, √9, …
- Cubic (*Im3m*) symmetry √1, √2, √4, √6, √8, √10, √12, …
- Hexagonal symmetry √1, √3, √4, √7, √9, √12, …

The d_{sp} represents the repeat distance of a lamellar system, and it is the sum of the thickness of the lamellar bilayer (d_{bi}) plus the width of the polar (often called water) layer (d_w), as represented in Figure 3.10. Thus, d_{sp} (d_{100}) is defined according to the following equation:

$$d_{sp} = d_w + d_{bi} \tag{3.8}$$

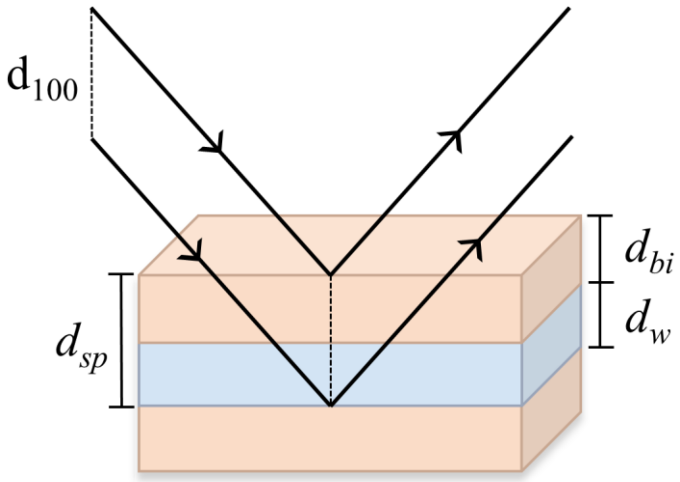

Figure 3.10 A schematic representation of the coherent scattering from a lamellar surfactant structure following the Bragg's law for diffraction, thus allowing to determine the interlamellar spacing (d_{sp}) of an aggregate system.

Other oriented (liquid crystalline) structures can also be identified from the scattering profile of their repeating units, Figure 3. 11.

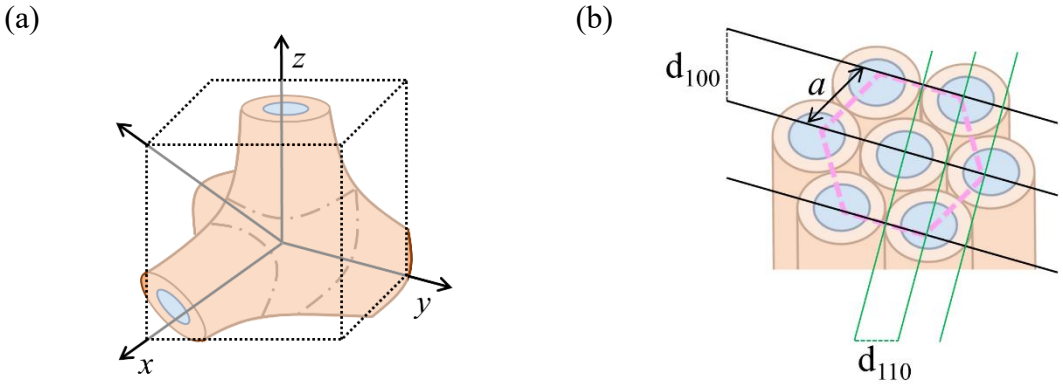

Figure 3.11 A schematic representation of the coherent scattering from (a) a cubic (*Pn3m*) structure and (b) a hexagonal structure following the Bragg's law for diffraction, thus allowing the determination of different distances between neighboring aligned structures.

3.5.4 Ellipsometry

The layer thickness and the adsorbed amount of the deposited layers were measured using an automated Rudolph Research thin-film null ellipsometer type 43603-200E, as described in Figure 3.12. The measurements were conducted using a xenon arc lamp with a filter at a wavelength of 4015 Å.

Null ellipsometry allows time-resolved measurements of both refractive index and thickness of an adsorbed film with high accuracy. This technique is based on measurement of changes in the ellipticity of polarized light, given by the relative change in amplitude, Ψ, and phase shift, Δ, upon reflection of polarized light against a surface. In order to convert Ψ and Δ into layer thickness and refractive index, a four-layer optical model assuming an isotropic medium and planar surface was applied [27]. From the obtained values of the thickness and refractive index, the adsorbed amount, Γ, was calculated using de Feijter's formula [28]:

$$\Gamma = \frac{d_f\left(n_f - n_0\right)}{dn/dc} \tag{3.9}$$

where Γ is the mass per surface area (mg m^{-2}), d_f is the thickness of the adsorbed layer (Å), n_f is the refractive index of the adsorbed film, n_0 is the refractive index of the bulk solution, and d_n/d_c is the refractive index increment.

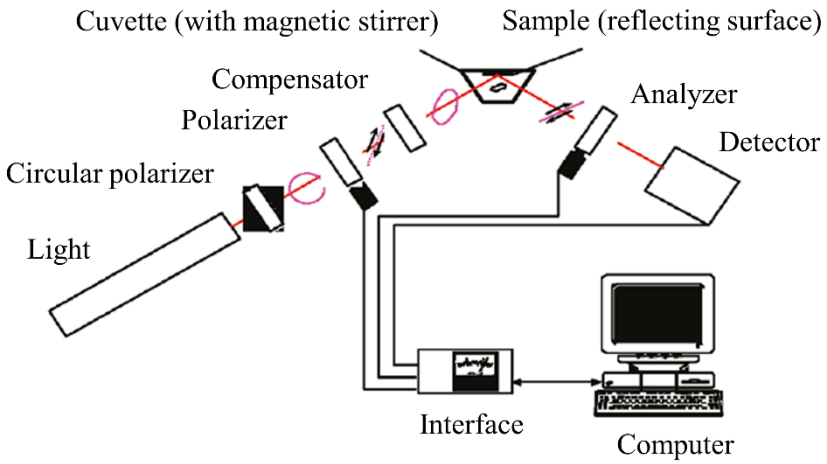

Figure 3.12 A schematic representation of the automated ellipsometer used in this study. The polarized light from the laser is depolarized with a circular polarizer. After the polarizer, the emerging linearly polarized light is transformed into elliptically polarized light when passing through the compensator, which is a quarter wave plate. The ellipticity can be varied by rotating the polarizer. As the reflection against the surface of the sample also changes the ellipticity of the light, the polarizer can be rotated in such a way that the light after reflection again is linearly polarized. The relative rotation of this light is measured by using another polarizer, the analyzer, which is rotated until a minima in light intensity as measured by the detector. (*Adapted with permission from Maryline Clauzel, Eric S. Johnson, Tommy Nylander, Rajan K. Panandiker, Mark R. Sivik, Lennart Piculell (2011) Surface Deposition and Phase Behavior of Oppositely Charged Polyion-Surfactant Ion Complexes. Delivery of Silicone Oil Emulsions to Hydrophobic and Hydrophilic Surfaces. ACS Applied Materials and Interfaces, 3, 2451–2462 Copyright 2011, American Chemical Society*) [29].

The optical characteristics of the silicon wafer, i.e., the refractive index of silicon as well as the thickness and refractive index of the silicon oxide layer, were determined in air and in deionized water as explained in detail by Tiberg and Landgren [30]. In order to account for the imperfections of the optical components, four-zone measurements [30] at the beginning of each experiment were used.

The adsorption from additive/surfactant mixtures was initiated by injecting 0.5 mL of the stock solution into the trapezoid cuvette filled with 4.5 mL of deionized water. The solution in the cuvette was agitated with a magnetic bead rotating at about 300 rpm. The adsorption process was followed by recording the ellipsometric angles for approximately 3500 s when

steady-state was reached. The experiments were conducted at 25 ^{o}C ± 0.1 ^{o}C by circulating water from a thermostat bath. In the rinse experiments, initially the bulk solution in the cuvette was exchanged by flowing deionized water through the measurement cell by means of a peristaltic pump under a flow rate of 10 mL min^{-1}.

A d_n/d_c value in the range 0.16-0.18 cm^3/g has been used for phospholipid systems [31, 32]. In this study, a d_n/d_c value of 0.18 cm^3/g was used, which is consistent with the X-ray characterization results of DODAC previously demonstrated (cf. chapter 4).

References

[1] E.F. Marques, B.F.B. Silva, Surfactant Self-Assembly, in: T. Tadros (Ed.), *Encyclopedia of Colloid and Interface Science*, *Springer Berlin Heidelberg*, Berlin, Heidelberg, 2013, pp. 1202-1241.

[2] W.M. Haynes, D.R. Lide, T.J. Bruno, CRC handbook of chemistry and physics : a ready-reference book of chemical and physical data, Boca Raton, Florida : CRC Press, [2016] 2016-2017, 97th Edition / Editor-in-Chief: W. M. Haynes.2016.

[3] M.J. Blandamer, B. Briggs, P.M. Cullis, J.A. Green, M. Waters, G. Soldi, J.B.F.N. Engberts, D. Hoekstra, Differential scanning microcalorimetric study of vesicles in aqueous solutions formed by dimethyldioctadecylammonium bromide, *Journal of the Chemical Society, Faraday Transactions* 88(23) **1992** 3431-3434.

[4] E.F. Marques, Size and stability of catanionic vesicles: Effects of formation path, sonication, and aging, *Langmuir* 16(11) **2000** 4798-4807.

[5] E.F. Marques, A. Khan, B.J. Lindman, A calorimetric study of the gel-to-liquid crystal transition in catanionic surfactant vesicles, *Thermochimica Acta* 394(1-2) **2002** 31-37.

[6] E.F. Marques, O. Regev, A. Khan, B. Lindman, Self-organization of double-chained and pseudodouble-chained surfactants: counterion and geometry effects, *Adv. Colloid Interface Sci.* 100 **2003** 83-104.

[7] M. Goto, Y. Ito, S. Ishida, N. Tamai, H. Matsuki, S. Kaneshina, Hydrostatic Pressure Reveals Bilayer Phase Behavior of Dioctadecyldimethylammonium Bromide and Chloride, *Langmuir* 27(5) **2011** 1592-1598.

[8] T. Iwata, Chapter 25 - Lamellar Gel Network, *Cosmetic Science and Technology*, *Elsevier*, Amsterdam, 2017, pp. 415-447.

[9] H. Kunieda, K. Shinoda, Solution behavior of dialkyldimethylammonium chloride in water. Basic properties of antistatic fabric softeners, *The Journal of Physical Chemistry* 82(15) **1978** 1710-1714.

[10] R.G. Laughlin, R.L. Munyon, Y.C. Fu, A.J. Fehl, Physical Science of the Dioctadecyldimethylammonium Chloride Water-System. 1. Equilibrium Phase-Behavior, *Journal of Physical Chemistry* 94(6) **1990** 2546-2552.

[11] A.V. Svensson, E.S. Johnson, T. Nylander, L. Piculell, Surface Deposition and Phase Behavior of Oppositely Charged Polyion−Surfactant Ion Complexes. 2. A Means to Deliver Silicone Oil to Hydrophilic Surfaces, *ACS Appl. Mater. Interfaces* 2(1) **2010** 143-156.

[12] K. Fontell, A. Ceglie, B. Lindman, B. Ninham, Some observations on phase-diagrams and structure in binary and ternary-systems of didodecyldimethylammonium bromide, *Acta Chemica Scandinavica Series a-Physical and Inorganic Chemistry* 40(4) **1986** 247-256.

[13] C.C. Muller-Goymann, Physicochernical characterization of colloidal drug delivery systems such as reverse micelles, vesicles, liquid crystals and nanoparticles for topical administration, *Eur. J. Pharm. Biopharm.* 58(2) **2004** 343-356.

[14] K. Holmberg, D.O. Shah, M.J. Schwuger, Handbook of applied surface and colloid chemistry, Chichester, England ; New York : Wiley, ©2002.2002.

[15] I. Dierking, Textures of liquid crystals. [electronic resource], Weinheim : Wiley-VCH, c2003.2003.

[16] J.M. Sturtevant, Biochemical Applications of Differential Scanning Calorimetry, *Annual Review of Physical Chemistry* 38(1) **1987** 463-488.

[17] R.L. Biltonen, D. Lichtenberg, The use of differential scanning calorimetry as a tool to characterize liposome preparations, *Chem. Phys. Lipids* 64(1) **1993** 129-142.

[18] M. Chiu, E. Prenner, Differential scanning calorimetry: An invaluable tool for a detailed thermodynamic characterization of macromolecules and their interactions, *Journal of Pharmacy And Bioallied Sciences* 3(1) **2011** 39-59.

[19] R.N. McElhaney, The use of differential scanning calorimetry and differential thermal-analysis in studies of model and biological-membranes, *Chem. Phys. Lipids* 30(2-3) **1982** 229-259.

[20] J.H. Hubbell, W.J. Veigele, E.A. Briggs, R.T. Brown, D.T. Cromer, R.J. Howerton, Atomic form factors, incoherent scattering functions, and photon scattering cross sections, *Journal of Physical and Chemical Reference Data* 4(3) **1975** 471-538.

[21] J.H. Hubbell, I. O/verbo/, Relativistic atomic form factors and photon coherent scattering cross sections, *Journal of Physical and Chemical Reference Data* 8(1) **1979** 69-106.

[22] J. Li, A. Jiao, S. Chen, Z. Wu, E. Xu, Z. Jin, Application of the small-angle X-ray scattering technique for structural analysis studies: A review, *Journal of Molecular Structure* 1165 **2018** 391-400.

[23] B.D. Cullity, Elements of x-ray diffraction, 3rd ed. ed., Prentice Hall, Upper Saddle River, NJ, 2001.

[24] G. Montalvo, A. Khan, Self-Assembly of Mixed Ionic and Zwitterionic Amphiphiles: Associative and Dissociative Interactions between Lamellar Phases, *Langmuir* 18(22) **2002** 8330-8339.

[25] H. Durchschlag, P. Zipper, Calculation of Partial Specific Volumes and Other Volumetric Properties of Small Molecules and Polymers, *Journal of Applied Crystallography* 30(5 Part 2) **1997** 803-807.

[26] J.N. Israelachvili, 4 - Interactions Involving Polar Molecules, in: J.N. Israelachvili (Ed.), *Intermolecular and Surface Forces (Third Edition)*, *Academic Press*, San Diego, 2011, pp. 71-90.

[27] R.M.A. Azzam, N.M. Bashara, Ellipsometry and polarized light, Amsterdam ; New York : North-Holland Pub. Co. ; New York : sole distributors for the U.S.A. and Canada, Elsevier North-Holland, 1977.1977.

[28] J.A. De Feijter, J. Benjamins, F.A. Veer, Ellipsometry as a tool to study the adsorption behavior of synthetic and biopolymers at the air–water interface, *Biopolymers* 17(7) **1978** 1759-1772.

[29] M. Clauzel, E.S. Johnson, T. Nylander, R.K. Panandiker, M.R. Sivik, L. Piculell, Surface Deposition and Phase Behavior of Oppositely Charged Polyion-Surfactant Ion Complexes. Delivery of Silicone Oil Emulsions to Hydrophobic and Hydrophilic Surfaces, *ACS Appl. Mater. Interfaces* 3(7) **2011** 2451-2462.

[30] F. Tiberg, M. Landgren, Characterization of Thin Nonionic Surfactant Films at the Silica Water Interface by Means of Ellipsometry, *Langmuir* 9(4) **1993** 927-932.

[31] A. Theisen, Refractive Increment Data-book for Polymer and Biomolecular Scientists, Nottingham University Press2000.

[32] T. Tumolo, L. Angnes, M.S. Baptista, Determination of the refractive index increment (dn/dc) of molecule and macromolecule solutions by surface plasmon resonance, *Anal. Biochem.* 333(2) **2004** 273-279.

Chapter 4

Packing in lamellar phases of double-chained cationic surfactants with bromide and chloride counterions

Double-chained surfactants spontaneously self-assemble into lamellar structures. This packing geometry extends their application to various fields because they can solubilize both polar and non-polar compounds. These lamellar structures also display an extensive swelling of their liquid crystalline phase, and though the swelling of the gel phase is constrained. In this chapter, the phase behavior and swelling behavior of dioctadecyldimethyl ammonium bromide and chloride were investigated. Surfactant solutions ranging from 5 to 37.5 wt. % were prepared. The phase identification was done using cross-polarizers, the thermal behavior was examined using differential scanning calorimetry and the surfactant packing was determined using small and wide-angle X-ray scattering. A lower gel-to-liquid crystalline phase transition temperature in the presence of chloride counterion was found when compared to bromide. The presence of chloride yielded stable lamellar surfactant phases below and above the Krafft temperature with a one-dimensional swelling.

4.1 Introduction

Double-tailed surfactants are known to spontaneously self-assemble into a lamellar architecture, in water [1-3]. The reason behind this geometrical arrangement lies in the volume occupied by its polar and non-polar domains, which results in a molecule with a cylindrical geometry. As mentioned in chapter two, these liquid crystalline phases comprised of different configurations, but planar lamellar structures were the focus of this work. Vesicle aggregates also formed bilayers, but with a curved interface.

Lamellar surfactant systems feature properties such as being able to solubilize both polar and non-polar compounds and display an extensive swelling of their domains, especially for ionic surfactants [2]. These properties are ideal in order to incorporate molecules with various structures without destroying the lamellar integrity. Planar bilayers are formed at surfactant concentration values where metastable vesicle structure collapses to form a structure with no curvature. These lamellar structures display two states of alkyl chain organization: a “solid-like” (L_β phase) where the hydrocarbon chains are motionless, and a “fluid-like” (L_α phase) state where the hydrocarbon chains are molten and have more rotational freedom. The main phase transition temperature (T_m) is the temperature where the L_β-L_α phase transition occurs and it can vary significantly depending on the preparation method, as summarized in Table 4.1.

Table 4.1 Thermodynamic parameters associated with the thermal transitions reported in the literature for DODAB and DODAC in water determined by differential scanning calorimetry.

DODAB				DODAC			
T_m (°C)	ΔH_m (kJ mol^{-1})	Phase	Ref	T_m (°C)	ΔH_m (kJ mol^{-1})	Phase	Ref
35.4	-	L_{c2}-L_β*1	[4]	19.7	32.7	L_c-L_β*2	[5]
44.5	45.2	L_β-L_α	[4]	39.9	41.9	L_β-L_α	[5]
52.9	101.2	L_{c1}-L_α*3	[4]	46.0	24.5	L_β-L_α	[6]
45.8	35.0	L_β-L_α	[7]	48.9	41.7	L_β-L_α	[7]
51.7	-	L_β-L_α	[8]	47.9	-	L_β-L_α	[9]
45.2	-	L_β-L_α	[10]	47.9	53.4	L_β-L_α	[11]
45.5	-	L_β-L_α	[9]				
45.3	44.8	L_β-L_α	[11]				

*1 L_{c2} was defined as a metastable lamellar crystal phase [4].

*2 L_c was defined as a lamellar crystal phase [5].

*3 L_{c1} was defined as a stable lamellar crystal phase [4].

This variation in the reported values does not allow to compare the behavior of these double tailed surfactants across literature for better understanding of their phase behavior. Using a consistent preparation method, stabilized dispersions of DODAB and DODAC in water at varying surfactant concentration were formulated and conducted a thermal behavior study, as well as investigate the self-assembled packing structure of these binary surfactant systems.

An investigation on the phase behavior of dioctadecyldimethyl ammonium bromide and chloride (DODAB and DODAC) in water was conducted. Surfactant solutions with concentration ranging from 5 to 37.5 wt. % were prepared and their stability, thermal behavior and self-assembled structure were evaluated. At these high concentrations, the phase shows low flexibility below the T_m and the L_β gel phase that exists is of great importance for different applications and should be better understood.

4.2 Results and discussion

4.2.1 Phase identification using visual observations (naked-eye and POM)

Direct sample examination, either by naked-eye observation or using an optical microscope equipped with cross-polarizers (also known as polarized optical microscope (POM)), is the most straightforward and versatile method to determine the phase of surfactant systems. This method alone do not confirm the packing structure but provide an easy way to predict it.

The solubility of these lamellar-forming surfactants in water is extremely low (10^{-5}-10^{-10} M) [1], which results in their inability to form micelles. Instead, they spontaneously form lamellar structures.

Figure A.4.1 and Figure A.4.2 (appendix) show the vials containing the dispersions of DODAB and DODAC in water at room temperature after equilibration. It can be seen that DODAC formed more stable dispersions in water as compared to DODAB. The phase behavior of these two double-tailed quaternary ammonium surfactants has been extensively studied [6, 12-21], and Schulz et al. suggested that both surfactant systems display a similar phase behavior in water [19].

The appearance of these two surfactants in water led us to reflect on the effect of the counterion to the stability of the surfactant system. Although the van der Waals packing radius (considered as a hard sphere) of bromide is 1.95 Å and chloride is 1.81 Å, they display the same hydrated radius of 3.3 Å [22]. However, bromide is more polarizable than the chloride anion, which results in a more densely packed bilayers whilst chloride is an easier “abandoning” anion than bromide; ergo, there is a stronger repulsion between head-groups for DODAC, thus avoiding the formation of a coagel phase.

The phase behavior of these two double-tailed cationic surfactants in water has been extensively studied [12-17, 19] and it has been found that the presence of gel phases is expected at temperatures below the Krafft point. From Figure A.4.1, it can be seen the presence of sample inhomogeneity in the vial containing DODAB in water, however, homogeneous dispersions were observed for DODAC below the Krafft temperature. This is in disagreement with the DODAC-water phase diagram [12, 16]. The unexpectedly higher stability of the DODAC gel phase may be attributed to the purity (97 %) of the surfactant used throughout our studies. The DODAC used was supplied by Evonik Corporation, USA, and contained an alkyl chain mixture of surfactant with 16-carbon chain (< 2 %) to provide additional stability. Whereas, the DODAB used in the studies had a purity of 100 %.

The mixtures with increasing surfactant concentration (5 – 37.5 wt. %) were placed on glass slides and observed under cross-polarizers at 25 ^{o}C. The micrographs were collected and can be seen in Figure 4.1 for DODAB in water, and Figure 4.2 for DODAC in water. Lamellar systems are anisotropic by nature and display unique textures when observed under an optical microscope with polarized light [23, 24]. Therefore, POM micrographs enabled quick identification of birefringent structures, such as lamellar, whereas isotropic mixtures will appear as a black image.

As discussed above, the presence of crystals in the dispersions of DODAB in water was visually identified. The inspection of the POM micrographs of DODAB (Figure 4.1) shows that anisotropic structures were formed but it was not a one-phase system, as seen in Figure A.4.1. These observations are in good agreement with the phase diagram of DODAB in water proposed by Schulz et al. [19] as the concentration studied fall in the region of the phase diagram where crystals immersed in a continuous isotropic liquid exists below the Krafft temperature.

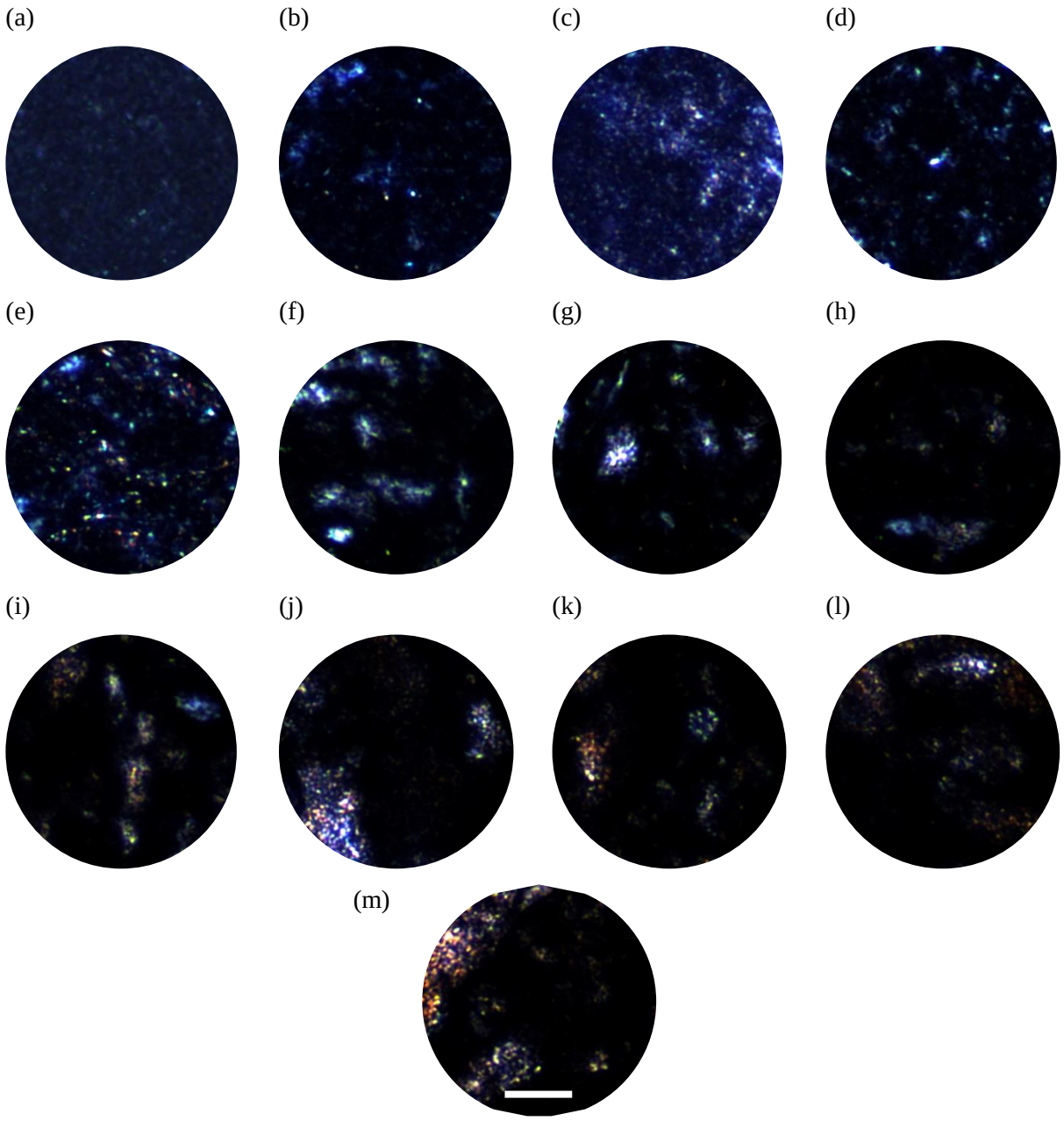

Figure 4.1 POM micrographs of the textures of DODAB in water at increasing surfactant concentration: (a) to (m) correspond to 5 wt. %, 7.5 wt. %, 10 wt. %, 12.5 wt. %, 15 wt. %, 17.5 wt. %, 20 wt. %, 22.5 wt. %, 25 wt. %, 30 wt. %, 32.5 wt. %, 35 wt. % and 37.5 wt. %, respectively. The scale was set at 50 µm and applied to all micrographs. Temperature was kept constant at 25 ^{o}C.

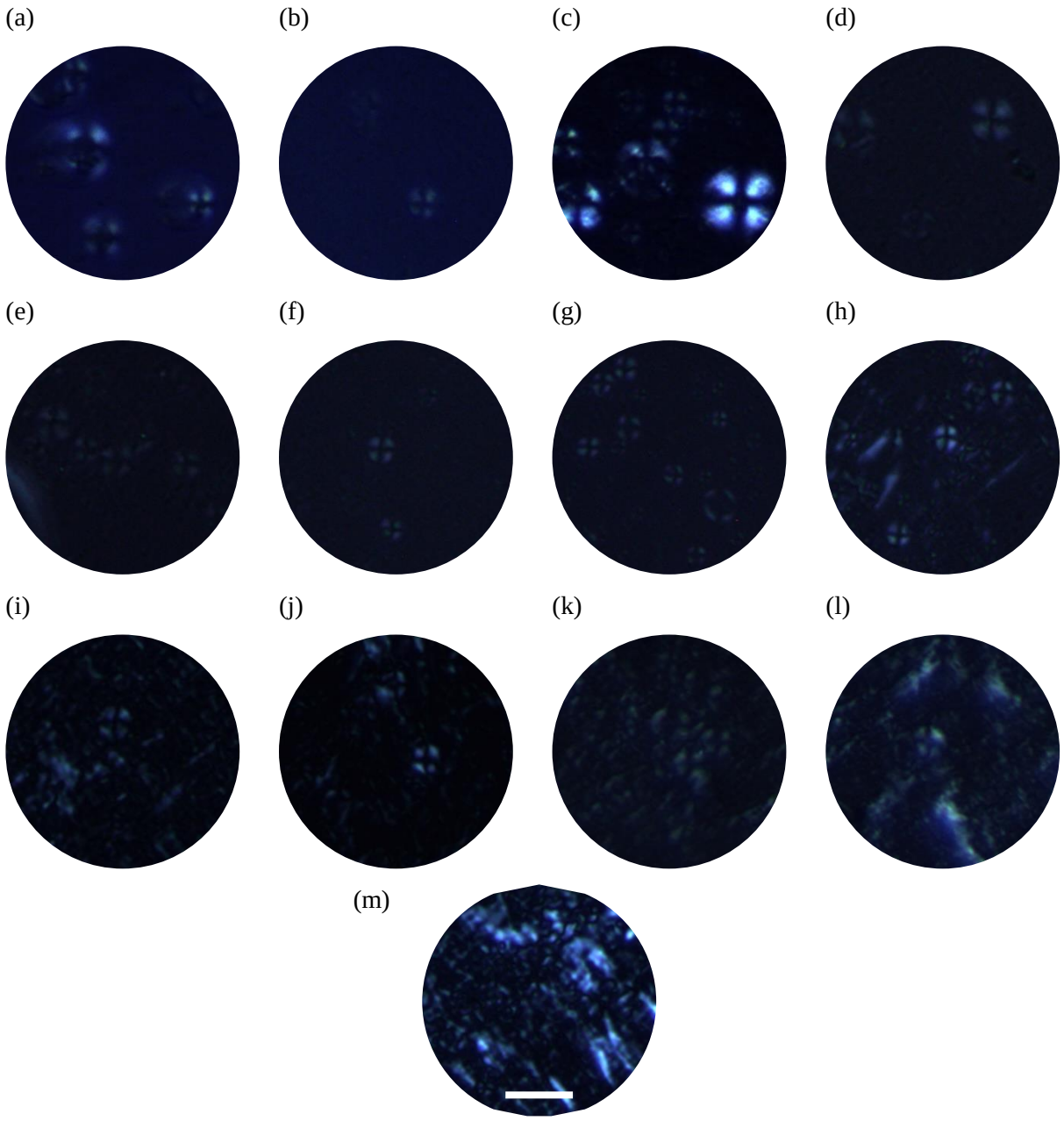

Figure 4.2 POM micrographs of the textures of DODAC in water at increasing surfactant concentration: (a) to (m) correspond to 5 wt. %, 7.5 wt. %, 10 wt. %, 12.5 wt. %, 15 wt. %, 17.5 wt. %, 20 wt. %, 22.5 wt. %, 25 wt. %, 30 wt. %, 32.5 wt. %, 35 wt. % and 37.5 wt. %, respectively. The scale was set at 50 μm and applied to all micrographs. Temperature was kept constant at 25 ^{o}C.

With increasing concentration of surfactant, the mixture became more viscous. The solutions of DODAB (Figure A.4.1) did not form a stable one-phase system, at temperatures below the Krafft temperature. However DODAC was easily dispersed in water, thus, self-assembled in a lamellar gel at room temperature (Figure A.4.2), at below the Krafft temperature for DODAC (45.3 ^{o}C) and this can be identified by the Maltese crosses or oily streaks pattern which is characteristic of a lamellar phase [23, 25].

Through initial inspection by naked eye and POM, these results suggest that the quaternary ammonium surfactant in water was more stable in the presence of chloride anion.

4.2.2 Thermal behavior

In order to examine the phase behavior of the surfactant in water, differential scanning calorimetry (DSC) measurements were conducted. The DSC experiment tracked thermal transitions and their associated thermodynamic properties, such as temperature and enthalpy (ΔH). This section starts with a study of the effect of the scan rate on the thermodynamic parameters to define the appropriate scan rate to be used in this study. Thereafter, the two surfactant systems were scanned and the main phase transition temperature observed during the heating cycle, often known as gel-to-liquid crystalline (L_{β}-L_{α}) phase transition temperature (T_m), the transition temperature under cooling (T_c) and the enthalpy of the phase transition associated with the endothermic event (ΔH_m) and the exothermic event (ΔH_c) were evaluated.

Effects of the scan rate

To understand the implications of the scan rate in the determination of the thermodynamic parameters associated to the phase transformations of the surfactant systems in water, a study of the thermal behavior at four different scan rates was performed. It has been previously discussed in literature that the sharp peak due to the first-order L_β-L_α phase transition of high purity double-tailed surfactant is affected by the scan rate and slow scan rates were recommended to avoid peak broadening [26]. In the case of lamellar surfactant systems, usually when the system was composed of vesicles, they showed to be sensitive to this parameter at low concentrations of surfactant [8]. Therefore, understanding the effect of scan rates was crucial to the identification of the thermal transitions present in the system. Our studies focused on systems with high concentration (35 wt. %) of surfactant which is seldom discussed in literature and DSC scans (both heating and cooling) are collected at various scan rates - 1, 2, 5 and 10 °C/min to investigate how the scan rate could affect the thermodynamic properties of DODAC in water at high concentration regime.

Figure 4.3 shows the thermograms obtained under four different scan rates for 35 wt. % of DODAC in water. The sample was heated from 10 to 60 ^{o}C (Figure 4.3 (a)), left to right), followed by cooling from 60 to 10 ^{o}C (Figure 4.3 (b)), right to the left), and the complete heating/cooling cycle can be obtained. The downward peaks of the thermograms indicate an endothermic event. By integrating of the area under or above the peak, the thermodynamic parameters associated with the thermal transitions were obtained, as summarized in Table 4.2.

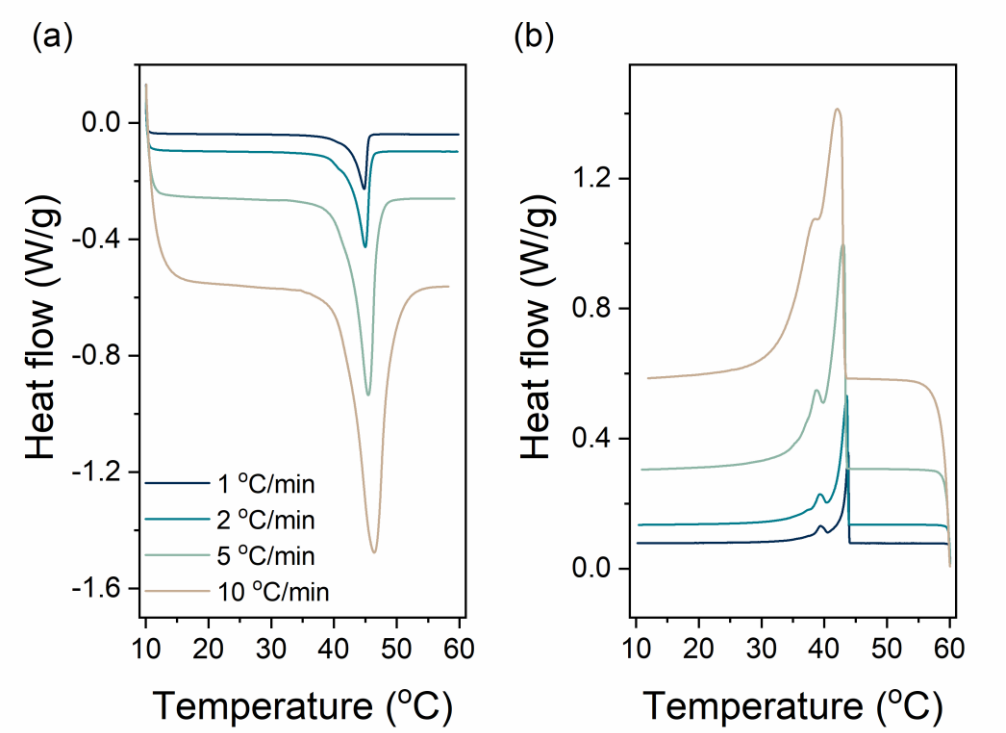

Figure 4.3 Thermograms under (a) heating and (b) cooling of 35 wt. % DODAC in water at four different scan rates (1, 2, 5, and 10 °C /min). The endothermic event corresponds to the downwards deflection.

Table 4.2 Normalized thermodynamic parameters of 35 wt. % DODAC in water under different scan rates.

	Heating		Cooling	
Scan rate	T_m (°C)	ΔH_m (kJ mol^{-1})	T_c (°C)	ΔH_c (kJ mol^{-1})
1 °C/min	44.8	49.2	43.8	50.7
2 °C/min	45.0	49.5	43.6	51.4
5 °C/min	45.4	49.9	43.0	53.8
10 °C/min	46.4	50.4	42.1	53.5

The results shows that different thermal scan rates did not affect the shape of the thermograms, both under heating and cooling conditions. One peak was detected during heating, whereas two thermal transition peaks were recorded during cooling, indicating a possible existence of a metastable phase not detected during the heating process. A careful

discussion of this unanticipated observation will be explored later in this chapter. Negligible differences in the T_m and ΔH_m values with increasing scan rates were observed, and a similar trend was found during the cooling scan. An average T_m of 45.4 ^oC with an average associated ΔH_m of 49.8 kJ mol^{-1} under heating scan were determined. Although scan rates do not seem to have an effect on the temperature and enthalpy associated with the phase transitions, other parameters such as the cooperativity of phase transition may have been affected. As the studies involved high concentration solutions (35 wt. %) of double-tailed surfactant, due to pure geometrical constraints between the polar head-group and the hydrophobic tails, such systems are expected to self-assemble into planar lamellar structures. Upon heating, the alkyl chains of one surfactant molecule will start melting and this event is propagated to the neighboring chains, which ultimately results in a lamellar system with the chains in a "fluid-like" state. The cooperativity of the phase transition was shown by the sharpness of the peaks. A sharper and narrower peak is observed when a slow scan rate was used (Figure 4.3) demonstrating that even if different scan rates did not significantly affect the T_m and ΔH_m values, it had affected the cooperativity of the alkyl chain melting process. It was verified that at fast scan rates, the phase transformation took place over longer times, thus, resulting in peak broadening. Therefore, the use of slow thermal scan rates to track the phase transformations of the surfactant system with temperature is preferred.

Though the original intention was to investigate the effect of the scan rate on the thermally induced phase transitions for a high surfactant concentration solution (35 wt. % of DODAC in water), it was found that the cooperativity of thermal transition was enhanced when the DSC scan was performed at slow scan rates. No significant differences were observed between scans at 1 or 2 ^oC/min thus, the thermal characterization of the surfactant samples was carried out at a scan rate of 2 ^oC/min.

Dioctadecyldimethyl ammonium bromide and chloride in water

Once a suitable scan rate is identified as discussed previously, the effect of counterions, bromide (Br^-) and chloride (Cl^-), on the thermal transitions of lamellar phases in water are discussed. In this section, solutions of dioctadecyldimethylammonium bromide (DODAB) and dioctadecyldimethylammonium chloride (DODAC) in water at various concentration ranging from 5 to 37.5 wt. % were scanned using DSC.

Figure 4.4 illustrates the thermograms of DODAB solutions from 5 to 37.5 wt. % of surfactant. The calculated transition temperature and enthalpy associated with the main phase transition under heating are summarized in Table 4.3. The thermal behavior of DODAB in water remains unchanged regardless of the amount of surfactant present in the system, as can be inferred by the thermograms (Figure 4.4) during the heating cycle and also during the cooling cycle. However, when the heating scans of the samples at various concentrations (Figure 4.4 (a)) are plotted in a stack, it masked another thermal transition (pre-transition) occurring under heating. In fact, this pre-transition was detected for all the samples and involved lower enthalpic energy compared to the main phase transition (T_m).

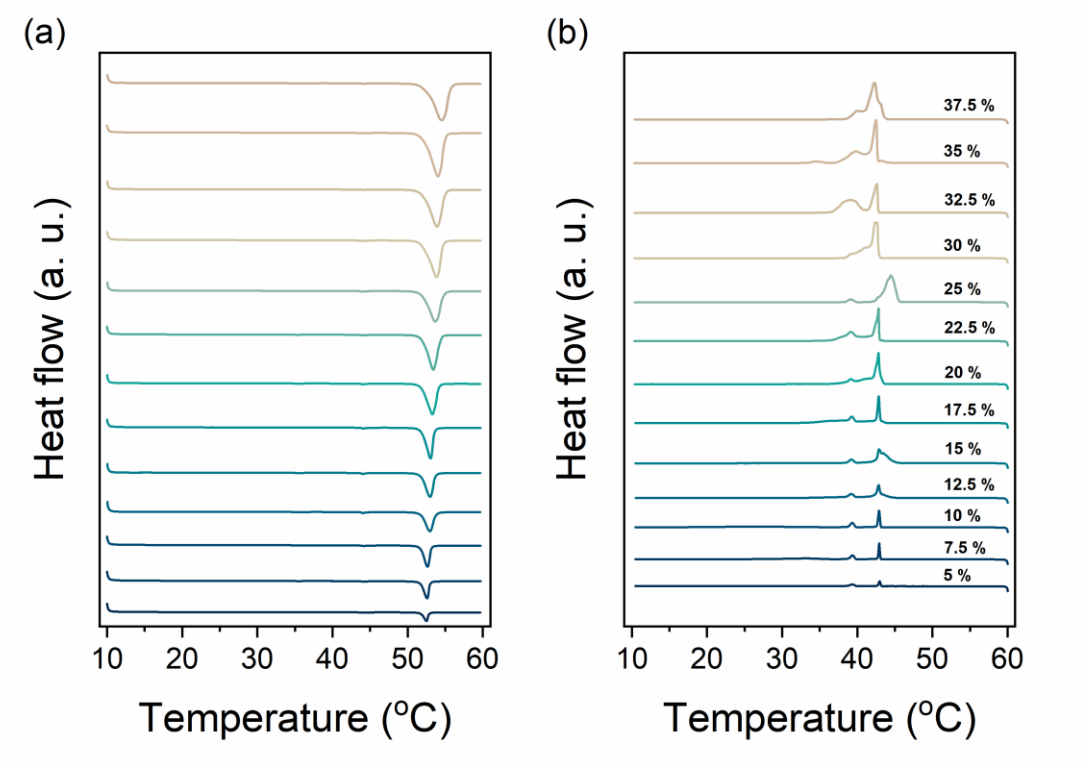

Figure 4.4 $DODA^+$ Br^- thermograms from 5 (bottom) to 37.5 wt. % of surfactant (top). On the left (a) is represented the heating scan, and on the right (b) is represented the cooling scan. The measurements were conducted from 10 to 60 °C, and back to 10 °C at 2 °C/min. The endothermic event corresponds to the downwards deflection.

Figure 4.5 shows the scans of two consecutive heating/cooling cycles from 10 to 60 °C and then back to 10 °C at 2 °C/min. Two thermal transitions both under heating and cooling cycles are identified. These transitions are present in the first and the second cycles, suggest no abnormalities in sample mixing. Upon heating, an energetically weak pre-transition (T_p*) at 44.1 °C with an associated enthalpy (ΔH) of 0.9 kJ mol^{-1} is determined, followed by the main phase transition (T_m) at 53.6 °C with an associated enthalpy of 108.2 kJ mol^{-1}. Under the cooling cycle, firstly, a main thermal transition (T_c) is detected at 44.4 °C with a ΔH of 79.3 kJ mol^{-1} and a second transition (T_c*) at 39.1 °C with a ΔH of 5.5 kJ mol^{-1}. These results are in agreement with the studies previously reported by Kodama et al. for a series of surfactants in water, including DODAB [14, 27]. They demonstrated that a gel phase exists in both stable and metastable states and that it could be tuned by cooling the sample to -20 °C, where the metastable gel phase was suppressed, and a stable coagel phase was

developed. After that thermal treatment of the sample, only one thermal transition under heating and cooling was detected, and it was identified as a stable coagel to a stable liquid crystalline phase transition. The lamellar packing of the DODAB at different temperatures was also examined, and it will be presented and discussed ahead in this chapter.

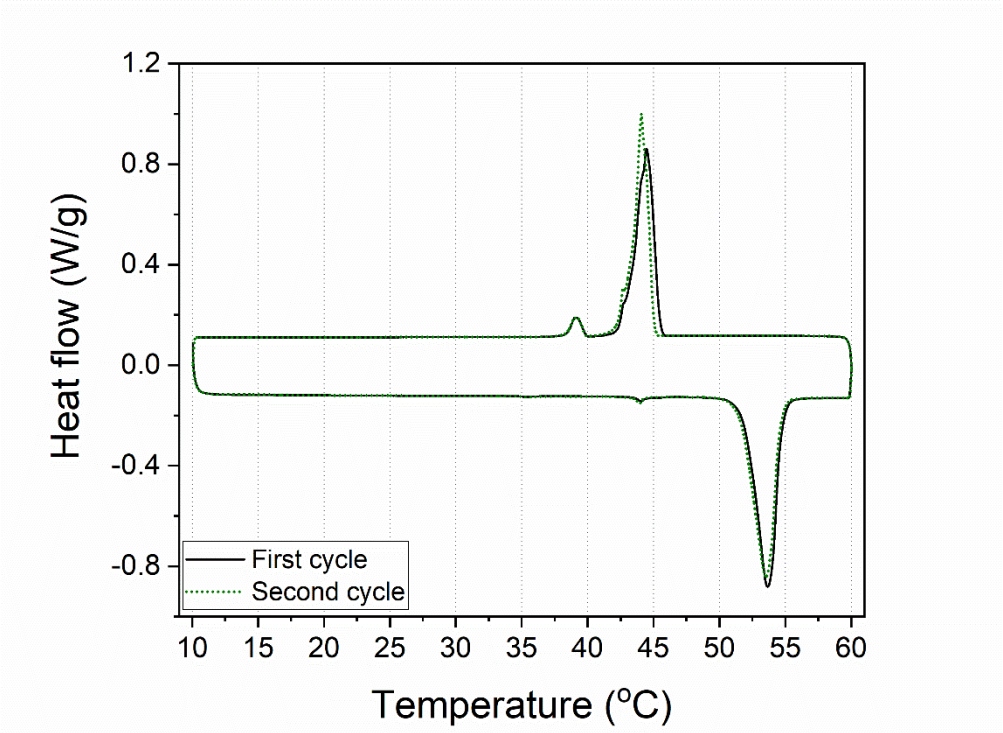

Figure 4.5 Two-cycle thermograms under heating and cooling of 25 wt. % DODAB in water. The full line corresponds to the first cycle and dotted line to the second cycle. The measurements were conducted from 10 to 60 °C, and back to 10 °C at 2 °C/min. The endothermic event corresponds to the downwards deflection.

A similar thermal study to look at the phase transitions of dioctadecyldimethylammonium chloride (DODAC) solutions with varying surfactant concentrations was conducted. Figure 4.6 shows the thermograms under heating (Figure 4.6 (a)) and cooling scan (Figure 4.6 (b)). DODAC solution shows only one thermal transition under heating, whereas DODAB displays two. However, thermal behavior under the cooling scan is rather different. DODAB displays two exothermic transformations under cooling, whereas DODAC shows a different trend where a second peak starts to develop with increasing concentration (Figure 4.6 (b)). From 5 to 15 wt. % of DODAC, one peak is detected and at some

concentrations, it is also possible to observe a small shoulder. From 15 wt. % of DODAC onwards, the intensity of that exothermic peak starts to decrease and a new peak developed. This phenomenon was also observed for DODAB under the cooling scan, however, it was detected for all the samples ranging from low to high surfactant concentration. In the case of DODAC, these two peaks appeared to have more significant effect when surfactant concentration was higher than 15 wt. %.

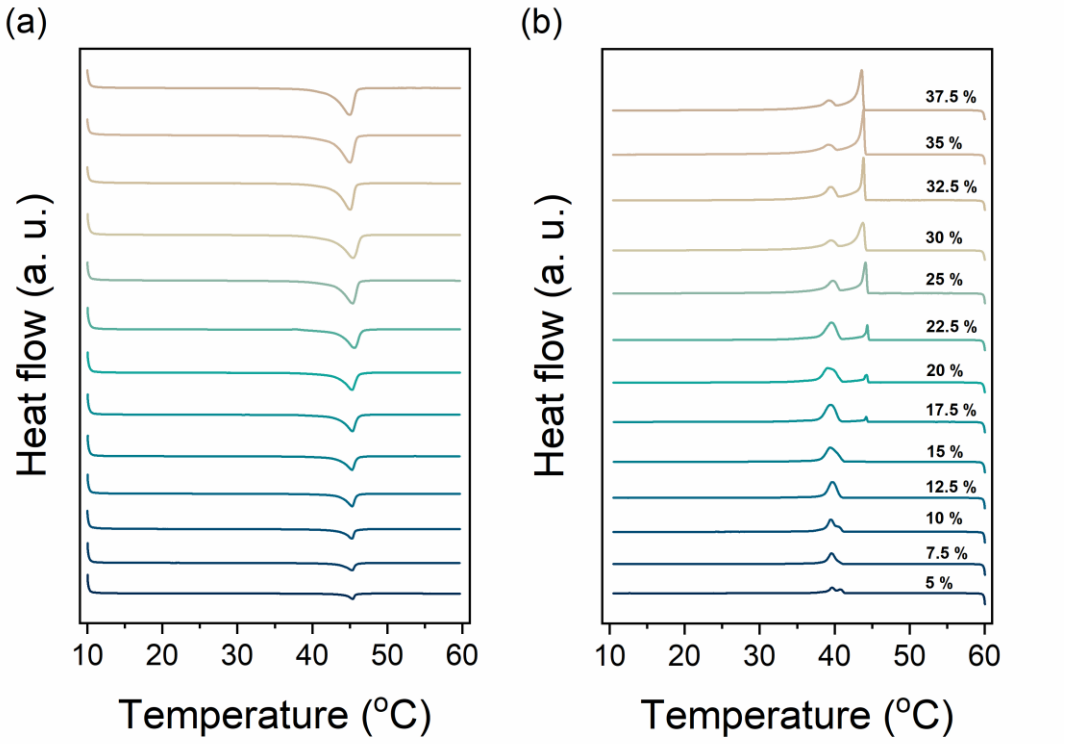

Figure 4.6 $DODA^+$ Cl^- thermograms from 5 (bottom) to 37.5 wt. % of surfactant (top). On the left (a) is represented the heating scan, and on the right (b) is represented the cooling scan. The measurements were conducted from 10 to 60 °C, and back to 10 °C at 2 °C/min. The endothermic event corresponds to the downwards deflection.

To better understand the nature of the thermal transitions, all the samples of DODAC in water were scanned for two consecutive heating/cooling cycles, as can be shown in Figure 4.7. The thermograms show hysteresis, which suggests that the samples did not experience extra thermal transformations upon a heating/cooling cycle. Unexpectedly, only one endothermal transformation under heating was detected at 45.1 ºC, with an associated enthalpy of 45.8 kJ mol^{-1}; and two overlapping exothermic peaks under cooling at 43.8 ºC with a total associated enthalpy of 52.0 kJ mol^{-1} were recorded. The values of the enthalpy of the endothermic and exothermic transitions were not significantly different suggesting that thermal transitions relating to similar phase transformation should be involved both under heating and cooling processes. Table 4.3 summarizes the main phase transition temperature and the enthalpy of melting during the heating cycle.

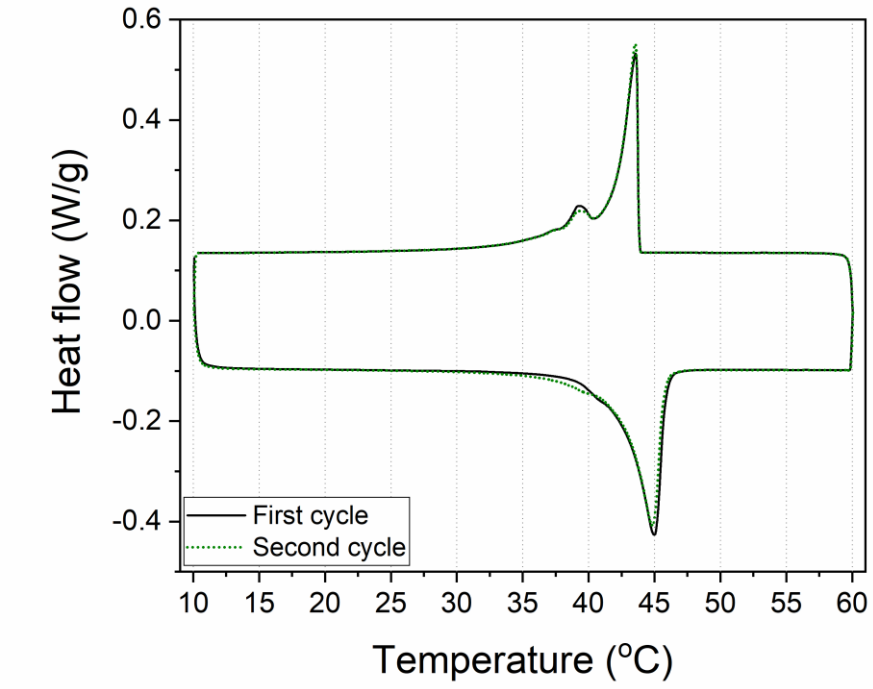

Figure 4.7 Two-cycle thermograms under heating and cooling of 35 wt. % of DODAC in water. The full line corresponds to the first cycle and dotted line to the second cycle. The measurements were conducted from 10 to 60 ºC, and back to 10 ºC at 2 ºC/min. The endothermic event corresponds to the downwards deflection.

Table 4.3 Normalized differential scanning calorimetry parameters of the DODAB and DODAC in water from 5 to 37.5 wt. % of surfactant.

	DODAB		**DODAC**	
Surfactant	Heating cycle		Heating cycle	
(wt. %)	**T_m (ºC)**	**ΔH_m (kJ mol^{-1})**	**T_m (ºC)**	**ΔH_m (kJ mol^{-1})**
5.0	52.5	63.6	45.4	40.2
7.5	52.6	94.7	45.3	42.5
10.0	52.6	96.7	45.3	39.2
12.5	53.0	97.2	45.3	41.4
15.0	53.0	98.0	45.3	42.9
17.5	53.0	95.4	45.3	46.0
20.0	53.3	109.6	45.3	46.0
22.5	53.4	113.0	45.6	46.7
25.0	53.6	108.2	45.4	45.9
30.0	53.8	99.6	45.4	47.5
32.5	53.9	102.3	45.1	44.3
35.0	54.0	109.3	45.1	45.8
37.5	54.5	102.7	45.0	44.4

These results (Table 4.3) show that the main phase transition temperature (T_m) and the enthalpy of melting (ΔH_m) were not dependent on the DODAC concentration. Under cooling, both surfactants in water displayed two exothermal transitions, and the phases at different temperatures will be determined in the next section. DODAB in water showed a higher T_m and associated ΔH_m when compared to DODAC. This happened because bromide is more polarizable than chloride, thus, there was less electrostatic repulsion between the head-group for DODAB. Therefore, the surfactant molecules pack closer to each other, which resulted in higher melting temperatures and required a large amount of energy for the melting transformation to occur.

The cross-polarizer micrographs show that these samples were anisotropic and DSC provided us with information on the thermal transformations upon heating and cooling. In order to determine the self-assembled structure of these surfactants in water, an X-ray scattering characterization over the heating and cooling scan was conducted. Consequently,

the packing structure of the surfactant systems can be determined using small and wide-angle X-ray scattering.

4.2.3 Surfactant self-assembled structure

According to DODAB and DODAC geometrical configuration, these surfactants are expected to pack into lamellar structures in water. Such structures can be in the gel phase (L_β), "solid" or in the liquid crystalline phase (L_α), "fluid" depending on the state of the surfactant alkyl chains. A system with the L_β phase is characterized by a short- and long-range packing order, whereas short-range disorder and a long-range order are found for a L_α phase. Simultaneous small and wide-angle X-ray scattering (SAXS and WAXS) characterization of the various phases detected in the previous DSC studies was conducted to determine the self-assembled structures observed for both DODAB and DODAC solutions.

Dioctadecyldimethyl ammonium bromide (DODAB)

SAXS/WAXS data was collected for DODAB solution at a temperature below the first endothermic peak (40 ^{o}C) and also from 47 to 58 ^{o}C using a 1 ^{o}C scan step, which covers the entire thermal transformations seen in the DSC studies. The pre-transition (T_p*) and T_m was determined at 44.1 and 53.6 ^{o}C, respectively. At 40 ^{o}C, two reflections were recorded (Figure 4.8 (a)), q_1 = 0.174 Å^{-1} and q_2 = 0.343 Å^{-1}. The q_2:q_1 peak ratio corresponds to a lamellar packing, with a corresponding interlamellar spacing (d_{sp}) of 36 Å. The WAXS profile (Figure 4.8 (b)) shows multiple crystalline peaks. The SAXS and WAXS profiles at 47 ^{o}C, which was above the T_p*, overlapped the profiles collected at 40 ^{o}C (Figure 4.8). As discussed previously, the hydrocarbon chains of the DODAB lamellae packed closer due to the electrostatic shielding provided by the counterion, which resulted in high melting temperature (53.6 ^{o}C). The two scattering profiles presented, in Figure 4.8, show that DODAB self-assembled into a lamellar gel structure below the main phase transition

temperature. Also, the pre-transition observed under heating did not correspond to a different lamellar structure. The SAXS profiles below and above the T_p* overlapped and displayed a lamellar structure with the same d_{sp} value. If visualized from the top, a gel phase is characterized by a hexagonal packing of the surfactant molecules (cf. section 2.2.1). This packing allows some level of rotational movement of the "frozen-like" hydrocarbon chains, and prevent the gel from packing closer and crystallizing [23]. Below the T_m of DODAB, several reflections at wide-angle were detected. These reflections suggest the existence of an orthorhombic packing with a chain-to-chain distance of 3.7 Å. The intensity of the peak corresponding to the orthorhombic packing detected at 47 °C was 4.5 times less intense compared to 40 °C. This was explained by the gain of free movement of the hydrocarbon chains on heating, allowing them to freely rotate and prevent the formation of closely packed structures (orthorhombic). These crystals coexisted in the gel phase because they are thermodynamically more stable than the hexagonally packed surfactant. These results suggest the existence of a gel phase in coexistence with crystals below the T_m, as reported by Schulz et al., and Kodama et al. [14, 19].

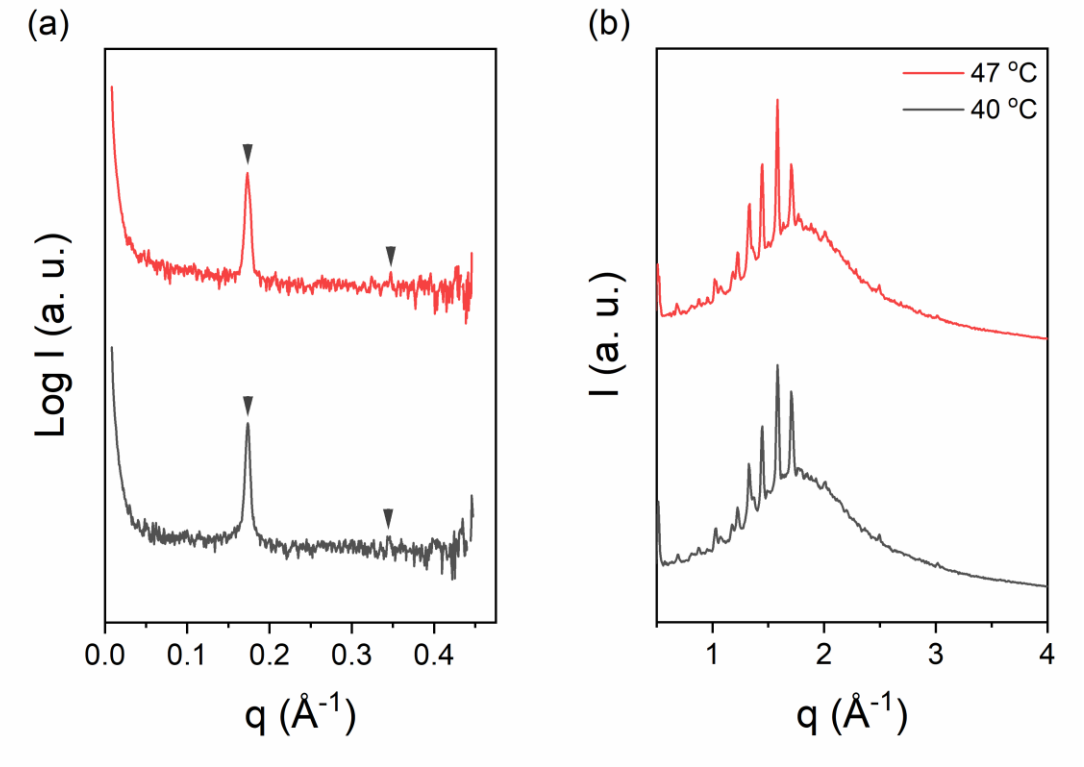

Figure 4.8 SAXS and WAXS profiles of 25 wt. % of DODAB in water under the heating cycle at 40 °C (grey; bottom profile) and 47 °C (red; top profile).

Figure 4.9 shows the SAXS (Figure 4.9 (a) and (c)) and WAXS (Figure 4.9 (b) and (d)) of 25 wt. % of DODAB in water during a heating/cooling cycle. The top two panels (Figure 4.9 (a) and (b)) show the SAXS and WAXS collected during the heating cycle. From top to bottom, the evolution of the packing structure with heating was presented. From 40 to 54 °C (Figure 4.9 (a)) the lamellar structure remained unchanged, showing a lamellar structure with a d_{sp} of 36 Å. Similarly, the WAXS profiles (Figure 4.9 (b)) exhibit crystalline peaks, showing the coexistence non-dispersed crystals and a gel phase below the T_m (53.6 °C). At 55 °C, the system undergoes the gel-to-liquid crystalline phase transition, and the development of other reflections occurred, and the reflections in the wide-angle regime were less intense (Figure 4.9 (a) and (b)), yet the peak of the L_β phase was more intense than the L_α phase peaks. When the system was equilibrated at 58 °C, reflections at q_1 = 0.050 Å^{-1}, q_2 = 0.101 Å^{-1}, q_3 = 0.151 Å^{-1} and q_4 = 0.203 Å^{-1}, and a peak broadening in the wide-angle regime allow to identify a L_α phase with a d_{sp} of 126 Å.

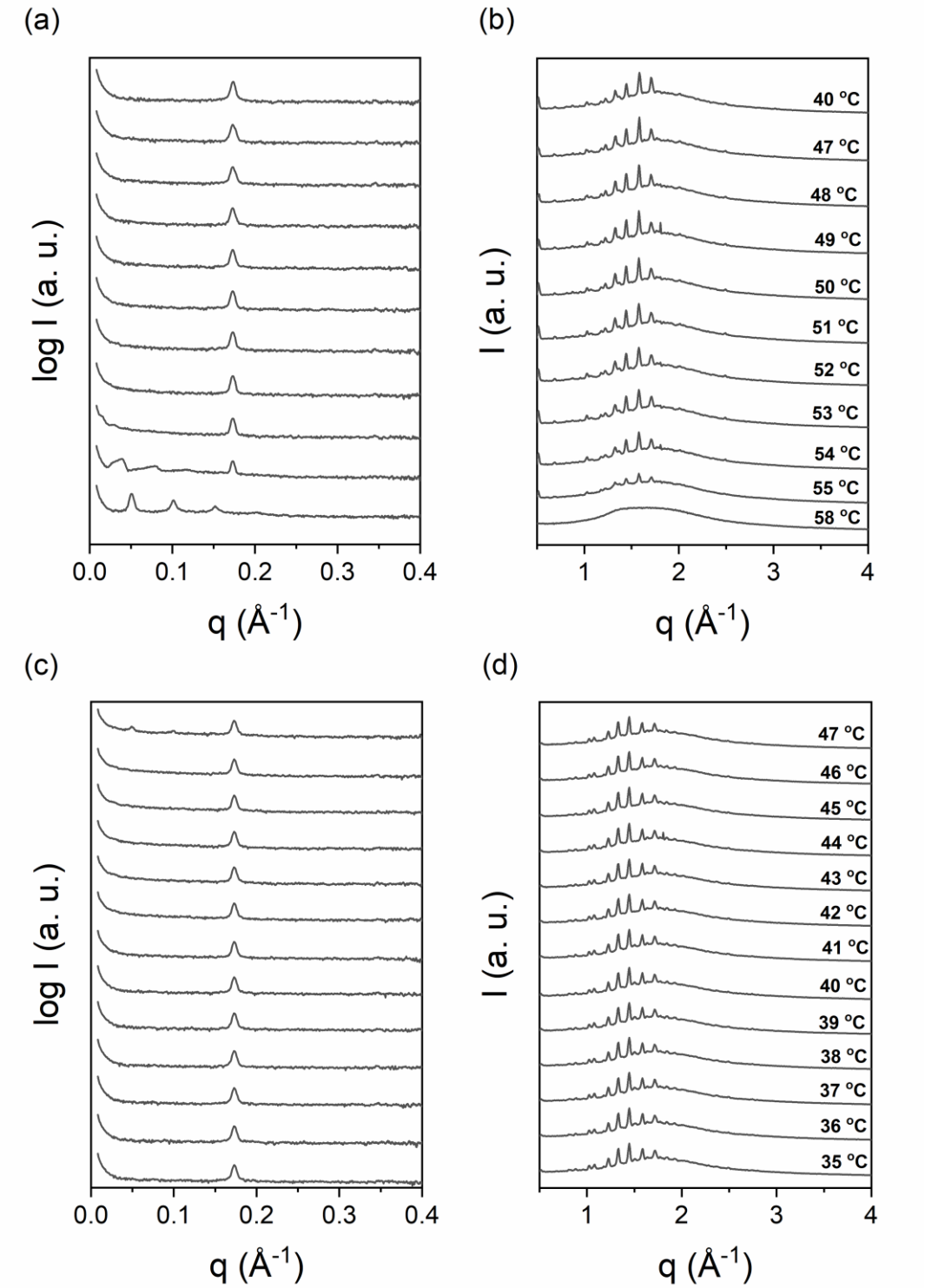

Figure 4.9 SAXS and WAXS profiles of 25 wt. % of DODAB in water under heating ((a) and (b)) and cooling ((c) and (d)) from top to bottom.

The behavior of the lamellar structure was also followed under cooling to determine the nature of the thermal transitions. The two bottom panels in Figure 4.9 show the SAXS (Figure 4.9 (c)) and WAXS (Figure 4.9 (d)) of 25 wt. % of DODAB in water under cooling. At 47 ^{o}C the alkyl chains of the DODAB bilayer started to "freeze", and the coexistence of the L_{β} and L_{α} phases are detected (Figure 4.10). A lamellar gel structure at temperatures below the T_c (44.4 ^{o}C) is determined with a d_{sp} of 36 Å. The DODAB hydrocarbon chains are composed of 18 carbons each, i.e., 36 carbons per non-polar domain in the lamellar structure. Consequently, using the Tanford's equation [28], the maximum thickness of the DODAB non-polar domain in the gel state can be found to be 48 Å. The experimental value of the DODAB, d_{sp}, in the gel phase was considerably smaller, which suggested the existence of lamellar structures with chains adopting a tilted and/or interdigitated configuration.

These results also show that DODAB in water undergoes a transition from the gel-to-liquid crystalline phase under heating, and the inverse is observed under cooling. However, this system did not show a single phase below the Krafft temperature, which results in the coexistence of non-dispersed crystals with a gel phase.

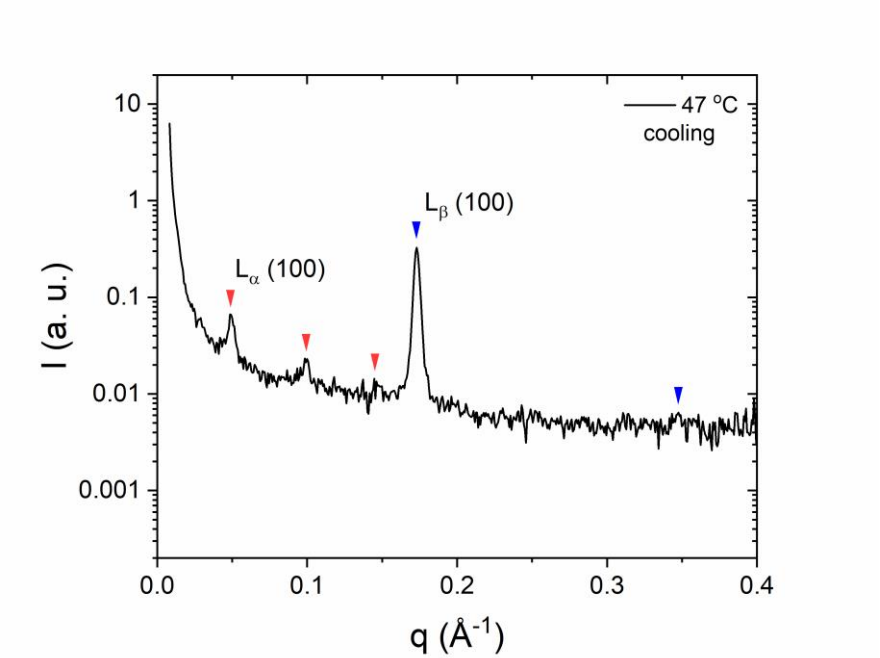

Figure 4.10 SAXS profile of 25 wt. % of DODAB in water at 47 °C under cooling showing the coexistence of two lamellar phases. The arrows represented lamellar reflections: in red the liquid crystalline phase and blue the gel phase.

Dioctadecyldimethyl ammonium chloride (DODAC)

The scan of DODAC using SAXS and WAXS over a temperature ramp was considered an essential step to investigate the self-assembled structure of the surfactant during the thermal transitions observed via DSC. The T_m of DODAC in water was determined to be 45.1 °C, and hence SAXS and WAXS data from 35 to 50 °C and back down to 35 °C using a 1 °C scan step were collected. The study aimed to elucidate the nature of the phase transitions that occur in DODAC solutions.

Figure 4.11 shows the SAXS (Figure 4.11 (a) and (c)) and WAXS (Figure 4.11 (b) and (d)) scans for 35 wt. % of DODAC in water during a heating/cooling cycle. The top two panels (Figure 4.11 (a) and (b)) show the SAXS and WAXS collected during the heating cycle. From top to bottom, the evolution of the packing structure with heating is presented. At 35 °C, the SAXS profile (Figure 4.11 (a)) shows a lamellar phase with a typical spacing of 69

Å. The WAXS profile displays a single and sharp reflection at q = 1.505 Å^{-1}, which corresponded to a distance of 4.2 Å. Therefore, these results indicate that DODAC self-assembled into a lamellar gel phase below the T_m.

The thermal scan of DODAC in water shows a broad endothermic peak under heating, thus, indicating that the melting of the chains occurred during a more extended time. These thermal transformations over time were tracked, and the gel-to-liquid crystalline transition phase was observed. Under heating, the development of two coexisting lamellar structures was observed starting from 40 ^{o}C, Figure 4.11 (a) - one with d_{sp} of 78 Å and a second with a d_{sp} of 69 Å (Figure 4.11 (b)). It can also be seen that the thinner lamellar structure, corresponding to the single gel phase existing below the T_m was three times more intense than the newly developed lamellar structure. The intensity of the peak corresponding to the thicker lamellar structure gradually became more intense until a temperature above the T_m was reached. With further increase in temperature, only one lamellar structure was identified at 47 ^{o}C with a d_{sp} of 84 Å, thus, revealing the L_α phase. The disordered fluid state of the alkyl chains of DODAC was easily confirmed by the disappearance of the sharp reflection in the wide-angle regime, and the development of a broad peak slightly shifted to lower q values during the heating scan (Figure 4.11 (b)). These scattering profiles indicate a transition of chains from a highly ordered gel phase, with a typical chain-to-chain spacing of 4.1-4.2 Å, to a fluid phase, liquid crystalline, with a 4.5-4.6 Å distance between alkyl chains. Therefore, small-angle X-ray diffraction profiles of the lamellar structures of the L_β and L_α phases can be confirmed and are in agreement with what was observed generally for these phases [29].

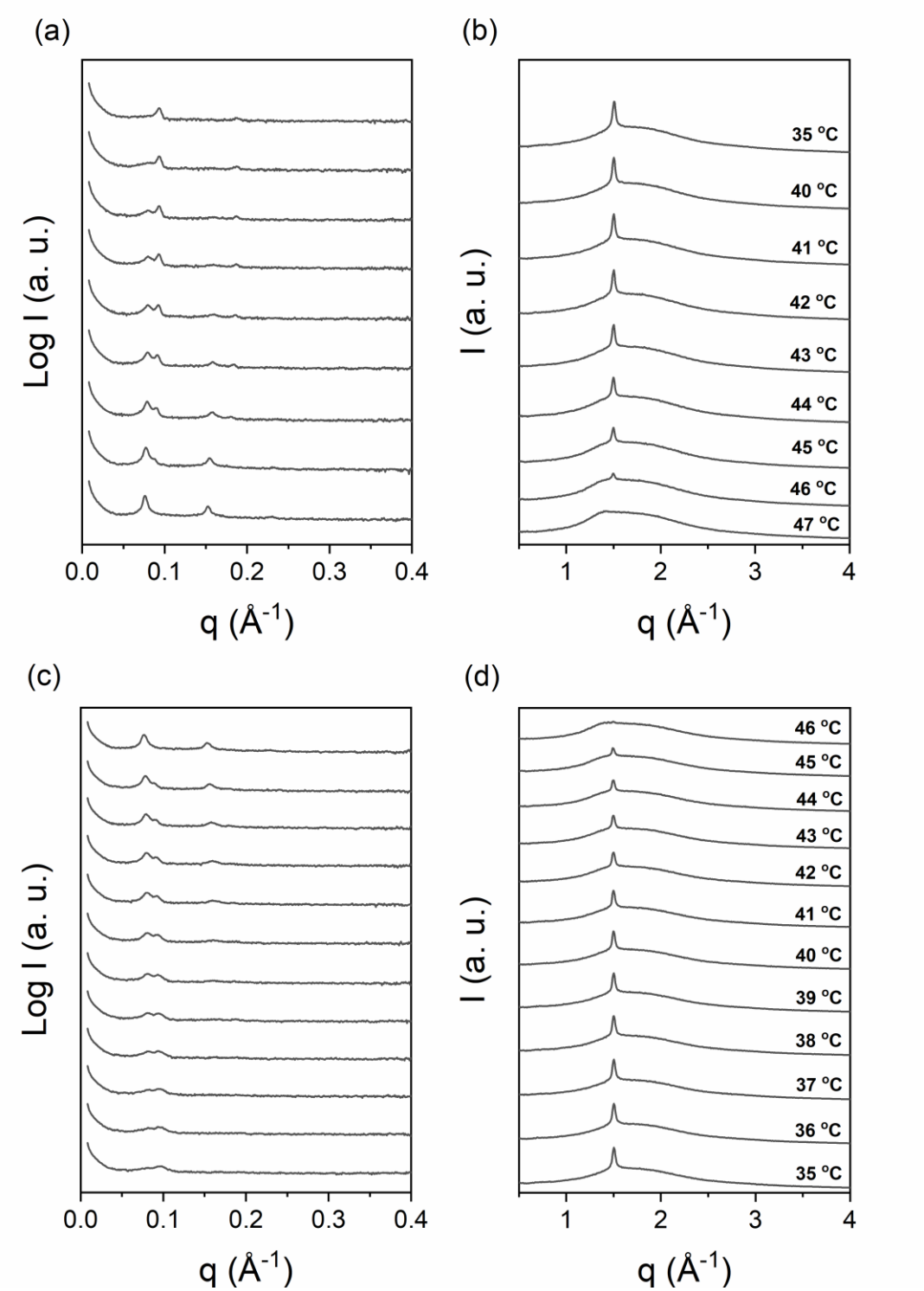

Figure 4.11 SAXS and WAXS profiles of 35 wt. % of DODAC in water under heating ((a) and (b)) and cooling ((c) and (d)) from top to bottom.

Under the cooling scan, the opposite behavior was observed. With decreasing temperature, DODAC experienced a L_α-L_β phase transition, with two coexisting gel phases appearing within the temperature gap where the transition occurred (45-35 ^oC), Figure 4.11 (c) and (d). At 35 ^oC, the lamellar system packed into a single, stable lamellar gel phase with a d_{sp} of 65 Å. These results demonstrate that no other phase coexisted. The existence of two overlapping thermal transitions is related to the existence of two lamellar gel structures coexisted during the L_β-L_α phase transition, and vice-versa.

The findings of SAXS and WAXS characterization of DODAB and DODAC in water is summarized in Table 4.4.

Table 4.4 Interlamellar spacing (d_{sp}) and associated phase transition of DODAB and DODAC in water at temperatures below and above their main phase transition temperature (T_m).

Surfactant	**Phase transition**	$d_{sp} < T_m$ **(Å)**	$d_{sp} > T_m$ **(Å)**
DODAB	L_β-L_α*	36	126
DODAC	L_β-L_α	69	84

* Hydrated crystals coexisting with the lamellar gel phase was found.

As discussed for DODAB in water, the maximum non-polar layer thickness, i.e., the DODAB and DODAC alkyl chain bilayer thickness should be 48 Å. For DODAC in water, the d_{sp} observed in both lamellar phases was larger than the maximum bilayer thickness. However, the d_{sp} value of DODAB in water, in the gel phase showed to be considerably smaller, which indicate rather thin bilayers (Table 4.4). Interestingly, both surfactants in water displayed a larger d_{sp} value in the liquid crystalline phase. The d_{sp} was expected to be higher in the gel phase since the alkyl chains should adopt an all-trans conformation and perpendicular to the interface. These findings suggest that a tilted and/or an interdigitated configuration may have been adopted by the alkyl chains in the gel phase, which resulted in thinner lamellar structures compared to the lamellar structures in the “fluid-like” state.

Quantification of the lamellar parameters

From the d_{sp} values presented in Table 4.4, the bilayer volume fraction (Φ_{bi}), bilayer thickness (d_{bi}) and area per surfactant molecule (a) of the DODAB and DODAC bilayers in water at temperatures below and above the main phase transition temperature (T_m) were calculated using the equations 3.5, 3.6 and 3.7. The results can be found in Table 4.5.

Table 4.5 Calculated values of the bilayer volume fraction (Φ_{bi}), bilayer thickness (d_{bi}) and area per surfactant molecule (a) of the 25 wt. % of the DODAB and 35 wt. % of the DODAC bilayers in water at temperatures below and above the main phase transition temperature (T_m).

		q (Å^{-1})	d_{sp} (Å)	Φ_{bi}	d_{bi} (Å)	a (Å^2)
< T_m	DODAB	0.174	36	0.240	9	237
	DODAC	0.093	69	0.349	24	85
> T_m	DODAB	0.050	126	0.240	30	68
	DODAC	0.075	84	0.349	29	70

Below the Krafft temperature, DODAB existed in the form of non-dispersed crystals and gel phase, whereas DODAC showed a single lamellar gel phase. Above the Krafft temperature, both surfactants displayed a large lamellar region, with DODAB developing two different lamellar mesophases at different DODAB concentrations [16, 19]. These results showed various new observations that can complement the previous phase studies conducted on these surfactants. Firstly, a rather small spacing (d_{sp} = 36 Å) was identified for DODAB below the T_m. This value was surprisingly small for a double-tailed surfactant with an 18-carbon alkyl chain and a large area per surfactant molecule was found in order to accommodate such lamellar structure (Table 4.5). Above the T_m, DODAB displayed a highly swollen lamellar phase (d_{sp} = 126 Å), an area per surfactant molecule of 68 Å^2, and a bilayer thickness of 30 Å which is in good agreement with the expected decrease of around 30% of the bilayer thickness from "solid-like" to "fluid-like" hydrocarbon state if the chains are in an all-trans conformation and perpendicular to the interface in the L_β phase [30, 31].

DODAC has shown a single lamellar phase below and above the T_m. This conclusion was drawn from the fact that the SAXS profiles only showed reflections of a single lamellar phase. In addition, below the T_m the simultaneously measured WAXS profile featured a single reflection peak characteristic of a chain-to-chain distance of 4.2 Å – corresponding to a gel phase. Above the T_m, the evolution of the sharp Bragg reflection peak to a broad peak at low *q* values was observed, thus, indicating a liquid crystalline phase with a chain-to-chain distance of 4.5 Å. These results showed that the DODAC in water experienced a transition from a single L_β phase to a single L_α phase at the Krafft temperature. More importantly, DODAC showed a lower T_m than DODAB, attributed to the fact that bromide is more polarizable than chloride, which resulted in a more densely packed DODAB bilayer with a smaller area per surfactant molecule (68 $Å^2$) in the L_α phase. These results suggested that there is a more favorable packing in the gel phase for DODAB thus resulting in higher T_m values.

The results from POM, DSC, SAXS and WAXS led us to choose DODAC in water as the surfactant system to carry out further investigations and address the main objective of this Ph.D. thesis, which is the design of a single and stable lamellar gel phase for hair-care applications.

4.2.4 Swelling of DODAC in water

In the previous section, it was shown that DODAC in water would be the most suitable surfactant to formulate a single and stable gel phase. However, the swelling of a gel phase can be challenging attributed to the "solid-like" state of the hydrocarbon chains, which resulted in kinetic limitations.

The findings on thermal behavior and stability of DODAC encouraged us to go further and investigate the behavior of DODAC in water, especially the swelling with water for surfactant concentrations that displays single and stable phase (> 33 wt. % [16]) down to a rather low surfactant concentration of 5 wt. %.

In this section, small and wide-angle X-ray scattering (SAXS and WAXS) measurements were carried out to determine the structural organization of the surfactant samples at temperatures below and above the gel-to-liquid crystalline phase transition (T_m).

The small and wide-angle X-ray scattering profiles collected at a temperature below and above the DODAC T_m, i.e., at 25 ^oC and 50 ^oC are presented in Figure A.4.3 (appendix). The analysis of the ratio of the peaks in the small angle regime combined with the scattering profiles at a wide-angle enabled to identify a single L_β-L_α phase transition for all the samples. Both L_β and L_α phase showed a shift of the first scattered peak towards lower q values with increasing amounts of water in the system, which suggests a progressive interlamellar swelling with the addition of water. With increasing amounts of water between the bilayers, the sharp reflection peak of the hydrocarbon chains in the "solid-state" in the wide-angle became progressively less intense, which is expected with the increase of the water layer thickness. Using Equations 3.5, 3.6 and 3.7, the values of the interlamellar spacing (d_{sp}), bilayer thickness (d_{bi}), polar layer thickness (d_w) and area per surfactant molecule (a) of DODAC bilayers in water at temperatures below (25 ^oC) and above (50 ^oC) the main phase transition temperature (T_m) were calculated and summarized in Table 4.6. Previously, it was verified that the sample with 35 wt. % of DODAC displayed a d_{sp} in the L_α phase larger than in the L_β phase. Here, the evaluation of the swelling of the gel and the liquid crystalline phases of DODAC in water is presented.

Table 4.6 Calculated values of the bilayer volume fraction (Φ_{bi}), the interlamellar spacing (d_{sp}), bilayer thickness (d_{bi}), polar layer thickness (d_w) and area per surfactant molecule (a) of DODAC bilayers in water at temperatures below (25 °C) and above (50 °C) the main phase transition temperature.

		25 °C				50 °C			
DODAC (wt. %)	Φ_{bi}	d_{sp} (Å)	d_{bi} (Å)	d_w (Å)	a (Å²)	d_{sp} (Å)	d_{bi} (Å)	d_w (Å)	a (Å²)
5.0	0.052	495	26	469	80	600	31	569	66
7.5	0.079	313	25	288	83	400	32	369	65
10.0	0.107	234	25	209	82	313	33	279	62
12.5	0.128	191	24	167	84	227	29	198	71
15.0	0.154	162	25	137	82	205	32	173	65
17.5	0.179	140	25	115	82	165	30	135	69
20.0	0.204	127	26	101	79	153	31	122	66
22.5	0.229	115	26	89	78	138	32	106	65
25.0	0.253	92	23	69	88	111	28	83	73
30.0	0.301	81	24	56	84	97	29	68	70
32.5	0.325	80	26	54	79	97	31	65	65
35.0	0.349	69	24	45	85	84	29	55	70
37.5	0.373	71	26	44	78	85	32	53	65

Figure 4.12 shows the swelling behavior of DODAC in water. The slope of the straight line of the swelling in the gel phase (Figure 4.12 (a)) was 0.97, and 1.00 for the liquid crystalline (Figure 4.12 (b)). The value of the slope of the two straight lines suggests that a one-dimensional swelling occurred because the interlamellar spacing is inversely proportional to the bilayer volume fraction, which demonstrates that the surfactant bilayer remains unaffected in the swelling process. The d_{sp} increased with the water content for both phases; this corresponded to an increased thickness of the water layers. This observation is generally expected for all the surfactants, the difference being that nonionic surfactants normally do not swell much. A large water uptake and swelling and can be understood from the electrostatic repulsions, mainly the counterion entropy [1, 3]. Therefore, only one phase, lamellar, was identified with no coexisting water phase, both below and above the T_m. These findings point to significant swelling of the DODAC in water in the gel phase, not only the liquid crystalline phase.

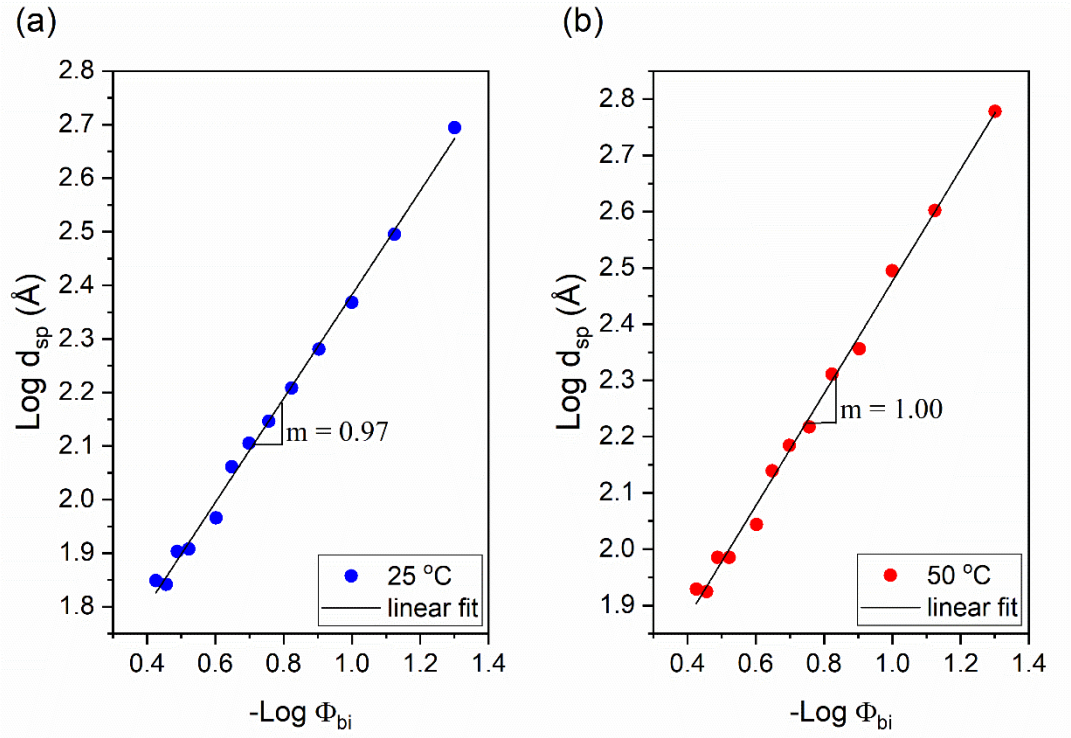

Figure 4.12 Plot of double logarithmic of interlamellar spacing (d_{sp}, Å) versus inverse bilayer volume fraction (Φ_{bi}) for DODAC in water at: (a) 25 °C and (b) 50 °C.

A comparison between the two phases revealed an interesting difference: d_{sp} values were larger for the liquid crystalline phase (Table 4.6 and Figure 4.13). On melting of the surfactant layers, there was a change in the conformation of the alkyl chains of the surfactant from an all-trans state to a more disordered one. This would lead to a shorter end-to-end distance of the alkyl chains and an increase in the effective cross-section area. If in the L_β phase, the hydrocarbon chains would adopt a conformation perpendicular to the interface, and higher d_{sp} values than those observed for the L_α phase are predicted. Thus, the gain in chain mobility in the L_α phase should result in Bragg reflections at higher q values, corresponding to smaller d_{sp} values. However, our results show an opposite behavior, which indicated an alternative chain packing or orientation in the L_β phase. Thus, suggesting that there is interdigitation or tilting of the hydrocarbon chains in the L_β phase or a combination of these. The existence of a mismatch between the cross-sectional areas of the hydrocarbon chains and the head-group may force the bilayer to change the conformation, avoiding unfavorable interactions [1].

The calculated average bilayer thickness at 50 ºC of 31 Å was in good agreement with the expected decrease of around 30% of the bilayer thickness from "solid-like" to "fluid-like" hydrocarbon state, if the chains are in an all-trans conformation and perpendicular to the interface in L_β phase [32]. Thus, the smaller bilayer thickness for the L_β compared to L_α phase, might be attributed to a significant tilting and/or interdigitation of the alkyl chains in the gel phase.

The underlying interactions for this phenomenon are not clear at this stage, but mismatches between the cross-sectional areas of the chains and the head-group could lead to variations in the critical packing parameter [33]. If the effect was ascribed to tilting alone, the tilting angle of a hydrocarbon chain must be approximately 59º, which seems to be an extremely large angle. Therefore, the existence of a tilted and interdigitated structure in the gel phase ($L_{\beta'\text{int}}$) is proposed. An alkyl chain with 18 carbons, fully stretched, perpendicular to the interface and in the "solid-like" state, was expected to measure around 24 Å in length. In the case of the DODAC bilayer, the thickness was predicted to be less than 48 Å, according to Tanford's equation [28].

The experimental results, displayed in Table 4.6, show that the bilayer of the gel phase was thinner than the bilayer of the liquid crystalline phase. These results suggest a non-perpendicular arrangement of the hydrocarbon chains or even interdigitation in the gel phase.

Figure 4.13 shows the lamellar swelling evolution for DODAC in water. In this graph the experimentally determined d_{sp} of the L_β and the L_α phase is compared with a theoretical maximum interlamellar spacing prediction (d_{max}), using Equation 4 [23]:

$$d_{max}\ (\text{Å}) = \frac{\sqrt{3} \times 10^{27}}{a^2 C R} \qquad (4)$$

where a is the chain-to-chain distance determined using wide-angle X-ray scattering as 4.2 Å and 4.6 Å for L_β and L_α phase, respectively [1, 21, 23, 34]. C is the surfactant concentration (mol/dm^3), and R is the Avogadro's constant.

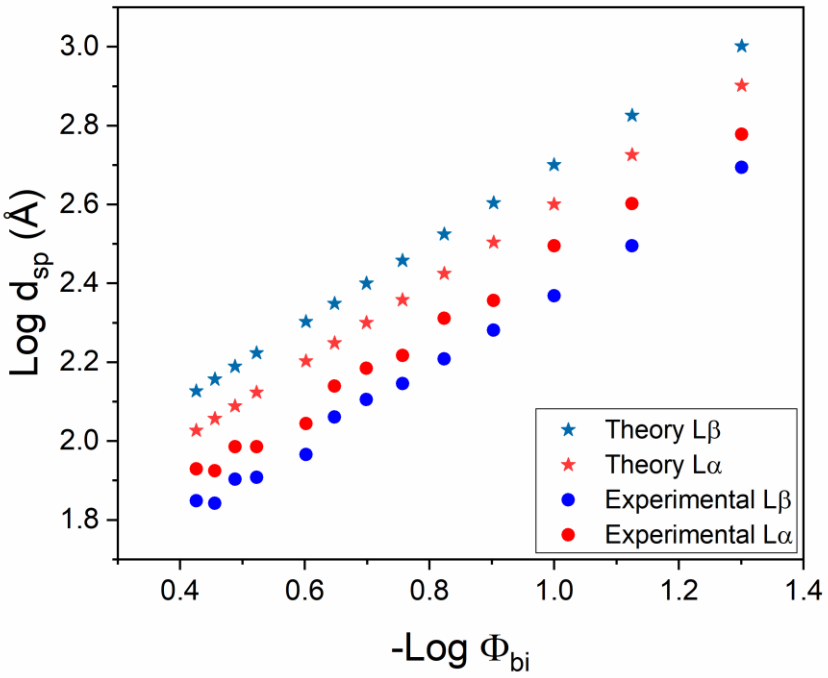

Figure 4.13 Double logarithmic plot of interlamellar spacing (d_{sp}, Å) versus inverse bilayer volume fraction (Φ_{bi}) for DODAC in water. Star symbol corresponds to the theoretical maximum interlamellar spacing (d_{max}, Å). Circle symbol corresponds to the experimental results calculated from SAXS and WAXS analysis of the L_β gel phase (25 °C, blue color) and L_α liquid crystalline phase (50 °C, red color).

By comparing the calculated d_{max} and the measured d_{sp}, two conclusions can be made. Firstly, the lamellar packing was not destroyed with water addition. This evidence suggests that the system was capable of taking up large amounts of water, corresponding to a progressive increase of the water layer thickness, due to mainly counterion entropy [3]. In addition, there was no significant effect on the T_m and the enthalpy of phase transition (ΔH_m) with increasing amounts of water, which supported the idea of the maintenance of the lamellar packing. Secondly, the measured d_{sp} values of the L_α phase were always larger than the L_β phase. As previously discussed, upon melting, the alkyl chains adopted a more disordered state. However, the results showed the opposite behavior, which suggests an alternative chain packing in the L_β phase. Regardless of the amount of water present in the system, the same trend was observed for all the samples. Therefore, a tilted and/or interdigitated structure in the gel phase was suggested.

4.3 Conclusions

The difference between bromide and chloride counterions in the lamellar bilayer structure of a double-tailed quaternary ammonium surfactant in water was evaluated. The observation and identification of the phases were conducted using cross-polarizers and the gel-to-liquid phase transition temperature (T_m) was studied using DSC. From the wide-angle X-ray scattering curves, the chain-chain distances were deduced and the values are as expected and in agreement with studies of different surfactants and lipid systems, larger above than below T_m [1, 23]. On the one hand, the small angle X-ray scattering data of DODAB showed the presence of non-dispersed crystals coexisting with the gel (L_β) phase below the T_m, and a transition to a liquid crystalline (L_α) phase above the T_m. On the other hand, a single transition from L_β to a single L_α phase for DODAC at a lower T_m was found. The experimental data suggests that DODAB had a more dense packing in the gel phase, and the conversion to a liquid crystalline phase occurred at a higher temperature and a higher energy cost when compared to DODAC and this attributed to bromide being more polarizable than chloride. Therefore, DODAC is suggested to formulate single and stable lamellar phases with a lower transition temperature.

The swelling behavior of DODAC in water showed a significant water uptake to the polar domain of the lamellar structure while keeping the lamellar integrity, which was characteristic of a one-dimensional swelling profile. Moreover, a larger repeat distance for the liquid crystalline than for the gel phase was found. With an orientation of the surfactant molecules perpendicular to the bilayers, the opposite situation was predicted. This indicates a considerable tilting and/or interdigitation of the alkyl chains in the L_β phase.

These results showed that DODAC formed a single lamellar phase in water, but more importantly, with a large swelling with water in the gel phase.

References

[1] D.F. Evans, H. Wennerström, The colloidal domain : where physics, chemistry, biology, and technology meet, 2nd ed. ed., New York : Wiley-VCH, 1999.1999.

[2] E.F. Marques, B.F.B. Silva, Surfactant Self-Assembly, in: T. Tadros (Ed.), *Encyclopedia of Colloid and Interface Science*, *Springer Berlin Heidelberg*, Berlin, Heidelberg, 2013, pp. 1202-1241.

[3] B. Kronberg, K. Holmberg, B. Lindman, Surface chemistry of surfactants and polymers, Chichester, West Sussex, United Kingdom : Wiley, 2014.2014.

[4] M. Goto, S. Ishida, Y. Ito, N. Tamai, H. Matsuki, S. Kaneshina, Thermotropic and Barotropic Phase Transitions of Dialkyldimethylammonium Bromide Bilayer Membranes: Effect of Chain Length, *Langmuir* 27(10) **2011** 5824-5831.

[5] M. Goto, Y. Ito, S. Ishida, N. Tamai, H. Matsuki, S. Kaneshina, Hydrostatic Pressure Reveals Bilayer Phase Behavior of Dioctadecyldimethylammonium Bromide and Chloride, *Langmuir* 27(5) **2011** 1592-1598.

[6] M. Kodama, M. Kuwabara, S. Seki, Thermal study of the interaction of crystalline surfactant with water; The dioctadecyldimethylammonium chloride-water system, *Thermochimica Acta* 50(1) **1981** 81-91.

[7] E. Feitosa, F.R. Alves, The role of counterion on the thermotropic phase behavior of DODAB and DODAC vesicles, *Chem. Phys. Lipids* 156(1–2) **2008** 13-16.

[8] F.R. Alves, W. Loh, Vesicles prepared with the complex salts dioctadecyldimethylammonium polyacrylates, *Journal of Colloid and Interface Science* 368(1) **2012** 292-300.

[9] P.C.A. Barreleiro, G. Olofsson, W. Brown, K. Edwards, N.M. Bonassi, E. Feitosa, Interaction of Octaethylene Glycol n-Dodecyl Monoether with Dioctadecyldimethylammonium Bromide and Chloride Vesicles, *Langmuir* 18(4) **2002** 1024-1029.

[10] C.R. Benatti, M.J. Tiera, E. Feitosa, G. Olofsson, Phase behavior of synthetic amphiphile vesicles investigated by calorimetry and fluorescence methods1Presented at the IUPAC International Symposium on Calorimetry and Chemical

Thermodynamics, April 5–9, 1998, Campinas, Brazil.1, *Thermochimica Acta* 328(1) **1999** 137-142.

[11] E. Feitosa, P.C.A. Barreleiro, G. Olofsson, Phase transition in dioctadecyldimethylammonium bromide and chloride vesicles prepared by different methods, *Chem. Phys. Lipids* 105(2) **2000** 201-213.

[12] H. Kunieda, K. Shinoda, Solution behavior of dialkyldimethylammonium chloride in water. Basic properties of antistatic fabric softeners, *The Journal of Physical Chemistry* 82(15) **1978** 1710-1714.

[13] K. Okuyama, Y. Soboi, N. Iijima, K. Hirabayashi, T. Kunitake, T. Kajiyama, Molecular and crystal-structure of the lipid-model amphiphile, dioctadecyldimethylammonium bromide monohydrate, *Bull. Chem. Soc. Jpn.* 61(5) **1988** 1485-1490.

[14] M. Kodama, T. Kunitake, S. Seki, Thermal characterization of the mode of phase transition in the dioctadecyldimethylammonium bromide-water system in relation to the stability of its gel phase, *The Journal of Physical Chemistry* 94(4) **1990** 1550-1554.

[15] R.G. Laughlin, R.L. Munyon, Y.C. Fu, A.J. Fehl, Physical Science of the Dioctadecyldimethylammonium Chloride Water-System. 1. Equilibrium Phase-Behavior, *Journal of Physical Chemistry* 94(6) **1990** 2546-2552.

[16] R.G. Laughlin, R.L. Munyon, Y.C. Fu, T.J. Emge, Physical science of the dioctadecyldimethylammonium chloride-water system. 2. Kinetic and mechanistic aspects, *Journal of Physical Chemistry* 95(9) **1991** 3852-3856.

[17] R.G. Laughlin, R.L. Munyon, J.L. Burns, T.W. Coffindaffer, Y. Talmon, Physical science of the dioctadecyldimethylammonium chloride-water system. 3. Colloidal aspects, *The Journal of Physical Chemistry* 96(1) **1992** 374-383.

[18] P.C. Schulz, J.E. Puig, The state of water in lyotropic liquid crystals, *Colloids and Surfaces A: Physicochemical and Engineering Aspects* 71(1) **1993** 83-90.

[19] P.C. Schulz, J.L. Rodriguez, F.A. Soltero-Martinez, J.E. Puig, Z.E. Proverbio, Phase behaviour of the dioctadecyldimethylammonium bromide water system, *J. Therm. Anal. Calorim.* 51(1) **1998** 49-62.

[20] P.S. Dubey, H. Srinivasan, V.K. Sharma, S. Mitra, V.G. Sakai, R. Mukhopadhyay, Dynamical Transitions and Diffusion Mechanism in DODAB Bilayer, *Scientific Reports* 8(1) **2018** 1862.

[21] R.A. Gonçalves, B. Lindman, M.G. Miguel, T. Iwata, Y.M. Lam, Elucidating the effect of additives on the alkyl chain packing of a double tail cationic surfactant, *Journal of Colloid and Interface Science* 528 **2018** 400-409.

[22] J.N. Israelachvili, 7 - Repulsive Steric Forces, Total Intermolecular Pair Potentials, and Liquid Structure, in: J.N. Israelachvili (Ed.), *Intermolecular and Surface Forces (Third Edition)*, *Academic Press*, San Diego, 2011, pp. 133-149.

[23] T. Iwata, Chapter 25 - Lamellar Gel Network, *Cosmetic Science and Technology*, *Elsevier*, Amsterdam, 2017, pp. 415-447.

[24] K. Holmberg, D.O. Shah, M.J. Schwuger, Handbook of applied surface and colloid chemistry, Chichester, England ; New York : Wiley, ©2002.2002.

[25] K. Holmberg, 21. Surfactant Liquid Crystals, *Handbook of Applied Surface and Colloid Chemistry*, *Volumes 1-2*, *John Wiley & Sons*2002.

[26] J.M. Sturtevant, Biochemical Applications of Differential Scanning Calorimetry, *Annual Review of Physical Chemistry* 38(1) **1987** 463-488.

[27] M. Kodama, S.z. Seki, Thermal study on the interaction of crystalline surfactant with water: Octadecyltrimethylammonium chloride-water system, *Journal of Colloid and Interface Science* 117(2) **1987** 485-496.

[28] C. Tanford, Micelle shape and size, *Journal of Physical Chemistry* 76(21) **1972** 3020-&.

[29] R. Tanasescu, M.A. Lanz, D. Mueller, S. Tassler, T. Ishikawa, R. Reiter, G. Brezesinski, A. Zumbuehl, Vesicle Origami and the Influence of Cholesterol on Lipid Packing, *Langmuir* 32(19) **2016** 4896-4903.

[30] J.N. Israelachvili, 15 - Solvation, Structural, and Hydration Forces, in: J.N. Israelachvili (Ed.), *Intermolecular and Surface Forces (Third Edition)*, *Academic Press*, San Diego, 2011, pp. 341-380.

[31] G.A. Ferreira, W. Loh, Structural Parameters of Lamellar Phases Formed by the Self-Assembly of Dialkyldimethylammonium Bromides in Aqueous Solution, *J. Braz. Chem. Soc.* 27(2) **2016** 392-+.

[32] J.N. Israelachvili, Intermolecular and surface forces. [electronic resource], Burlington, MA : Academic Press, 2011.

3rd ed.2011.

[33] T. Tadros, Encyclopedia of Colloid and Interface Science. [electronic resource], Berlin, Heidelberg : Springer Berlin Heidelberg : Imprint: Springer, 2013.2013.

[34] A.M. Percebom, L. Piculell, W. Loh, Polyion–Surfactant Ion Complex Salts Formed by a Random Anionic Copolyacid at Different Molar Ratios of Cationic Surfactant: Phase Behavior with Water and n-Alcohols, *The Journal of Physical Chemistry B* 116(8) **2012** 2376-2384.

Chapter 5*

Elucidating the effects of additives on the alkyl chain packing of a double tail cationic surfactant

The effects of additives on the surfactant packing are of fundamental interest and also important for applications such as in personal-care applications where formulations are complex mixtures. In our studies, a large number of additives was investigated and different types of physico-chemical behavior were observed. In this chapter, the results for fifteen additives showing distinctly different characteristics, namely "ureas", short-chain fatty acids, hydrotrope molecules and short- and intermediate-chain fatty alcohols are presented.

*This section has been published substantially as: Rui A. Gonçalves, B. Lindman, M. G. Miguel, T. Iwata and Yeng Ming Lam. *J Colloid Interface Sci.* 528 (**2018**) 400-409.

Rui A. Gonçalves, B. Lindman, M. G. Miguel, T. Iwata and Yeng Ming Lam. *J Colloid Interface Sci., to be submitted*.

5.1 Introduction

Amphiphilic molecules, such as surfactants and polar lipids, can be used for many novel health-care and personal-care applications as solution behavior modifiers [1-5]. Since the first investigations by Kunieda and Shinoda on the solution behavior of long di-alkyl quaternary ammonium salts [6], there has been much work done to understand the properties of the bilayer structures that dominate the phase diagrams of binary surfactant-water systems [3, 7-9]. Two types of lamellar structures are found for these systems – the lamellar gel phase (L_β) with highly ordered alkyl chains with little conformational freedom, and the lamellar liquid crystalline phase (L_α) characterized by liquid-like properties of the alkyl chains. Kunieda and Shinoda established the first phase diagram of dioctadecyldimethylammonium chloride (DODAC) in solution, and it was found that DODAC and other cationic surfactants with two long alkyl chains displayed relatively high stability as a two-phase solution, only splitting into two phases with the aid of centrifugation [6]. Laughlin et al. had also performed in-depth studies on the phase behavior of the DODAC-water system [10-12]. They observed the presence of a lamellar liquid crystalline phase coexisting with water at temperatures above 45 ^{o}C, with the surfactant molecules spontaneously self-assembling in bilayer structures. When the solution temperature exceeded 45 ^{o}C, they also identified a single and stable lamellar phase at a surfactant concentration of around 33 wt. % up to nearly 90 wt. %.

The phase behavior of ionic surfactants has enabled them to be potentially useful as drug carriers, wetting agents and anti-static agents [13]. Carmona-Ribeiro et al. explored the colloidal stability of DODAC vesicles in the presence of electrolytes and microspheres as well as the effect of pH [14-16]. It was found that the bilayers in the fluid-like phase can vary their shape depending on the conditions, whereas in the gel phase, the vesicles are more resistant to deformation. Furthermore, the vesicle instability can be related to the asymmetry of charge distribution. Feitosa et al. presented several studies on bilayer surfactant systems in solution and demonstrated variations in the gel-to-liquid transition temperature (T_m) for DODAC in solution when prepared between 37.5 and 48 ^{o}C [17-23]. Recently, Goto et al. confirmed that the gel-to-liquid crystal transition from a stable gel

phase (L_β) to a stable liquid crystalline phase (L_α) occurs at 40 ^oC [24, 25]. An increase in the phase complexity with the increasing number of carbons in the alkyl chains was also shown [24]. Kodama et al. investigated the concentrated regime and established a T_m of 46 ^oC for samples with 80-15 wt. % DODAC [26]. Although extensive work reports that DODAC forms lamellar structures, the phase identification is not consistent across various studies in the literature, indicating that phase stability and concentration effects remain ambiguous [18, 25, 26]. In addition, investigations on the DODAC-water phase behavior in the high concentration regime where only the pure lamellar phase exists, without any co-existence of a water phase, are largely lacking.

Double-chain cationic surfactant systems are expected to display many analogies with other double-chain amphiphile systems. Among these amphiphiles, phospholipids, and notably lecithin, have received a considerable amount of attention and are the most studied in this category. It is for example, well known that small polar additives with low vapor pressure may modulate the bilayer structure of this family of surfactants. Considerable work has been reported on the effect of small polar additives on liquid crystalline structures of lipids and block copolymers as well as on the stabilization of the amphiphilic aggregates [2-5, 27-29]. Costa-Balogh et al. demonstrated that the presence of urea has the effect of favoring the liquid crystalline structure of a series of double chain amphiphile systems in solution [2]. In their work, the phase behavior and the interlamellar spacing were determined, and a decrease in the T_m with urea addition to the lecithin system was demonstrated. Björklund et al. showed the potential of urocanic acid and pyrrolidone carboxylic acid in increasing the alkyl chain mobility, resulting in a T_m decrease which can be attributed to the additives residing in the non-polar domains of the lamellae [5]. Sparr and Wennerström also studied the interlamellar forces and thermodynamic properties of a phospholipid system and how it swells. The lamellar swelling was found to be entropically driven, and the presence of polar solutes resulted in a long-ranged interlamellar repulsion force [3, 30]. Such polar molecules act as stabilizers of the L_α phase, showing a higher swelling potential than the L_β phase [4].

Many studies have shown the effects of different molecules on lamellar structures and how their location affects the lamellar structure packing differently. Most of these studies were done on a zwitterionic amphiphile, lecithin, revealing different interactions between the additive and the polar head-group of the surfactant.

It is hypothesized that by perturbing the alkyl chain mobility with additives whilst keeping the lamellar integrity, a decrease in the T_m of the ternary DODAC-additive-water systems compared to the binary DODAC-water system should be observed. Since the currently used double-tail quaternary ammonium surfactants have relatively high T_m, limiting their applicability, and the effect of additives on the phase behavior has been little investigated, the aim of this chapter is to provide better understanding of how the molecular structure of the additives affect where they are located and their role in destabilizing the lamellar packing and hence reducing the L_β-L_α phase transition temperature. In view of this, the effect of four quite different families of additives namely "ureas", short-chain fatty acids, hydrotrope molecules, and short and intermediate-chain fatty alcohols on the DODAC lamellar structure is presented. In particular, the molecular organization and the effect of these additives on the gel-to-liquid phase transition in the high concentration regime are evaluated.

5.2 Results and discussion

5.2.1 The DODAC-additive-water ternary systems (visual observations)

In chapter four, single and stable lamellar phases of dioctadecyldimethyl ammonium chloride (DODAC) in water in comparison to dioctadecyldimethyl ammonium bromide (DODAB) were demonstrated. DODAC self-assembled into stable lamellar structures: a lamellar gel (L_β) phase below the Krafft temperature and a liquid crystalline (L_α) phase with hydrocarbon chains in a molten state above that temperature.

The relatively high gel-to-liquid crystalline (L_β-L_α) phase transition temperature (T_m) of DODAC, which has been a limiting factor for its usage, was the focus of the studies discussed in this chapter. The effect of additives on the lamellar DODAC-water system was evaluated and the impact on the T_m and self-assembled structure was investigated and discussed. The composition of the surfactant-water-additive mixtures studied is shown in the phase diagram in Figure 5.1. Mixtures of a fixed concentration of surfactant (35 wt. %) and increasing concentration of additive (5-20 wt. %) were prepared. The additives studied can be divided into four main categories: "ureas" which comprises of urea, methyl urea and dimethyl urea; short-chain fatty acids (SCFAs) corresponding to acetic, propionic, butyric and hexanoic acid, and sodium butyrate; hydrotrope molecules such as benzyl alcohol and phenoxyethanol; and fatty alcohols such as, butanol, hexanol, octanol, decanol and dodecanol. With these 15 different additives, a holistic understanding of the effect of additives on the lamellar packing of DODAC in water is provided.

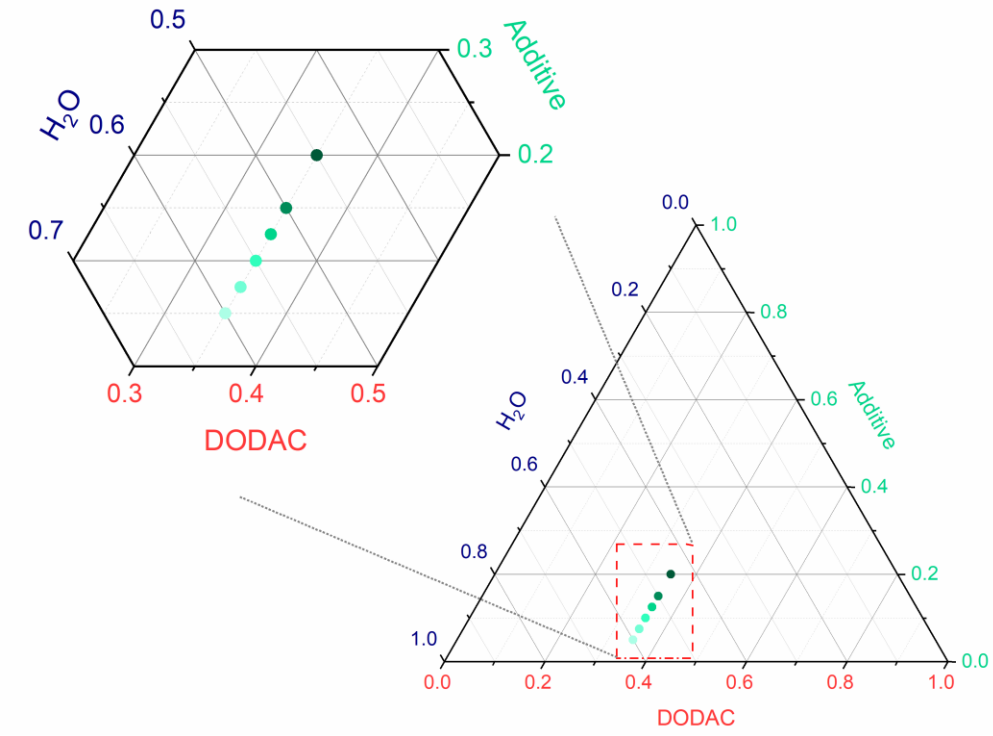

Figure 5.1 Schematic representation of the region of study in the phase diagram of DODAC-water-additive mixtures. A fixed concentration of 35 wt. % of DODAC and varying concentration from 5-20 wt. % of additive was chosen.

The preliminary phase identification of the ternary surfactant systems was conducted by naked-eye observations and complemented with the textures obtained using polarized optical microscopy (POM) at room temperature. Figure A.5.1 to Figure A.5.15 (appendix) show the photos of the surfactant mixtures in glass vials at room temperature. A naked eye inspection helped to understand the effects of the different additives on the DODAC bilayer.

The mixtures of DODAC with "ureas" resulted in macroscopically stable and strong gels (Figure A.5.1, Figure A.5.2 and Figure A.5.3) with no phase separation detected.

The SCFAs showed a different effect on the DODAC bilayer with acetic and propionic acid exhibiting a decrease in the sample turbidity with increasing concentration, Figure A.5.4 and Figure A.5.5. Whereas a similar trend was observed when butyric acid was added, excess amounts of this additive (20 wt. %) induced a phase-separated system, Figure A.5.6. On the other hand, its salt counterpart sodium butyrate revealed firm gels with a "milky" appearance over wide ranges of additive present in the mixture. The mixtures of DODAC with a six-carbon alkyl chain fatty acid - hexanoic acid, exhibited phase separation. For this group of SCFAs, the effect on the DODAC bilayer changes according to the polarity of the additive. The hydrophobic domain of these SCFAs is too short to induce self-assembly but still yielded dramatic effects when mixed with DODAC. One can regard them as "polar oils", especially those with longer alkyl chain such as propionic, butyric and hexanoic acid. It is suggested that when a SCFA with a two to five-carbon tail was added, it introduced a certain level of chain length mismatch which destabilizes the bilayer, thus resulting in increased system fluidity.

The mixtures with benzyl alcohol and phenoxyethanol, Figure A.5.9 and Figure A.5.10, considered as hydrotrope molecules, also displayed a similar behavior as the SCFAs when mixed with DODAC. The higher the concentration of the additive, the clearer the mixture became unless excess amounts of benzyl alcohol (20 wt. %) were added, which resulted in a phase separation (Figure A.5.9).

The addition of fatty alcohols to the DODAC bilayer resulted in distinctly different behavior depending on the hydrocarbon chain length. Butanol, which can be compared with butyric acid, did not induce phase separation of the surfactant system. Interestingly, even at excess amounts of butanol (20 wt. %), phase separation was not detected, in opposition to its fatty acid counterpart, Figure A.5.11. This may be attributed to a smaller polar domain, which facilitates favorable interactions to keep the lamellar structure. Hexanol showed phase separation, Figure A.5.12, suggesting a more complex phase behavior. As for hexanoic acid, the samples with 5, 7.5, and 10 wt. % of additive developed a phase-separated system, and increasing amounts of hexanol (12.5 and 15 wt. %) resulted in a gel with no evidence of phase separation. When the ratio of this intermediate-chain fatty alcohol per DODAC was three times higher, phase separation was detected. For both additives, hexanoic acid and hexanol, a single macroscopic phase developed only when the DODAC/additive molar ratio was 1:2. In the presence of excess amounts (20 wt. %), the mixture presented a clear phase on top, and a "milky" phase deposited on the bottom of the vial. These observations suggest that when there is three times more additive than surfactant, a transition to another phase may occur. Octanol displayed a less complex behavior when mixed with the surfactant, yet by visual inspection of the mixtures, Figure A.5.13, it was not possible to draw conclusions about the phase. The mixture presented a "milky" appearance in the presence of small amounts of octanol, it gradually became less turbid with the addition of more octanol, and a "milky" phase reappeared once the number of octanol molecules was 2.5 times higher than the number of DODAC molecules. These transitions on additive addition suggest a complex phase behavior, which will be further discussed using other characterization techniques. In the presence of long-chain fatty alcohols, such as decanol and dodecanol, no macroscopic phase separation was identified, and the mixtures became less fluid at room temperature. These two additives acted as a co-surfactant, which provided the lamellar system with a long hydrocarbon tail, thus promoting stronger hydrophobic interactions, and the hydroxyl group provided electrostatic screening. The combination of these contributed to a closer packing of the lamellar structure and consequently, a stronger gel phase.

Figure 5.2 shows the textures of the DODAC-additive-water mixtures observed under a cross-polarizers/polarized optical microscope (POM). In the previous chapter, the existence of textures observed under cross-polarizers when a sample is anisotropic was demonstrated. Specifically, Maltese crosses or oily streaks patterns, characteristic of lamellar structures were observed for all the surfactant systems at room temperature. Collectively, these observations and the naked eye inspection of the mixtures have shown that lamellar surfactant systems are present for all of the additives selected in this study.

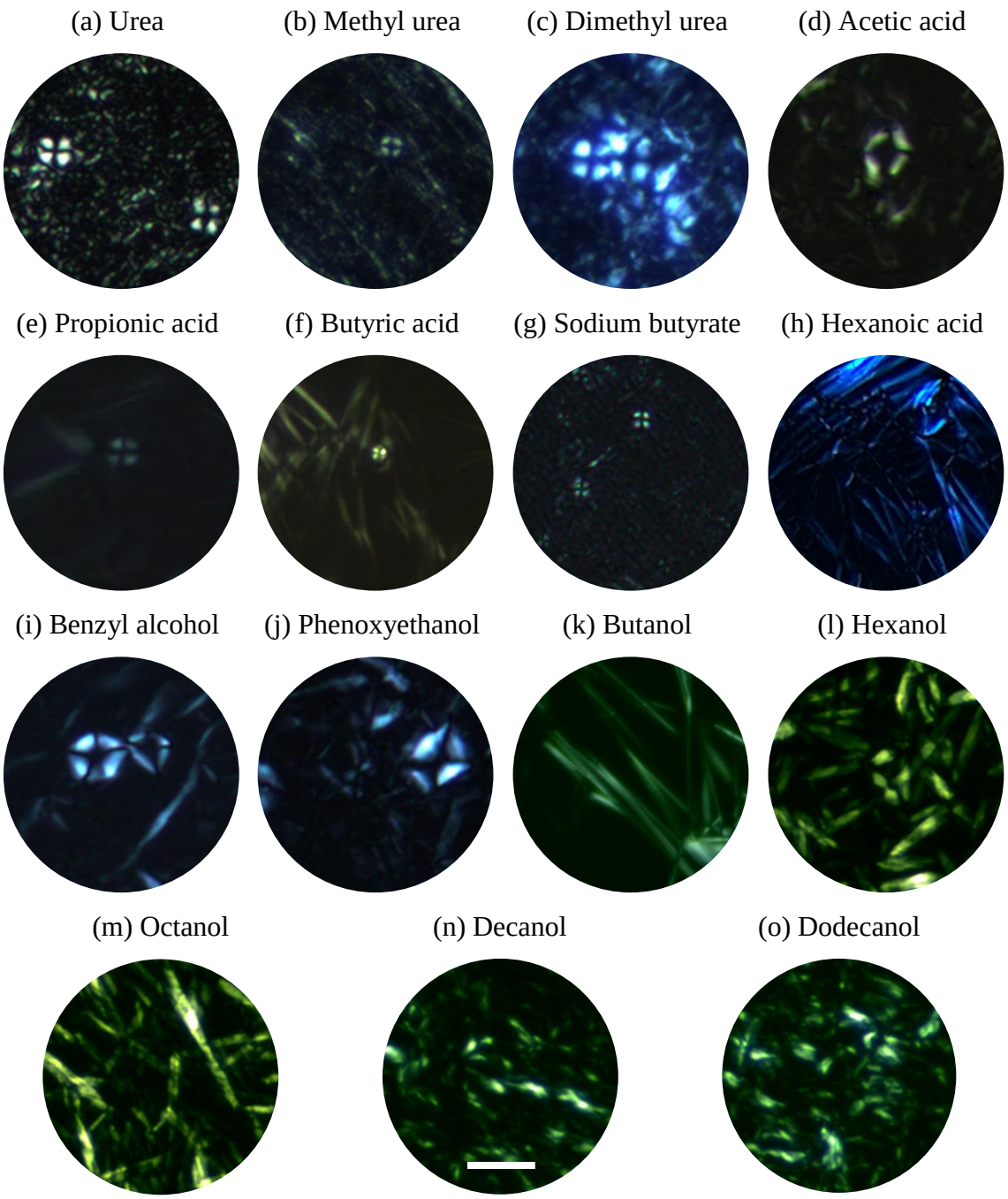

Figure 5.2 POM micrographs of the textures of DODAC in the presence of 5 wt. % of additive at 25 ^{o}C: (a) to (o) correspond to urea, methyl urea, Dimethyl urea, acetic acid, propionic acid, butyric acid, sodium butyrate, hexanoic acid, benzyl alcohol, phenoxyethanol, butanol, hexanol, octanol, decanol and dodecanol, respectively. The scale is 50 μm and applies to all micrographs.

5.2.2 Thermal behavior of DODAC in the presence of additives

The main phase transition temperatures (T_m) are expected to vary depending on the type and amount of additive present in the system. The type of additive and its intrinsic properties, such as melting point, density and partition coefficient, will determine their location in the lamellar structure.

The phase behavior of the ternary systems was examined using differential scanning calorimetry (DSC). A heating/cooling run at a scan rate of 2 ^oC/min was performed. The thermograms were recorded and plotted and they can be found in the appendix (Figure A.5.16 to Figure A.5.30). Previously, one thermal transition under heating and two transitions under cooling were observed for DODAC in water. Using a variable temperature SAXS experiment, which will be discussed later in this chapter, it is suggested the co-existence of two lamellar phases below the T_m. These phases have a similar melting point and therefore their transition peaks overlap and make their differentiation in the heating scan challenging. However, those two lamellar phases showed two independent exothermic peaks under cooling. In order to understand how phase transitions are affected by these additives, the thermal behavior was investigated using DSC.

Ureas

The presence of "ureas" with different polarities, namely urea, methyl urea, and dimethyl urea in the DODAC solutions did not show any significant change in the DSC thermograms, Figure A.5.16, Figure A.5.17 and Figure A.5.18 (appendix). Also, the thermograms do not display any relevant difference compared to the DODAC-water thermogram. One endothermic transformation under heating and two exothermic transformations on cooling were recorded. "Ureas" had a virtually insignificant effect on the transition temperature and enthalpy, Figure 5.3 and Table 5.1. The shape and intensity of the endothermic peaks are similar across the "ureas" samples. This points to an essentially ideal mixing in the water layers and little tendency for association with the surfactant alkyl chains. Though

urea is known as a chaotropic agent in other systems because its presence disrupts the local water structure, this effect on DODAC was not unexpected in view of the very weak amphiphilic character of urea [31]. However, with increasing amounts of dimethyl urea in the system, the second exothermic transition was getting progressively less intense and it was suppressed when the number of molecules of dimethyl urea was almost four times higher than that of the surfactant (Figure A.5.18). The calculated enthalpy of solution of dimethyl urea was determined to be 14 times lower than urea, and this is due to its structure and the reduced hydrogen bond formation in comparison to urea [32-34]. Therefore, it is suggested that dimethyl urea, which is a less polar molecule, may be located closer to the head-group/hydrocarbon interface which prevented the formation of a metastable gel phase under cooling. Nonetheless, the T_m and the enthalpy associated to the chain melting (ΔH_m) recorded for these three ternary systems was similar and did not significantly vary from the values recorded in the absence of additive as shown in Figure 5.3 and Table 5.1.

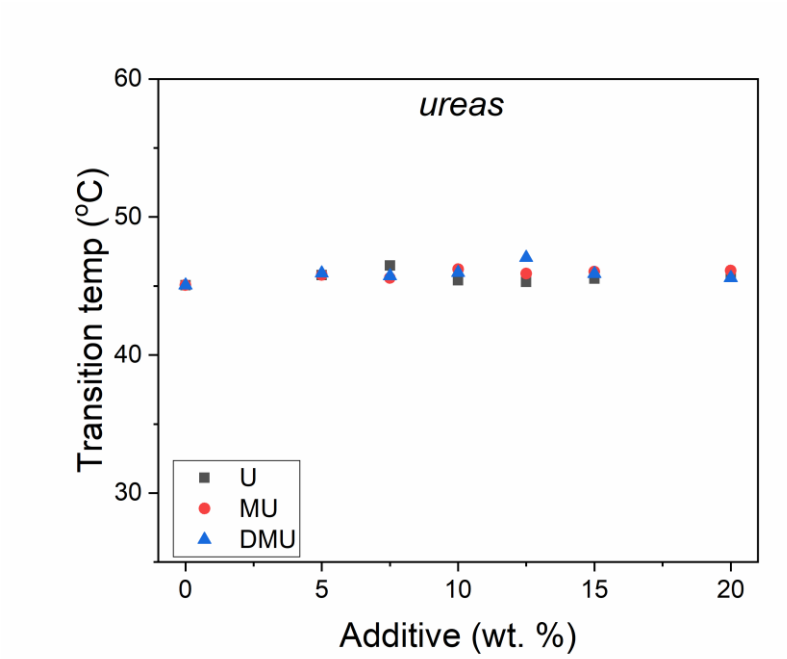

Figure 5.3 Effect of added additives on the main phase transition temperature of DODAC-*ureas*-water ternary systems. U- urea, MU- methyl urea, DMU- dimethyl urea.

Table 5.1 Values for the main phase transition temperature (T_m) and the normalized enthalpy of endothermic transition (ΔH_m) for DODAC-*ureas*-water ternary systems.

	Composition (wt. %)		Molar ratio	T_m	ΔH_m
	DODAC	additive	(S:A:W)	(°C)	(kJ mol^{-1})
DODAC in water	35.0	0.0	1:0.0:60	45.1	45.8
Urea	35.0	5.0	1:1.4:56	45.8	42.6
	35.0	7.5	1:2.1:53	46.5	42.0
	35.0	10.0	1:2.8:51	45.4	46.8
	35.0	12.5	1:3.5:49	45.3	39.8
	35.0	15.0	1:4.2:47	45.5	43.7
	35.0	20.0	1:5.6:42	45.7	44.7
Methyl urea	35.0	5.0	1:1.1:56	45.8	41.7
	35.0	7.5	1:1.7:53	45.6	37.5
	35.0	10.0	1:2.3:51	46.2	37.4
	35.0	12.5	1:2.8:49	45.9	36.7
	35.0	15.0	1:3.4:47	46.0	44.2
	35.0	20.0	1:4.5:42	46.1	39.9
Dimethyl urea	35.0	5.0	1:1.0:56	45.9	41.8
	35.0	7.5	1:1.4:53	45.7	32.1
	35.0	10.0	1:1.9:51	46.0	50.3
	35.0	12.5	1:2.4:49	47.1	35.2
	35.0	15.0	1:2.9:47	45.9	46.7
	35.0	20.0	1:3.8:42	45.6	43.5

Short-chain fatty acids

The thermograms of the heating and cooling cycles of the DODAC in the presence of short-chain fatty acids (SCFAs) are displayed in the appendix, Figure A.5.19 to Figure A.5.23. No significant variations in the shape of the endothermic peaks were found, but differences under cooling were observed. The second exothermic peak detected on cooling was progressively suppressed with the addition of SCFAs, resulting in a peak broadening. The two less polar SCFAs, butyric and hexanoic acid, appeared to be more effective in suppressing the second thermal transition even at small amounts of additive (<5 wt. %). These observations suggested that the presence of SCFAs increased the relative stability of the phase above the T_m. However, the thermograms of the mixtures of DODAC-sodium butyrate suggested a different behavior. The thermal transitions showed to be insensitive to the presence of sodium butyrate regardless of the amount added, Figure A.5.22.

Out of the five fatty acids used, only acetic acid is completely water-soluble and will to a large extent stay in the polar domain of the lamellar structure. Propionic acid, butyric acid, sodium butyrate, and hexanoic acid are also soluble in water but to a smaller extent [35].

All SCFAs displayed a striking ability to lower the transition temperature but sodium butyrate, which has a structure very similar to butyric acid behave differently, Figure 5.4. The DSC results showed that the effect was more pronounced with a decreased polarity of the SCFAs. It is also noted that with increasing amount of butyric and hexanoic acid, the transition became less well defined. With 20 wt. % of additive the L_β phase was not formed; instead, there was a macroscopic separation into two phases, the major phase being a clear liquid phase. Butyric acid addition resulted in a very significant decrease of T_m, as well as a decrease in the enthalpy change of the phase transition, Table 5.2. On top of this, a marked progressive broadening of the peak in DSC was observed. These results seem to indicate a strong interaction between DODAC and butyric acid, leading to a lowered stability of the gel phase. For sodium butyrate, the variation in the T_m was negligible (Figure 5.4 and Table 5.2). This additive provides the system with the weakly amphiphilic butyrate ions and the sodium ions. The butyrate ions, in excess for most of the samples, are expected to associate rather strongly with the cationic surfactant ions. The increased ionic strength is expected to affect the electrostatic interactions in the system leading to a complex phase behavior.

The average transition, T_m = 44.8 ^oC, remained virtually unchanged with the addition of sodium butyrate. As can be seen from Figure 5.4, the shape of the thermograms was similar to those when no additive was added to the surfactant in water. This was surprising given the nature of the additive, and the characterization of the self-assembled structures using X-rays will allow us to elucidate the effects of these short-chain fatty acids on the packing structure of DODAC.

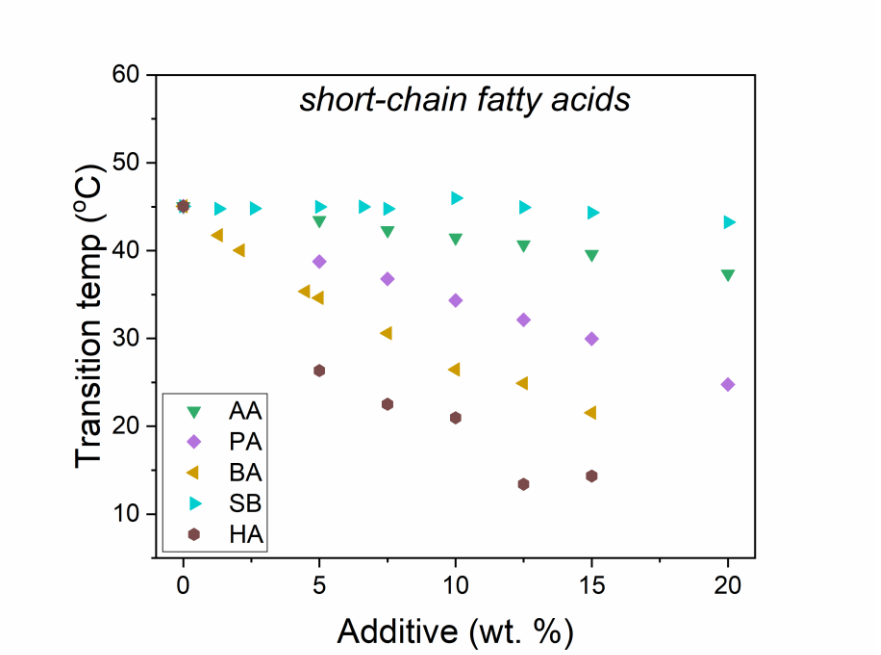

Figure 5.4 Effect of added additives on the main phase transition temperature of DODAC-*SCFAs*-water ternary systems. AA- acetic acid, PA- propionic acid, BA- butyric acid, SB- sodium butyrate, HA- hexanoic acid.

Table 5.2 Values for the main phase transition temperature (T_m) and the normalized enthalpy of endothermic transition (ΔH_m) for DODAC-*SCFAs*-water ternary systems.

	Composition (wt. %)		Molar ratio	T_m	ΔH_m
	DODAC	additive	(S:A:W)	(°C)	(kJ mol^{-1})
DODAC in water	35.0	0.0	1:0.0:60	45.1	45.8
Acetic acid	35.0	5.0	1:1.4:56	43.5	44.5
	35.0	7.5	1:2.1:53	42.3	43.6
	35.0	10.0	1:2.8:51	41.5	43.5
	35.0	12.5	1:3.5:49	40.7	42.9
	35.0	15.0	1:4.2:47	39.6	42.7
	35.0	20.0	1:5.6:42	37.4	41.1
Propionic acid	35.0	5.0	1:1.1:56	38.8	37.1
	35.0	7.5	1:1.7:53	36.8	39.8
	35.0	10.0	1:2.3:52	34.3	38.9
	35.0	12.5	1:2.9:49	32.1	40.8
	35.0	15.0	1:3.4:46	30.0	39.9
	35.0	20.0	1:4.5:42	24.7	43.0
Butyric acid	35.0	1.3	1:0.2:60	41.8	37.7
	35.0	2.1	1:0.4:58	40.0	36.2
	35.0	4.5	1:0.8:56	35.4	37.1
	35.0	5.0	1:1.0:56	34.6	31.6
	35.0	7.5	1:1.5:53	30.6	32.0
	35.0	10.0	1:1.9:51	26.5	28.6
	35.0	12.5	1:2.4:49	24.9	25.8
	35.0	15.0	1:2.9:47	21.6	25.1
	35.0	20.0	1:3.8:42	-*[1]	-*[1]
Sodium butyrate	35.0	1.3	1:0.2:60	44.8	41.1
	35.0	2.6	1:0.4:58	44.8	41.5
	35.0	5.0	1:0.8:56	45.0	43.0
	35.0	6.6	1:1.0:56	45.0	40.9
	35.0	7.5	1:1.1:53	44.8	43.8
	35.0	10.0	1:1.5:51	46.0	40.6
	35.0	12.5	1:1.9:49	44.9	41.8
	35.0	15.0	1:2.3:47	44.3	43.5
	35.0	20.0	1:3.1:42	43.2	42.3
Hexanoic acid	35.0	5.0	1:0.7:56	26.4	29.4
	35.0	7.5	1:1.1:54	22.5	24.1
	35.0	10.0	1:1.4:51	21.0	18.5
	35.0	12.5	1:1.8:49	13.4	4.6
	35.0	15.0	1:2.2:47	14.3	-*[2]
	35.0	20.0	1:2.9:42	-*[1]	-*[1]

*[1] Absence of thermal transition.

*[2] More than one thermal transition identified.

Hydrotrope molecules

The effect of the addition of two hydrotrope molecules, benzyl alcohol and phenoxyethanol, to the thermal behavior of DODAC was investigated, and the DSC thermograms are presented in the appendix, Figure A.5.24 and Figure A.5.25.

Hydrotropes are small and highly water-soluble molecules known to increase the solubility of surfactants in water greatly. As detected when SCFAs were added to the DODAC bilayer, the introduction of these two hydrotrope molecules resulted in a single endothermic and exothermic transitions under heating and cooling scans, respectively. Interestingly, benzyl alcohol and phenoxyethanol also suppressed the second exothermal transformation under cooling, which suggests to correspond to a metastable phase. Previously, it was discussed that a naked eye observation of the mixtures revealed a possibly more complex phase behavior, and indeed the thermograms (Figure A.5.24 and Figure A.5.25) display less defined thermal transitions. These observations indicate a high likelihood of a strong interaction between these two molecules and the cationic surfactant ions.

Figure 5.5 and Table 5.3 summarize the effects of these molecules on the main phase transition temperature and the enthalpy of phase transition. Both additives gave a progressive decrease in the T_m values, but different trends for the ΔH_m were recorded. On the one hand, the calculated enthalpy associated with the phase transformation did not significantly vary with increasing concentration of benzyl alcohol in the system. However, the peak broadened which increased the area under the peak, thus high values of ΔH_m were measured. Under heating, the thermal peaks were less defined as they were for the SCFAs mixtures, and excess amounts of benzyl alcohol (20 wt. %) led the mixture to phase separate. These observations suggested that a more complex ternary system was formed in the presence of benzyl alcohol. On the other hand, the addition of phenoxyethanol resulted in macroscopically stable gels at room temperature, and thermograms with defined transitions were recorded. The T_m and ΔH_m were found to decrease with additive addition, which suggested that phenoxyethanol facilitated the thermal transformation. However, at high concentrations of this additive (20 wt. %), even though the mixture was in a

macroscopically homogeneous phase, the DSC scan suggested more than one thermal transition. These were detected when the number of molecules of phenoxyethanol was two times higher than the surfactant molecules. For that reason, the phase transformation displayed higher ΔH_m, thus suggesting a transition with an enthalpic loss.

A more detailed packing structure characterization of these systems will be presented to investigate this complex phase behavior, but it is suggested that these two additives have a markedly different effect on the phase behavior of DODAC, thus resulting in a remarkable decrease of the main transition temperature.

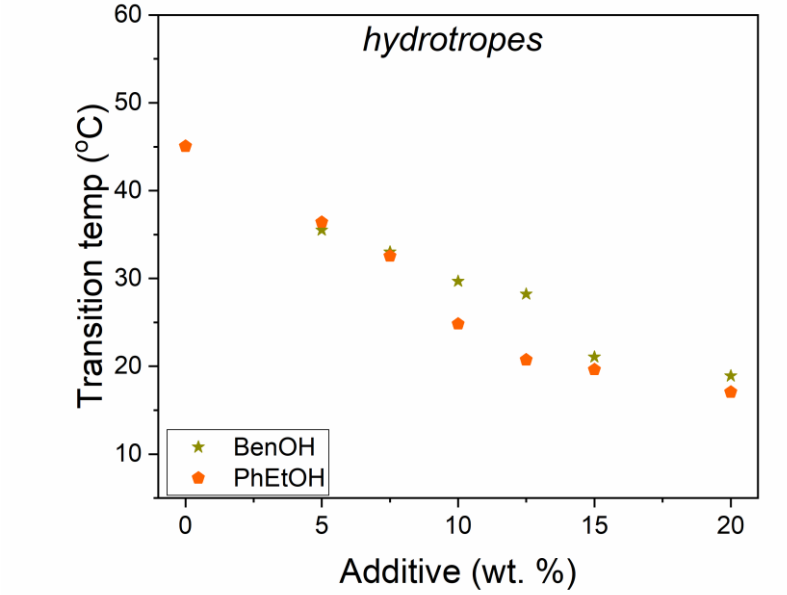

Figure 5.5 Effect of added additives on the main phase transition temperature of DODAC-*hydrotropes*-water ternary systems. BenOH- benzyl alcohol, PhEtOH- phenoxyethanol.

Table 5.3 Values for the main phase transition temperature (T_m) and the normalized enthalpy of endothermic transition (ΔH_m) for DODAC-*hydrotropes*-water ternary systems.

	Composition (wt. %)		Molar ratio	T_m	ΔH_m
	DODAC	additive	(S:A:W)	(°C)	(kJ mol^{-1})
DODAC in water	35.0	0.0	1:0.0:60	45.1	45.8
Benzyl alcohol	35.0	5.0	1:0.9:56	35.5	35.7
	35.0	7.5	1:1.2:53	33.0	34.3
	35.0	10.0	1:1.6:51	29.7	34.5
	35.0	12.5	1:1.9:49	28.2	34.4
	35.0	15.0	1:2.3:47	21.1	31.5
	35.0	20.0	1:3.1:43	18.9	31.4
Phenoxyethanol	35.0	5.0	1:0.6:56	36.4	46.6
	35.0	7.5	1:0.9:53	32.6	35.2
	35.0	10.0	1:1.2:52	24.8	25.7
	35.0	12.5	1:1.5:49	20.7	19.8
	35.0	15.0	1:1.8:46	19.6	19.6
	35.0	20.0	1:2.4:42	17.1	27.1

Fatty alcohols

The effects of the presence of fatty alcohols in the surfactant bilayer were studied with five alcohols of different polarities. Two short-chain length alcohols: butanol and hexanol, and three intermediate-chain length alcohols: octanol, decanol, and dodecanol were tested. The latter two are expected to act as co-surfactants and strengthen the gel phase, whereas butanol, hexanol, and octanol, would operate as "perturbing agent" molecules, thus resulting in a decrease in the main transition temperature. Figure A.5.26 to Figure A.5.30 (appendix) show the heating/cooling thermal scans for DODAC in the presence of different alcohols. The variation of the T_m with alcohol inclusion in the system is presented in Figure 5.6, and the calculated thermodynamic parameters associated with the thermal transition are summarized in Table 5.4. One endothermic transition and one exothermic transition were detected in the heating and cooling scans, respectively. Occasionally, particular mixtures displayed a different thermal scan, and those will be discussed later. As expected, the observations vary depending on the polarity of these aliphatic organic molecules, but the addition of alcohol helped to suppress the second exothermic thermal transition detected for the DODAC in water under cooling, which suggested a transition to a more stable phase.

Butanol, hexanol and octanol show a great ability to decrease the T_m, but a complex phase behavior is indicated from the thermograms obtained when hexanol and octanol are present. Butanol effectively shifted the T_m to lower temperatures and suppressed the metastable phase. These results point to the increased relative stability of the phase above the T_m, as observed for butyric acid.

The addition of hexanol resulted in a phase separation (cf. above), similarly to its fatty acid counterpart. When the surfactant-to-hexanol ratio was higher than 1:1.3, the mixture showed a complex thermal behavior accompanied by the development of a second thermal transition. The six-carbon alkyl chain of this alcohol may not be long enough to penetrate the surfactant bilayer and align parallel to the DODAC tails to create cohesive and strong hydrophobic interactions. Instead, they perturbed the bilayer packing resulting in phase separation. An even more pronounced effect was found when excess amounts (20 wt. %) of hexanol were added to the surfactant, which produced a separation into two distinct phases.

Octanol, when present in small amounts (5 wt. %), had a significant influence on the T_m, but this amount was not enough to suppress the metastable phase. This result suggests that at least one molecule of octanol per molecule of surfactant was needed to accomplish a stable phase transition. With successive inclusion of octanol to the bilayer, the development of more than one thermal transition and peak broadening were detected, which suggested that the system evolved to a metastable phase.

The mixtures of DODAC and decanol in water did not show any macroscopic phase separation, but an increased viscosity at room temperature was noticed. Despite a progressive inclusion of alcohol to the surfactant bilayer, the T_m remained unaffected. This observation can be explained because decanol was acting as a co-surfactant. The ten-carbon alkyl chain was long enough to penetrate the bilayer core, and the hydroxyl group provided electrostatic shielding, which ultimately did not change the T_m. Likewise, when the ratio of surfactant-to-decanol was smaller than unity, the thermogram shows a second thermal transformation, which is suppressed with increasing amounts in the lamellar system.

However, if the amount of decanol was double the amount of surfactant, the thermogram shows two distinct thermal transition peaks, Figure A.5.29. It is suggested that two phases may have developed: one surfactant-rich phase, and another alcohol-rich phase, which resulted in T_m at distinctively different temperatures.

Dodecanol produced somewhat similar effects on the DODAC lamellar structure as decanol. However, with this 12-carbon aliphatic alcohol, the T_m was found to increase. Dodecanol acted as a co-surfactant, thus causing more densely packed bilayer structures, which requires more energy for the thermal transition to occur (Table 5.4). The hydroxyl group resides at the water/hydrocarbon interface that reduces the head-group electrostatics, and concurrently the long hydrocarbon tails associated rather strongly via hydrophobic interactions, which stabilizes the gel phase.

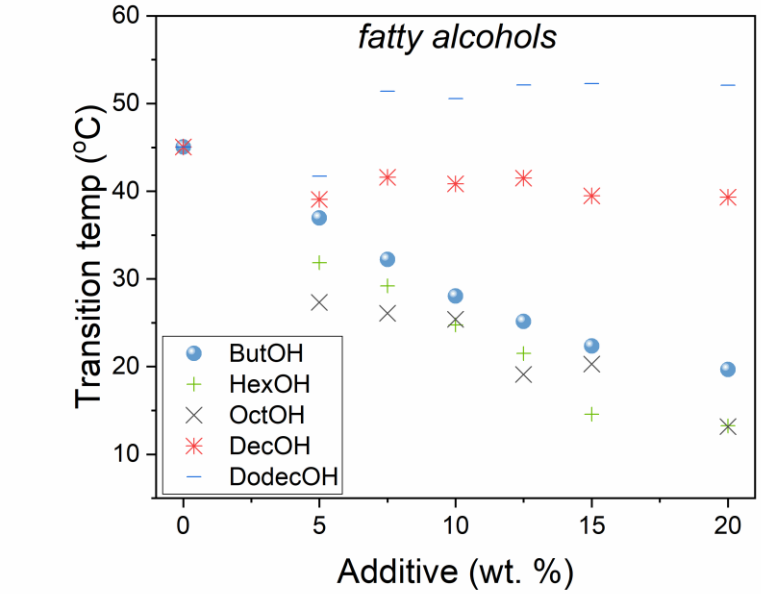

Figure 5.6 Effect of added additives on the main phase transition temperature of DODAC-*fatty alcohols*-water ternary systems. ButOH- butanol, HexOH- hexanol, OctOH- octanol, DecOH- decanol, DodecOH- dodecanol.

Table 5.4 Values for the main phase transition temperature (T_m) and the normalized enthalpy of endothermic transition (ΔH_m) for DODAC-*fatty alcohols*-water ternary systems.

	Composition (wt. %)		Molar ratio	T_m	ΔH_m
	DODAC	additive	(S:A:W)	(°C)	(kJ mol^{-1})
DODAC in water	35.0	0.0	1:0.0:60	45.1	45.8
Butanol	35.0	5.0	1:1.2:56	37.0	43.9
	35.0	7.5	1:1.7:54	32.2	42.9
	35.0	10.0	1:2.3:51	28.1	42.6
	35.0	12.5	1:2.8:49	25.2	37.9
	35.0	15.0	1:3.4:47	22.4	32.2
	35.0	20.0	1:4.6:42	19.7	24.6
Hexanol	35.0	5.0	1:0.8:56	31.9	30.9
	35.0	7.5	1:1.3:54	29.2	22.0
	35.0	10.0	1:1.6:51	24.8	11.1
	35.0	12.5	1:2.1:49	21.5	-*[1]
	35.0	15.0	1:2.5:47	14.6	-*[1]
	35.0	20.0	1:3.3:42	13.3	-*[1]
Octanol	35.0	5.0	1:0.7:56	27.3	-*[1]
	35.0	7.5	1:1.0:54	26.1	-*[1]
	35.0	10.0	1:1.3:51	25.4	-*[1]
	35.0	12.5	1:1.7:50	19.1	-*[1]
	35.0	15.0	1:1.9:47	20.3	-*[1]
	35.0	20.0	1:2.6:42	13.2	-*[1]
Decanol	35.0	5.0	1:0.5:56	39.1	39.7
	35.0	7.5	1:0.8:54	41.6	32.3
	35.0	10.0	1:1.1:51	40.8	31.9
	35.0	12.5	1:1.3:49	41.5	31.2
	35.0	15.0	1:1.6:47	39.5	31.9
	35.0	20.0	1:2.1:42	39.3	-*[1]
Dodecanol	35.0	5.0	1:0.5:56	41.7	55.0
	35.0	7.5	1:0.7:54	51.4	48.3
	35.0	10.0	1:0.9:51	50.6	50.6
	35.0	12.5	1:1.1:49	52.1	54.2
	35.0	15.0	1:1.3:47	52.3	60.5
	35.0	20.0	1:1.8:43	52.1	65.6

*[1] More than one thermal transition identified.

The presence of urea molecules of different polarities in the DODAC lamellar structure did not show any significant effect on the main phase transition temperature and the enthalpy of thermal transition, although excess amounts of the least polar of the "ureas", dimethyl urea, suppressed the metastable thermal transition observed under cooling.

On the one hand, the incorporation of acetic acid, propionic acid, butyric acid, benzyl alcohol, phenoxyethanol, and butanol was shown to be more effective in lowering the T_m without developing unexpected thermal transitions. On the other hand, hexanoic acid,

hexanol and octanol developed a complex phase behavior resulting in less defined thermal transitions. Also, decanol and dodecanol take part in both the polar and the non-polar domains, as co-surfactants, thus resulting in stable and strong gels with a more organized bilayer structure, showing higher transition temperatures when compared with short-chain fatty acids, hydrotropes, and butanol.

In conclusion, the addition of additives that partition into both polar and non-polar domains showed an increase in the mobility of the hydrocarbon chains, which led to a depression in the melting point of the phase. The systems which displayed a single thermal transition are believed to experience a phase transition of the same nature as the one observed in the DODAC-water system, a gel-to-liquid crystalline phase transition.

To understand the underlying surfactant molecular packing in the presence of additives, small and wide-angle X-ray scattering studies were performed. The results and discussion of this characterization are presented in the next section.

5.2.3 Self-assembled structures in the presence of additives

Similar to the binary surfactant system, the self-assembled structure of the ternary systems was investigated using small and wide-angle X-ray scattering (SAXS and WAXS) at temperatures below and above the T_m, determined and presented in the previous section. The SAXS and WAXS profiles are presented in Figure A.5.31 to Figure A.5.45 (appendix). A careful interpretation and analysis of the scattering data resulted in the identification of the packing structure of the ternary surfactant systems and the characterization of the lamellar systems through the determination of the interlamellar spacing (d_{sp}), the bilayer thickness (d_{bi}) and the area per surfactant molecule (a) as summarized in Table 5.5 to Table 5.8.

Ureas

The presence of "ureas" with different polarities did not give any significant change in the main phase transition temperature, which indicated that the nature of the thermal transitions observed without and with these additives is of the same nature.

From the SAXS profiles (Figure A.5.31, Figure A.5.32 and Figure A.5.33) and based on the relation between observed Bragg peak positions, it was confirmed that all the mixtures self-assembled into a lamellar aggregate below and above the T_m. Moreover, the simultaneous collection of WAXS profiles provided evidence of a gel-to-liquid crystalline phase transition (L_β-L_α) occurring at the T_m. The analyses of the SAXS results are summarized in Table 5.5.

Figure 5.7 shows that the different types of urea molecules affect the d_{sp}, d_{bi}, and a, in the L_β and L_α phases, similarly. The effect of urea molecules on the spacing and thus on the surfactant layer thickness was found to be negligible. These results are in good agreement with the urea effect on the T_m, where no significant variation was observed. The small variations in the bilayer thickness corresponded to small variations in the area per surfactant molecule. Due to their polar properties, "ureas" are solubilized into the polar domain, which means that the reduction in water content is accompanied by the addition of a polar compound, resulting in no significant d_{sp} variation.

To this effect, urea promotes enlargement of the interlamellar spacing as it is known to weaken the hydrophobic interactions [36]. However, this weakening was not strong enough to disturb the surfactant layer thickness but reduced the values of the interfacial area per surfactant molecule. Ergo, the results of the interlamellar spacing at a temperature above the T_m show a slight decrease, especially in the case of methyl urea and dimethyl urea. Two factors may contribute to this observation: firstly, the two urea molecules become less polar with an increase in temperature and secondly, the volume occupied by water is larger than for urea, and such difference is even more pronounced in the case of dimethyl urea. Therefore, urea molecules can also promote interlamellar contraction in L_α state. This

contraction is consistent with the gain in chain movement, which promotes disorder, thus resulting in a decrease of the d_{sp}.

The chaotropic effect of urea in water, related to changes in the intermolecular water bonding, has been extensively studied [36-38]. Since urea distributes itself in the aqueous domain, the impact on chain packing is small; hence urea molecules had virtually no effect on the bilayer thickness, or the area per surfactant molecule, Table 5.5. In addition, the L_β and L_α phases were observed to behave in similar ways when these urea molecules were present in the system. Though the trend for the effects of "ureas" was generally the same, the results suggest that their polarity plays an important role in their location in the lamellar structure and therefore their ability to decrease the main phase transition temperature.

Table 5.5 Values for the bilayer volume fraction (Φ_{bi}), the interlamellar spacing (d_{sp}), the bilayer thickness (d_{bi}) and the area per surfactant molecule (a) for DODAC-*ureas*-water ternary systems below and above the T_m.

Additive	wt. % additive	Molar ratio (S:A:W)	Φ_{bi}	Below T_m			Above T_m			Transition	T_m (°C)
				d_{sp} (Å)	d_{bi} (Å)	a (Å^2)	d_{sp} (Å)	d_{bi} (Å)	a (Å^2)		
	0.0	1:0.0:60	0.349	69	24	85	84	29	70	L_β-L_α	45.1
Urea	5.0	1:1.4:56	0.360	78	28	80	93	34	67	L_β-L_α	45.8
	7.5	1:2.1:53	0.366	75	27	83	88	32	70	L_β-L_α	46.5
	10.0	1:2.8:51	0.372	75	28	81	90	34	67	L_β-L_α	45.4
	12.5	1:3.5:49	0.378	74	28	81	89	34	67	L_β-L_α	45.3
	15.0	1:4.2:47	0.385	74	28	79	89	34	65	L_β-L_α	45.5
	20.0	1:5.6:42	0.399	75	30	75	90	36	63	L_β-L_α	45.7
Methyl urea	5.0	1:1.1:56	0.359	73	26	85	85	31	73	L_β-L_α	45.8
	7.5	1:1.7:53	0.365	76	28	81	89	32	70	L_β-L_α	45.6
	10.0	1:2.3:51	0.371	83	31	73	97	36	63	L_β-L_α	46.2
	12.5	1:2.8:49	0.377	75	28	80	86	32	70	L_β-L_α	45.9
	15.0	1:3.4:47	0.384	71	27	83	81	31	73	L_β-L_α	46.0
	20.0	1:4.5:42	0.397	69	28	82	78	31	73	L_β-L_α	46.1
Dimethyl urea	5.0	1:1.0:56	0.359	77	28	81	87	31	72	L_β-L_α	45.9
	7.5	1:1.4:53	0.365	75	27	82	87	32	71	L_β-L_α	45.7
	10.0	1:1.9:51	0.370	75	28	81	87	32	70	L_β-L_α	46.0
	12.5	1:2.4:49	0.376	77	29	77	88	33	68	L_β-L_α	47.1
	15.0	1:2.9:47	0.383	73	28	81	81	31	72	L_β-L_α	45.9
	20.0	1:3.8:42	0.396	71	28	81	78	31	73	L_β-L_α	45.6

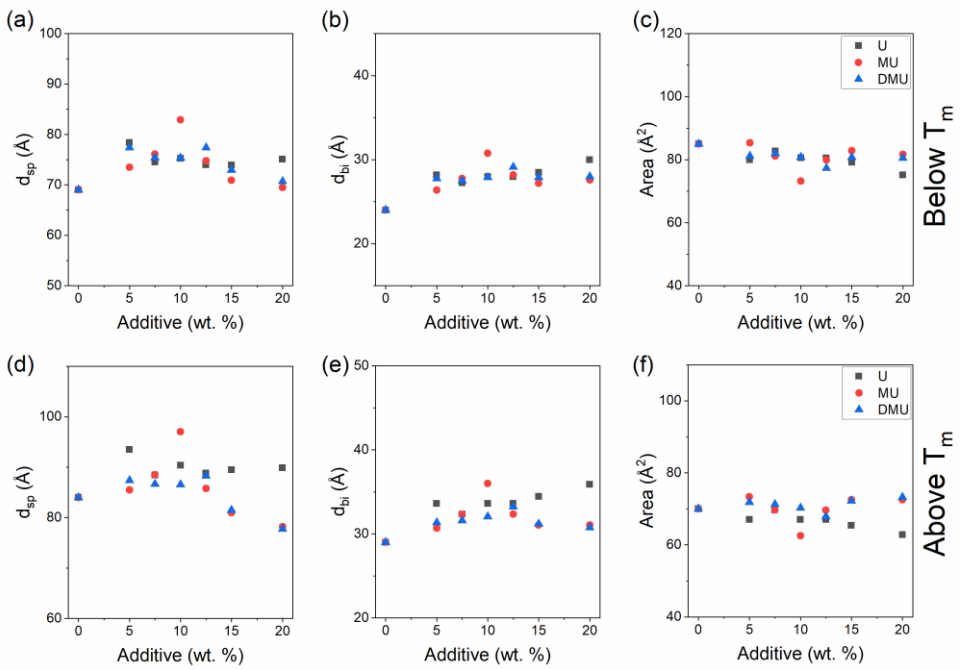

Figure 5.7 Effects of the presence of *ureas* in the interlamellar spacing (d_{sp}), bilayer thickness (d_{bi}), and area per surfactant molecule (a) of the DODAC lamellar structure. The variation of interlamellar spacing, bilayer thickness and area per surfactant molecule as a function of additive concentration is a useful view of the trends, but data are referred to different T_m temperatures. The top panels (a, b and c) correspond to the gel phase, and the bottom panels (d, e and f) correspond to the liquid crystalline phase. U- urea (black square), MU- methyl urea (red circle), DMU- dimethyl urea (blue triangle).

Short-chain fatty acids

The inclusion of short-chain fatty acids (SCFAs) with increasing hydrocarbon chain length in the DODAC bilayer gave significant changes in the main phase transition temperature, which indicates that this class of additives significantly affects the lamellar packing resulting in a more complex phase behavior (cf. section 5.2.2).

From the SAXS profiles, Figure A.5.34 to Figure A.5.38 (appendix), and based on the relation between observed Bragg peak positions, it was deduced that these SCFAs lead to the co-existence of different phases. Moreover, the simultaneous collection of WAXS profiles provided the data needed to determine the “frozen” or “melted” state of the

hydrocarbon chains at temperatures below and above the T_m. The analyses of the SAXS results are summarized in Table 5.6. This table presents striking and unpredictable results – some additives did not show a L_β-L_α phase transition with a temperature increase, while others developed a non-lamellar phase at room temperature. The discussion of these interesting results will be presented in detail, but the focus of this study will primarily be on those surfactant systems that self-assembled into lamellar structures.

Table 5.6 Values for the bilayer volume fraction (Φ_{bi}), the interlamellar spacing (d_{sp}), the bilayer thickness (d_{bi}) and the area per surfactant molecule (a) for DODAC-*SCFAs*-water ternary systems below and above the T_m.

Additive	wt. % additive	Molar ratio (S:A:W)	Φ_{bi}	Below T_m			Above T_m			Transition	T_m (°C)
				d_{sp} (Å)	d_{bi} (Å)	a (Å^2)	d_{sp} (Å)	d_{bi} (Å)	a (Å^2)		
	0.0	1:0.0:60	0.349	69	24	85	84	29	70	L_β-L_α	45.1
Acetic acid	5.0	1:1.4:56	0.347	75	26	79	84	29	70	L_β-L_α	43.5
	7.5	1:2.1:53	0.347	72	25	82	79	27	75	L_β-L_α	42.3
	10.0	1:2.8:51	0.346	73	25	82	77	27	77	L_β-L_α	41.5
	12.5	1:3.5:49	0.346	73	25	81	75	26	79	L_β-L_α	40.7
	15.0	1:4.2:47	0.343	71	24	84	71	24	84	L_β-L_α	39.6
	20.0	1:5.6:42	0.343	71	24	84	68	23	87	L_β-L_α	37.4
Propionic acid	5.0	1:1.1:56	0.348	72	25	82	77	27	77	L_β-L_α	38.8
	7.5	1:1.7:53	0.350	72	25	81	73	25	81	L_β-L_α	36.8
	10.0	1:2.3:52	0.346	73	25	81	71	24	84	L_β-L_α	34.3
	12.5	1:2.9:49	0.349	71	25	82	66	23	89	L_β-L_α	32.1
	15.0	1:3.4:46	0.349	73	25	81	64	22	91	L_β-L_α	30.0
	20.0	1:4.5:42	0.347	60	21	98	57	20	103	L_β-L_α	24.7
Butyric acid	5.0	1:1.0:56	0.375	73	27	81	77	29	76	L_β-L_α	34.6
	7.5	1:1.5:54	0.388	72	28	79	70	27	82	L_β-L_α	30.6
	10.0	1:1.9:51	0.402	72	29	77	69	28	79	L_β-L_α	26.5
	12.5	1:2.4:49	0.415	74	31	72	72	30	74	L_β-L_α	24.9
	15.0	1:2.9:47	0.430	69	30	74	66	28	78	-*[1]	21.6
Sodium butyrate	1.3	1:0.2:60	0.353	65	23	96	82	29	76	L_β-L_α	44.8
	2.6	1:0.4:58	0.360	46	16	135	78	28	79	L_β-L_α	44.8
	5.0	1:0.8:56	0.373	35	13	169	55	20	108	L_β-L_α	45.0
	6.6	1:1.0:56	0.376	35	13	168	52	20	112	L_β-L_α	45.0

	7.5	1:1.1:53	0.386	35	13	165	-	-	-	L_β-L_3	44.8
	10.0	1:1.5:51	0.398	35	14	160	-	-	-	L_β-L_3	46.0
	12.5	1:1.9:49	0.412	36	15	150	-	-	-	L_β-L_3	44.98
	15.0	1:2.3:47	0.422	37	16	140	-	-	-	L_β-L_3	44.3
	20.0	1:3.1:42	0.452	38	17	128	-	-	-	L_β-L_3	43.2
Hexanoic acid	5.0	1:0.7:56	0.390	68	27	89	84	33	72	-*2	26.4
	7.5	1:1.1:54	0.410	57	23	95	58	24	93	-*2	22.5
	10.0	1:1.4:51	0.430	70	30	73	-	-	-	-*2	21.0
	12.5	1:1.8:49	0.450	-	-	-	-	-	-	*Cub-Cub*	13.4
	15.0	1:2.2:47	0.471	54	26	86	-	-	-	-*2	14.3

*1 The system was in the L_α phase at 25 ºC.

*2 Co-existence of phases was identified.

Figure 5.8 shows how the different short-chain fatty acid molecules affect d_{sp}, d_{bi} and a, in the L_β and L_α phases. The fatty acids with one-, two-, and three-carbon chain length, namely acetic, propionic, and butyric acid, exhibit a more consistent trend. In the fluid phase, regardless of acid, all of them show a decrease in the interlamellar spacing consistent with an increase in the area per surfactant molecule, and an increase in the hydrocarbon disorder resulting in a contraction. The decrease in the d_{sp} in the gel phase is due to a reduction in water content in the system and an increased area per surfactant molecule. The effects on the T_m become more pronounced with the increasing length of the alkyl chain, and the same trend was observed for the lamellar packing.

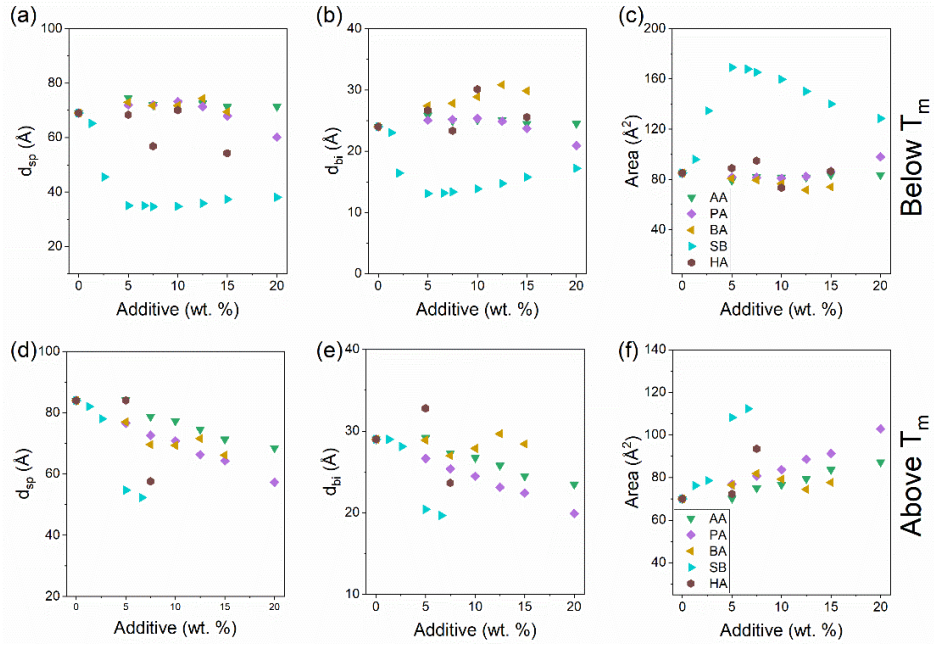

Figure 5.8 Effects of the presence of *SCFAs* in the interlamellar spacing (d_{sp}), bilayer thickness (d_{bi}), and area per surfactant molecule (a) of the DODAC lamellar structure. The variation of interlamellar spacing, bilayer thickness and area per surfactant molecule as a function of additive concentration is a useful view of the trends, but data are referred to different T_m temperatures. The top panels (a, b and c) correspond to the gel phase, and the bottom panels (d, e and f) correspond to the liquid crystalline phase. AA- acetic acid (green triangle), PA- propionic acid (purple rhombus), BA- butyric acid (yellow triangle), SB- sodium butyrate (cyan triangle), HA- hexanoic acid (brown hexagon).

Butyric acid molecules are expected to be located at the interface, according to their chemical nature. From the thermal behavior of this surfactant system, it was detected that small quantities of butyric acid give rise to a very significant reduction in the T_m. These results suggest that butyric acid has a distinct effect on the packing structure. In fact, d_{bi} increases upon butyric acid addition to the system, at 25 ^oC, Figure 5.8 (b). Thus, it can be inferred to reduce the chain interdigitation, and a smaller area per surfactant molecule is deduced. At 50 ^oC, where the alkyl chains have a fluid-like nature, there is no significant effect on the bilayer thickness. Small variations of the d_{bi} were observed corresponding to variations of a. Ergo, a lateral expansion or compression will result in the bilayer thinning or thickening in order to accommodate the same volume.

The addition of sodium butyrate causes significant and interesting effects. As can be inferred from Table 5.6, relatively small amounts dramatically reduce the spacing in the L_β phase, reaching values that are ca. half of those of the surfactant alone. A minimum in spacing is observed around charge stoichiometry between surfactant and butyrate while at higher butyrate contents, there was a minor increase. For the calculations of the bilayer thickness and the area per head-group, it is assumed that sodium butyrate does not differ significantly in volume from butyric acid. To derive the volume, the use of partial molar volume will be not appropriate due to electrostriction effect, leading to smaller volumes per molecule [39]. Therefore, the volume occupied by sodium butyrate was considered to be the same as butyric acid.

The deduced values for the bilayer thickness are much smaller with butyrate than for the surfactant alone; actually, they are close to the length of one surfactant molecule rather than two as expected for an "ideal" L_β phase (as discussed in the previous chapter). This would correspond to a close to total interdigitation of the surfactant alkyl chains. Such a packing, as indicated in Figure 5.9, can be understood from the geometric packing restrictions in a system of two surfactants with very different alkyl chain lengths. As butyrate is amphiphilic, the propyl chain was expected to mix with the surfactant alkyl chains in the bilayers. The resulting structure suggested (Figure 5.9) reflects a minor contribution from butyrate to the hydrophobic volume but a significant contribution to the head-group area. On further inclusion of butyrate, when it is in charge excess, there is a weak progressive increase in the bilayer thickness; the lowest rate of change occurs in the region of charge stoichiometry of butyrate and surfactant. It has been suggested previously that specific interactions are not significant in the formation of an interdigitated structure [40, 41]. Thus, the main driving force was seen to be an increase in the surfactant head-group area.

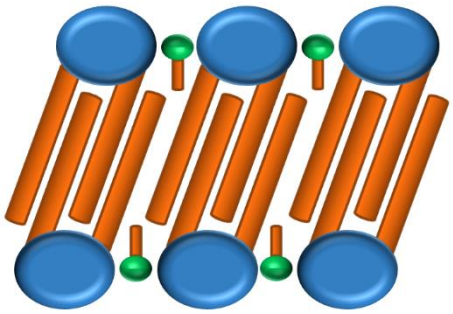

Figure 5.9 Schematic representation of the packing structure for the fully interdigitated DODAC-sodium butyrate-water system.

For the L_α phase in the butyrate system, it was observed that at small additive amounts a similar picture for the observed spacing and the bilayer thickness as for the L_β phase and this was attributed to the same type of packing restrictions. However, a significant difference compared to the surfactant alone is that the diffraction profiles were less distinct and peaks smeared out (Figure 5.10 (a)). This suggests a less ordered L_α phase.

As approximate charge stoichiometry between butyrate and cationic surfactant was attained, the diffraction profile at 50 ^oC changes dramatically (Figure 5.10 (b)), and no lamellar ordering is indicated. Thus, with sodium butyrate, the melting of the L_β phase did not lead to the L_α phase as observed for the other additives and the surfactant alone. Instead, the loss of birefringence, as well as of X-ray diffraction peaks, suggest an isotropic phase. There are two possible isotropic phases in this case, a vesicle solution and a sponge (L_3) phase. Vesicle solutions are commonly observed for mixed cationic-anionic surfactant systems but only for dilute solutions [42, 43]. The present systems appear to be too concentrated to allow for vesicles. Only multi-layered vesicles would be possible from geometric packing considerations, and these would show X-ray diffraction peaks. In addition, studies of an anionic double-chain surfactant also demonstrated the effect of electrolytes to induce a transition from lamellar phase to an isotropic phase, identified as the sponge phase [44]. Therefore, it was concluded that a reversed L_3 phase is formed after the phase transition temperature for the samples with excess butyrate ions. The SAXS data were fitted to the Teubner-Strey model [45] for bicontinuous systems where a single broad peak and a q^{-4} decay at the Porod region (large q) were observed allowing the identification of a reversed L_3 phase. On the other hand, as mentioned, it was possible to identify a L_β-L_α phase

transition when the amount of butyrate was below the charge neutrality, as represented in Figure 5.9. These observations highlight a substantial effect of butyrate ions on the surfactant packing. It is noted that a transition from a L_α phase to a bicontinuous L_3 phase is expected from simple packing considerations. Thus, the spontaneous curvature of an ionic surfactant film goes from positive (towards the oil part) to negative both as the charge is neutralized (by butyrate ions) and as the ion concentration in the aqueous parts is increased.

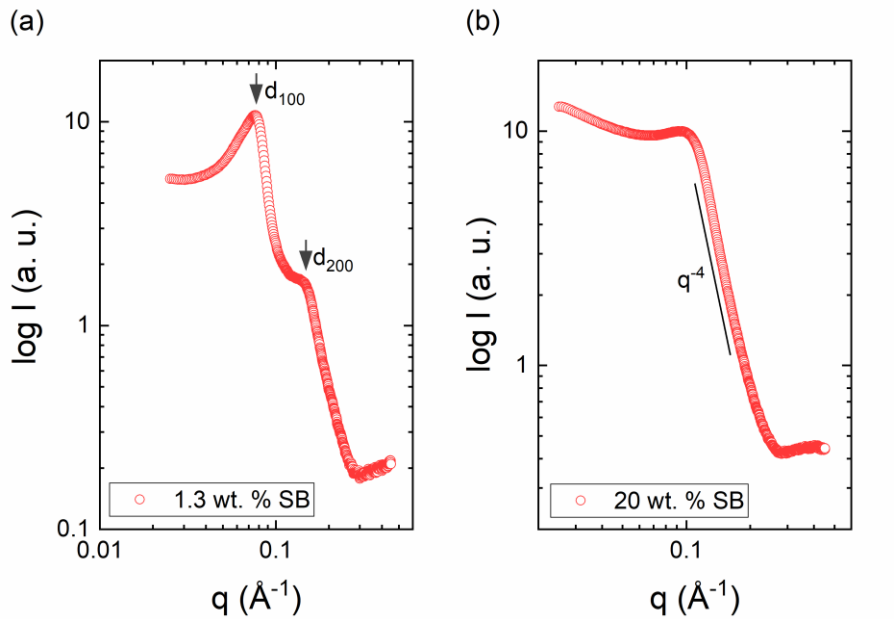

Figure 5.10 SAXS and WAXS profiles for DODAC with (a) 1.3 and (b) 20 wt. % of sodium butyrate at 50 ºC showing the L_α-L_3 phase transition with excess amounts of additive.

The addition of hexanoic acid to the DODAC bilayer resulted in mixtures that displayed a distinct phase behavior. Phase separation at naked eye was identified, and the inclusion of small amounts (5 wt. %) of hexanoic acid had a tremendous effect on the T_m which dropped to very low values. With increasing inclusion into the bilayer, a continuous drop of the T_m value was verified up to a limit (20 wt. %) at which no thermal transition was detected (from 10 to 60 ^oC). These initial results suggest a rather complex phase behavior of DODAC in the presence of this six-carbon carboxylic acid.

To ensure that phase identification was correctly done below and above the T_m, the SAXS and WAXS measurements at 12 and 50 ^oC were conducted, and those scattering profiles can be found in the appendix, Figure A.5.38. Except for one of the mixtures, all the other five mixtures showed co-existence of different phases. In the presence of small amounts of hexanoic acid (5 wt. %), a lamellar gel phase co-exists with a cubic phase. A lamellar gel with 68 Å of interlamellar spacing and with a scattering intensity two times higher than the cubic phase was determined below the T_m, as can be seen in Figure 5.11 (a). At 50 ^oC, i.e., above the T_m, a thicker L_α phase with a d_{sp} of 84 Å co-existing with a cubic phase was identified (Figure 5.11 (b)) However, in the melted phase, the intensity of the lamellar structure was five times higher than in the cubic. Figure 5.11 (c) and (d) show the scattering profiles of DODAC in the presence of 12.5 wt. % of hexanoic acid at a temperature below and above the T_m, respectively. Here, the number of molecules of hexanoic acid is twice the number of molecules of the surfactant and a cubic phase both below and above the T_m was determined. The addition of a more hydrophobic additive suggests a remarkable decrease in the head-group area, which led the system to develop a reversed bicontinuous cubic phase. These observations suggest a substantial effect of hexanoic acid on the surfactant packing. As detected for DODAC in the presence of sodium butyrate, a transition from a lamellar phase to a reversed cubic phase was expected from simple packing considerations.

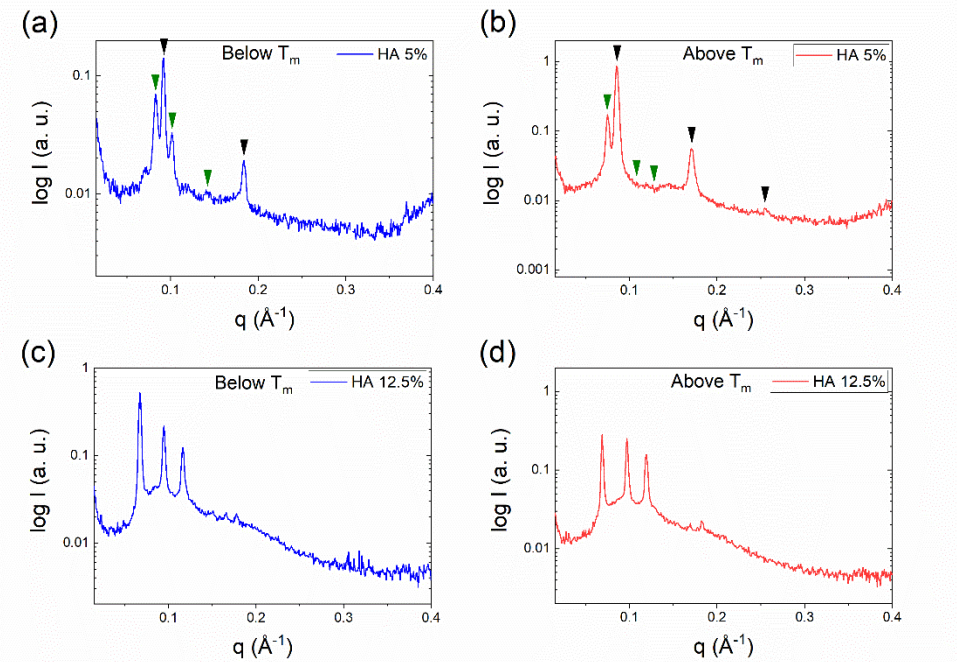

Figure 5.11 SAXS profiles for DODAC in the presence of hexanoic acid. Top panels: 5.0 wt. % of the additive, T_m = 26.4 ºC: (a) below the T_m, and (b) above the T_m. Bottom panels: 12.5 wt. % of the additive, T_m = 13.4 ºC: (c) below the T_m, and (d) above the T_m. In the top two panels, a co-existence of a lamellar and cubic (*Pn3m*) phase was found, and the bottom two panels show the evolution to a reversed cubic (*Pn3m*) phase. The green color arrows represented cubic phase reflections, the black arrows represented lamellar phases.

Hydrotrope molecules

The addition of benzyl alcohol and phenoxyethanol, to the DODAC bilayer, gives a significant depression of the main phase transition temperature (T_m). The SAXS and WAXS profiles can be found in Figure A.5.39 and Figure A.5.40 (appendix) and the characterization of these surfactant systems resulted in the values presented in Table 5.7. The effect of the inclusion of these two hydrotrope molecules in the DODAC bilayer in terms of the interlamellar spacing (d_{sp}), surfactant bilayer thickness (d_{bi}) and area per surfactant molecule (a) at temperatures below and above the T_m is presented in Figure 5.12.

At a temperature below the T_m, DODAC packed in a lamellar structure with alkyl chains in the "frozen" state (L_β phase). Above the T_m, the surfactant underwent a gel-to-liquid crystalline phase transition, resulting in the "fluid" state of the hydrocarbon chains. However, with excess amounts of benzyl alcohol (12.5 and 15 wt. %), a gel-to-cubic phase transition was identified. The addition of benzyl alcohol results in smaller areas per surfactant molecule in the L_β phase, which in turn led to a bilayer thickening arising from a closer chain-to-chain packing when compared to pure DODAC in water. This decrease in the *a* values suggests that benzyl alcohol is located at the polar/non-polar interface at 25 ^oC. Strikingly, with the temperature increase, the phase behavior changes. At 50 ^oC, the results show that DODAC occupies a larger area compared to the surfactant in the gel phase and without additive, resulting in bilayer thinning to accommodate the increase in the area to keep the lamellar packing. These results suggest a different location of benzyl alcohol. Ultimately, with excess amounts of benzyl alcohol the system develops a cubic phase. With the increase in temperature, benzyl alcohol becomes less polar and possibly penetrates into the bilayer core. Once there, it significantly contributes to an increase of the volume of the non-polar domain, driving the surfactant to adopt a structure with negative mean curvature thus resulting in a reversed structure, particularly a reversed cubic phase.

It is noteworthy that below the T_m, the SAXS profiles show that the addition of small amounts of benzyl alcohol (5.0 and 7.5 wt. %) results in mixtures with two co-existing gel phases (Figure A.5.39 (a)). When 5 wt. % was added, a lamellar gel with a d_{sp} of 78 Å and another with 70 Å were determined. Increasing amounts of benzyl alcohol in the surfactant system (7.5 wt. %) resulted in two lamellar gels with d_{sp} of 75 Å and 70 Å. Further inclusion of benzyl alcohol led to the suppression of one of the lamellar structures, thus resulting in a single lamellar gel phase. The progressive decrease of the d_{sp} value could be explained by the replacement of water with benzyl alcohol, a less polar molecule, thus resulting in thinner water layers. However, an unexpected larger d_{sp} value when the amount of benzyl alcohol almost doubled the amount of DODAC molecules was observed.

The addition of phenoxyethanol to the surfactant bilayers did not show any significantly different effect. Notably, the lamellar surfactant packing remained unaffected, which suggests that the presence of phenoxyethanol might stabilize the lamellar DODAC structure. At 50 ^{o}C, a significant increase in the area per surfactant molecule was ascertained. These results suggest that phenoxyethanol might be located at the polar/non-polar interface and possibly forming aggregates.

Table 5.7 Values for the bilayer volume fraction (Φ_{bi}), the interlamellar spacing (d_{sp}), the bilayer thickness (d_{bi}) and the area per surfactant molecule (a) for DODAC-*hydrotropes*-water ternary systems below and above the T_m.

Additive	wt. % additive	Molar ratio (S:A:W)	Φ_{bi}	Below T_m			Above T_m			Transition	T_m (^{o}C)
				d_{sp} (Å)	d_{bi} (Å)	a (Å^2)	d_{sp} (Å)	d_{bi} (Å)	a (Å^2)		
	0.0	1:0.0:60	0.349	69	24	85	84	29	70	L_β-L_α	45.1
Benzyl alcohol	5.0	1:0.9:56	0.384	78	30	77	75	29	80	L_β-L_α	35.5
	7.5	1:1.2:53	0.401	75	30	77	65	26	89	L_β-L_α	33.0
	10.0	1:1.6:51	0.417	72	30	77	66	27	85	L_β-L_α	29.7
	12.5	1:1.9:49	0.435	80	35	67	-	-	-	L_β-*Cub*	28.2
	15.0	1:2.3:47	0.452	68	31	76	-	-	-	L_β-*Cub*	21.1
Phenoxyethanol	5.0	1:0.6:56	0.375	75	28	83	64	24	98	L_β-L_α	36.4
	7.5	1:0.9:53	0.390	74	29	81	72	28	83	L_β-L_α	32.6
	10.0	1:1.2:52	0.402	67	27	87	66	27	88	L_β-L_α	24.8
	12.5	1:1.5:49	0.418	62	26	90	61	25	92	L_β-L_α	20.7
	15.0	1:1.8:46	0.431	64	27	85	52	22	105	L_β-L_α	19.6
	20.0	1:2.4:42	0.456	68	31	76	54	25	94	L_β-L_α	17.1

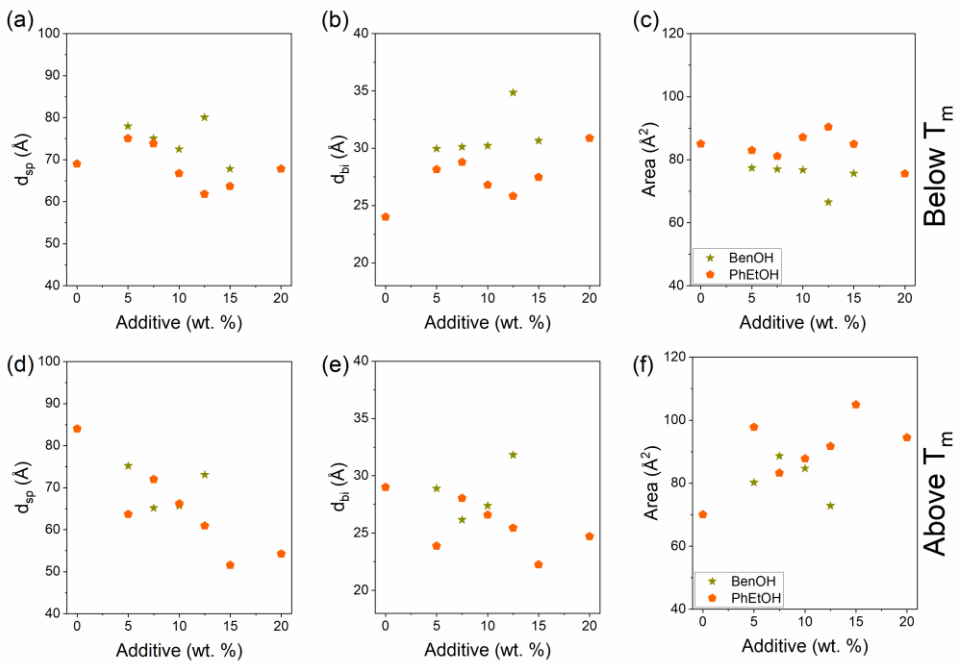

Figure 5.12 Effects of the presence of *hydrotropes* in the interlamellar spacing (d_{sp}), bilayer thickness (d_{bi}), and area per surfactant molecule (a) of the DODAC lamellar structure. The variation of interlamellar spacing, bilayer thickness and area per surfactant molecule as a function of additive concentration is a useful view of the trends, but data are referred to different T_m temperatures. The top panels (a, b and c) correspond to the gel phase, and the bottom panels (d, e and f) correspond to the liquid crystalline phase. BenOH- benzyl alcohol (yellow star), PhEtOH- phenoxyethanol (orange pentagon).

Fatty alcohols

The presence of short and intermediate-chain alcohol molecules in the DODAC bilayer gives distinct changes in the main phase transition temperature. Depending on the polarity of these aliphatic alcohols, different effects on the thermal behavior were detected, which suggests that this class of additives develops a more complex phase behavior.

From the SAXS profiles, Figure A.5.41 to Figure A.5.45 (appendix), and based on the relation between observed Bragg peaks position, it was observed that similar to the observations for the SCFAs, these fatty alcohol molecules may lead to the co-existence of different phases. SAXS and WAXS characterization at 12, 25, and 50 ^{o}C was conducted to ensure a correct phase identification below, during and above the main phase transition temperature. The discussion of the various self-assembly structures identified at different temperatures is presented and the analysis of the lamellar-forming structures is summarized in Table 5.8 and Figure 5.13.

Table 5.8 Values for the bilayer volume fraction (Φ_{bi}), the interlamellar spacing (d_{sp}), the bilayer thickness (d_{bi}) and the area per surfactant molecule (a) for DODAC-*fatty alcohols*-water ternary systems below and above the T_m.

Additive	wt. % additive	Molar ratio (S:A:W)	Φ_{bi}	Below T_m			Above T_m			Transition	T_m (°C)
				d_{sp} (Å)	d_{bi} (Å)	a (Å^2)	d_{sp} (Å)	d_{bi} (Å)	a (Å^2)		
	0.0	1:0.0:60	0.349	69	24	85	84	29	70	L_β-L_α	45.1
Butanol	5.0	1:1.2:56	0.382	71	27	81	72	28	80	L_β-L_α	37.0
	7.5	1:1.7:54	0.400	67	27	83	67	27	83	L_β-L_α	32.2
	10.0	1:2.3:51	0.419	64	27	82	62	26	85	L_β-L_α	28.1
	12.5	1:2.8:49	0.435	60	26	85	60	26	85	L_β-L_α	25.2
	15.0	1:3.4:47	0.454	75	34	65	-	-	-	L_β-L_3	22.4
	20.0	1:4.6:42	0.490	71	35	63	-	-	-	L_β-L_3	19.7
Hexanol	5.0	1:0.8:56	0.392	114	45	53	73	29	83	L_β/*Cub*-L_α	31.9
	7.5	1:1.3:54	0.415	150	62	38	-	-	-		29.2
	10.0	1:1.6:51	0.436	172	75	32	-	-	-		24.8
	12.5	1:2.1:49	0.457	172	78	30	-	-	-		21.5
	15.0	1:2.5:47	0.480	-	-	-	-	-	-		14.6
Octanol	5.0	1:0.7:56	0.395	131	52	48	79	31	79	L_β/*Cub*-L_α	27.3
	7.5	1:1.0:54	0.417	96	40	62	75	31	79	L_β/*Cub*-L_α	26.1
	10.0	1:1.3:51	0.441	98	43	57	-	-	-		25.4
	12.5	1:1.7:50	0.459	105	48	51	-	-	-		19.1
	15.0	1:1.9:47	0.485	104	50	49	-	-	-		20.3
	20.0	1:2.6:42	0.530	125	66	37	-	-	-		13.2
Decanol	5.0	1:0.5:56	0.395	99	39	66	77	30	85	L_β-L_α	39.1
	7.5	1:0.8:54	0.419	101	42	61	74	31	84	L_β-L_α	41.6
	10.0	1:1.1:51	0.442	90	40	65	84	37	70	L_β-L_α	40.8
	12.5	1:1.3:49	0.465	84	39	66	82	38	68	L_β-L_α	41.5
	15.0	1:1.6:47	0.488	81	39	66	-	-	-	L_β-*Hex*	39.5
	20.0	1:2.1:42	0.534	75	40	64	-	-	-	L_β-*Hex*	39.3
Dodecanol	5.0	1:0.5:56	0.396	83	33	82	63	25	107	L_β-L_α	41.7
	7.5	1:0.7:54	0.420	94	39	69	67	28	96	L_β-L_α	51.4
	10.0	1:0.9:51	0.443	89	39	69	-	-	-	L_β-*Hex*	50.6
	12.5	1:1.1:49	0.466	81	38	71	-	-	-	L_β-*Hex*	52.1
	15.0	1:1.3:47	0.489	79	38	70	-	-	-	L_β-*Hex*	52.3
	20.0	1:1.8:43	0.534	76	40	67	-	-	-	L_β-*Hex*	52.1

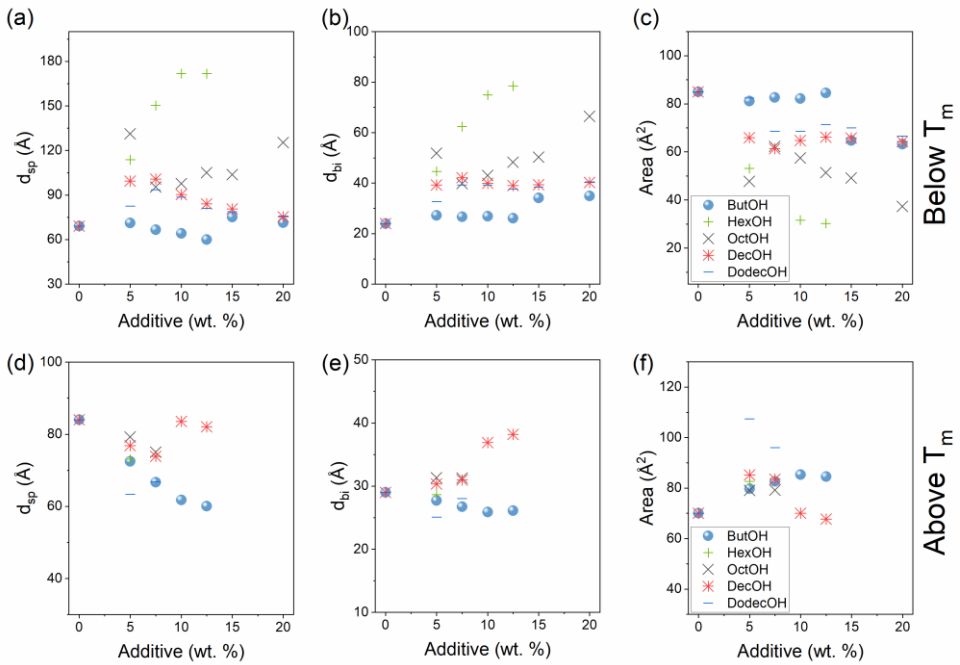

Figure 5.13 Effects of the presence of *fatty alcohols* in the interlamellar spacing (d_{sp}), bilayer thickness (d_{bi}), and area per surfactant molecule (a) of the DODAC lamellar structure. The variation of interlamellar spacing, bilayer thickness and area per surfactant molecule as a function of additive concentration is a useful view of the trends, but data are referred to different T_m temperatures. The top panels (a, b and c) correspond to the gel phase, and the bottom panels (d, e and f) correspond to the liquid crystalline phase. ButOH- butanol (blue dot), HexOH- hexanol (green plus), OctOH- octanol (black cross), DecOH- decanol (red plus-crossed), DodecOH- dodecanol (blue minus).

Table 5.8 illustrates the different phase transitions that DODAC experiences depending on the polarity of the alcohol. Butanol induces a L_β-L_α phase transition at low temperatures, which results in relatively high stability of the liquid crystalline phase. The surfactant in the presence of small amounts of butanol (5 and 7.5 wt. %) shows the coexistence of two lamellar gel phases (Figure A.5.41), which evolves to a single liquid crystalline phase above the T_m. This could be explained by the poor solvency of DODAC in water. However, when the number of moles of butanol tripled the moles of DODAC, a gel-to-reversed sponge (L_3) phase transition was found, refer to Figure 5.14. These results are similar to those of sodium butyrate and suggest a strong interaction at the polar/non-polar interface between the additive and the surfactant. Therefore, at high amounts of butanol, thinner bilayers were found accompanied by an increase in the area per surfactant molecule. The

concomitant increase in *a* drives the surfactant to form a reversed bicontinuous sponge phase to accommodate unfavorable interactions with water. A broad peak and the power law of the form factor (-4) at large *q* [45] characterizes the bicontinuous sponge phase, as illustrated in Figure 5.14 (d).

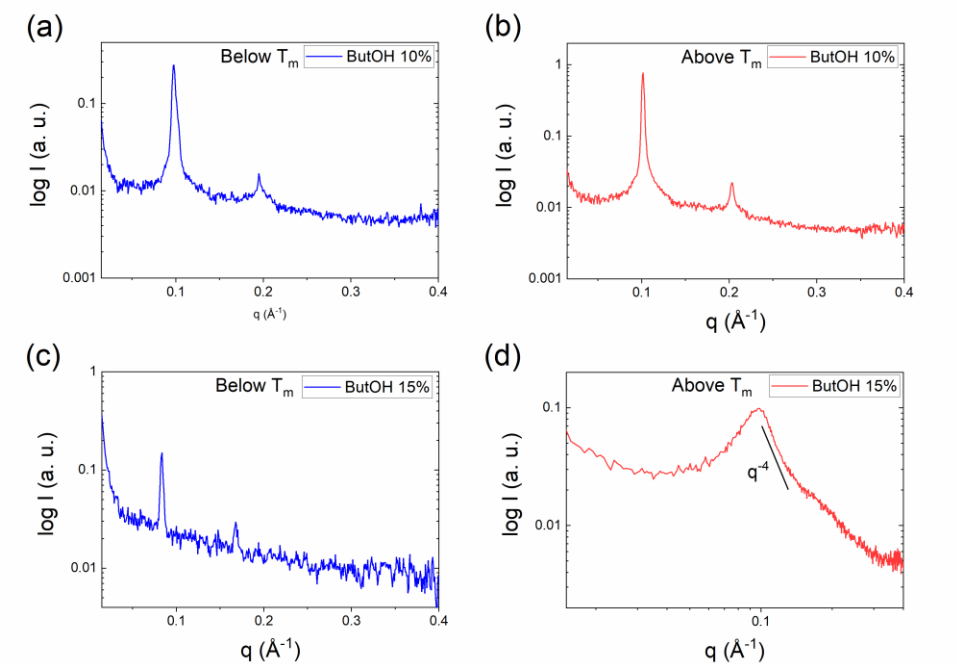

Figure 5.14 SAXS profiles for DODAC in the presence of butanol. Top panels: 10.0 wt. % of the additive: (a) below the T_m, and (b) above the T_m. Bottom panels: 15.0 wt. % of the additive: (c) below the T_m (12 ^oC), and (d) above the T_m. In the top two panels, a L_β-L_α phase transition was found, and the bottom two panels show the evolution to a reversed sponge (L_3) phase was determined.

The inclusion of hexanol in the surfactant bilayers developed a complex phase behavior. As discussed in section 5.2.1, the macroscopic inspection of the samples allowed to anticipate a special effect of hexanol on the surfactant packing. A similar complex phase behavior was found for its fatty acid counterpart. The T_m was extensively depressed by hexanol, which led us to conduct the SAXS and WAXS characterization at 12, 25, and 50 ^oC to ensure a correct phase determination below and above the T_m. At a temperature below the T_m, hexanol led the surfactant to adopt two coexisting phases, one lamellar gel phase, and one reversed cubic phase, as demonstrated in Figure 5.15 (a). The gel phase displays a significant increase in the d_{sp} values, thicker bilayers and smaller areas per surfactant

molecule. This pointed to a possibly different location of hexanol in the lamellar structure. Hexanol is believed to interact rather strongly with the surfactant head-groups, thus decreasing the *a* values by screening the electrostatic repulsion. However, the large increase in bilayer thickness, up to 78 Å, is somewhat surprising. The thickness of a bilayer composed of two 18-carbon alkyl chain monolayers in the L_β phase, oriented perpendicular to the interface is 48 Å. From the results, there is a 30 Å thickness increase, which suggests that hexanol is able to penetrate the bilayer core and swell the non-polar domain. It is noteworthy that a cubic phase always coexists with the gel phase below the T_m (Figure A.5.42). The cubic phase arose from the formation of a structure with even smaller *a* values thus forcing the surfactant to curve towards the oil phase and develop a reversed cubic phase.

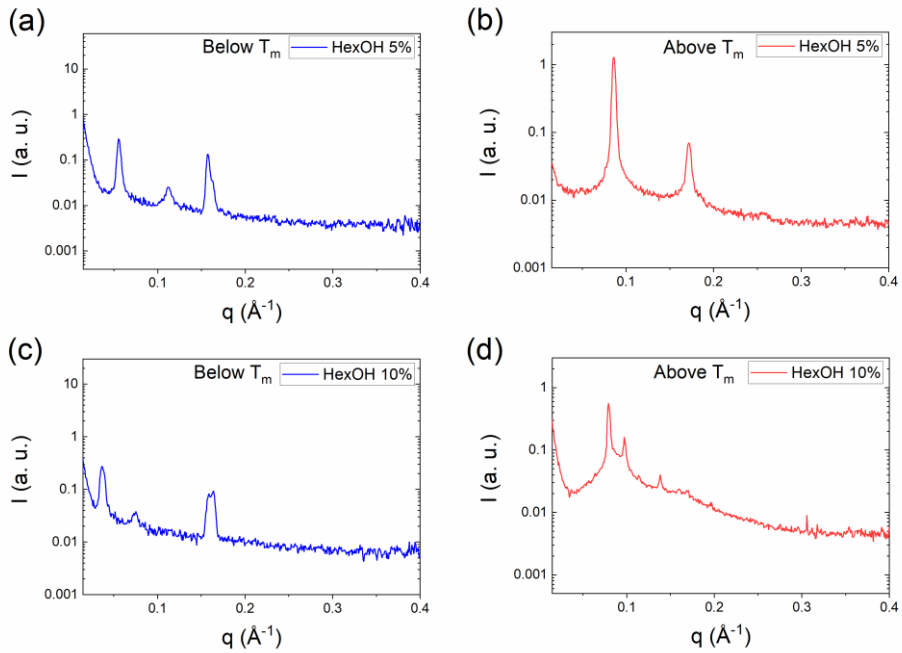

Figure 5.15 SAXS profiles for DODAC in the presence of hexanol. Top panels: 5.0 wt. % of the additive: (a) below the T_m (12 °C), and (b) above the T_m. Bottom panels: 10.0 wt. % of the additive: (c) below the T_m (12 °C), and (d) above the T_m. In the top two panels, a L_β-L_α phase transition was found, and the bottom two panels show the evolution to a reversed cubic phase was determined.

At 50 °C, a temperature above the T_m, the increased hydrophobicity of hexanol leads the surfactant to experience a transition from coexisting reversed cubic and L_β phases to a single reversed cubic phase as seen in Figure 5.15 (c) and (d). This transition arises from a smaller area per surfactant molecule due to the presence of hexanol at the polar/non-polar

interface. The electrostatic screening provided by hexanol reduces the *a* values to the extent that the surfactant was forced to adopt a reversed packing. A transition to a single liquid crystalline phase was only identified at small amounts of hexanol (5 wt. %), refer to Figure 5.15 (a) and (b). The bilayer thickness remains similar to the value without hexanol, but a decrease in the d_{sp} and increase in *a* were detected. These evidences suggest that at a DODAC-hexanol ratio of 1:1, hexanol might create some instability at the polar/non-polar interface, which in turn increases the area per surfactant molecule. However, this perturbation is not strong enough to disrupt the lamellar packing. The addition of excess amounts of hexanol (20 wt. %) leads to phase separation of the surfactant into a clear supernatant, and a deposited "milky" phase, which does not show any thermal transition and, therefore, no SAXS and WAXS characterization was performed (Figure A.5.12).

Octanol also induced a complex phase behavior. T_m is affected with the presence of this 8-carbon chain alcohol, which led us to conduct the SAXS and WAXS characterization at 15, 25 and 50 ^oC to ensure correct phase determination below and above the T_m. Octanol is not amphiphilic enough to self-assemble, and like hexanol, the length of the hydrophobic chain is not long enough to stabilize the lamellar surfactant structures. Despite its 8-carbon alkyl chain, the lamellar packing of the surfactant is transformed once octanol is added to the bilayers. At a temperature below the T_m, the SAXS profiles of DODAC-octanol-water system show that a gel phase always coexist with a reversed phase (Figure A.5.43 (a)). This reversed phase was determined to be a reversed cubic phase, and it evolves to a reversed hexagonal phase when the number of molecules of octanol is twice the number of molecules of surfactant, as schematically demonstrated in Figure 5.16.

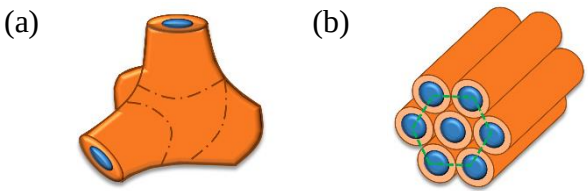

Figure 5.16 Schematic representation of (a) a reversed cubic (cub_b) phase and (b) a reversed hexagonal (rev hex) phase.

Figure 5.17 shows the phase evolution with temperature when DODAC is in the presence of 5 and 12.5 wt. % of octanol. The remarkable effect of octanol in the DODAC lamellar packing is observed even at the smallest amount of additive (5 wt. %). Figure 5.17 (a) displays the SAXS profile of DODAC in the presence of 5 wt. % of octanol and the coexistence of two phases was verified. A lamellar phase with a d_{sp} of 131 Å, and a reversed cubic (cub_b) phase, with the lamellar phase peak being nine times more intense than that of the cubic phase, were identified. With the increase in temperature, the cubic phase was gradually suppressed and a L_α phase with a d_{sp} of 79 Å above the T_m was determined. This was the only sample that gave a single and stable lamellar phase in the presence of octanol (Figure 5.17 (c)). The development of coexisting phases at a temperature below the Krafft point may be attributed to the poor solvency of the surfactant in water and the slow kinetics when the alkyl chains are in the "frozen" state.

With increasing chain fluidity, the surfactant could accommodate the octanol molecules in its lamellar structure, thus resulting in a single phase. Strikingly, if the lamellar gel structures formed is examined, unexpected observations are obtained. First, there was a pronounced increase in the interlamellar spacing, which in turn leads to a decrease in the area per surfactant molecule. Second, a noticeable increase in the bilayer thickness was established, which in some cases is more than double the value without additive. These observations suggest that octanol penetrates the bilayer core and swells this non-polar domain.

Nonetheless, a single phase was never observed. The two samples that show a L_α phase (5 and 7.5 wt. % of octanol) display a small decrease of the d_{sp} expected from the replacement of water by the alcohol. The corresponding increase in the *a* values, and a bilayer thickness reduction of about 30% is due to the expected melting of a bilayer with 36 carbons in the "frozen" state and perpendicular to the interface [46]. Figure 5.17 (d) to (f) display the phase evolution of DODAC in the presence of excess amounts (12.5 wt. %) of octanol with temperature, and the formation of a reversed hexagonal phase was identified (Figure 5.17 (f)). With the increase in temperature, the alcohol becomes less polar, which favors the

formation of reversed structures. Here, the system is in excess of alcohol, which "boosts" the formation of reversed cubic and reversed hexagonal phases.

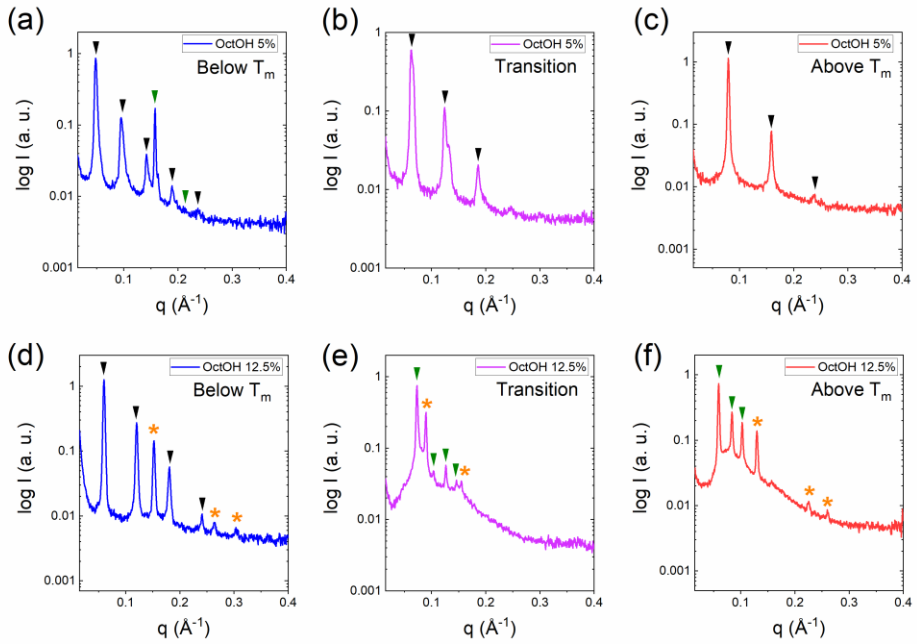

Figure 5.17 SAXS profiles for DODAC in the presence of octanol. Top panels: 5.0 wt. % of the additive: (a) below the T_m (15 °C), (b) during the phase transition (25 °C), and (c) above the T_m (50 °C). Bottom panels: 12.5 wt. % of the additive: (d) below the T_m (15 °C), (e) during the phase transition (25 °C), and (f) above the T_m (50 °C). In the top panels, a coexistence of lamellar gel and cubic phase evolution to a single lamellar liquid crystalline phase was found, and the bottom panels a coexistence of lamellar gel and hexagonal phase evolution to cubic and hexagonal phase transition was determined. The black color arrows represented lamellar phase reflections, the green arrows represented cubic phase, and the orange stars represented hexagonal phase.

Decanol and dodecanol mark the change to a trend different from the previously discussed aliphatic alcohols. The T_m of the surfactant in the presence of decanol remains virtually unchanged, and it increases in the presence of dodecanol. The SAXS and WAXS profiles of these two surfactant systems are presented in Figure A.5.44 and Figure A.5.45 (appendix). Using simultaneous SAXS and WAXS characterization, a single lamellar gel phase below T_m was ascertained for both surfactant systems. In the L_β phase, the values of the bilayer thickness increases and the area per surfactant molecule decreases (accompanied by an increase in the d_{sp} values) when compared to DODAC in water. These alcohols should act primarily as a second surfactant in this system and facilitate the

structure packing favoring the hydrophobic interactions. On top of this, their presence help to shield the electrostatic repulsion between charged head-groups.

X-ray scattering profiles at a temperature above the T_m were different from those of the L_β phase. The increase in the temperature led to the development of a reversed hexagonal phase. With these two alcohols present in the system, the increased interlayer spacing observed for the gel phase was no longer observed for the L_α phase.

From the X-ray data, it was possible to deduce the changes in d_{sp}, d_{bi} and a in both the gel and liquid crystalline phases. The variation in these values with varying additive concentration can be seen in Figure 5.13. Different trends can be observed compared to shorter-chain alcohols. Firstly, in the gel phase, the addition of decanol and dodecanol promoted an increase of the interlayer spacing of the phase referred to the masking of the electrostatic repulsions at the interface. This led to a decrease in the area per surfactant molecule, hence helped in the packing of the hydrocarbon chains. The subsequent decrease in the d_{sp} values with further increase in additive concentration was due to a reduction in water amounts. The two alcohols in the L_α phase did not promote an interlayer space increase. With the gain in the amphiphile hydrocarbon chain mobility, their presence was not enough to provide the needed additional stability. The effect on the alkyl chain bilayer provided by these two intermediate-chain alcohols was supported by DSC measurements, where it was possible to observe a negligible effect on T_m. Increasing amounts of decanol showed no effect on the T_m, and the addition of dodecanol led to a small increase of the T_m, thus increasing the stability of the gel phase. The development of reversed structures above the T_m in the presence of excess amounts of decanol and dodecanol was attributed to two vectors: the decrease in polarity of this additives at higher temperatures that increased the volume of the non-polar domain, and the reduced area per surfactant molecule. Therefore, reversed structures were expected to be formed with the increase in temperature from pure geometrical considerations.

In short, the presence of alcohols with different polarities manifested distinctly different effects on the surfactant phase behavior. The shorter alkyl chain alcohol, butanol, showed a similar effect in the surfactant bilayers as its carboxylic acid counterpart. Hexanol and

octanol displayed a rather complex phase behavior with a marked effect on the surfactant bilayers, thus developing systems with more than one phase. Decanol and dodecanol contributed to a single and stable gel phase but developed reversed structures at temperatures above the surfactant T_m. Interestingly, the latter two alcohols seem to disrupt the interdigitated or tilted gel phase observed for DODAC in water. DODAC with these 10- and 12-carbon alcohols developed stable gel phases with thicker bilayers.

5.3 Conclusions

The effects of "ureas", short-chain fatty acids (SCFAs), hydrotrope molecules and short- and intermediate-chain alcohols on the alkyl chain packing in the lamellar bilayer structure of DODAC in water were evaluated. The gel-to-liquid phase transition temperature (T_m) was studied using DSC. From the small-angle X-ray scattering profiles, the surfactant packing was determined, and the wide-angle X-ray scattering profile allowed to determine the chain-chain distances for the lamellar gel and liquid crystalline phases.

Additives were found to have very different effects on the surfactant system. Whereas the "ureas", sodium butyrate and decanol had only minor effects on T_m, similar to other additives [3, 5], SCFAs, hydrotropes, and butanol gave a significant decrease of the T_m, corresponding to stabilizing the L_α phase with respect to the L_β phase. For "ureas", SCFAs and butanol, melting led to a lamellar phase whereas significant addition of sodium butyrate, hexanoic acid, and fatty alcohols gave origin to reversed phases; bicontinuous or sponge type (often denoted L_3), reversed cubic (cub_b) and reversed hexagonal (rev hex) phases were identified.

The small angle X-ray scattering data imply distinctively different effects of the additives on the surfactant packing in the gel and liquid crystalline phases. Replacing water by "ureas" had minimal effects on the lamellar spacing both below and above the chain melting temperature. In line with the value of T_m being unaffected, it is deduced that the surfactant-surfactant interactions are not appreciably different in water and water-urea environments. Acetic, propionic and butyric acid as well as the two hydrotropes had intermediate effects

on the bilayer thickness, with a moderate increase for the L_β phase and a moderate decrease for the L_α phase. This effect was more pronounced for butyric acid, which formed mixed aggregates with DODAC. From the reduced average size of the amphiphile, the lower chain melting temperature can be understood. Furthermore, there appears to be a decreased tilting or interdigitation in the gel phase in the presence of butyric acid. In the liquid crystalline phase, the decreased average amphiphile length leads to a minor thinning of the bilayers. Sodium butyrate, hexanoic acid, and the fatty alcohols gave the most complex and interesting behavior, and one can identify several factors, which can operate in opposite directions and give cancellation effects. Butyrate will act as a short-chain oppositely charged amphiphile and it will also give electrostatic screening by acting as an electrolyte. From the SAXS data for the gel phase, it is inferred a dramatic thinning of the surfactant layers from additions corresponding to rough charge neutrality. For larger additions, the thickness of the surfactant layer increases moderately. Strikingly, the layer thickness over a wide range of compositions corresponds to the length of one surfactant molecule in the all-trans conformation, which would suggest a maximal interdigitation of surfactant molecules. These results show that, although the interdigitation phenomenon has been widely discussed, challenges remain to characterize it. Excess amounts of fatty alcohol in the system induced a transition from a gel phase to reversed structures such as a sponge, cubic, and hexagonal phases.

Generally, addition of “ureas”, SCFAs (except hexanoic acid), hydrotrope molecules and butanol (to a certain extent) maintained the integrity of the lamellar structure at temperatures below and above the main phase transition, whereas addition of sodium butyrate, hexanoic acid and aliphatic alcohols with more than four-carbon chains addition gave rise to reversed phases above the Tm. Hence, the importance of the location of the additive in the bilayer is highlighted, which may result in drastic changes in the hydrocarbon chain packing.

References

[1] I.M. Banat, R.S. Makkar, S.S. Cameotra, Potential commercial applications of microbial surfactants, *Applied Microbiology and Biotechnology* 53(5) **2000** 495-508.

[2] F.O. Costa-Balogh, H. Wennerstrom, L. Wadso, E. Sparr, How small polar molecules protect membrane systems against osmotic stress: The urea-water-phospholipid system, *Journal of Physical Chemistry B* 110(47) **2006** 23845-23852.

[3] E. Sparr, H. Wennerstrom, Interlamellar forces and the thermodynamic characterization of lamellar phospholipid systems, *Current Opinion in Colloid & Interface Science* 16(6) **2011** 561-567.

[4] A. Nowacka, S. Douezan, L. Wadso, D. Topgaard, E. Sparr, Small polar molecules like glycerol and urea can preserve the fluidity of lipid bilayers under dry conditions, *Soft Matter* 8(5) **2012** 1482-1491.

[5] S. Bjorklund, J.M. Andersson, Q.D. Pham, A. Nowacka, D. Topgaard, E. Sparr, Stratum corneum molecular mobility in the presence of natural moisturizers, *Soft Matter* 10(25) **2014** 4535-4546.

[6] H. Kunieda, K. Shinoda, Solution behavior of dialkyldimethylammonium chloride in water. Basic properties of antistatic fabric softeners, *The Journal of Physical Chemistry* 82(15) **1978** 1710-1714.

[7] G.A. Ferreira, W. Loh, Structural Parameters of Lamellar Phases Formed by the Self-Assembly of Dialkyldimethylammonium Bromides in Aqueous Solution, *J. Braz. Chem. Soc.* 27(2) **2016** 392-+.

[8] P. Kudla, T. Sokolowski, B. Blumich, K.P. Wittern, Phase behavior of liquid-crystalline emulsion systems, *Journal of Colloid and Interface Science* 349(2) **2010** 554-559.

[9] R. Koynova, J. Brankov, B. Tenchov, Modulation of lipid phase behavior by kosmotropic and chaotropic solutes - Experiment and thermodynamic theory, *European Biophysics Journal with Biophysics Letters* 25(4) **1997** 261-274.

[10] R.G. Laughlin, R.L. Munyon, J.L. Burns, T.W. Coffindaffer, Y. Talmon, Physical science of the dioctadecyldimethylammonium chloride-water system. 3. Colloidal aspects, *The Journal of Physical Chemistry* 96(1) **1992** 374-383.

[11] R.G. Laughlin, R.L. Munyon, Y.C. Fu, T.J. Emge, Physical science of the dioctadecyldimethylammonium chloride-water system. 2. Kinetic and mechanistic aspects, *Journal of Physical Chemistry* 95(9) **1991** 3852-3856.

[12] R.G. Laughlin, R.L. Munyon, Y.C. Fu, A.J. Fehl, Physical Science of the Dioctadecyldimethylammonium Chloride Water-System. 1. Equilibrium Phase-Behavior, *Journal of Physical Chemistry* 94(6) **1990** 2546-2552.

[13] E.F. Marques, O. Regev, A. Khan, B. Lindman, Self-organization of double-chained and pseudodouble-chained surfactants: counterion and geometry effects, *Adv. Colloid Interface Sci.* 100 **2003** 83-104.

[14] A.M. Carmona-Ribeiro, Theoretical and experimental stabilities of amphiphile vesicles in the presence of sodium chloride, *The Journal of Physical Chemistry* 93(6) **1989** 2630-2634.

[15] A.M. Carmona-Ribeiro, B.R. Midmore, Surface potential in charged synthetic amphiphile vesicles, *The Journal of Physical Chemistry* 96(8) **1992** 3542-3547.

[16] L.R. Tsuruta, A.M. Carmona-Ribeiro, Counterion Effects on Colloid Stability of Cationic Vesicles and Bilayer-Covered Polystyrene Microspheres, *The Journal of Physical Chemistry* 100(17) **1996** 7130-7134.

[17] E. Feitosa, W. Brown, Fragment and Vesicle Structures in Sonicated Dispersions of Dioctadecyldimethylammonium Bromide, *Langmuir* 13(18) **1997** 4810-4816.

[18] E. Feitosa, P.C.A. Barreleiro, G. Olofsson, Phase transition in dioctadecyldimethylammonium bromide and chloride vesicles prepared by different methods, *Chem. Phys. Lipids* 105(2) **2000** 201-213.

[19] E. Feitosa, P.C.A. Barreleiro, The effect of ionic strength on the structural organization of dioctadecyldimethylammonium bromide in aqueous solution, *Surface and Colloid Science*, *Springer Berlin Heidelberg*, Berlin, Heidelberg, 2004, pp. 163-168.

[20] E. Feitosa, G. Karlsson, K. Edwards, Unilamellar vesicles obtained by simply mixing dioctadecyldimethylammonium chloride and bromide with water, *Chem. Phys. Lipids* 140(1–2) **2006** 66-74.

[21] E. Feitosa, F.R. Alves, The role of counterion on the thermotropic phase behavior of DODAB and DODAC vesicles, *Chem. Phys. Lipids* 156(1–2) **2008** 13-16.

[22] A. Lopes, K. Edwards, E. Feitosa, Extruded vesicles of dioctadecyldimethylammonium bromide and chloride investigated by light scattering and cryogenic transmission electron microscopy, *Journal of Colloid and Interface Science* 322(2) **2008** 582-588.

[23] I.M.S.C. Oliveira, J.P.N. Silva, E. Feitosa, E.F. Marques, E.M.S. Castanheira, M.E.C.D. Real Oliveira, Aggregation behavior of aqueous dioctadecyldimethylammonium bromide/monoolein mixtures: A multitechnique investigation on the influence of composition and temperature, *Journal of Colloid and Interface Science* 374(1) **2012** 206-217.

[24] M. Goto, S. Ishida, Y. Ito, N. Tamai, H. Matsuki, S. Kaneshina, Thermotropic and Barotropic Phase Transitions of Dialkyldimethylammonium Bromide Bilayer Membranes: Effect of Chain Length, *Langmuir* 27(10) **2011** 5824-5831.

[25] M. Goto, Y. Ito, S. Ishida, N. Tamai, H. Matsuki, S. Kaneshina, Hydrostatic Pressure Reveals Bilayer Phase Behavior of Dioctadecyldimethylammonium Bromide and Chloride, *Langmuir* 27(5) **2011** 1592-1598.

[26] M. Kodama, M. Kuwabara, S. Seki, Thermal study of the interaction of crystalline surfactant with water; The dioctadecyldimethylammonium chloride-water system, *Thermochimica Acta* 50(1) **1981** 81-91.

[27] P. Holmqvist, P. Alexandridis, B. Lindman, Modification of the microstructure in poloxamer block copolymer-water-"oil" systems by varying the "oil" type, *Macromolecules* 30(22) **1997** 6788-6797.

[28] T. Iwanaga, M. Suzuki, H. Kunieda, Effect of added salts or polyols on the liquid crystalline structures of polyoxyethylene-type nonionic surfactants, *Langmuir* 14(20) **1998** 5775-5781.

[29] P. Alexandridis, R. Ivanova, B. Lindman, Effect of glycols on the self-assembly of amphiphilic block copolymers in water. 2. Glycol location in the microstructure, *Langmuir* 16(8) **2000** 3676-3689.

[30] N. Markova, E. Sparr, L. Wadsö, H. Wennerström, A Calorimetric Study of Phospholipid Hydration. Simultaneous Monitoring of Enthalpy and Free Energy, *The Journal of Physical Chemistry B* 104(33) **2000** 8053-8060.

[31] J.N. Israelachvili, 8 - Special Interactions: Hydrogen-Bonding and Hydrophobic and Hydrophilic Interactions, in: J.N. Israelachvili (Ed.), *Intermolecular and Surface Forces (Third Edition)*, *Academic Press*, San Diego, 2011, pp. 151-167.

[32] A. Rouw, G. Somsen, Solvation and hydrophobic hydration of alkyl-substituted ureas and amides in NN-dimethylformamide + water mixtures, *Journal of the Chemical Society, Faraday Transactions 1: Physical Chemistry in Condensed Phases* 78(11) **1982** 3397-3408.

[33] H. Piekarski, G. Somsen, Enthalpies of solution of urea in water–alkanol mixtures and the enthalpic pair interaction coefficients of urea and several nonelectrolytes in water, *Canadian Journal of Chemistry* 64(9) **1986** 1721-1724.

[34] J.N. Spencer, J.W. Hovick, Solvation of urea and methyl-substituted ureas by water and DMF, *Canadian Journal of Chemistry* 66(4) **1988** 562-565.

[35] J.N. Losso, R.R. Bansode, 18 - Anti-angiogenic functional food, degenerative disease and cancer, in: C. Remacle, B. Reusens (Eds.), *Functional Foods, Ageing and Degenerative Disease*, *Woodhead Publishing*2004, pp. 485-523.

[36] S.M.B. Souza, E.B. Alvarez, M.J. Politi, Effect of Urea on Surfactant Aggregates: A Comprehensive Review, *Recent Trends in Surface and Colloid Science* 12 **2012** 155-169.

[37] D.R. Robinson, W.P. Jencks, The Effect of Compounds of the Urea-Guanidinium Class on the Activity Coefficient of Acetyltetraglycine Ethyl Ester and Related Compounds1, *Journal of the American Chemical Society* 87(11) **1965** 2462-2470.

[38] D.B. Watlaufer, S.K. Malik, L. Stoller, R.L. Coffin, Nonpolar Group Participation in the Denaturation of Proteins by Urea and Guanidinium Salts. Model Compound Studies, *Journal of the American Chemical Society* 86(3) **1964** 508-514.

[39] Y. Marcus, The Standard Partial Molar Volumes of Ions in Solution. Part 5. Ionic Volumes in Water at 125–200 °C, *The Journal of Physical Chemistry B* 116(24) **2012** 7232-7239.

[40] M. Kranenburg, M. Venturoli, B. Smit, Phase Behavior and Induced Interdigitation in Bilayers Studied with Dissipative Particle Dynamics, *The Journal of Physical Chemistry B* 107(41) **2003** 11491-11501.

[41] S. Furuike, V.G. Levadny, S.J. Li, M. Yamazaki, Low pH induces an interdigitated gel to bilayer gel phase transition in dihexadecylphosphatidylcholine membrane, *Biophysical Journal* 77(4) **1999** 2015-2023.

[42] M.R.A. Matos, B.F.B. Silva, E.F. Marques, Chain length mismatch and packing effects on the thermotropic phase behavior of salt-free catanionic surfactants, *Journal of Colloid and Interface Science* 405 **2013** 134-144.

[43] C. Bize, J.-C. Garrigues, M. Blanzat, I. Rico-Lattes, O. Bistri, B. Colasson, O. Reinaud, Spontaneous formation of vesicles in a catanionic association involving a head and tail functionalized amino-calix[6]arene, *Chemical Communications* 46(4) **2010** 586-588.

[44] K. Fontell, Influence of Electrolyte on Phase Equilibria and Phase Structure in the Binary System of Di-2-Ethylhexyl Sulphosuccinate and Water, *Colloidal Dispersions and Micellar Behavior, American Chemical Society*1975, pp. 270-277.

[45] M. Teubner, R. Strey, Origin of The Scattering Peak in Microemulsions, *Journal of Chemical Physics* 87(5) **1987** 3195-3200.

[46] J.N. Israelachvili, 21 - Interactions of Biological Membranes and Structures, in: J.N. Israelachvili (Ed.), *Intermolecular and Surface Forces (Third Edition), Academic Press*, San Diego, 2011, pp. 577-616.

Chapter 6*

Tunable surfactant phase transition in the presence of additives – Deposition of surfactant gel phase

An investigation of the tunability of the surfactant gel-to-liquid crystalline phase transition temperature (T_m) of a bilayer-forming cationic surfactant in the presence of small water-soluble additives, the phase behavior of such surfactant systems on dilution, and the deposition on silica are presented. Differential scanning calorimetry (DSC) allowed to track the T_m, and synchrotron and laboratory-based small and wide-angle X-ray scattering (SAXS and WAXS) were used to determine the self-assembled structure. A spontaneous transition from a liquid crystalline (L_α) phase to a gel (L_β) phase on dilution was demonstrated, which indicated that additives could be taken out from the L_α phase. By means of in-situ null ellipsometry, the deposition of a diluted surfactant L_β phase upon replacement of bulk solution by deionized water was followed. Robust layers at least one bilayer-thick were deposited onto the surface and shown to be irreversibly adsorbed due to poor surfactant solvency in water. The thickest layer of surfactant deposited after dilution was found for mixtures with small amounts of additive since high amounts might lead to a phase-separated system.

---

*This section is under review as: Rui A. Gonçalves, Polina Naidjonoka, Tommy Nylander, M. G. Miguel, B. Lindman and Yeng Ming Lam. *RSC Advances* (2020).

6.1 Introduction

The function of materials is often determined by their surface properties, i.e. where the material meets the surrounding medium. Deposition of a functional layer on a surface is, therefore, crucial for controlling material properties like lubrication and protection against contamination. It is challenging to prepare molecularly thin layers, and in particular, with controlled thickness and surface properties for such studies. Amphiphilic molecules, such as surfactants and lipids, adsorb from aqueous solution in monomolecularly thin layers on hydrophobic and hydrophilic surfaces. Such layers are, however, not very stable when exposed to water or humid air since they are made from substances with a significant solubility in water. Stable layers can be obtained by chemical coupling either the molecules onto the surface or between the adsorbed molecules. One example where the former concept is used is in the case where molecules with thiol end groups are used to modify gold surfaces and this has led to the development of some important practical applications [1-3].

Another principle for the preparation of monomolecular layers is built on spreading insoluble amphiphilic compounds on the air-water interface. This monolayer can be transferred to solid surface passing through the interface. Multilayers can be obtained in this way by letting the solid surface pass through the water-air interface several times. This is the basis for the well-established Langmuir-Blodgett method [4].

The adsorption of soluble low molecular weight substances is typically reversible, however polymers often display a more or less irreversible adsorption, especially for high molecular weight polymers. Charged polymers have a higher solubility in water and adsorbed strongly when the surface is oppositely charged [5]. This adsorption is effectively irreversible for higher molecular weight polymers. Polyelectrolyte adsorption has been thoroughly studied during recent decades and is exploited in many applications. For example, it is possible to charge up surfaces through adsorption and by using the irreversibility also reverse the charge of a surface. A practical application of charging up surfaces is in conditioning (“two-in-one”) hair shampoo where a cationic polymer is

deposited on hair from a mixed solution of an anionic surfactant and a cationic polymer. With an excess of surfactant, such a formulation is thermodynamically stable, and no adsorption onto hair occurs. However, on rinsing with water, the system falls into the two-phase region of the phase diagram and deposition occurs; further rinsing leads to removal of the surfactant whereas the polymer remains and gives the substrate the desired positive charge and a conditioning effect. The mechanism is well understood from phase diagrams, and the deposition has been demonstrated in in-situ adsorption studies using ellipsometry [6-10].

Alternatively, surfactants can be used for hair conditioning. Normally cationic surfactants or different mixed systems are used [11]. A good conditioning effect normally is based on achieving a layer of cationic surfactant in the lamellar gel (normally referred to as L_β) state. Here the surfactant molecules are in a solid-like state whereby robust layers are formed, and that desorption is slow because of very low solubility. Often cationic surfactants with two long alkyl chains are used. Problems with such formulations include the limited kinetic stability of the formulations and the difficulty in controlling the thickness of the deposited layers. In our previous work, the ability to tune the main phase transition temperature by using additives which are preferably located at the surfactant-water interface was demonstrated [12]. In addition, hydrotrope molecules have been used in the formulation of personal care products which make them favorable candidates to tune the phase behavior of surfactant mixtures.

The purpose of the present study was to reveal whether a well-defined layer of surfactant in the L_β state could be achieved from a controlled phase transition from a stable surfactant phase, in particular, a lamellar liquid crystalline phase (L_α). For this purpose, it was investigated whether addition of water-soluble components acting as co-surfactants can induce the requested phase transition. Furthermore, in-situ null ellipsometry studies were performed to determine the amount of surfactant deposited and the adsorbed layer thickness. It is shown that ternary surfactant-additive-water mixtures in the lamellar liquid crystalline state can be designed in such a way that they

are converted into the lamellar gel phase in excess of water. These are then deposited on surfaces in thin layers of well-defined thickness.

6.2 Results and discussion

6.2.1 Effects of the presence of an additive on the T_m

The gel-to-liquid crystalline (L_β-L_α) phase transition temperature (T_m) and the enthalpy of phase transition (ΔH_m) of the surfactant mixtures were determined by differential scanning calorimetry (DSC). The corresponding surfactant chain packing was determined by small and wide-angle X-ray scattering and will be discussed in the next section.

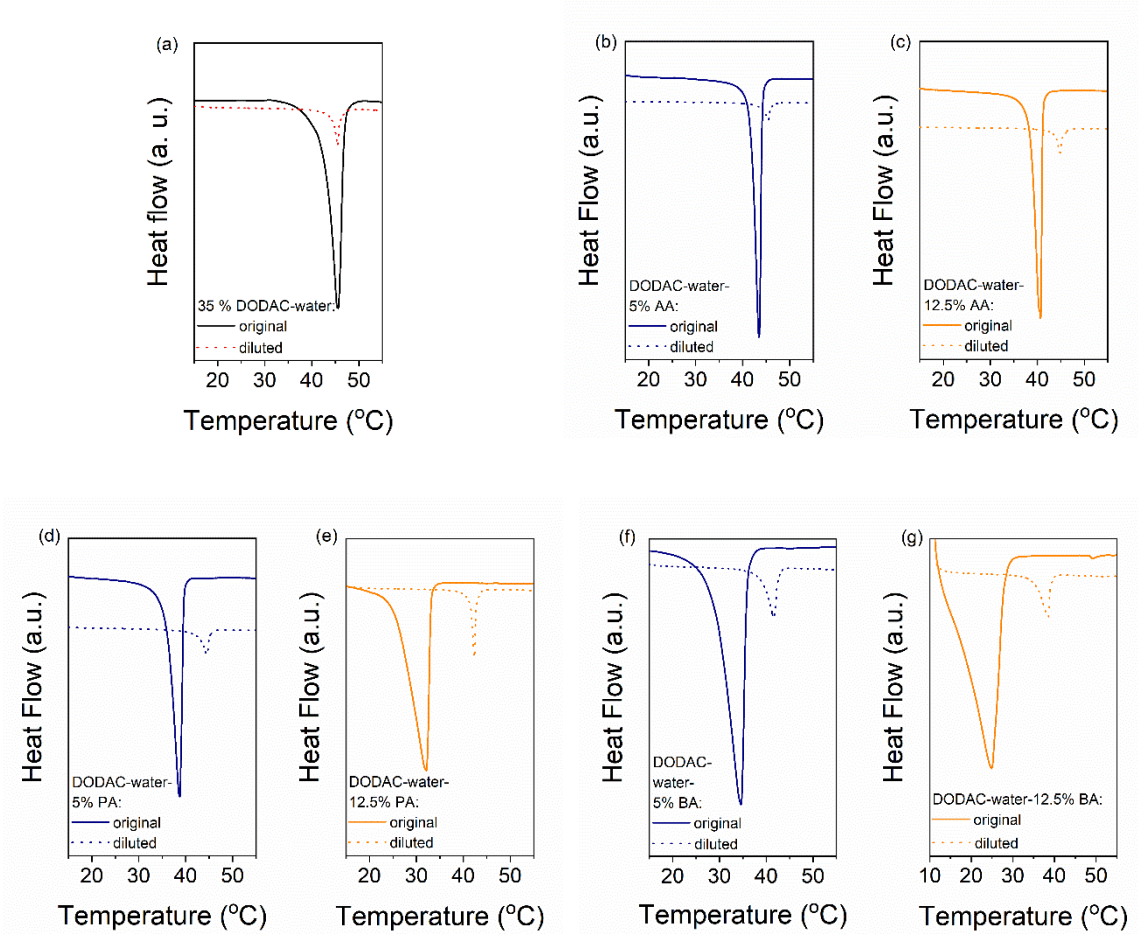

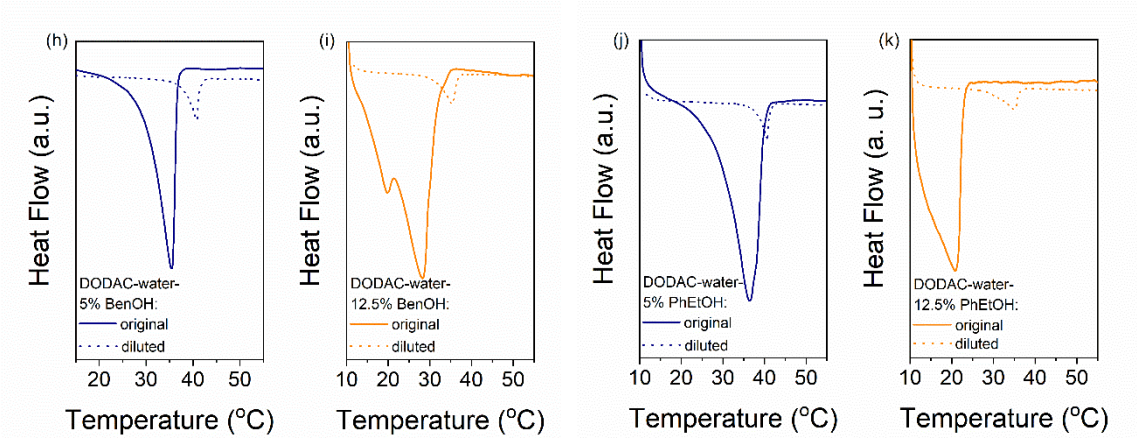

Figure 6.1 (a) DSC heating thermograms of 35 wt. % DODAC in water. Ternary surfactant mixtures with 5 wt. % (blue color) and 12.5 wt. % (orange color) of additive. Full line represents the original sample and dotted line corresponds to the sample diluted ten times. (b-c) Acetic acid (AA) samples. (d-e) Propionic acid (PA) samples. (f-g) Butyric acid (BA) samples. (h-i) Benzyl alcohol (BenOH) samples. (j-k) Phenoxyethanol (PhEtOH) samples. Endothermic down.

Figure 6.1 shows the DSC heating thermograms of the ternary surfactant-additive-water mixtures. Here the effect of three short-chain fatty acids (SCFAs): acetic, propionic and butyric acid; and two hydrotrope molecules: benzyl alcohol and phenoxyethanol on the thermal behavior of dioctadecyldimethylammonium chloride (DODAC) in water is presented. The full line represents the original samples (35 wt. % DODAC in water), and the dotted line corresponds to the diluted samples with 5 (blue color) and 12.5 wt. % (orange color) of additive in the system. As discussed in the earlier chapter, at these concentrations, only one thermal transition was detected for all the mixtures within the investigated temperature range (10 to 60 ^{o}C), for both the original sample as well as the same sample after dilution ten times with water. This suggests that with the dilution of the mixtures using water, the same type of self-assembled structure was maintained below and above the T_m, i.e. the lamellar arrangement. The original and diluted samples therefore appear to be in a gel (L_β) phase below the T_m and a liquid crystalline (L_α) phase above the T_m. A shift of the T_m to a higher temperature with water dilution was observed for all the samples. For instance, Figure 6.1 (b) displays the thermal behavior of the DODAC in the presence of small amount (5 wt. %) of acetic acid. A T_m of around 43.5 and 45.5 ^{o}C was found for the original sample and the diluted sample, respectively. By small amount of additive, the system is in excess concentration of surfactant.

The shape of the endothermic peaks is similar for all the mixtures. This suggests that additives affect the phase transition temperature by a similar mechanism and that they do not change the nature of the transition. However, the thermograms of the original samples of benzyl alcohol and phenoxyethanol, Figure 6.1 (h) to (k) full line, appear to be different as they show a small plateau before the phase transition, which almost disappears with excess amount (12.5 wt. %) of additive in the mixture. By excess amount, the system consists of larger additive molar concentration than of the surfactant. Also, excess amount of benzyl alcohol results in a peak split, indicating the possible formation of an intermediate phase. The presence of these hydrotropes results in a significant decrease in the L_β-L_α transition temperature (to 21 ^oC). Figure 6.2 summarizes the T_m and ΔH_m values obtained for aqueous mixtures of DODAC in the presence of small and excess amounts of the three SCFAs and the two hydrotrope molecules. These results show that the presence of the cosolutes in the surfactant system facilitates the transition from bilayers in the "solid" state to a "melted" state. A longer hydrophobic moiety of the cosolute results in a more significant decrease in the T_m.

The results from the diluted samples show that the addition of water to the surfactant system shifts the T_m back to higher temperatures, Figure 6.1. This indicates that these additives can be removed from the bilayers by water addition, thus restoring the gel phase. The enthalpy of the phase transition per mole of DODAC for the diluted samples was quite similar, although slightly lower, when compared to the values of the "original" samples as shown in Figure 6.2. This effect can be attributed to a residual amount of cosolute remaining in the bilayers. However, the enthalpy of phase transition of the diluted mixtures with butyric acid is higher than the original sample. Butyric acid is the least polar molecule of the studied series of additives. Therefore, this additive may partially remain at the surfactant-water interface reducing the electrostatic repulsion between surfactant head-groups.

The presence of SCFAs and hydrotropes on the lamellar structure, helped to tune the T_m. In addition, upon dilution the T_m was shifted to higher temperatures, thus increasing the relative stability of the lamellar gel phase.

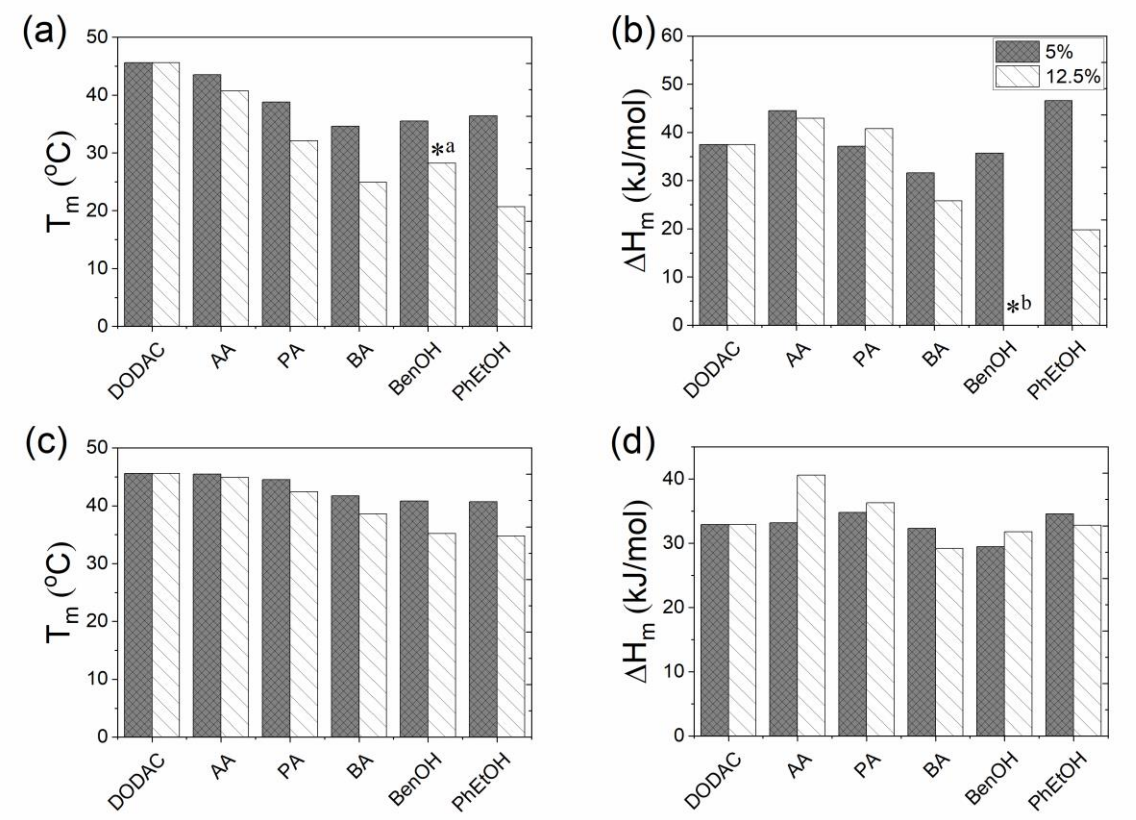

Figure 6.2 Thermodynamic parameters of the gel-to-liquid crystalline phase transition temperature (T_m) and the enthalpy of phase transition (ΔH_m) of the DODAC-water-additive mixtures at the original composition ((a) and (b)) and after dilution ten times ((c) and (d)). DODAC was fixed at 35 wt. % for all the samples. *a: Main phase transition peak; *b: Peak split that appears to indicate two thermal transitions, hence ΔH_m could not be determined.

6.2.2 Surfactant packing in the diluted regime

Small and wide-angle X-ray scattering (SAXS/WAXS) was used to determine the chain packing and structure of the diluted surfactant-additive mixtures at temperatures below and above the gel-to-liquid crystalline (L_β-L_α) phase transition (T_m). The characteristic Bragg reflections with a peak ratio of 1:2:3… corresponding to lamellar structures were clearly observed in the small-angle regime. In addition, the wide-angle scattering profiles allow to determine the solid-like or fluid-like state of the alkyl chains of the bilayer. For bilayers in the gel state (L_β), a sharp peak at around 1.5 $Å^{-1}$ is expected that corresponds to the characteristic inter-acyl chain distance of 4.2 Å, whereas, for the fluid-like state (L_α), a shift to lower q values and a peak broadening is observed. Indeed the reflections in the wide-angle regime correspond to an inter-acyl chain distance of 4.1-4.2 Å for the L_β phase, and ca. 4.5-4.6 Å for the L_α phase [13]. The SAXS profiles of the original DODAC mixtures with short-chain fatty acids (SCFAs) and hydrotropes at temperatures below and above their T_m (ascertained by DSC)) were also recorded and the data confirms the lamellar structures, Figure A.6.1 to Figure A.6.4 (appendix). Additional features can be extracted from the SAXS and WAXS profiles, such as interlamellar d-spacing, polar layer thickness, non-polar layer thickness and the area per surfactant molecule as discussed in detail in our previous study [12].

The surfactant mixtures were diluted ten times with water. These diluted mixtures display a rather thick water layer as demonstrated by means of synchrotron SAXS/WAXS analysis. The additive is expected to be at least partly removed from the water-DODAC interface. Indeed, after dilution the surfactant mixtures showed an increase in the T_m as discussed above. Thus, this suggests that the additives can be “washed away” from the mixed surfactant Lα phase, so that the DODAC gel phase is restored. To verify this expected behavior, the alkyl chain packing was determined using WAXS data collected from synchrotron source, both below and above the transition temperature of these diluted mixtures.

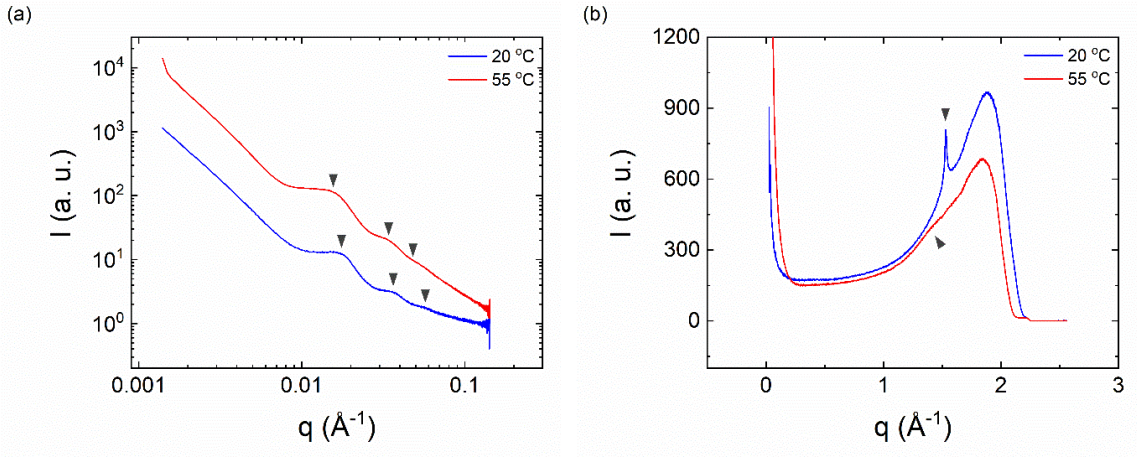

Figure 6.3 Synchrotron scattering profiles of diluted mixtures of 5 wt. % acetic acid in DODAC-water at 20 °C (below T_m) and 55 °C (above T_m). (a) SAXS and (b) WAXS.

The mixtures showed only one thermal transition under heating also after dilution of the sample (Figure 6.1). As previously reported, it can be assumed that lamellar surfactant systems display a large osmotic swelling which results in thick water layers in the lamellar structure [14]. Therefore, one may expect the same behavior for the DODAC-water-additive mixtures. Figure 6.3 shows the SAXS and WAXS profiles of diluted mixtures of DODAC in the presence 5 wt. % of acetic acid at 20 and 55 °C. As identified in Figure 6.3 (a), the Bragg reflections follow an order of 1: 2: 3: … which corresponds to a lamellar packing of the DODAC. At 20 °C, a sharp peak at 1.5 $Å^{-1}$, which corresponds to the hydrocarbon chains in the gel phase with an inter-acyl chain distance of 4.2 Å, is observed (Figure 6.3 (b)). This confirms that the system features a L_β phase at 20 °C. The sharp Bragg peak in the WAXS data has disappeared at 55 °C and is replaced by a broad peak at lower *q* values, typically observed for bilayers in the fluid-like state. These results suggest that after dilution, the system does not lose its lamellar packing. This demonstrates the ability to tune the phase behavior of this surfactant system in the presence of additives by simple dilution. The original samples in the presence of additives display a lower T_m as compared to the sample in the absence of additives. The L_α phase in the presence of additives is thus more stable for neat DODAC. The additive can be partially removed from the bilayers and leading to a recovery of the L_β phase and consequently increase the T_m simply by dilution of the mixture with water. The same trend was found for all the diluted mixtures in the

presence of 5 and 12.5 wt. % of propionic and butyric acid, benzyl alcohol and phenoxyethanol, Figure A.6.5 to Figure A.6.9 (appendix).

6.2.3 Adsorbed amount and layer thickness upon rinsing

The potential to tune the phase behavior by water addition lead us to explore the ability of these surfactant systems to be deposited onto surfaces. Silica was chosen as substrate to examine the deposition profile from the surfactant mixtures as a mimic of a negatively charged surface common in many applications. Previously it was demonstrated that deposition from surfactant/additive mixtures onto hydrophilic and hydrophobic silica are rather independent of the surface properties. Instead, deposition was found to be largely controlled by the solvency conditions rather than the attraction to the surface [7]. Here in-situ null ellipsometry was used to provide us with information on the equilibrium and kinetic aspects of the adsorption process, both in terms of the surfactant adsorbed amount, Γ, and average thickness of the adsorbed film, *d*. In addition, the area occupied per surfactant molecule, *a*, can be derived from the adsorbed amount. This study focuses on the surface deposition when DODAC mixtures with a small amount of additive (5 wt. %) and excess of additive (12.5 wt. %) were diluted.

In-situ, time-resolved adsorption measurements were conducted using aqueous dispersions of DODAC in the presence of three short-chain fatty acids (SCFAs): acetic acid, propionic acid, butyric acid; and two hydrotrope molecules: benzyl alcohol and phenoxyethanol. The adsorption/deposition process was performed in a two-cycle fashion, start/stop rinsing and repeat of rinsing, as illustrated in Figure 6.4. The average thickness and adsorbed amount are presented in Figure 6.5 and Figure 6.6.

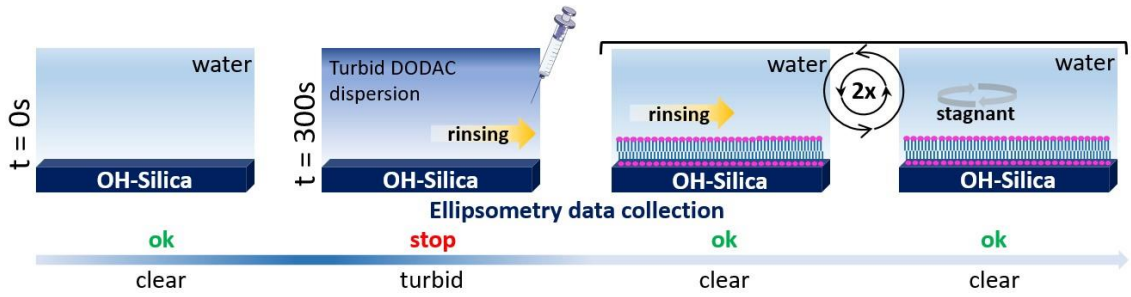

Figure 6.4 Schematic representation of the experimental procedure used to study the deposition from DODAC-water-additive mixtures at the silica/water interface at 25 °C by in-situ null ellipsometry. At t = 0 s the silica wafer was immersed in water. The diluted surfactant sample was injected into the cuvette at t = 300 s, followed by start/stop rinsing and repeat of rinsing.

Before discussing the details of the results for the different conditions (presented below in Figure 6.5 to Figure 6.8), some general observations are made. One striking aspect is that throughout a surfactant layer is deposited on the substrate and that both the adsorbed amount and the thickness of the adsorbed layers are in a rather limited range in spite of large differences in the composition of the bulk surfactant phase. Stable plateau values are obtained, which do not vary over long waiting times and do not change on dilution. This rather well defined behavior is striking in view of the non-equilibrium conditions of the experiments.

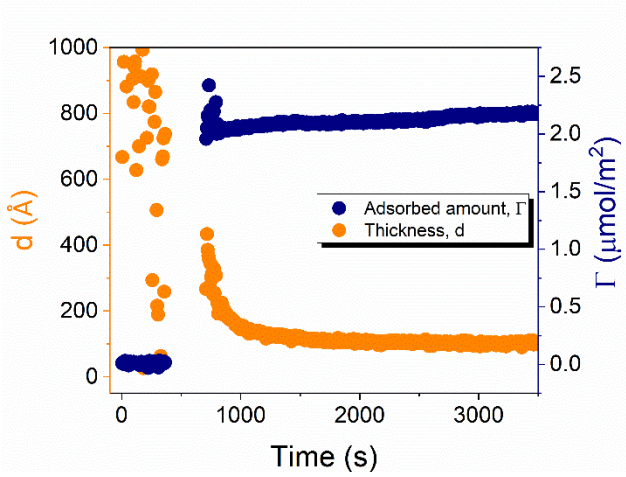

Figure 6.5 Time evolution of the adsorbed amount (Γ) and average layer thickness (*d*) of DODAC-water mixture at the silica/water interface (T = 25 °C).

A stable plateau of the values of Γ and *d* is thus obtained after ca. 1000 s, with the exception of the sample with 12.5 wt. % of propionic acid, Figure 6.6 (c). The time required to reach steady-state conditions depends on factors like the turbidity of the sample, the bulk concentration, etc...[15] Since ellipsometry is an optical technique, it requires a certain transparency of the medium. The turbid nature of the surfactant mixtures used here does not allow enough light to pass through the solution to follow the adsorption process. Nevertheless, seconds after the rinsing process started, the instrument resumed the data collection. Therefore, there is a gap in the data between the moment that the sample was injected (t = 300 s) and a few seconds after the rinsing started (t = 700 s). Once the solution was sufficiently clear, the amount of surfactant adsorbed was determined to 2.13 μmol/m^2, and the average layer thickness 107 Å. From the adsorbed amount, the area per surfactant molecule was determined to be 78 $Å^2$. This result is consistent with the area per surfactant molecule of bulk DODAC-water mixtures determined by SAXS in our previous study [12].

Table 6.1 summarizes the properties of the adsorbed layers from the diluted DODAC-water-additive mixtures. Since all the films onto the hydrophilic silica are deposited from a highly diluted medium they are expected to be in the gel phase at 25 ^oC as demonstrated by the DSC and WAXS results. After the deposition on the surface, two cycles of rinsing were conducted, with no desorption being observed. Regarding the driving force, the formation of the surfactant film is attributed mainly to the inherent insolubility of DODAC in water but there is also an electrostatic attraction of the cationic surfactant to the negatively charged surface. The composition of the formed surfactant layer cannot be determined using ellipsometry, hence one can only evaluate the data in terms of the total amount deposited and the thickness of the formed layer. In the corresponding bulk sample, the DODAC bilayer was determined to be 28 Å-thick (using X-rays). This bilayer is rather thin when compared to the expected total thickness of two monolayers formed by an 18 carbon-chain oriented perpendicular to the interface. Such a small thickness value can be explained by the formation of a tilted and interdigitated DODAC bilayer in the gel phase [12].

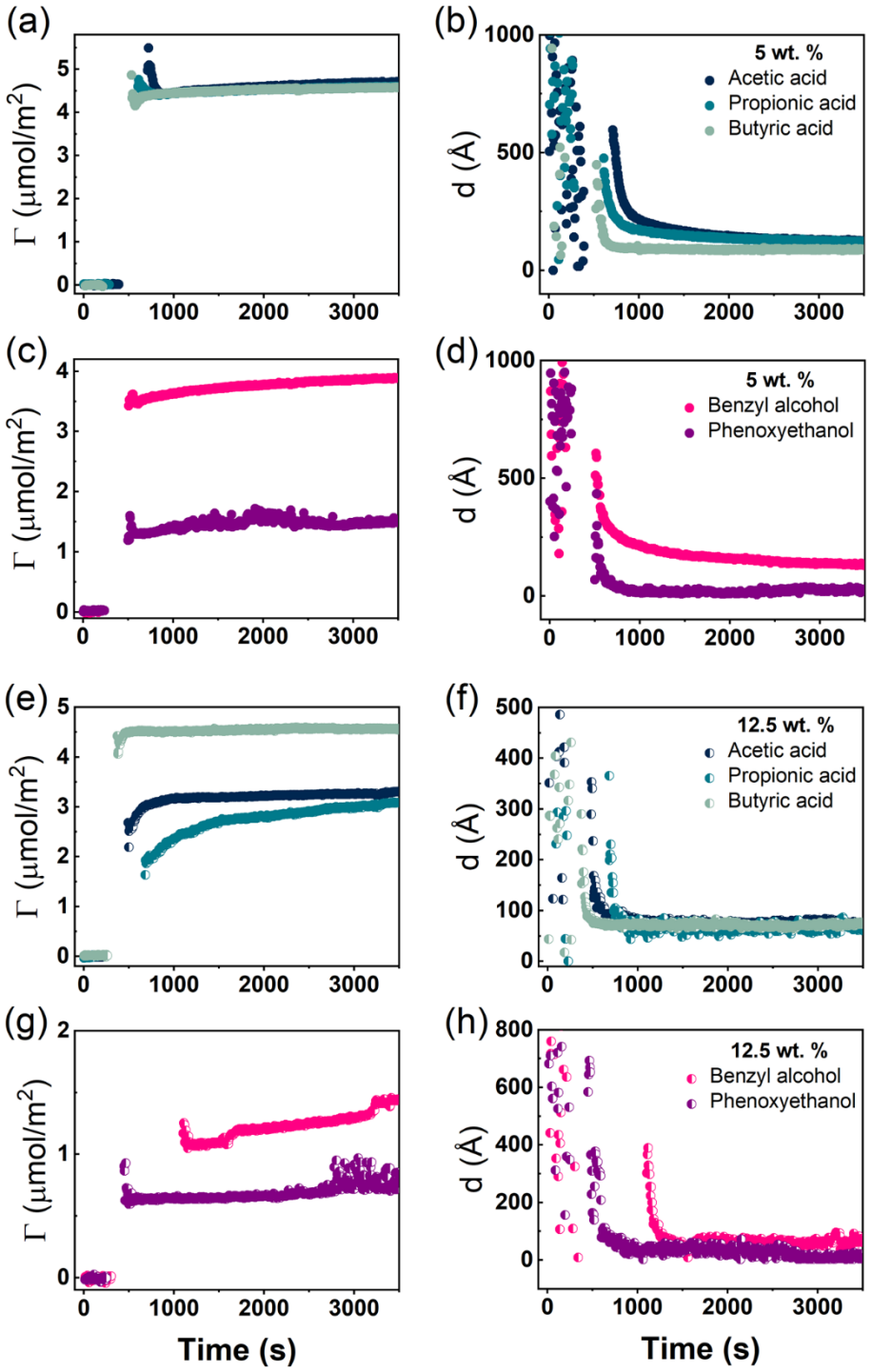

Figure 6.6 Time evolution of the adsorbed amount (cf. equation 3.9), Γ, and average layer thickness, *d*, of DODAC-water-additive mixtures at the silica/water interface (T = 25 °C). (a) to (d) DODAC-water-5 wt. % additive. (e) to (h) DODAC-water-12.5 wt. % additive.

Deposition with added short-chain fatty acids

As mentioned above the phase transition between the gel and liquid crystalline phases can be tuned by the addition of certain solutes [12, 16-18]. Here the effect of addition of three short-chain fatty acids (SCFAs), namely, acetic, propionic and butyric acid was investigated, which decrease the transition temperature markedly, on the amount of DODAC adsorbed on silica and the thickness of the deposited layer. The more hydrophobic the SCFA is, the less turbid the dispersion. This was also supported by the DSC data that demonstrated that butyric acid contributed to a more stable DODAC L_α phase. This is shown in Figure 6.6 (a) and (b). The ellipsometer first resumed the data collection for butyric acid, followed by propionic acid, and last by acetic acid. However, in excess of SCFA, the turbidity of the mixtures increased in the order butyric < acetic < propionic acid, hence a different behavior was observed. Therefore, the opaque DODAC dispersion in excess of propionic acid took longer time to reach a steady-state value. These results point to a stronger affinity of propionic acid to DODAC when in excess in the system. Consequently, a longer time is needed to remove the propionic acid from the DODAC bilayer during the rinsing process.

The mixtures with a small amount of short-chain fatty acid gave a larger adsorbed amount than the corresponding mixtures with an excess of short-chain fatty acid, except for the mixture with an excess of butyric acid. The same trend was found for the average film thickness. In line with previous results for polyelectrolyte-surfactant mixtures deposition increases when rinsing starts closer to the phase border [8]. On rinsing, a residual amount of SCFAs remains in the bilayers, which reduced the electrostatic repulsion between DODAC molecules, thus resulting in larger adsorbed amounts, and consequently, a smaller area per surfactant molecule.

Hydrotropes

The presence of hydrotrope molecules, benzyl alcohol and phenoxyethanol, results in smaller adsorbed amounts of DODAC, with the exception of benzyl alcohol at low concentration. Small amount (5 wt. %) of benzyl alcohol in the mixture boosts the adsorbed amount by producing a closely packed DODAC bilayer with an area per surfactant molecule of 43 $Å^2$. On the contrary, small amount of phenoxyethanol and excess amount of both hydrotrope molecules results in lesser adsorbed amounts (< 1.81 μmol/m^2) corresponding to larger areas per surfactant molecule (> 92 $Å^2$), Figure 6.6 (c), (g) and Table 6.1. Ellipsometry measures the mean optical thickness, thus a thin layer or low adsorbed amount does not rule out that inhomogeneities with dense patches of adsorbed surfactant bilayers partially cover the substrate area.

The mixture with excess amount of benzyl alcohol was rather opaque, therefore it took a long time to resume ellipsometry data collection after the rinsing process had started, Figure 6.6 (g). Furthermore, three steady-state plateaus are identified during successive rinsing cycles, which feature an increase of the adsorbed amount with each rinsing step. This suggests that benzyl alcohol is removed gradually, with more DODAC deposited at each step. For all the other mixtures, the additive was "washed away" immediately during the first rinsing cycle. This evidence highlights the DODAC solvency effect as the driving force for surfactant adsorption onto silica.

It is noteworthy that the addition of these additives led to a significant variation of the pH, Table 6.1. This suggests a carboxylate formation with the release of protons (hydrogen ions), thus resulting in an acidification of the dispersion. For all the investigated additives, robust layers with a thickness of at least twice the length of the surfactant molecules are seen to be irreversibly deposited on hydrophilic silica.

Table 6. 1 Values of the adsorbed amount, Γ, average layer thickness, *d*, area per surfactant molecule, *a*, and pH of the diluted DODAC-water-additive mixtures.

	Diluted sample	Adsorbed amount, Γ (μmol/m^2)	Average thickness, *d* (Å)	Area per molecule, *a* (Å^2)	pH
	No additive	2.13	107	78	6.16
Small amount	**5 % Acetic acid**	4.71	124	35	2.99
	5% Propionic acid	4.54	136	37	3.10
	5 % Butyric acid	4.53	89	37	3.14
	5% Benzyl alcohol	3.84	144	43	4.43
	5% Phenoxyethanol	1.48[a]	26	112	7.22
Excess amount	**12.5 % Acetic acid**	3.22	76	52	2.77
	12.5 % Propionic acid	2.91	63	57	2.84
	12.5 % Butyric acid	4.55	72	36	2.82
	12.5 % Benzyl alcohol	1.81[b]	62	92	3.89
	12.5 % Phenoxyethanol	0.73	38	-	6.76

[a] Large scattering observed;

[b] Result from the plateau in the steady-state.

Concentration effect

To understand the effects of the concentration of the mixture on the adsorbed DODAC amount and the thickness of the film formed, four different mixtures in the presence of excess butyric acid were studied. From the same diluted sample with butyric acid, increasing volumes (0.3, 0.5, 0.6 and 1.0 mL) were collected and added to the ellipsometry cuvette, and the volume was adjusted with water to a final volume of 5.0 mL. The added volume of the DODAC mixtures corresponds to concentrations of 3.6 mM (C1), 6.0 mM (C2), 7.2 mM (C3) and 12.0 mM (C4). The results of the adsorbed amount and layer thickness are presented in Figure 6.7 and summarized in Table 6. 2.

The turbidity of the mixtures increased with concentration in the order C1 < C2 < C3 < C4, which is noticeable in Figure 6.7. After the rinsing process started, only 158 seconds were needed to resume the data collection for the C1 mixture, whereas extra time was needed for the mixtures with high concentrations. The C4 mixture profile shows a considerably higher level of scattering when compared to the lower concentration samples, and stabilized at a steady-state plateau only around 2400 s. This suggests that a more homogeneous layer of surfactant at low concentration was formed.

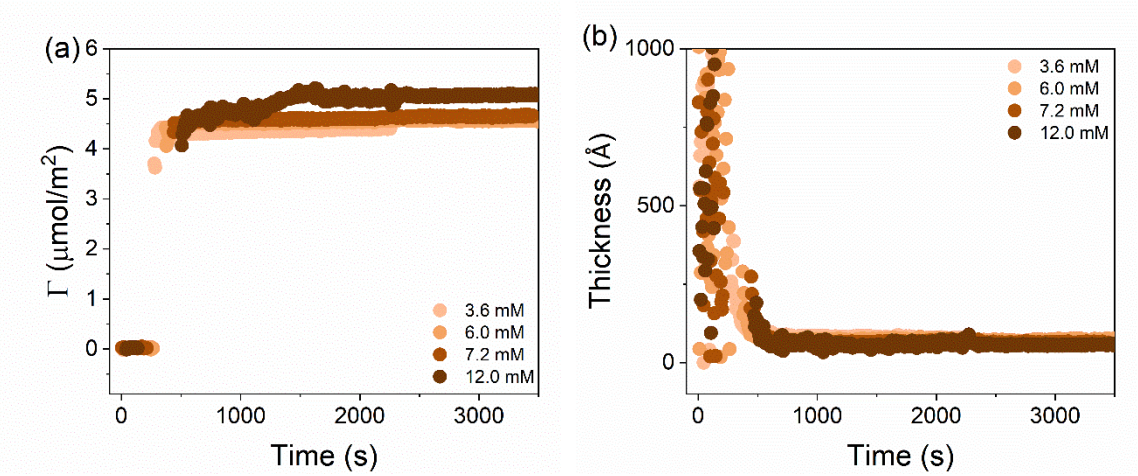

Figure 6.7 (a) Time evolution of the adsorbed amount, Γ, and (b) average layer thickness, d, of DODAC-water-butyric acid mixtures at the silica/water interface (T = 25 ºC). Mixtures with increasing concentration in the ellipsometry cuvette, 3.6 mM (C1), 6.0 mM (C2), 7.2 mM (C3) and 12.0 mM (C4).

Whereas the adsorbed amount is higher and the adsorbed layer thinner in the presence of butyric acid than for the surfactant alone there is only a moderate variation of the deposition data with the concentration, Figure 6.8. There is a slight increase of the adsorbed amount with the concentration. The origin of this effect is not clear but as discussed previously, the presence of SCFAs contributes to shield the electrostatic repulsion between DODAC head groups, which might enhance the amount of surfactant adsorbed on the substrate. As a result, the area per surfactant molecule was determined to decrease when compared to the mixture in the absence of SCFAs. The mixture C4 resulted in a slightly larger adsorbed amount of DODAC and smaller area per molecule, and the deposited layer from this mixture took longer time to reach steady-state values. It is noteworthy that the adsorbed amounts from mixtures with increasing concentration appear to be the same. More importantly, from the first and second columns in Figure 6.8 (a), the results suggest that butyric acid facilitates the deposition of robust and homogeneous layers of DODAC onto hydrophilic silica, even for the lowest concentration studied. The deposited layer of DODAC in the presence of butyric acid (from 56 to 89 Å) was slightly thinner compared to the deposited layer in the absence of additive (107 Å).

In the previous section, it was shown that thicker layers of DODAC were deposited when the solute was present in small amount (5 wt. %), and the excess of solute (12.5 wt. %) lead to a deposition of thinner layers of surfactant. The mixtures C1, C2, C3 and C4 are in the presence of excess of butyric acid giving slightly thinner deposited layers of surfactant. Whereas there are some differences, a main finding is that well-defined layers are deposited and have a thickness slightly above the double length of the surfactant molecule.

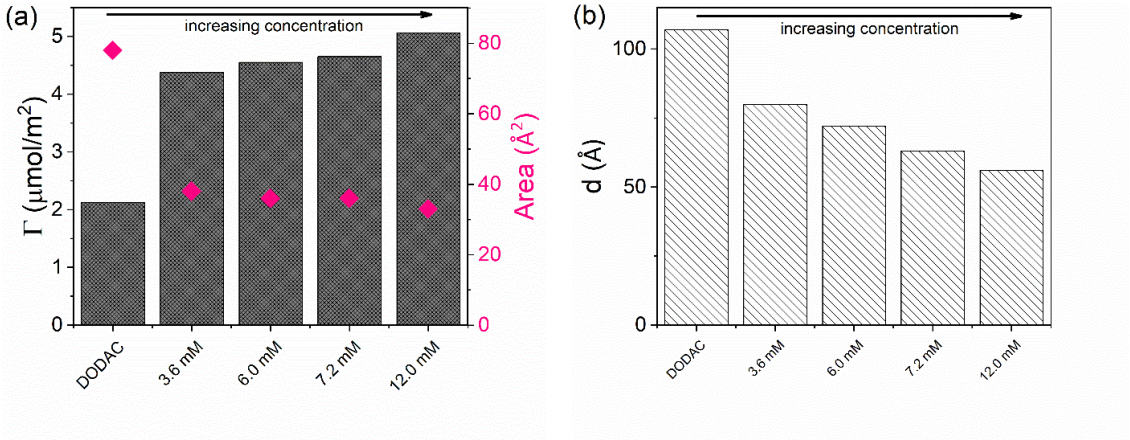

Figure 6.8 (a) Adsorbed amount (Γ) and area per surfactant molecule, and (b) average layer thickness (*d*) of mixtures of 12.5 wt. % of butyric acid in DODAC-water. Mixtures with increasing concentration in the ellipsometry cuvette, 3.6 mM (C1), 6.0 mM (C2), 7.2 mM (C3) and 12.0 mM (C4).

Table 6. 2 Values of the adsorbed amount, Γ, average layer thickness, d, and area per surfactant molecule, a, of the diluted DODAC-water-12.5 wt. % butyric acid samples with increasing concentration of the solution in the ellipsometry cuvette. Concentration increases from C1 to C4.

Diluted sample	**Adsorbed amount, Γ (µmol/m²)**	**Average thickness, *d* (Å)**	**Area per molecule, *a* (Å²)**
C1 – 3.6 mM	4.37	80	38
C2 – 6.0 mM	4.55	72	36
C3 – 7.2 mM	4.65	63	36
C4 – 12.0 mM	5.06	56	33

6.3 Conclusions

The double-chain cationic surfactant, DODAC, has very low solubility in water but a large tendency to form bilayer structures swelling with water. At low temperatures, a gel phase, L_β, is formed with the surfactant molecules in a solid-like state whereas above a well-defined transition temperature, T_m, a liquid crystalline phase, L_α, is formed.

As described in this work, a number of low molecular weight water-soluble compounds can lower the transition temperature substantially. Interestingly, on diluting samples of surfactant, additive and water, there is a spontaneous transition from the L_α to the L_β phase, ascribed to the dissociation of additive from the bilayers. Surfactants of the type studied have important applications for surface modification, like in hair conditioning. This is based on covering the substrate with the L_β phase. One problem in applications is to form stable formulations of the surfactant, the formulation typically consisting of kinetically stable dispersed particles of the L_β phase. The L_α phase, on the other hand, is thermodynamically stable over wide ranges and easier to formulate.

One purpose of the present work was to investigate if stable samples of the L_α phase can spontaneously be changed into the L_β phase and subsequently deposited on a substrate. This was achieved via lowering the T_m using a water-soluble additive. On dilution, it is washed away, and the composition of the surfactant bilayer changed so that T_m is raised and a gel structure is formed. The WAXS results show that a sharp crystalline peak appears on dilution and that the chain-to-chain distance decreases, thus demonstrating the formation of a gel phase. Ellipsometry studies demonstrate that dilution of the surfactant-additive-water phases leads to the deposition of well-defined robust layers on a substrate. The adsorbed surfactant layers have a thickness of the order of the double surfactant molecule length and are stable and not affected by extensive dilution.

References

[1] R.G. Nuzzo, D.L. Allara, Adsorption of bifunctional organic disulfides on gold surfaces, *Journal of the American Chemical Society* 105(13) **1983** 4481-4483.

[2] E.B. Troughton, C.D. Bain, G.M. Whitesides, R.G. Nuzzo, D.L. Allara, M.D. Porter, Monolayer films prepared by the spontaneous self-assembly of symmetrical and unsymmetrical dialkyl sulfides from solution onto gold substrates - structure, properties, and reactivity of constituent functional-groups, *Langmuir* 4(2) **1988** 365-385.

[3] C.D. Bain, E.B. Troughton, Y.T. Tao, J. Evall, G.M. Whitesides, R.G. Nuzzo, Formation of monolayer films by the spontaneous assembly of organic thiols from solution onto gold, *Journal of the American Chemical Society* 111(1) **1989** 321-335.

[4] I.R. Peterson, Langmuir-Blodgett films, *Journal of Physics D: Applied Physics* 23(4) **1990** 379-395.

[5] B. Lindman, B. Medronho, L. Alves, C. Costa, H. Edlund, M. Norgren, The relevance of structural features of cellulose and its interactions to dissolution, regeneration, gelation and plasticization phenomena, *Physical Chemistry Chemical Physics* 19(35) **2017** 23704-23718.

[6] E. Terada, Y. Samoshina, T. Nylander, B. Lindman, Adsorption of cationic cellulose derivatives/anionic surfactant complexes onto solid surfaces. I. Silica surfaces, *Langmuir* 20(5) **2004** 1753-1762.

[7] E. Terada, Y. Samoshina, T. Nylander, B. Lindman, Adsorption of Cationic Cellulose Derivative/Anionic Surfactant Complexes onto Solid Surfaces. II. Hydrophobized Silica Surfaces, *Langmuir* 20(16) **2004** 6692-6701.

[8] A.V. Svensson, L. Huang, E.S. Johnson, T. Nylander, L. Piculell, Surface Deposition and Phase Behavior of Oppositely Charged Polyion/Surfactant Ion Complexes. 1. Cationic Guar versus Cationic Hydroxyethylcellulose in Mixtures with Anionic Surfactants, *ACS Appl. Mater. Interfaces* 1(11) **2009** 2431-2442.

[9] O. Santos, E.S. Johnson, T. Nylander, R.K. Panandiker, M.R. Sivik, L. Piculell, Surface Adsorption and Phase Separation of Oppositely Charged Polyion−Surfactant Ion Complexes: 3. Effects of Polyion Hydrophobicity, *Langmuir* 26(12) **2010** 9357-9367.

[10] A.V. Svensson, E.S. Johnson, T. Nylander, L. Piculell, Surface Deposition and Phase Behavior of Oppositely Charged Polyion−Surfactant Ion Complexes. 2. A Means to Deliver Silicone Oil to Hydrophilic Surfaces, *ACS Appl. Mater. Interfaces* 2(1) **2010** 143-156.

[11] M. Kodama, M. Kuwabara, S. Seki, Thermal study of the interaction of crystalline surfactant with water; The dioctadecyldimethylammonium chloride-water system, *Thermochimica Acta* 50(1) **1981** 81-91.

[12] R.A. Gonçalves, B. Lindman, M.G. Miguel, T. Iwata, Y.M. Lam, Elucidating the effect of additives on the alkyl chain packing of a double tail cationic surfactant, *Journal of Colloid and Interface Science* 528 **2018** 400-409.

[13] D.F. Evans, H. Wennerström, The colloidal domain : where physics, chemistry, biology, and technology meet, 2nd ed. ed., New York : Wiley-VCH, 1999.1999.

[14] E.F. Marques, B.F.B. Silva, Surfactant Self-Assembly, in: T. Tadros (Ed.), *Encyclopedia of Colloid and Interface Science*, *Springer Berlin Heidelberg*, Berlin, Heidelberg, 2013, pp. 1202-1241.

[15] F. Tiberg, M. Landgren, Characterization of Thin Nonionic Surfactant Films at the Silica Water Interface by Means of Ellipsometry, *Langmuir* 9(4) **1993** 927-932.

[16] R.A. Demel, B. De Kruyff, The function of sterols in membranes, *Biochimica et Biophysica Acta (BBA) - Reviews on Biomembranes* 457(2) **1976** 109-132.

[17] J.R. Usher, R.M. Epand, D. Papahadjopoulos, The effect of free fatty acids on the thermotropic phase transition of dimyristoyl glycerophosphocholine, *Chem. Phys. Lipids* 22(3) **1978** 245-253.

[18] R.N. McElhaney, The use of differential scanning calorimetry and differential thermal-analysis in studies of model and biological-membranes, *Chem. Phys. Lipids* 30(2-3) **1982** 229-259.

Chapter 7

Impact and Outstanding Questions

The research outcomes in this dissertation suggest the development of a novel approach for the formulation of a stable gel phase and modification of surfaces. This chapter will therefore attempt to draw a comprehensive rationale from work conducted, its scientific impact, and make suggestions for future studies in this field of research. The unanswered questions remaining from this work are presented, and opportunities for future investigations inspired by other pieces of work are discussed and suggested.

7.1 Impact

This Ph.D. work has investigated the effect of additives with different chemical nature on the deposition of a lamellar surfactant gel phase on surfaces using a phase behavior approach. It started with the study of the stability of "swelling-type" surfactant systems with water, followed by the effect of additives on the lamellar structure and its characterization. The main focus of this thesis work is also on the investigation of the underlying additive/surfactant interactions and how this correlate to the ability of the additive to tune the gel-to-liquid crystalline phase transition temperature. The mechanism of deposition of robust layers of surfactant in a stable gel phase induced by a shift towards a two-phase region of the phase diagram by water addition was also investigated. The application of this new approach of surfactant deposition and surface modification was demonstrated.

This dissertation was organized by investigation of the stability of lamellar surfactant phases in the presence of different counterions (chapter 4), the effects of the inclusion of additives to the surfactant system packing structure (chapter 5) and the phase tunability and surfactant deposition upon dilution with water (chapter 6). The selection of additives was based on their polarity, which determines their partitioning in the lamellar structure. For instance, urea is a polar molecule which disperses in an aqueous medium, hydrotrope molecules are amphiphilic and facilitate the solubilization of hydrophobic compounds in water and long-tailed fatty acids and alcohols are expected to affect the lamellar stability via electrostatic effects and hydrophobic interactions. Therefore, the lamellar phase stability of surfactant in water studied in chapter 4; the effects of additives to tune the gel-to-liquid crystalline phase transition temperature was examined in chapter 5; chapter 6 demonstrated the role of water addition on dilution by removing the water-soluble additives from the bilayers and deposit robust layers of surfactant in the gel phase on a surface.

The scientific impact drawn from these chapters is listed as follows:

1) Stable lamellar surfactant phases, which are capable of taking up large amounts of water, have been successfully formulated. A one-dimensional swelling profile was determined for both gel (L_β) and liquid crystalline (L_α) phases. These results demonstrated a large swelling of a surfactant gel phase with potential hair-care applications.
2) The interlamellar spacing determination has revealed a larger repeat distance for the L_α phase than for the L_β phase. With an orientation of the surfactant molecules perpendicular to the bilayers, the opposite situation is predicted. This indicates a considerable tilting and/or interdigitation of the alkyl chains in the L_β phase.
3) The gel-to-liquid crystalline (L_β-L_α) phase transition temperature has been tuned by incorporating water-soluble additives in the bilayer. The surfactant systems showed hysteresis revealing only one thermal transition. Additives which partition at the polar/non-polar interface have resulted in stable lamellar phases, and those with a long hydrophobic tail stabilized the gel phase, thus showing higher L_β-L_α phase transition temperatures. Reversed bicontinuous phases have been confirmed in the presence of more hydrophobic additives above the main phase transition temperature. The inclusion of butyric acid has demonstrated a reduction of the alkyl chain interdigitation in the gel phase.
4) Well-defined robust layers of lamellar surfactant gel phase have been adsorbed on a hydrophilic silica surface; the rinsing process has led to removal of the water-soluble additives from the bilayers; the adsorbed layer has been irreversibly deposited on the surface and not affected by extensive dilution; this strategy has the potential to tune the phase behavior achievable by water dilution. This new principle of surfactant deposition/surface modification unravels the potential of small polar molecules which partition at the bilayer interface to act as active compounds with tunable phase behavior properties that enables the formulation of a variety of new products for conditioning applications.

In summary, this thesis demonstrated that the inclusion of selected additives is a versatile approach to formulate stable lamellar surfactant systems. Stable mixtures of the liquid crystalline phase can spontaneously be changed into the gel phase and subsequently deposited on a substrate (as schematically depicted in the hypothesis, Figure 1.1). The strategy established in this work, highlighted in chapter 6, provides new avenues to formulate new products for a wide variety of applications.

7.2 Outstanding questions and future work

The location of the additive molecules in the lamellar structure essentially determines the additive-bilayer structure interactions. The effect of these additives on the packing structure is pivotal to formulate single and stable gel and liquid crystalline phases.
Gel phases are inherently more complex partially due to their "solid-like" properties, which results in a kinetically stable state. For instance, the high viscosity has been a limiting factor to the phase characterization.

Therefore, it is essential to further investigate the phase behavior of "swelling-type" surfactant systems from a perspective of the stability and enhance the gel phase characterization methods.

7.2.1 Stability perspective

The packing in lamellar phases of double-tailed cationic surfactants with bromide and chloride reveals that the counterion is critical to achieving stable and highly swollen phases. The swelling of these ionic surfactants is governed by electrostatic interactions, meaning that the electric double-layer dominates the interbilayer interaction.

Bromide counterion associates rather strongly to the interface, resulting in fewer counterions in the diffuse double-layer and therefore less repulsion between bilayers. On the other hand, a more solvated ion like acetate contributes more to the diffuse part of the

double-layer, thus resulting in a more considerable swelling by electrostatic repulsion. Charged surfaces are described by a surface charge density (σ) and a potential (Φ_0); the adjacent electrolyte solution is described by bulk concentration (c_{i0}) valency (z_i), and the dielectric constant of the solvent [1]. This effect is illustrated in Figure 7.1 and used the Poisson-Boltzmann equation to derive and model the Gouy-Chapman theory. As reported in Table 6.1, some additives modify pH, and very likely can change the surface charge. The stability of the layer is firstly addressed by counterion dissociation and hydration, thus the role of additives that can modify Debye length should be considered. Therefore, the effect of molecules on the Debye length of positively charged DODAC interface is recommended for future investigations.

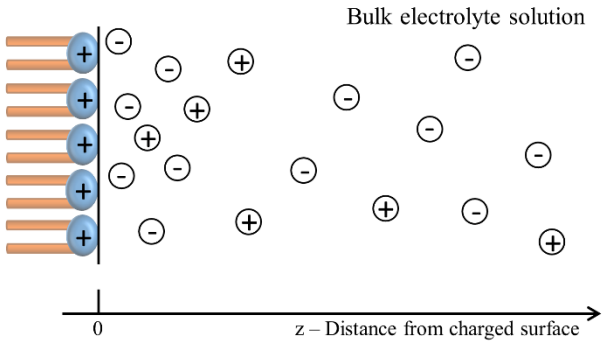

Figure 7.1 The model used to derive the Gouy-Chapman theory from the Poisson-Boltzmann equation. A positively charged wall that it infinite in *x* or *y* direction has associated with it a charge density and a potential. Valency and concentration of electrolyte and the dielectric permittivity of the solvent determine the variation in potential in *z* direction. The ions are treated as point charges.

In addition, the effect of water hardness on the transition temperatures and on the removal of the additives should be evaluated for commercial applications. In this work all experiments are performed in distilled water.

An investigation that further elucidates the effects of the addition of additives that tune the structure of DODAC is recommended. A complementary study on the removal of additives by water with different dissolved minerals is also suggested. This may also provide details

on how to prevent the formation of a thermodynamically more stable gel phase (coagel).

The outcomes of the work presented in this dissertation can be further exploited not only in the cosmetic industry but also to investigate applications in other fields such as different types of detergency, nano-medicine, and perhaps in food technology also.

7.2.2 Characterization perspective

Small and wide-angle X-ray scattering has been employed to characterize the packing structure of lamellar phases. A common limiting factor could be when the contrast between the scattering level of background and sample is very similar [2]. The large scattering length difference of hydrogen and deuterium provides the contrast needed, and it is widely used to overcome this limitation. The use of small-angle neutron scattering would provide complementary information on the alkyl chain packing in the gel phase and elucidate the underlying phenomena causing the chain interdigitation. Nagao et al. have been studying lamellar systems and investigating how the interlamellar distance (*d*) is affected by thickness fluctuations in a swollen lamellar phase, Figure 7.2. Membranes with low bilayer thickness value became rigid, and large bilayer thickness values resulted in more flexible membranes. The reason is that the membrane thickness is a function of the bending rigidity [3].

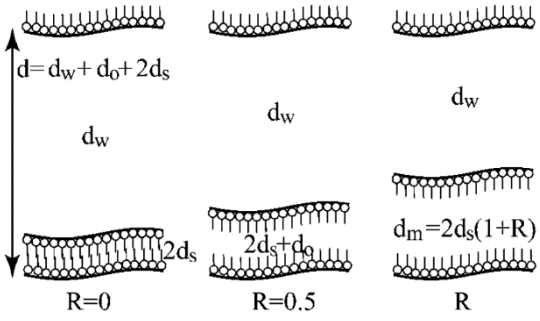

Figure 7.2 A schematic illustration of the lamellar system. Addition of oil to the system swells the $C_{12}E_5$ bilayers. Since the volume fraction of surfactant is kept constant, the interlamellar distance, *d*, is constant, while the bilayer thickness, $d_m = 2d_s + d_o = 2d_s\,(1 + R)$, increases with increasing R, where d_s and d_o are the surfactant molecular length and the oil layer thickness. R = 0 corresponds to the case of pure bilayers. R is the ratio between the volume fraction of oil ϕ_o and that of

surfactant ϕ_s, $R = \phi_o/\phi_s$. (*Reproduced from M. Nagao, S. Chawang and T. Hawa, Soft Matter, 2011, 7, 6598-6605 with permission from The Royal Society of Chemistry*) [2].

Recently, Nagao et al. showed in different studies [4, 5] that the membrane rigidity can drive the surfactant packing in different self-assembled structures and it also affected the diffusion of molecules throughout the membrane, Figure 7.3. A series of phosphatidylcholine bilayers were studied and shown different membrane properties and encouraged new investigations on the mechanical properties of bilayers.

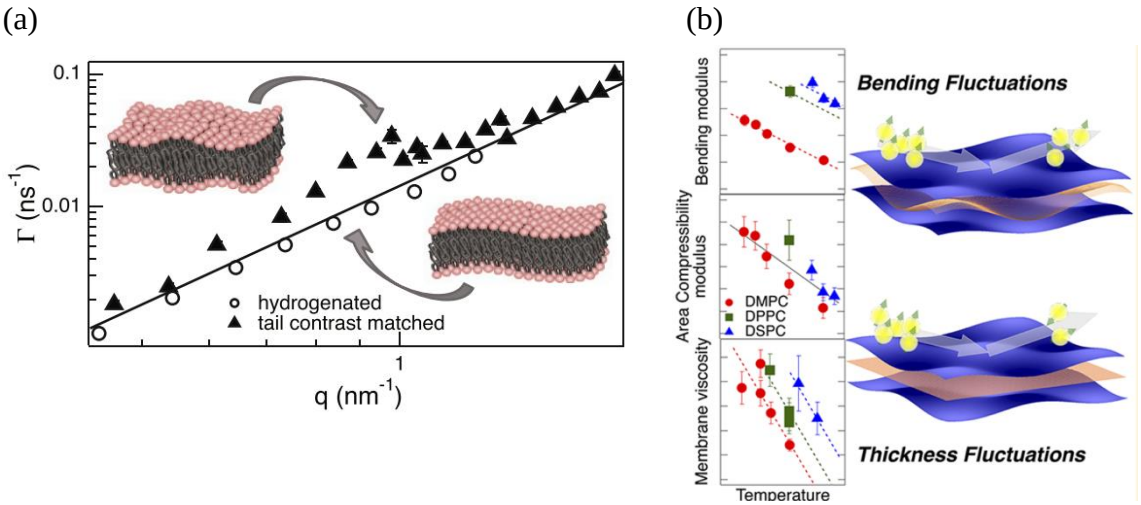

Figure 7.3 (a) The *q* dependence of relaxation state (Γ) for hydrogenated and tail-contrast-matched samples at T = 65ºC. The enhancement in the decay rates of the tail-contrast-matched sample corresponds to membrane thickness fluctuations. Error bars represent ± 1 SD in the entire article and are smaller than the symbol size in this figure. (*Reprinted with permission from Rana Ashkar, Michihiro Nagao, Paul D. Butler, Andrea C. Woodka, Mani K. Sen and Tadanori Koga (2015) Tuning Membrane Thickness Fluctuations in Model Lipid Bilayers. Biophysical Journal, 109(1), 106–112. Copyright 2015*) [4]. (b) A schematic illustration of the lamellar system. Addition of oil to the system swells the $C_{12}E_5$ bilayers. Since the volume fraction of surfactant is kept constant, the interlamellar distance, *d*, is constant, while the bilayer thickness, $d_m = 2d_s + d_o = 2d_s\,(1 + R)$, increases with increasing R, where d_s and d_o are the surfactant molecular length and the oil layer thickness. R = 0 corresponds to the case of pure bilayers. (*Reprinted with permission from Michihiro Nagao, Elizabeth G. Kelley, Rana Ashkar, et al. (2017) Probing Elastic and Viscous Properties of Phospholipid Bilayers Using Neutron Spin Echo Spectroscopy. J. Phys. Chem. Lett., 8, 4679-4684 Copyright (2017) American Chemical Society*) [5].

This dissertation demonstrates a facile method to formulate a stable lamellar phase, and the deposition on a surface can be triggered by the formation of a gel phase when the additive is diluted away from the lamellar structure. The effect of deposition of these lamellar structures can be monitored, and the adsorbed amount, refractive index and layer thickness have been determined using ellipsometry, but only after dilution and removing aggregates from the solution. The turbid nature of these surfactant mixtures does not allow to follow the adsorption process using an optical technique like ellipsometry. It is suggested a study that takes advantage of neutrons and monitors the deposition of deuterated DODAC mixtures and thus studies the adsorption processes onto the silica surface. Neutrons reflectometry, in combination with selective deuteration of DODAC, also allows to determine the composition of the layer structure in terms of additives, DODAC, and water.

Nylander et al. presented a comprehensive review of lipid and DNA delivery to interfaces using neutron reflectometry. The principle of neutron scattering length density difference between hydrogen and deuterium was demonstrated once more, allowing to characterize the films formed from lamellar surfactant systems on surfaces. The authors showed that careful data treatment and analysis is essential to extract valuable quantitative structural and compositional information. Figure 7.4 (a) highlights the importance of isotopic labeling to distinguish and characterize compounds with different neutron scattering length density, which resulted in enhanced contrast. Levicky et al. investigated the effects of surface treatment to control the DNA conformation once adsorbed on a substrate, as depicted in Figure 7.4 (b). Once again, due to poor contrast between different elements, this study was successful by using a neutron reflection technique [6].

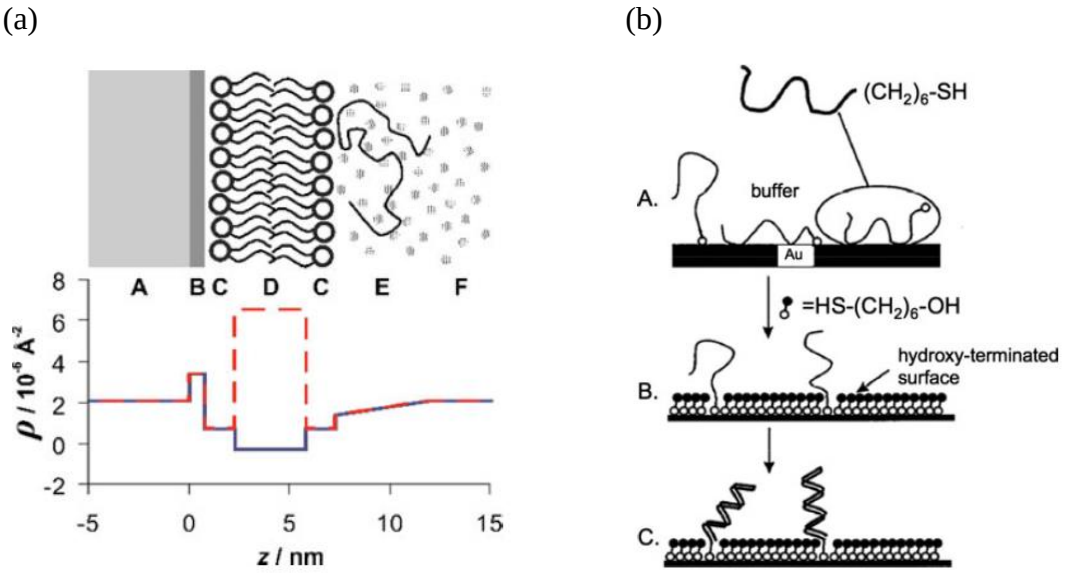

Figure 7.4 (a) A schematic of a model liquid/silica interface with a lipid bilayer and an adsorbed biopolymer. The lower panel shows profiles of the scattering length density ρ as a function of the distance z from the planar surface in the cases where the alkyl chain regions of the lipids are normal hydrogenous groups (continuous blue line) and deuterated groups (dashed red line). In both cases, the solvent is matched in scattering length density to that of the substrate. The different regions shown are (A) silicon, (B) silicon dioxide, (C) lipid head groups, (D) lipid alkyl chains, (E) adsorbed biopolymer, and (F) solvent. (*Reprinted with permission from T. Nylander, R. A. Campbell, P. Vandoolaeghe, et al. (2008) Neutron reflectometry to investigate the delivery of lipids and DNA to interfaces (Review) Biointerphases, Vol. 3, No. 2, FB64-82 Copyright (2008) AIP Publishing*) [7]. (b) (A) Functionalized single-stranded DNA (HS-ss-DNA) that adsorbs to the gold substrate through the thiol end group as well as through backbone-substrate contacts. A multitude of adsorption states exists. (B) The formation of a mercaptohexanol (MCH) monolayer that prevents contacts between the DNA backbone and the substrate, the HS-ss-DNA is left attached by the thiol end. (C) The end-tethered HS-ss-DNA is shown after hybridization to complementary oligonucleotides. (*Reprinted with permission from R. Levicky, T. M. Herne, M. J. Tarlov and S. K. Satija (1998) Using Self-Assembly To Control the Structure of DNA Monolayers on Gold: A Neutron Reflectivity Study J. Am. Chem. Soc., 120, 38, 9787-9792 Copyright (1998) American Chemical Society*) [6].

The use of neutrons to characterize lamellar surfactant systems in the gel phase appears as an excellent alternative to acquire more knowledge on this “solid-like” phase. With the increased use of surfactant systems in a wide range of applications, the use of neutron techniques to better understand the alkyl chain packing and surfactant adsorption on surfaces is suggested.

This Ph.D. dissertation focused on the effects of additives on lamellar surfactant systems and this strategy has been followed to achieve different goals. One such example is given by Isabettini et al. which developed mixed surfactant complexes to generate magnetically responsive systems. Interestingly, they have used cholesterol in the system to induce the lamellar geometry and enhance magnetic alignment. This was attained by repeated heating/cooling cycles during sample preparation. Previously, the importance of these cycles to obtain stable lamellar phases was discussed, which in here, they are shown to have additional positive effects [8].

Early this year, Guo et al. examined the effects of butanol on microbial membranes. The authors concluded that this small polar molecule contributed to membrane fluidization, which resulted in thicker bilayers attributed to a reduction in the alkyl chain interdigitation. Among other techniques, simulations showed reliable results and matched significantly well with experimental results [9]. This study showed the potential use of water-soluble molecules to control the chain stability, and it also agrees with the results obtained in the present dissertation using the fatty acid counterpart, butyric acid. More importantly, the use of small molecules that locate at the surfactant head group/water interface has been analyzed and demonstrated efficient to tune the lamellar phase behavior. The use of simulations to elucidate the underlying surfactant/additive interactions appears as an effective complementary technique to provide a better understanding of the system. The phase stability and concentration effects remain ambiguous, and more work in characterizing surfactant lamellar systems is recommended. Therefore, further SAXS investigations and simulation studies discussed in this Ph.D. work to further pursue the optimization of the surfactant systems are suggested.

References

[1] D.F. Evans, H. Wennerström, The colloidal domain : where physics, chemistry, biology, and technology meet, 2nd ed. ed., New York : Wiley-VCH, 1999.1999.

[2] Y. Fan, Y. Wang, Applications of small-angle X-ray scattering/small-angle neutron scattering and cryogenic transmission electron microscopy to understand self-assembly of surfactants, *Current Opinion in Colloid & Interface Science* 42 **2019** 1-16.

[3] M. Nagao, S. Chawang, T. Hawa, Interlayer distance dependence of thickness fluctuations in a swollen lamellar phase, *Soft Matter* 7(14) **2011** 6598-6605.

[4] R. Ashkar, M. Nagao, Paul D. Butler, Andrea C. Woodka, Mani K. Sen, T. Koga, Tuning Membrane Thickness Fluctuations in Model Lipid Bilayers, *Biophysical Journal* 109(1) **2015** 106-112.

[5] M. Nagao, E.G. Kelley, R. Ashkar, R. Bradbury, P.D. Butler, Probing Elastic and Viscous Properties of Phospholipid Bilayers Using Neutron Spin Echo Spectroscopy, *The Journal of Physical Chemistry Letters* 8(19) **2017** 4679-4684.

[6] R. Levicky, T.M. Herne, M.J. Tarlov, S.K. Satija, Using Self-Assembly To Control the Structure of DNA Monolayers on Gold: A Neutron Reflectivity Study, *Journal of the American Chemical Society* 120(38) **1998** 9787-9792.

[7] T. Nylander, R.A. Campbell, P. Vandoolaeghe, M. Cárdenas, P. Linse, A.R. Rennie, Neutron reflectometry to investigate the delivery of lipids and DNA to interfaces (Review), *Biointerphases* 3(2) **2008** FB64-FB82.

[8] S. Isabettini, M.E. Baumgartner, P.Q. Reckey, J. Kohlbrecher, T. Ishikawa, P. Fischer, E.J. Windhab, S. Kuster, Methods for Generating Highly Magnetically Responsive Lanthanide-Chelating Phospholipid Polymolecular Assemblies, *Langmuir* 33(25) **2017** 6363-6371.

[9] J. Guo, J.C.S. Ho, H. Chin, A.E. Mark, C. Zhou, S. Kjelleberg, B. Liedberg, A.N. Parikh, N.-J. Cho, J. Hinks, Y. Mu, T. Seviour, Response of microbial membranes to butanol: interdigitation vs. disorder, *Physical Chemistry Chemical Physics* 21(22) **2019** 11903-11915.

APPENDIX

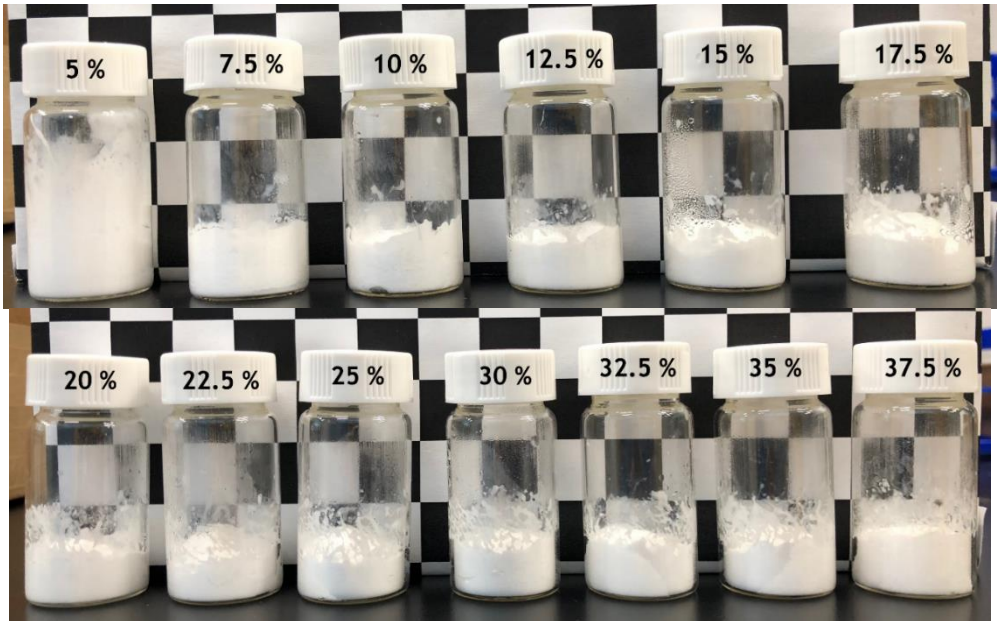

Figure A.4.1 Screw-cap glass vials containing the dispersions of DODAB in water (5 to 37.5 wt. % of surfactant) at room temperature after equilibration.

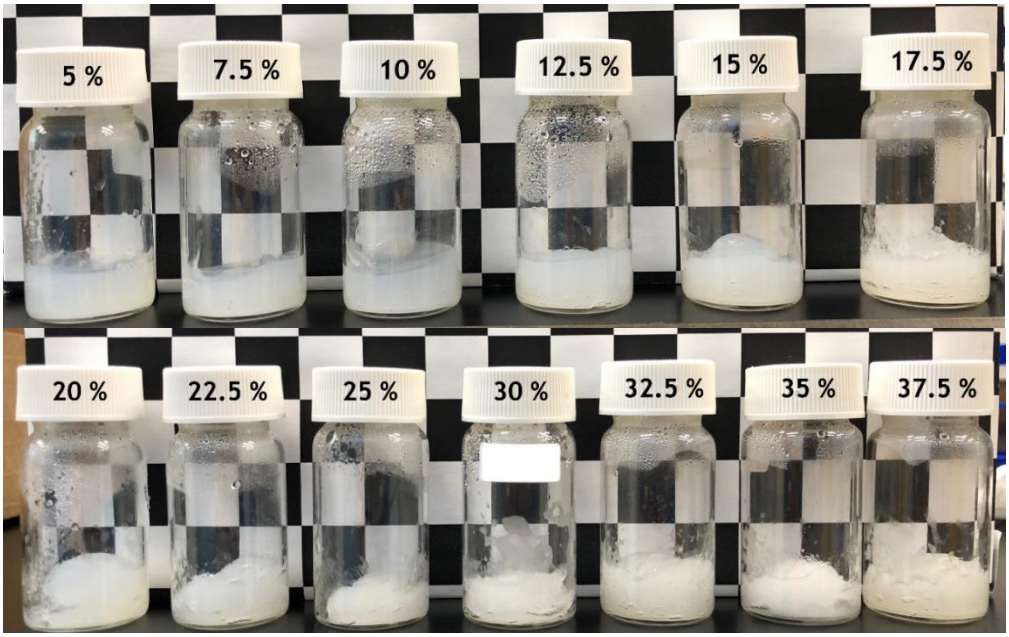

Figure A.4.2 Screw-cap glass vials containing the dispersions of DODAC in water (5 to 37.5 wt. % of surfactant) at room temperature after equilibration.

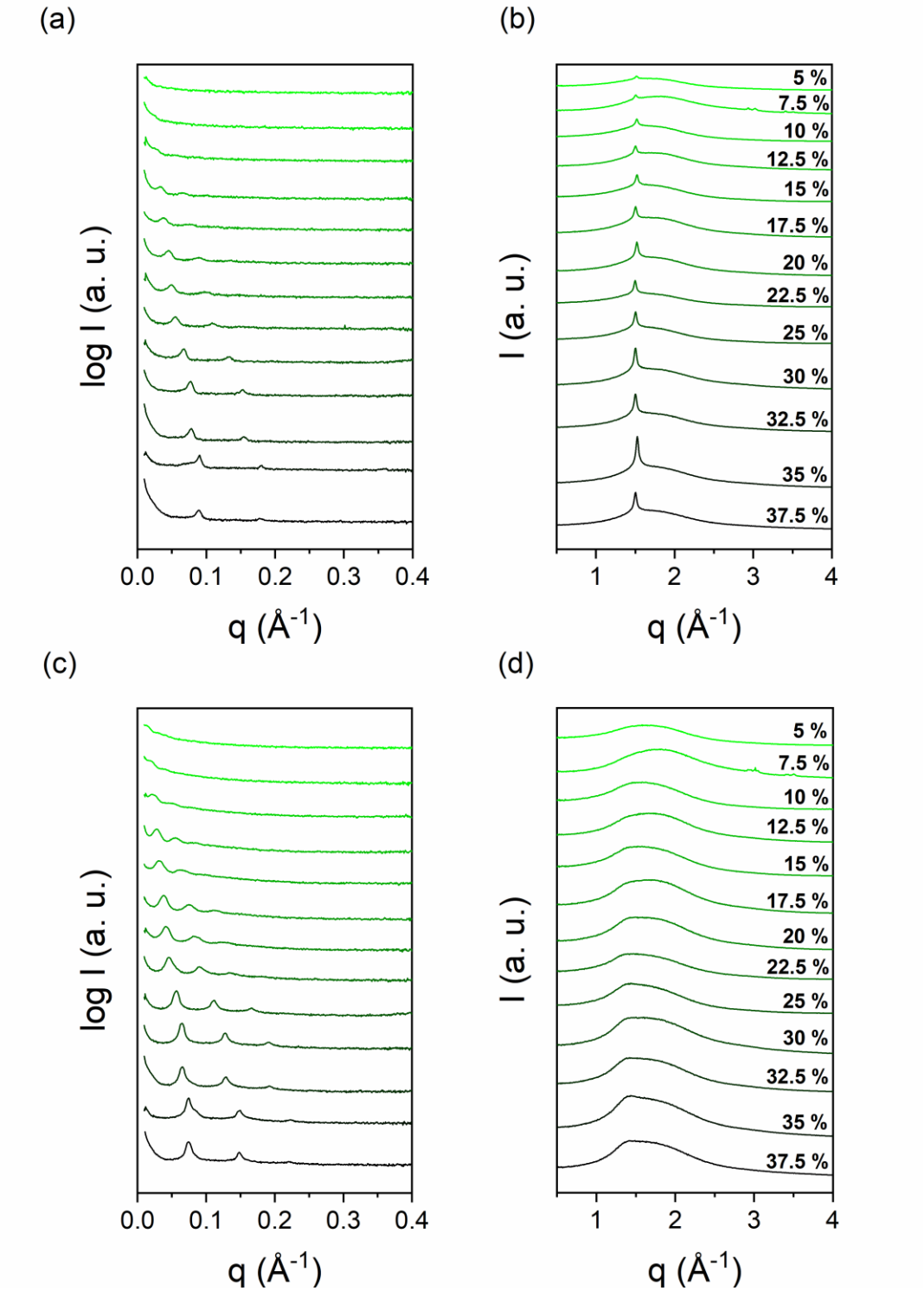

Figure A.4.3 SAXS and WAXS profiles of DODAC in water with increasing surfactant concentration from top to bottom (5-37.5 wt. %). Top panels (a) and (b) corresponds to measurements at 25 ^{o}C, and the bottom panel (c) and (d) to 50 ^{o}C.

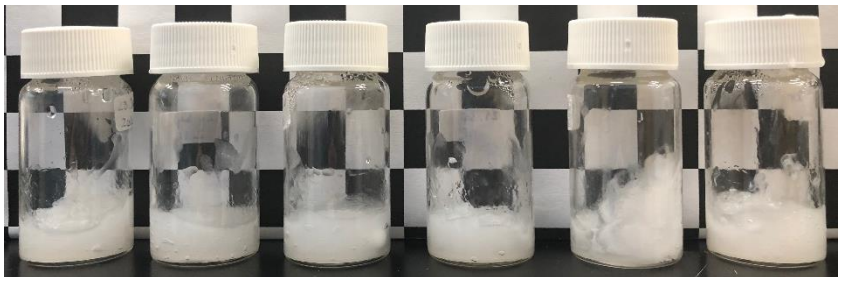

Figure A.5.1 Glass vials with the ternary DODAC-water-urea mixtures. Increasing additive concentration from left to right (5.0, 7.5, 10.0, 12.5, 15.0 and 20.0 wt. %).

Figure A.5.2 Glass vials with the ternary DODAC-water-methyl urea mixtures. Increasing additive concentration from left to right (5.0, 7.5, 10.0, 12.5, 15.0 and 20.0 wt. %).

Figure A.5.3 Glass vials with the ternary DODAC-water-dimethyl urea mixtures. Increasing additive concentration from left to right (5.0, 7.5, 10.0, 12.5, 15.0 and 20.0 wt. %).

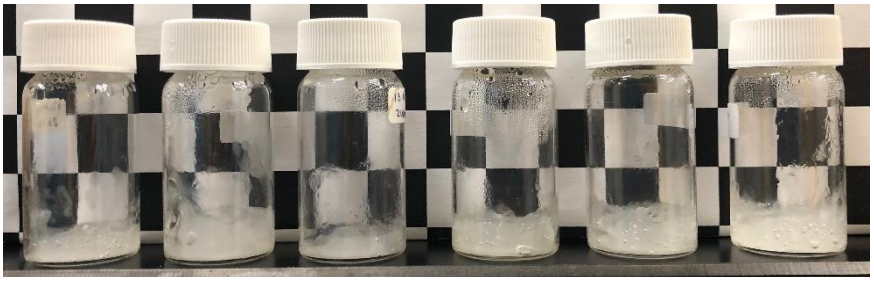

Figure A.5.4 Glass vials with the ternary DODAC-water-acetic acid mixtures. Increasing additive concentration from left to right (5.0, 7.5, 10.0, 12.5, 15.0 and 20.0 wt. %).

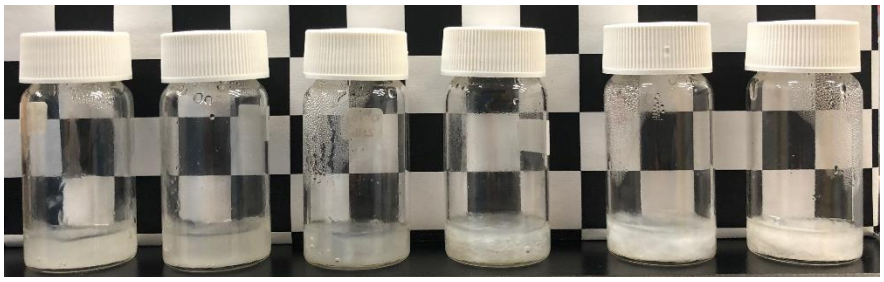

Figure A.5.5 Glass vials with the ternary DODAC-water-propionic acid mixtures. Increasing additive concentration from left to right (5.0, 7.5, 10.0, 12.5, 15.0 and 20.0 wt. %).

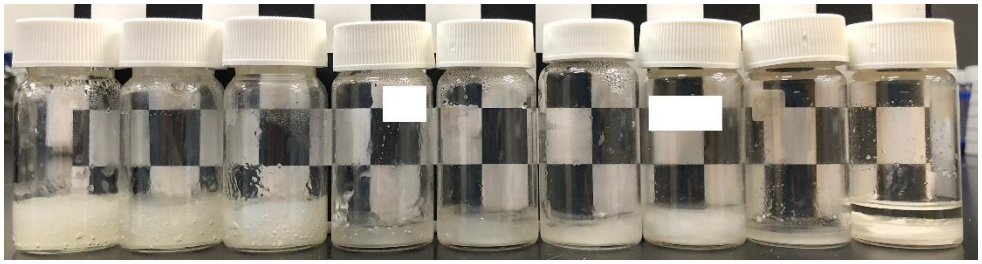

Figure A.5.6 Glass vials with the ternary DODAC-water-butyric acid mixtures. Increasing additive concentration from left to right (1.3, 2.1, 4.5, 5.0, 7.5, 10.0, 12.5, 15.0 and 20.0 wt. %).

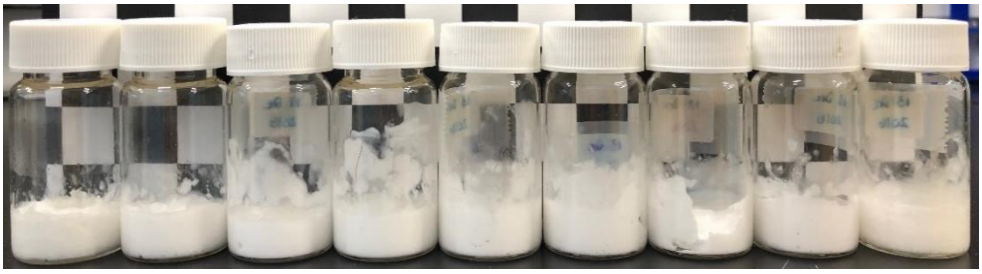

Figure A.5.7 Glass vials with the ternary DODAC-water-sodium butyrate mixtures. Increasing additive concentration from left to right (1.3, 2.6, 5.0, 6.6, 7.5, 10.0, 12.5, 15.0 and 20.0 wt. %).

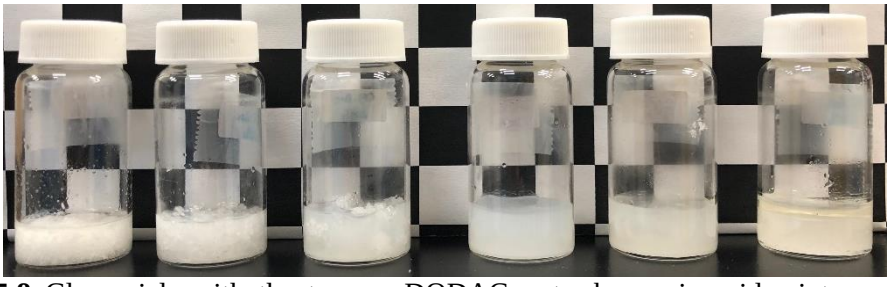

Figure A.5.8 Glass vials with the ternary DODAC-water-hexanoic acid mixtures. Increasing additive concentration from left to right (5.0, 7.5, 10.0, 12.5, 15.0 and 20.0 wt. %).

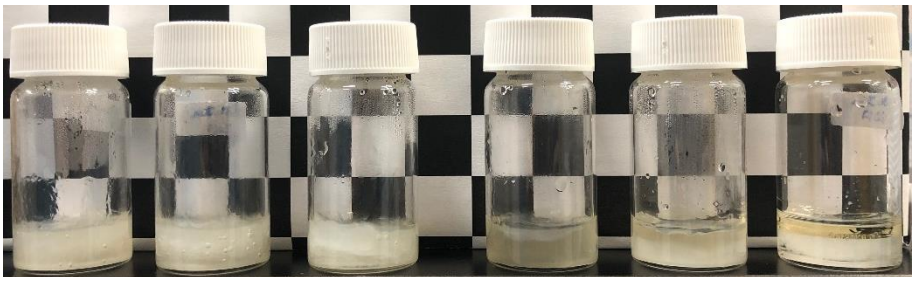

Figure A.5.9 Glass vials with the ternary DODAC-water-benzyl alcohol mixtures. Increasing additive concentration from left to right (5.0, 7.5, 10.0, 12.5, 15.0 and 20.0 wt. %).

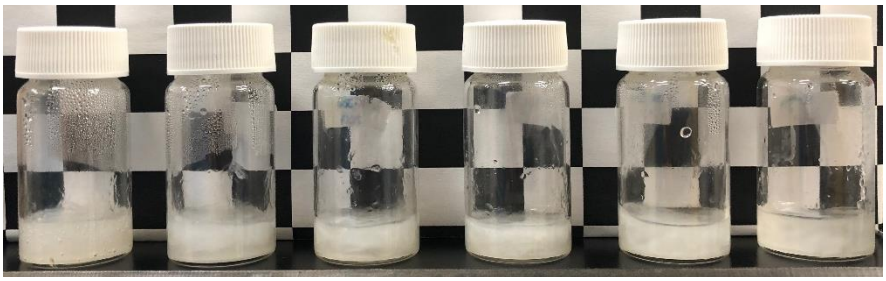

Figure A.5.10 Glass vials with the ternary DODAC-water-phenoxyethanol mixtures. Increasing additive concentration from left to right (5.0, 7.5, 10.0, 12.5, 15.0 and 20.0 wt. %).

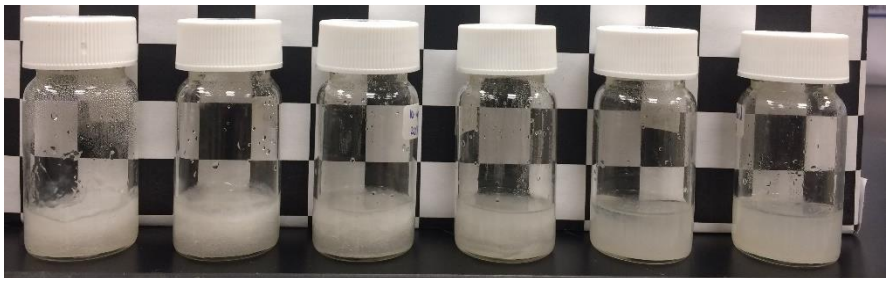

Figure A.5.11 Glass vials with the ternary DODAC-water-butanol mixtures. Increasing additive concentration from left to right (5.0, 7.5, 10.0, 12.5, 15.0 and 20.0 wt. %).

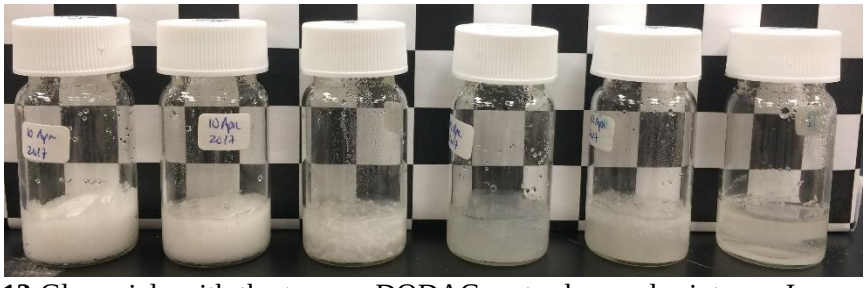

Figure A.5.12 Glass vials with the ternary DODAC-water-hexanol mixtures. Increasing additive concentration from left to right (5.0, 7.5, 10.0, 12.5, 15.0 and 20.0 wt. %).

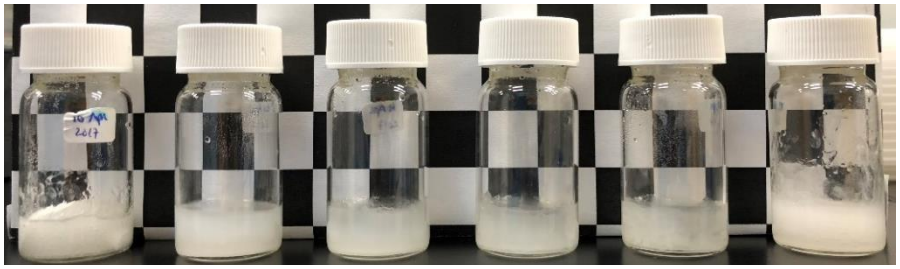

Figure A.5.13 Glass vials with the ternary DODAC-water-octanol mixtures. Increasing additive concentration from left to right (5.0, 7.5, 10.0, 12.5, 15.0 and 20.0 wt. %).

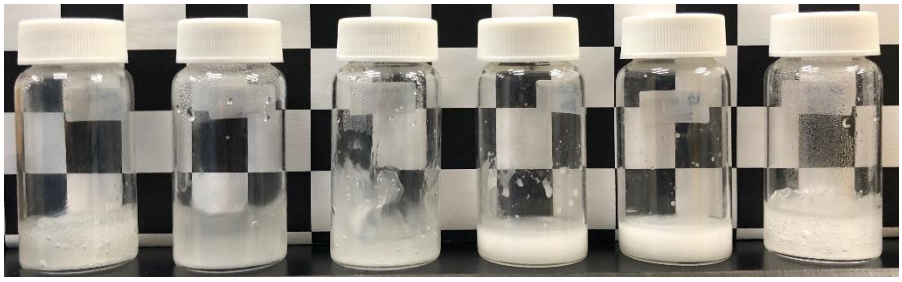

Figure A.5.14 Glass vials with the ternary DODAC-water-decanol mixtures. Increasing additive concentration from left to right (5.0, 7.5, 10.0, 12.5, 15.0 and 20.0 wt. %).

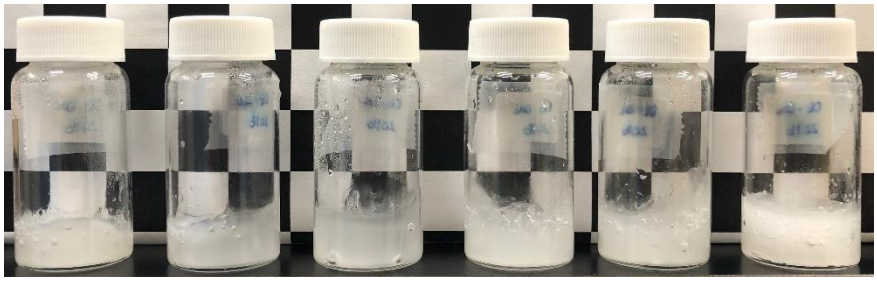

Figure A.5.15 Glass vials with the ternary DODAC-water-dodecanol mixtures. Increasing additive concentration from left to right (5.0, 7.5, 10.0, 12.5, 15.0 and 20.0 wt. %).

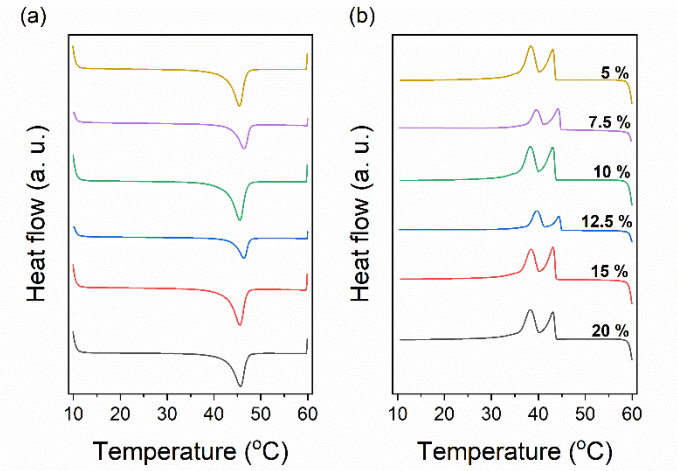

Figure A.5.16 DODAC-water-urea thermograms from 5 (top) to 20 wt. % urea (bottom) at fixed 35 wt. % surfactant. On the left (a) is represented the heating scan, and on the right (b) is represented the cooling scan. The measurements were conducted from 10 to 60 °C, and back to 10 °C at 2 °C/min. The endothermic event corresponds to the downwards deflection.

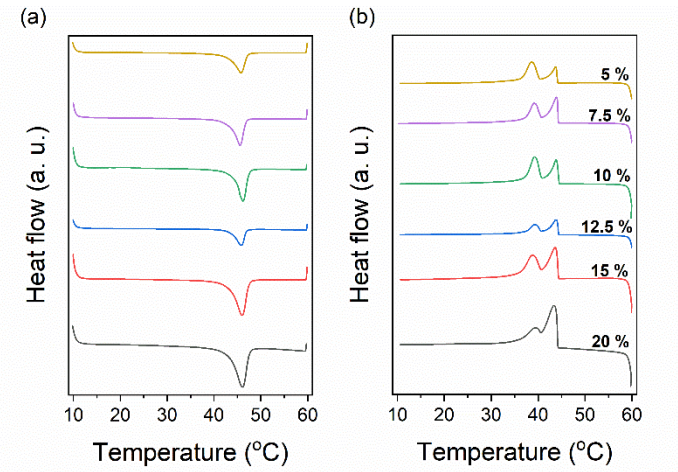

Figure A.5.17 DODAC-water-methyl urea thermograms from 5 (top) to 20 wt. % methyl urea (bottom) at fixed 35 wt. % surfactant. On the left (a) is represented the heating scan, and on the right (b) is represented the cooling scan. The measurements were conducted from 10 to 60 °C, and back to 10 °C at 2 °C/min. The endothermic event corresponds to the downwards deflection.

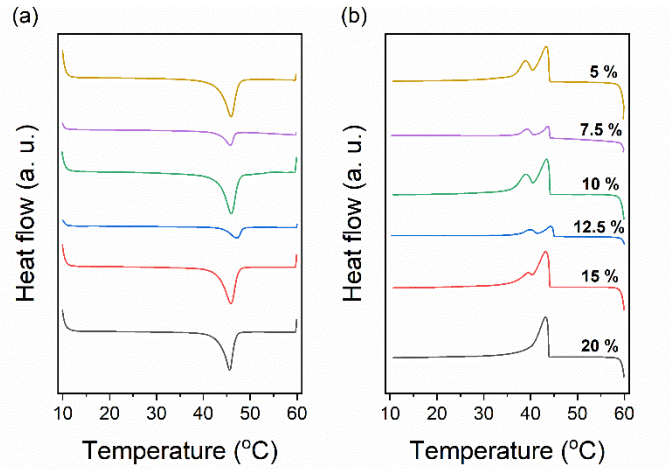

Figure A.5.18 DODAC-water-dimethyl urea thermograms from 5 (top) to 20 wt. % dimethyl urea (bottom) at fixed 35 wt. % surfactant. On the left (a) is represented the heating scan, and on the right (b) is represented the cooling scan. The measurements were conducted from 10 to 60 °C, and back to 10 °C at 2 °C/min. The endothermic event corresponds to the downwards deflection.

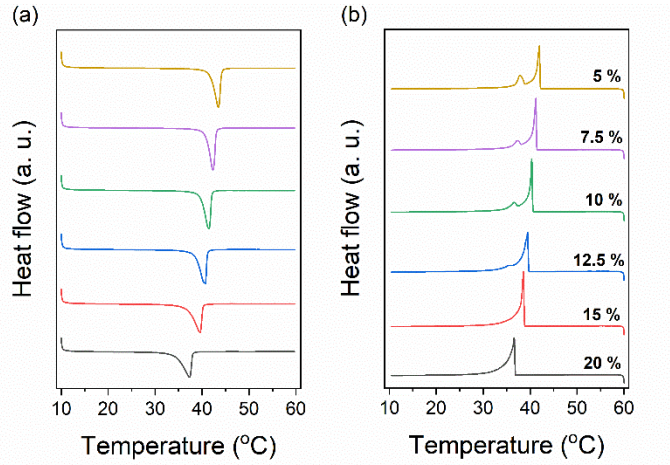

Figure A.5.19 DODAC-water-acetic acid thermograms from 5 (top) to 20 wt. % acetic acid (bottom) at fixed 35 wt. % surfactant. On the left (a) is represented the heating scan, and on the right (b) is represented the cooling scan. The measurements were conducted from 10 to 60 °C, and back to 10 °C at 2 °C/min. The endothermic event corresponds to the downwards deflection.

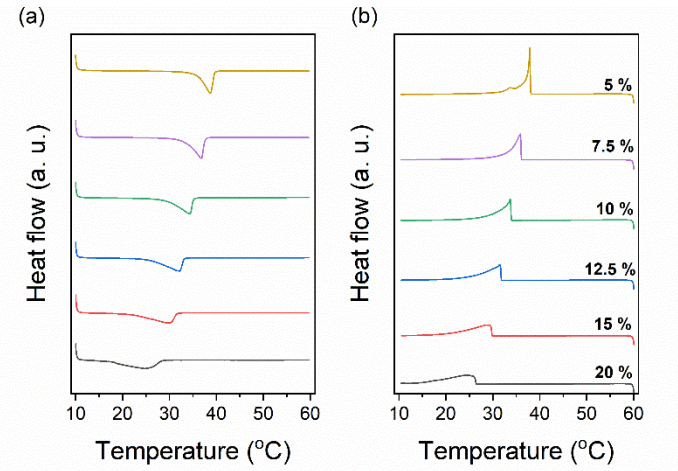

Figure A.5.20 DODAC-water-propionic acid thermograms from 5 (top) to 20 wt. % propionic acid (bottom) at fixed 35 wt. % surfactant. On the left (a) is represented the heating scan, and on the right (b) is represented the cooling scan. The measurements were conducted from 10 to 60 °C, and back to 10 °C at 2 °C/min. The endothermic event corresponds to the downwards deflection.

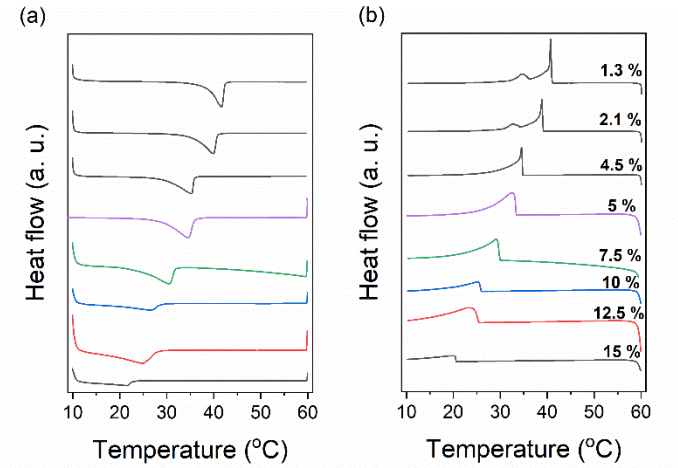

Figure A.5.21 DODAC-water-butyric acid thermograms from 1.3 (top) to 20 wt. % butyric acid (bottom) at fixed 35 wt. % surfactant. On the left (a) is represented the heating scan, and on the right (b) is represented the cooling scan. The measurements were conducted from 10 to 60 °C, and back to 10 °C at 2 °C/min. The endothermic event corresponds to the downwards deflection.

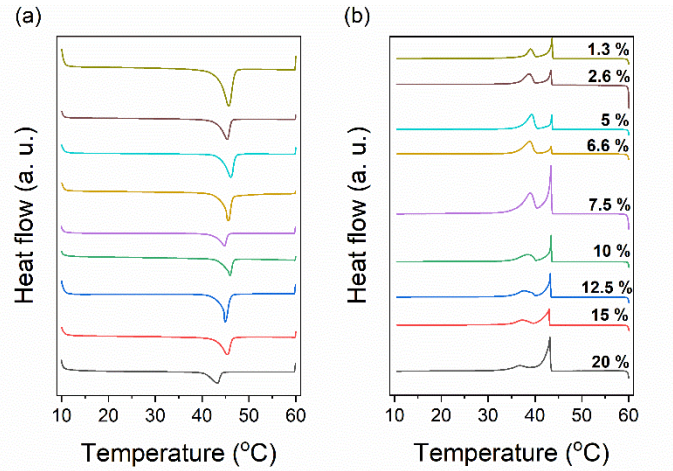

Figure A.5.22 DODAC-water-sodium butyrate thermograms from 1.3 (top) to 20 wt. % sodium butyrate (bottom) at fixed 35 wt. % surfactant. On the left (a) is represented the heating scan, and on the right (b) is represented the cooling scan. The measurements were conducted from 10 to 60 °C, and back to 10 °C at 2 °C/min. The endothermic event corresponds to the downwards deflection.

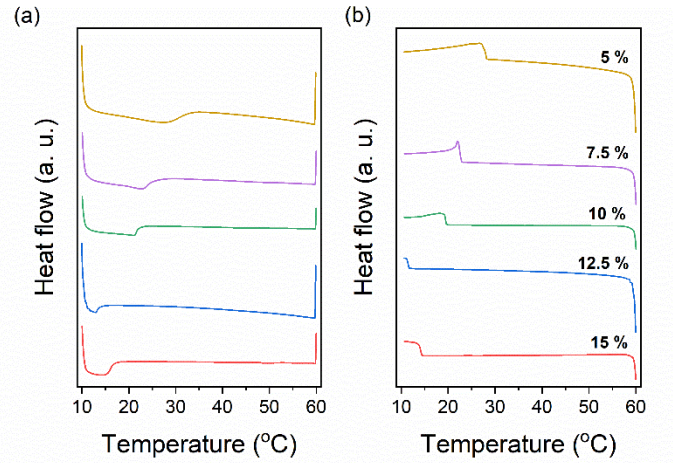

Figure A.5.23 DODAC-water-hexanoic acid thermograms from 5 (top) to 20 wt. % hexanoic acid (bottom) at fixed 35 wt. % surfactant. On the left (a) is represented the heating scan, and on the right (b) is represented the cooling scan. The measurements were conducted from 10 to 60 °C, and back to 10 °C at 2 °C/min. The endothermic event corresponds to the downwards deflection.

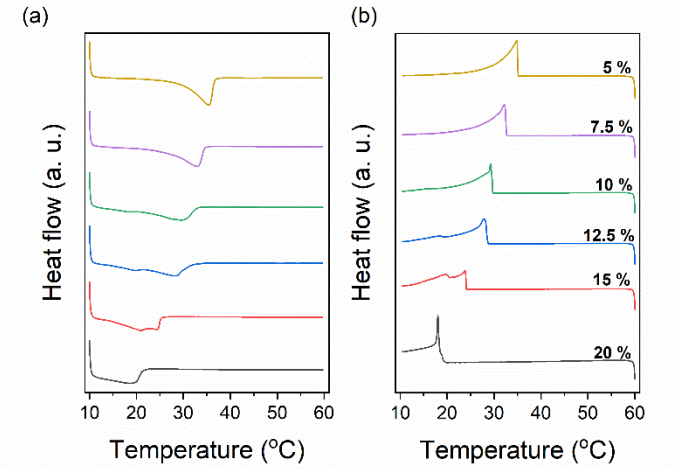

Figure A.5.24 DODAC-water-benzyl alcohol thermograms from 5 (top) to 20 wt. % benzyl alcohol (bottom) at fixed 35 wt. % surfactant. On the left (a) is represented the heating scan, and on the right (b) is represented the cooling scan. The measurements were conducted from 10 to 60 °C, and back to 10 °C at 2 °C/min. The endothermic event corresponds to the downwards deflection

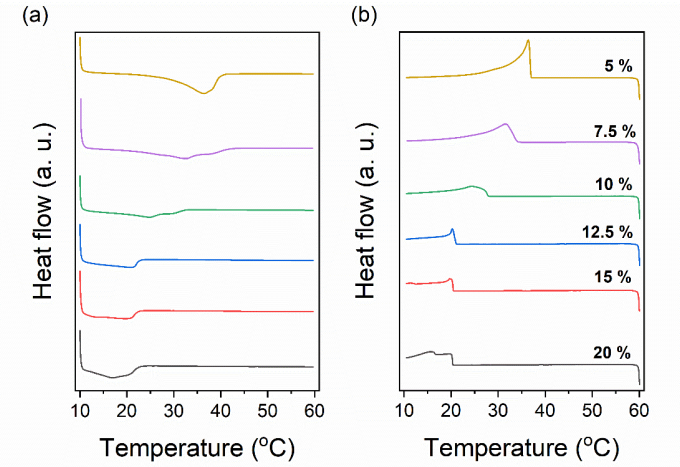

Figure A.5.25 DODAC-water-phenoxyethanol thermograms from 5 (top) to 20 wt. % phenoxyethanol (bottom) at fixed 35 wt. % surfactant. On the left (a) is represented the heating scan, and on the right (b) is represented the cooling scan. The measurements were conducted from 10 to 60 °C, and back to 10 °C at 2 °C/min. The endothermic event corresponds to the downwards deflection.

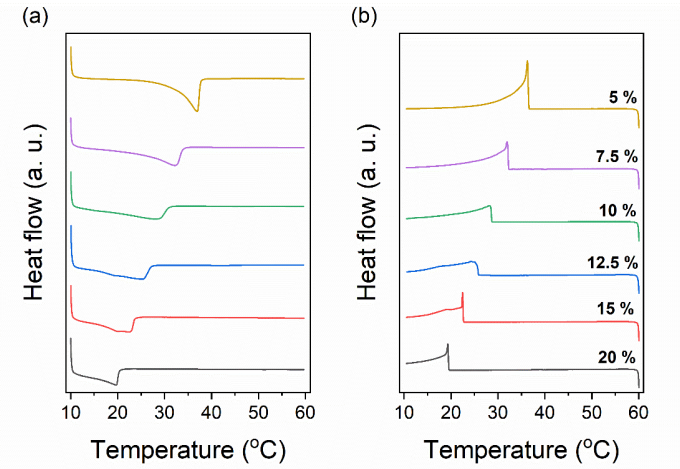

Figure A.5.26 DODAC-water-butanol thermograms from 5 (top) to 20 wt. % butanol (bottom) at fixed 35 wt. % surfactant. On the left (a) is represented the heating scan, and on the right (b) is represented the cooling scan. The measurements were conducted from 10 to 60 °C, and back to 10 °C at 2 °C/min. The endothermic event corresponds to the downwards deflection.

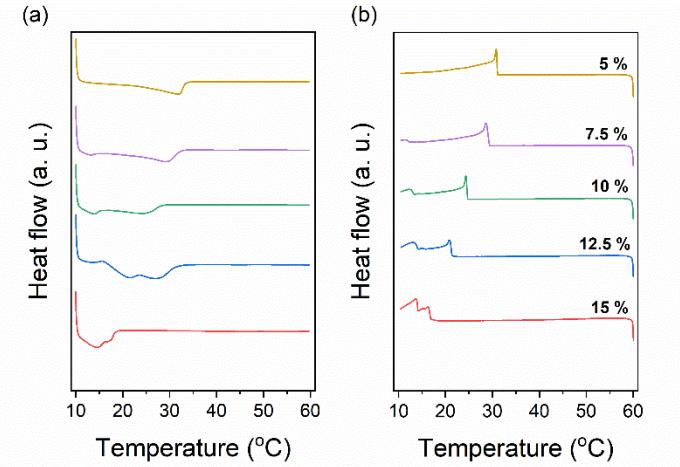

Figure A.5.27 DODAC-water-hexanol thermograms from 5 (top) to 15 wt. % hexanol (bottom) at fixed 35 wt. % surfactant. On the left (a) is represented the heating scan, and on the right (b) is represented the cooling scan. The measurements were conducted from 10 to 60 °C, and back to 10 °C at 2 °C/min. The endothermic event corresponds to the downwards deflection.

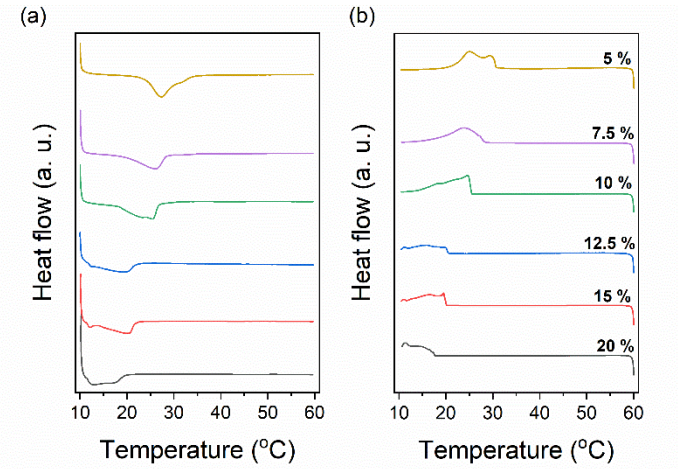

Figure A.5.28 DODAC-water-octanol thermograms from 5 (top) to 20 wt. % octanol (bottom) at fixed 35 wt. % surfactant. On the left (a) is represented the heating scan, and on the right (b) is represented the cooling scan. The measurements were conducted from 10 to 60 °C, and back to 10 °C at 2 °C/min. The endothermic event corresponds to the downwards deflection.

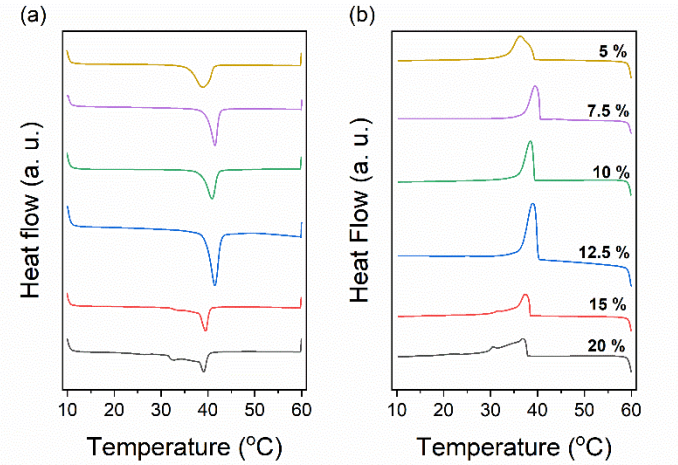

Figure A.5.29 DODAC-water-decanol thermograms from 5 (top) to 20 wt. % decanol (bottom) at fixed 35 wt. % surfactant. On the left (a) is represented the heating scan, and on the right (b) is represented the cooling scan. The measurements were conducted from 10 to 60 °C, and back to 10 °C at 2 °C/min. The endothermic event corresponds to the downwards deflection.

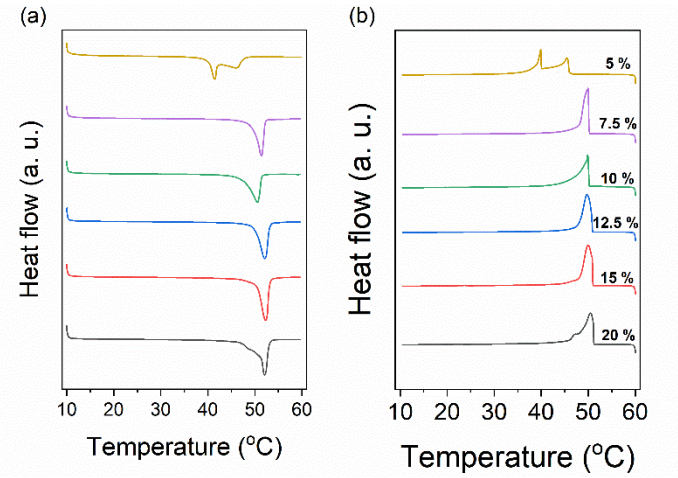

Figure A.5.30 DODAC-water-dodecanol thermograms from 5 (top) to 20 wt. % dodecanol (bottom) at fixed 35 wt. % surfactant. On the left (a) is represented the heating scan, and on the right (b) is represented the cooling scan. The measurements were conducted from 10 to 60 °C, and back to 10 °C at 2 °C/min. The endothermic event corresponds to the downwards deflection.

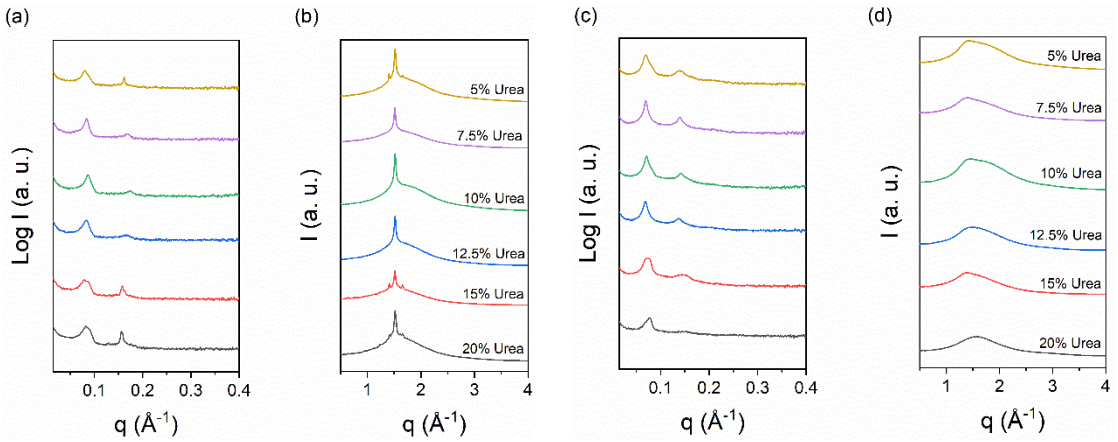

Figure A.5.31 SAXS and WAXS profiles of DODAC in water with increasing urea concentration from top to bottom (5-20 wt. %). (a) and (b) correspond to measurements at 25 ºC, and (c) and (d) to 50 ºC.

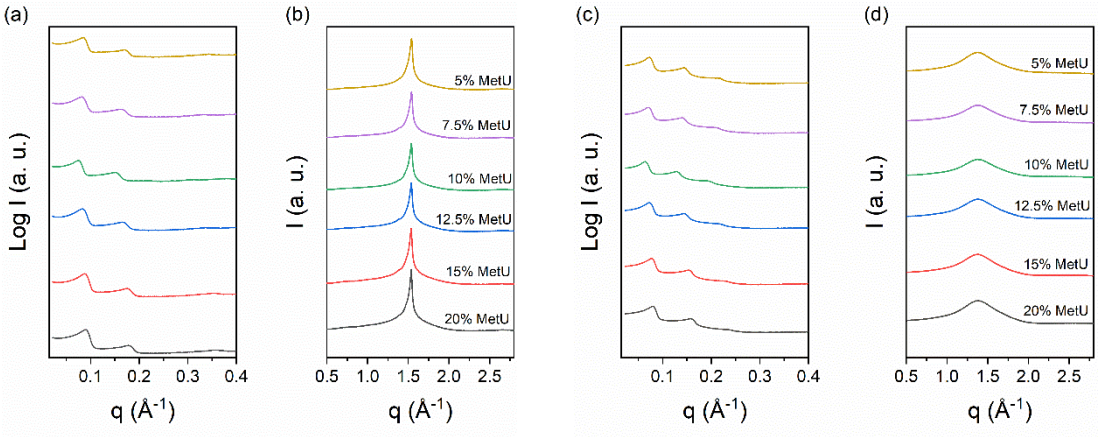

Figure A.5.32 SAXS and WAXS profiles of DODAC in water with increasing methyl urea concentration from top to bottom (5-20 wt. %). (a) and (b) correspond to measurements at 25 ºC, and (c) and (d) to 50 ºC.

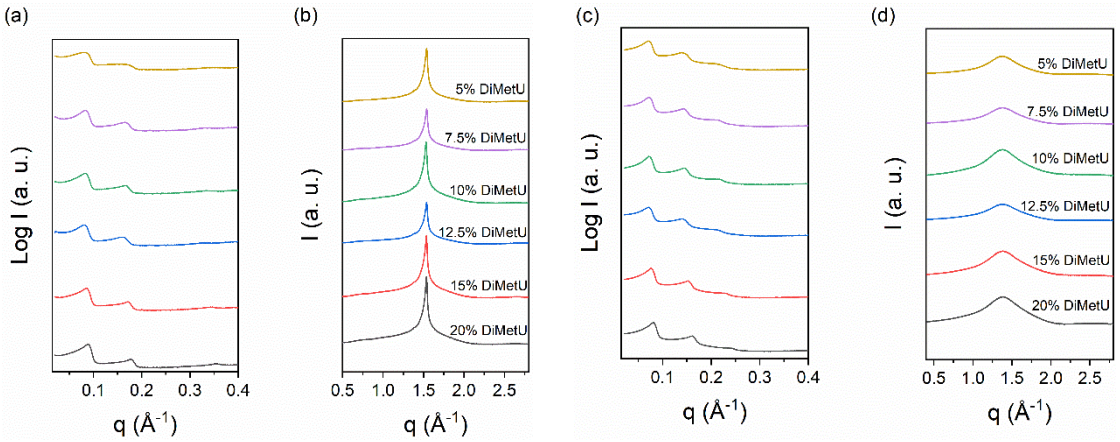

Figure A.5.33 SAXS and WAXS profiles of DODAC in water with increasing dimethyl urea concentration from top to bottom (5-20 wt. %). (a) and (b) correspond to measurements at 25 ºC, and (c) and (d) to 50 ºC.

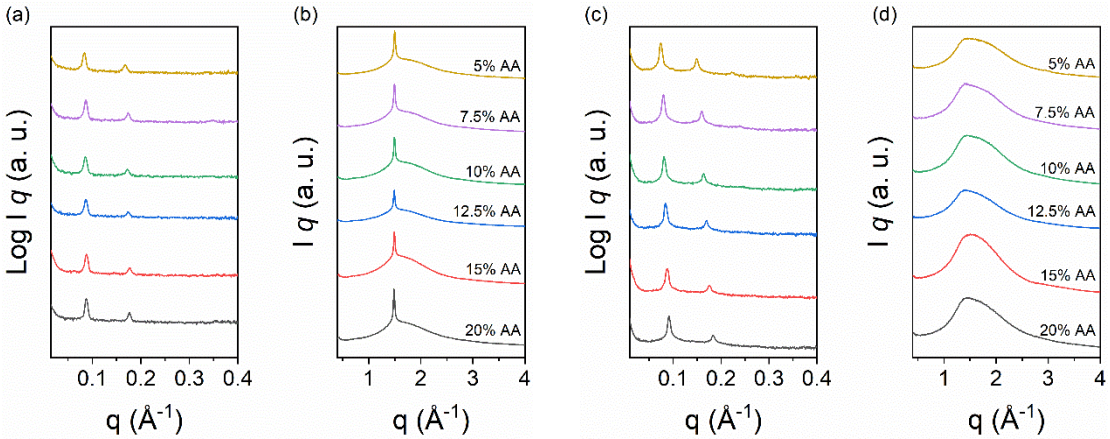

Figure A.5.34 SAXS and WAXS profiles of DODAC in water with increasing acetic acid concentration from top to bottom (5-20 wt. %). (a) and (b) correspond to measurements at 25 ºC, and (c) and (d) to 50 ºC.

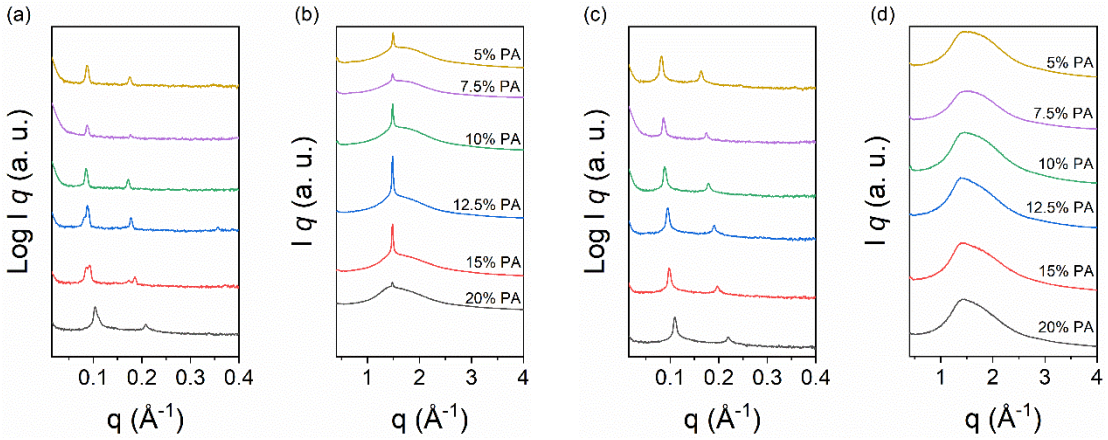

Figure A.5.35 SAXS and WAXS profiles of DODAC in water with increasing propionic acid concentration from top to bottom (5-20 wt. %). (a) and (b) correspond to measurements at 25 ºC, and (c) and (d) to 50 ºC.

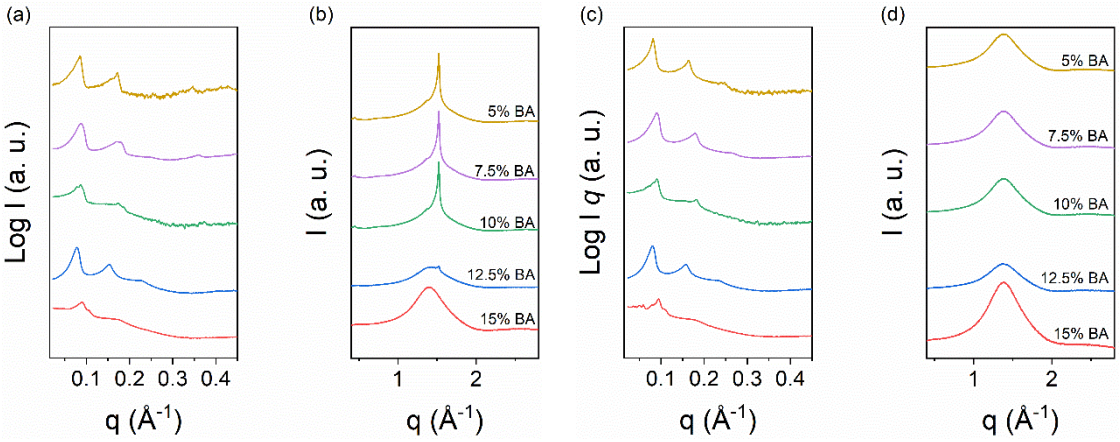

Figure A.5.36 SAXS and WAXS profiles of DODAC in water with increasing butyric acid concentration from top to bottom (5-20 wt. %). (a) and (b) correspond to measurements at 25 ºC, and (c) and (d) to 50 ºC.

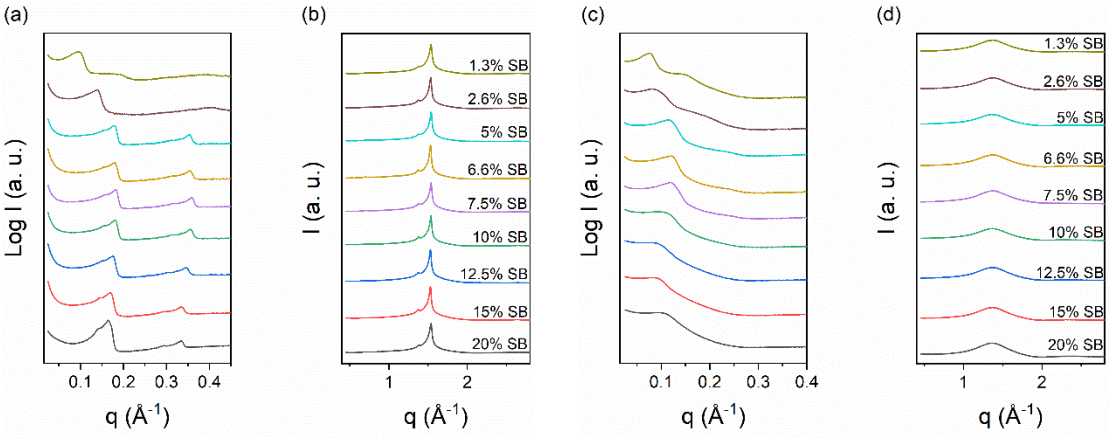

Figure A.5.37 SAXS and WAXS profiles of DODAC in water with increasing sodium butyrate concentration from top to bottom (1.3-20 wt. %). (a) and (b) correspond to measurements at 25 ºC, and (c) and (d) to 50 ºC.

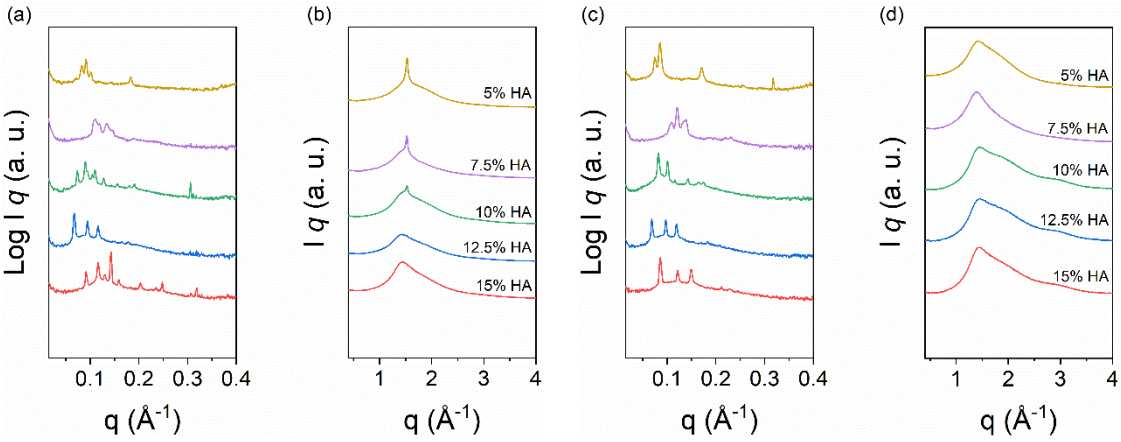

Figure A.5.38 SAXS and WAXS profiles of DODAC in water with increasing hexanoic acid concentration from top to bottom (5-20 wt. %). (a) and (b) correspond to measurements at 12 ºC, and (c) and (d) to 50 ºC.

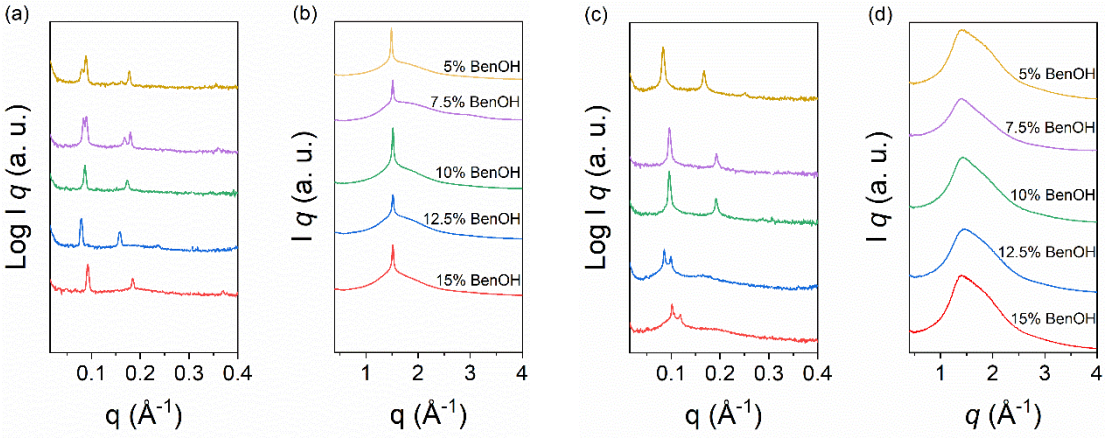

Figure A.5.39 SAXS and WAXS profiles of DODAC in water with increasing benzyl alcohol concentration from top to bottom (5-20 wt. %). (a) and (b) correspond to measurements at 25 ºC, and (c) and (d) to 50 ºC.

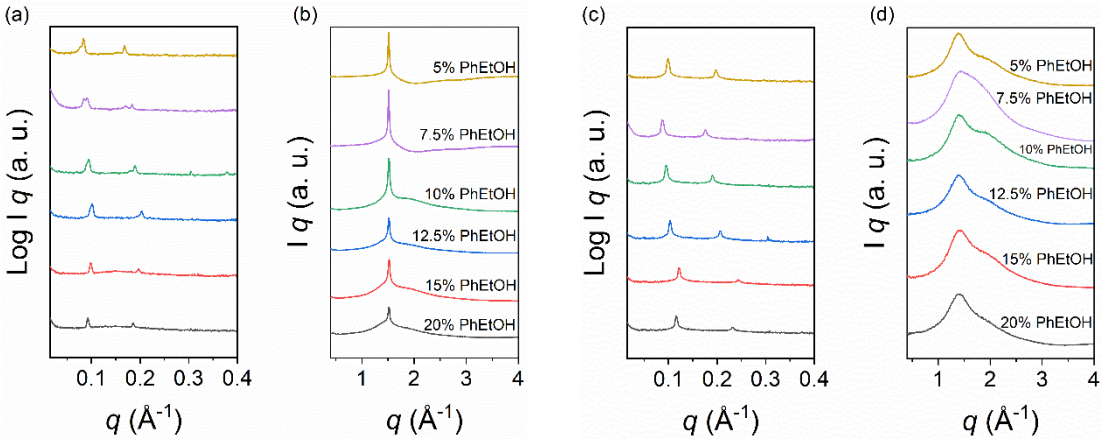

Figure A.5.40 SAXS and WAXS profiles of DODAC in water with increasing phenoxyethanol concentration from top to bottom (5-20 wt. %). (a) and (b) correspond to measurements at 25 ºC, and (c) and (d) to 50 ºC.

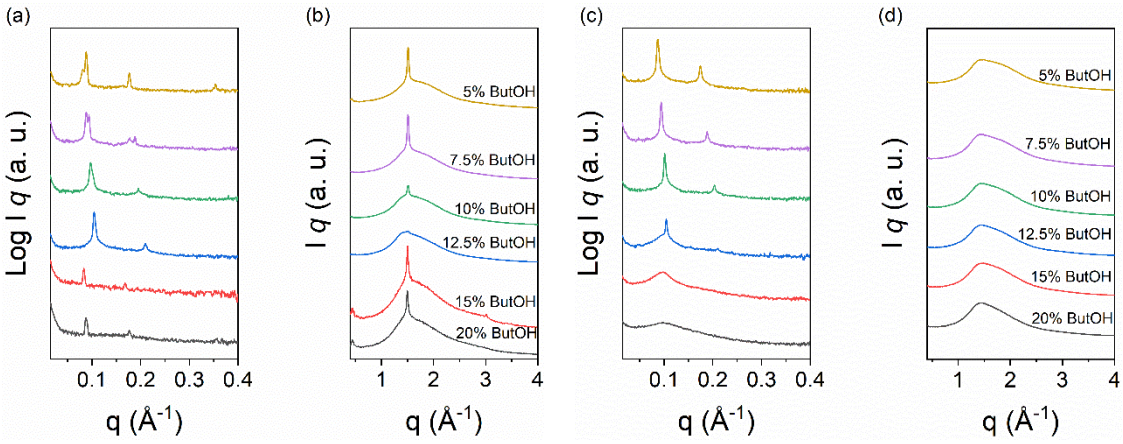

Figure A.5.41 SAXS and WAXS profiles of DODAC in water with increasing butanol concentration from top to bottom (5-20 wt. %). (a) and (b) correspond to measurements at 12 ºC, and (c) and (d) to 50 ºC.

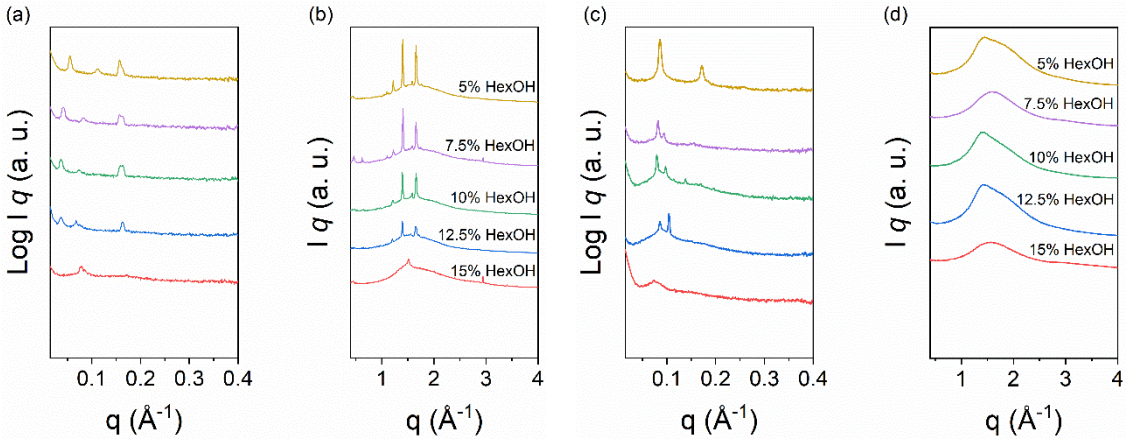

Figure A.5.42 SAXS and WAXS profiles of DODAC in water with increasing hexanol concentration from top to bottom (5-20 wt. %). (a) and (b) correspond to measurements at 12 ºC, and (c) and (d) to 50 ºC.

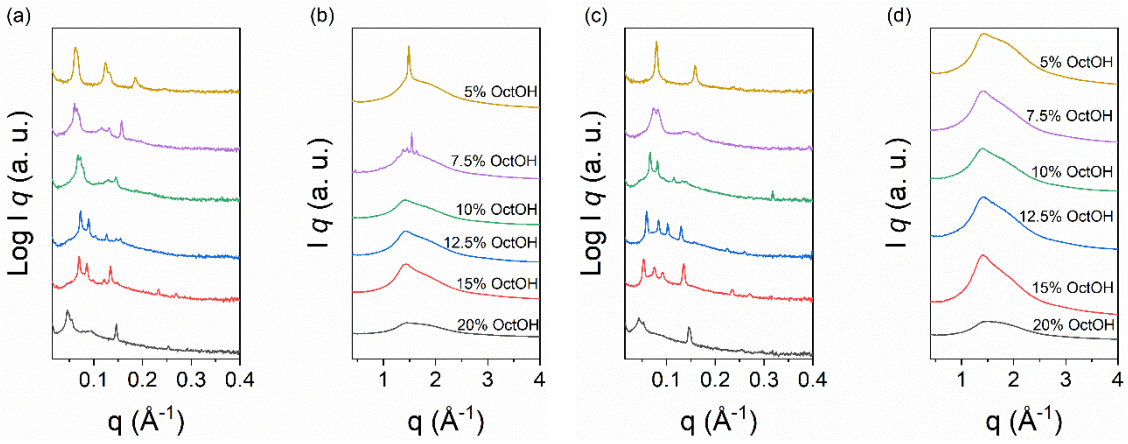

Figure A.5.43 SAXS and WAXS profiles of DODAC in water with increasing octanol concentration from top to bottom (5-20 wt. %). (a) and (b) correspond to measurements at 25 ºC, and (c) and (d) to 50 ºC.

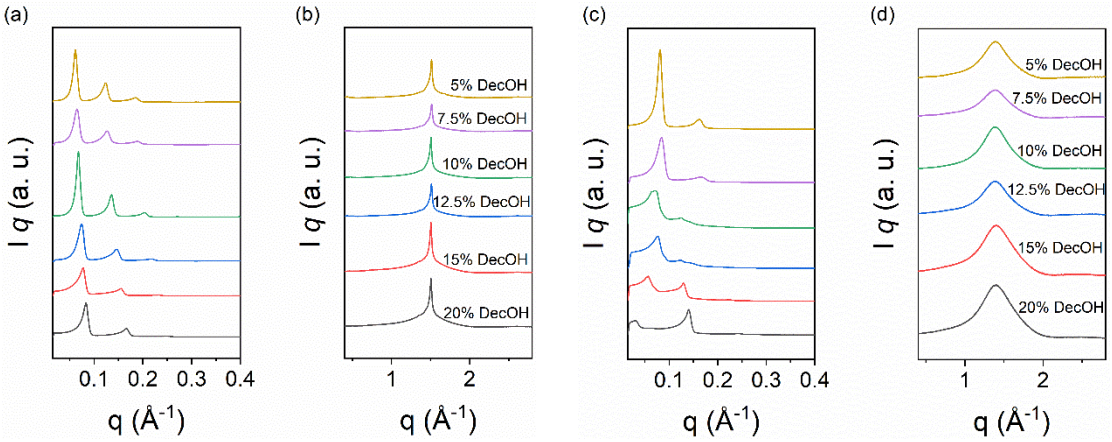

Figure A.5.44 SAXS and WAXS profiles of DODAC in water with increasing decanol concentration from top to bottom (5-20 wt. %). (a) and (b) correspond to measurements at 25 ºC, and (c) and (d) to 50 ºC.

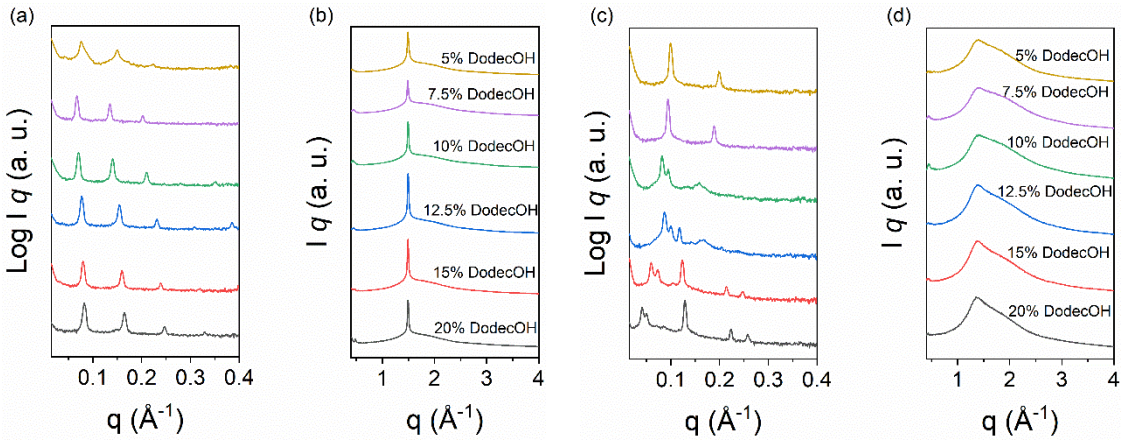

Figure A.5.45 SAXS and WAXS profiles of DODAC in water with increasing dodecanol concentration from top to bottom (5-20 wt. %). (a) and (b) correspond to measurements at 25 ºC, and (c) and (d) to 50 ºC.

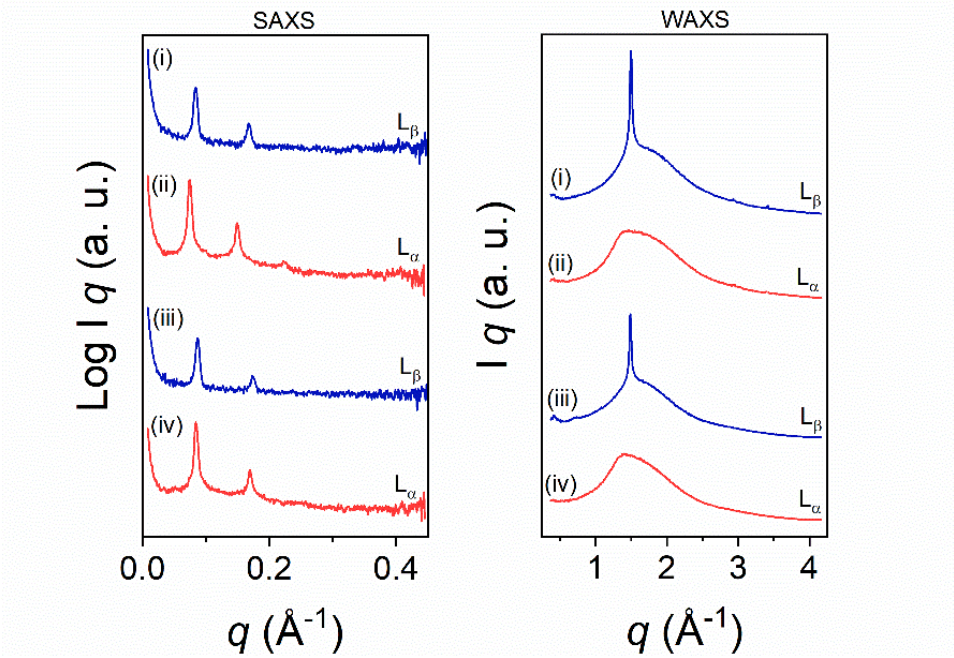

Figure A.6.1 Stacked SAXS/WAXS profiles for the original mixtures of 35 wt. % DODAC-water-acetic acid (AA). (i) SAXS/WAXS of 5 wt. % AA in the L_β (gel) phase; (ii) SAXS/WAXS of 5 wt. % AA in the L_α (liquid crystalline) phase; (iii) SAXS/WAXS of 12.5 wt. % AA in the L_β phase; (iv) SAXS/WAXS of 12.5 wt. % AA in the L_α phase. The Bragg reflections on SAXS reveal the lamellar peak ratio of 1: 2: 3… On the WAXS regime the L_β phase peak at q = 1.50 Å^{-1}, and the L_α phase peak broadening at ca. 1.42 Å^{-1} are determined.

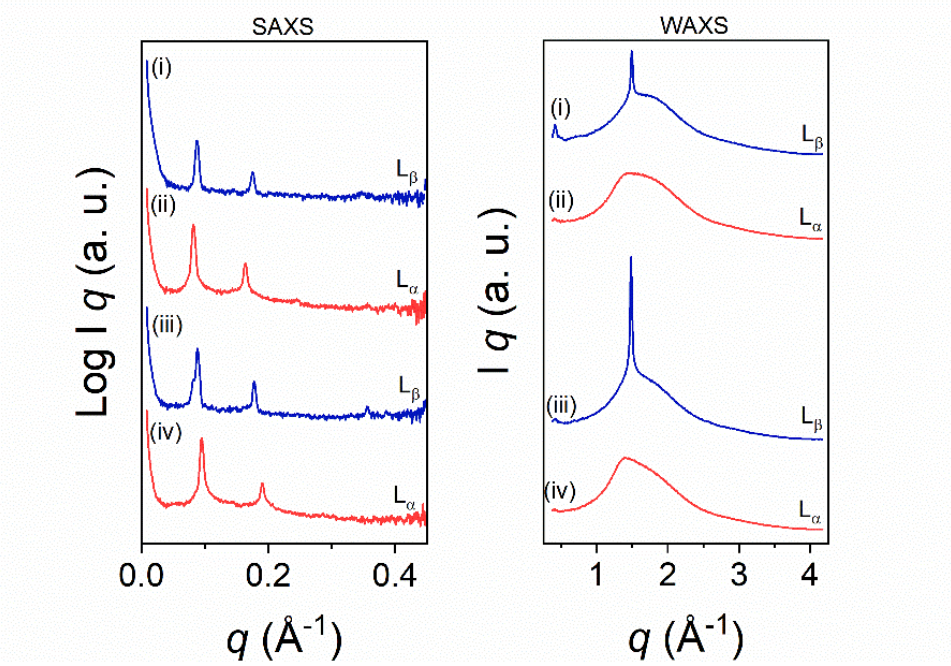

Figure A.6.2 Stacked SAXS/WAXS profiles for the original mixtures of 35 wt. % DODAC-water-propionic acid (PA). (i) SAXS/WAXS of 5 wt. % PA in the L_β (gel) phase; (ii) SAXS/WAXS of 5 wt. % PA in the L_α (liquid crystalline) phase; (iii) SAXS/WAXS of 12.5 wt. % PA in the L_β phase; (iv) SAXS/WAXS of 12.5 wt. % PA in the L_α phase. The Bragg reflections on SAXS reveal the lamellar peak ratio of 1: 2: 3… On the WAXS regime the L_β phase peak at q = 1.49 Å^{-1}, and the L_α phase peak broadening at ca. 1.38 Å^{-1} are determined.

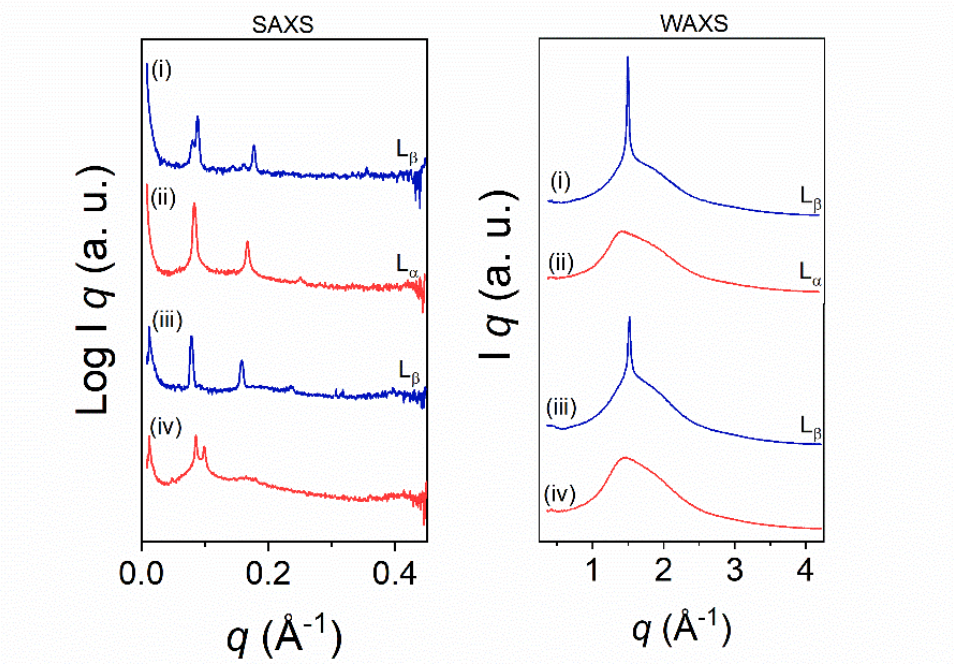

Figure A.6.3 Stacked SAXS/WAXS profiles for the original mixtures of 35 wt. % DODAC-water-benzyl alcohol (BenOH). (i) SAXS/WAXS of 5 wt. % BenOH in the L_β (gel) phase; (ii) SAXS/WAXS of 5 wt. % BenOH in the L_α (liquid crystalline) phase; (iii) SAXS/WAXS of 12.5 wt. % BenOH in the L_β phase; (iv) SAXS/WAXS of 12.5 wt. % BenOH (unidentified phase). The Bragg reflections on SAXS reveal the lamellar peak ratio of 1: 2: 3… On the WAXS regime the L_β phase peak at q = 1.49 $Å^{-1}$, and the L_α phase peak broadening at ca. 1.40 $Å^{-1}$ are determined.

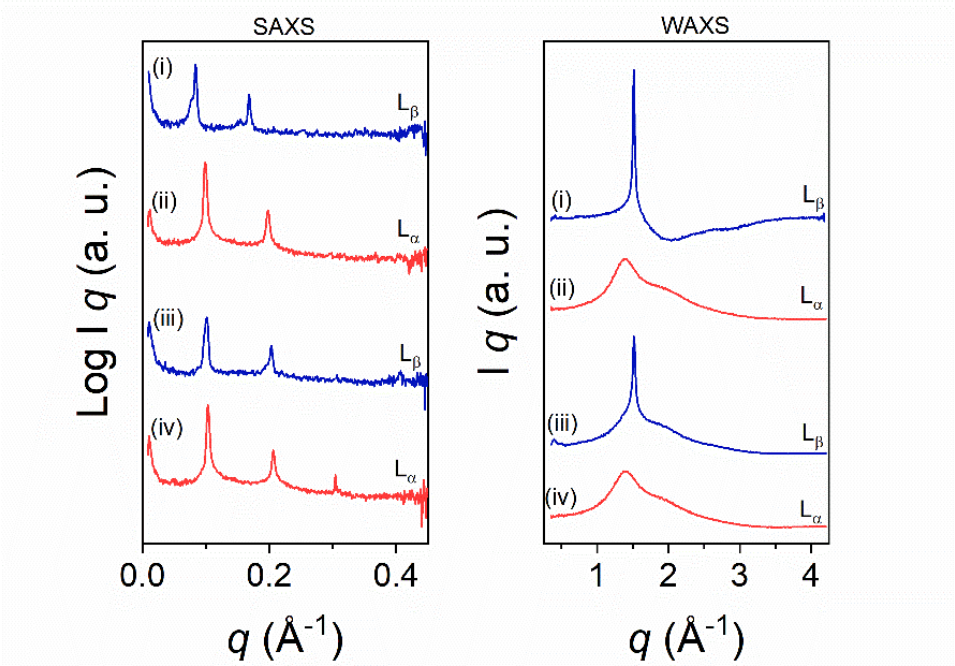

Figure A.6.4 Stacked SAXS/WAXS profiles for the original mixtures of 35 wt. % DODAC-water-phenoxyethanol (PhEtOH). (i) SAXS/WAXS of 5 wt. % PhEtOH in the L_β (gel) phase; (ii) SAXS/WAXS of 5 wt. % PhEtOH in the L_α (liquid crystalline) phase; (iii) SAXS/WAXS of 12.5 wt. % PhEtOH in the L_β phase; (iv) SAXS/WAXS of 12.5 wt. % PhEtOH in the L_α (liquid crystalline) phase. The Bragg reflections on SAXS reveal the lamellar peak ratio of 1: 2: 3… On the WAXS regime the L_β phase peak at q = 1.52 $Å^{-1}$, and the L_α phase peak broadening at ca. 1.38 $Å^{-1}$ are determined.

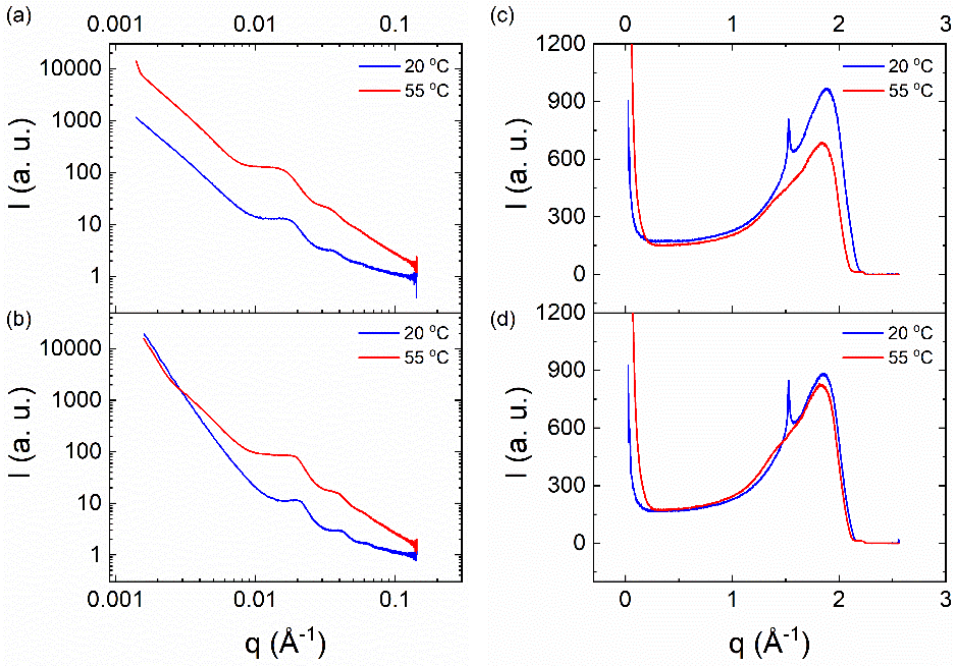

Figure A.6.5 Scattering profiles of diluted mixtures at 20 °C (below T_m) and 55 °C (above T_m). (a) SAXS of 5 wt. % acetic acid in DODAC-water, (b) SAXS of 12.5 wt. % acetic acid in DODAC-water, (c) WAXS of 5 wt. % acetic acid in DODAC-water, and (d) WAXS of 12.5 wt. % acetic acid in DODAC-water.

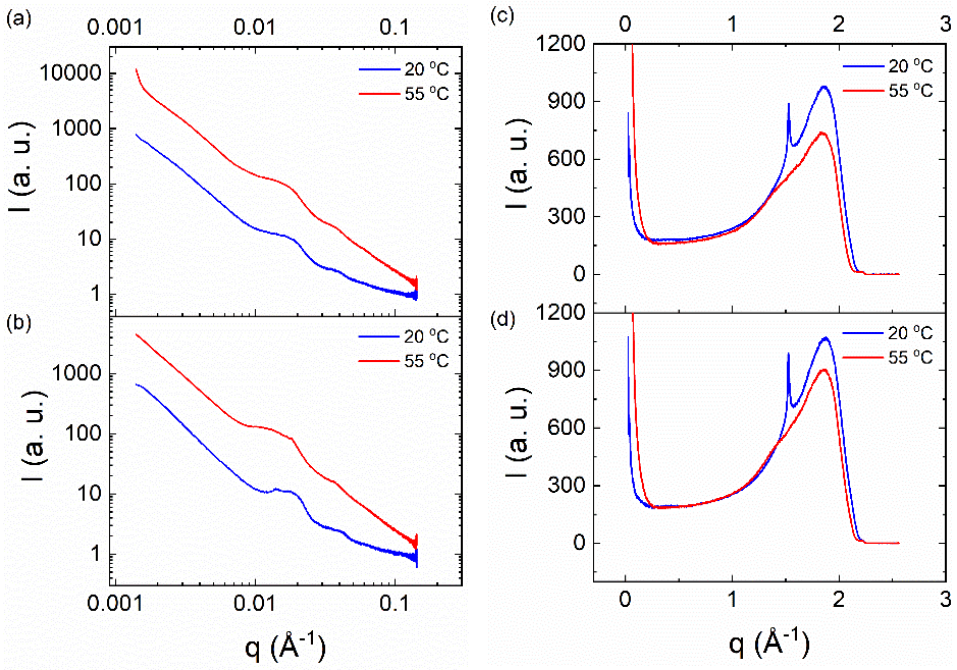

Figure A.6.6 Scattering profiles of diluted mixtures at 20 °C (below T_m) and 55 °C (above T_m). (a) SAXS of 5 wt. % propionic acid in DODAC-water, (b) SAXS of 12.5 wt. % propionic acid in DODAC-water, (c) WAXS of 5 wt. % propionic acid in DODAC-water, and (d) WAXS of 12.5 wt. % propionic acid in DODAC-water.

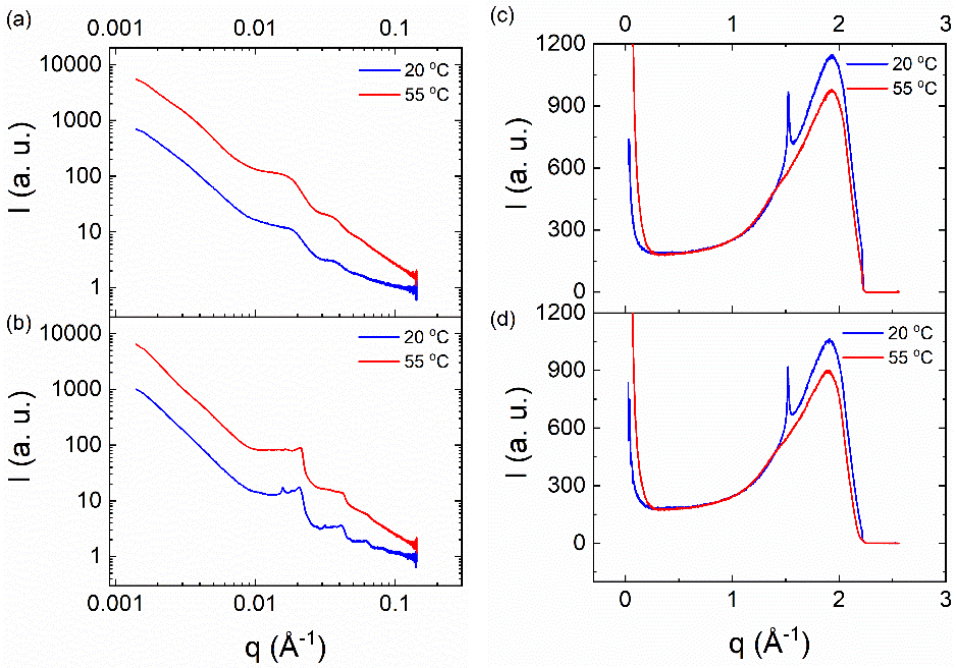

Figure A.6.7 Scattering profiles of diluted mixtures at 20 °C (below T_m) and 55 °C (above T_m). (a) SAXS of 5 wt. % butyric acid in DODAC-water, (b) SAXS of 12.5 wt. % butyric acid in DODAC-water, (c) WAXS of 5 wt. % butyric acid in DODAC-water, and (d) WAXS of 12.5 wt. % butyric acid in DODAC-water.

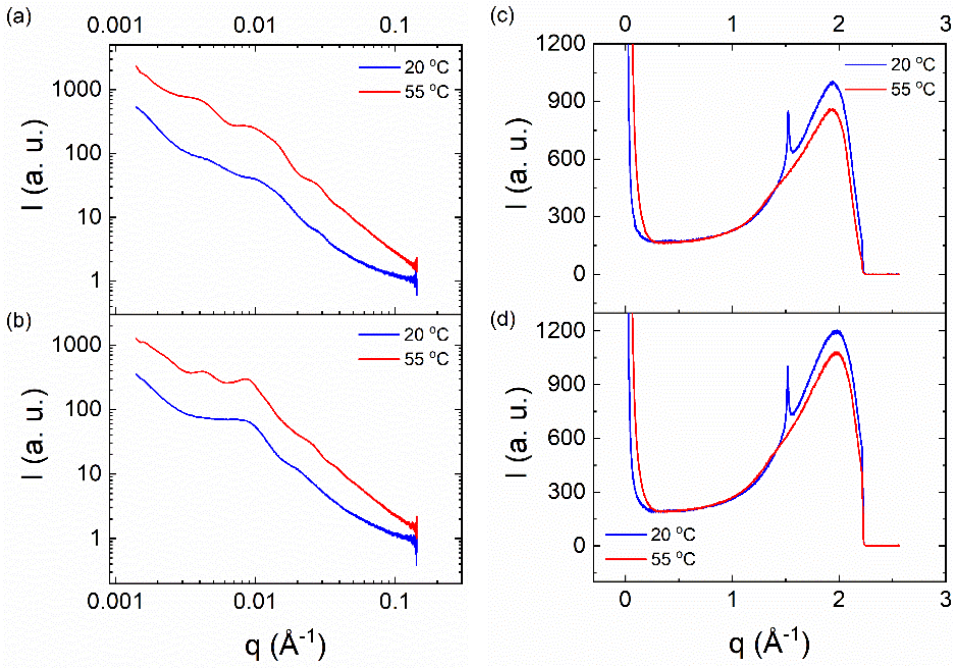

Figure A.6.8 Scattering profiles of diluted mixtures at 20 °C (below T_m) and 55 °C (above T_m). (a) SAXS of 5 wt. % benzyl alcohol in DODAC-water, (b) SAXS of 12.5 wt. % benzyl alcohol in DODAC-water, (c) WAXS of 5 wt. % benzyl alcohol in DODAC-water, and (d) WAXS of 12.5 wt. % benzyl alcohol in DODAC-water.

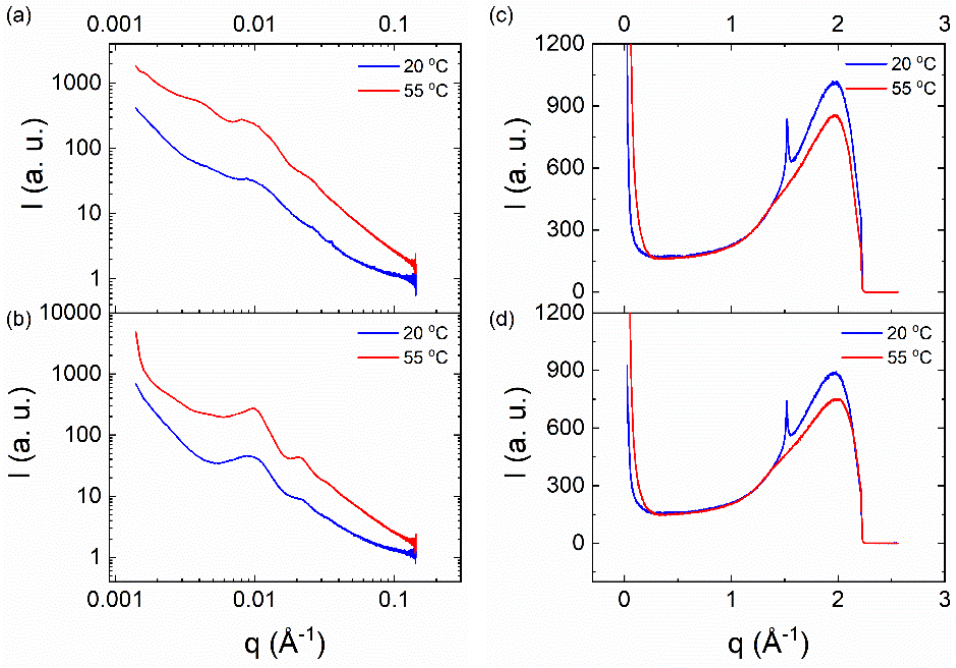

Figure A.6.9 Scattering profiles of diluted mixtures at 20 °C (below T_m) and 55 °C (above T_m). (a) SAXS of 5 wt. % phenoxyethanol in DODAC-water, (b) SAXS of 12.5 wt. % phenoxyethanol in DODAC-water, (c) WAXS of 5 wt. % phenoxyethanol in DODAC-water, and (d) WAXS of 12.5 wt. % phenoxyethanol in DODAC-water.